DEVELOPMENT OF ANALYSIS TOOLS FOR THE EVALUATION OF FAULT DETECTION AND DIAGNOSTICS FOR CHILLERS

Sponsored by
ASHRAE
Deliverable for Research Project 1043-RP
Fault Detection and Diagnostic (FDD)
Requirements and Evaluation Tools for Chillers

HL 99-20 Report #4036-3

Submitted by: Mathew C. Comstock, Graduate Research Assistant
James E. Braun, Principal Investigator

Approved by: Robert J. Bernhard, Director
Ray W. Herrick Laboratories

DECEMBER 1999

ACKNOWLEDGEMENTS

In working on projects such as this one, it is difficult to ignore the fact that there are tasks bigger than can be accomplished by any one person. In addition, this project brought more difficulties than most projects due to the large amount of experimental work performed. Thankfully, there is a God bigger than all our problems who was able to provide the right people at the right time to enable the completion of this project.

Much of the financial support of this project came from ASHRAE and its members. In addition, McQuay donated the chiller used in the experiments, Johnson Controls Inc. donated much of the instrumentation, and ITT provided many additional structural components at reduced cost through their subsidiary, Hydronic and Steam.

The shop personnel at Herrick Labs spent many hours building and wiring the chiller test stand that was used to collect the data. Bob Brown and Frank Lee did much of the heavy construction work, while Gilbert Gordon did the electronics work.

Tom Watson, my contact at McQuay, was an invaluable link to the industrial world. He arranged the donation of the chiller, provided technical assistance, and managed to get the major chiller manufacturers to participate in the chiller survey.

Many other people have provided assistance in countless ways: Todd Rossi, Kirk Drees, Jonathan West, Sriram Srinivasan, Bin Chen, John Seem, and Rich Hackner, among others, helped in different phases of the project. Moreover, I am thankful for Dr. Braun, Dr. Groll, and Dr. Schoenhals; whose technical assistance and general encouragement motivated me to pursue this degree. In particular, I am indebted to Dr. Braun for his patience and vision that made this project possible.

I am also grateful for the many lifelong friends made at Herrick Laboratories who shared in my experiences here and will carry me through the years to come.

TABLE OF CONTENTS

Page

Page

Page

LIST OF TABLES

Table Page

Page

Page

LIST OF FIGURES

Page

NOMENCLATURE

A	-	Area (ft^2)
Building Tons	-	Simulated Cooling Load due to Steam Heating (tons)
c_p	-	Specific Heat at Constant Pressure (Btu/lb_m-R)
Cond Energy Balance	-	1st Law Energy Balance for Condenser Water Loop (tons)
Cond Tons	-	Condenser Heat Rejection Rate (tons)
Cooling Tons	-	City Water Cooling Rate (tons)
COP	-	Coefficient of Performance
C_f	-	Correction Factor
C_{min}	-	Minimum Heat Capacity Rate (Btu/hr-R)
D	-	Diameter (ft)
ε	-	Effectiveness
Evap Energy Balance	-	1st Law Energy Balance for Evaporator Water Loop (tons)
Evap Tons	-	Evaporator Cooling Rate (tons)
f	-	Friction Factor
ff	-	Fouling Factor (hr-R/Btu)
FWB	-	Condenser Water Bypass Flow Rate (gpm)
FWC	-	Flow Rate of Condenser Water (gpm)
FWE	-	Flow Rate of Evaporator Water (gpm)
FWH	-	Hot Water Flow Rate (gpm)
FWW	-	City Water Flow Rate (gpm)
g_c	-	Gravitational Constant (32.2 ft/s^2)
h	-	Heat Transfer Coefficient ($Btu/hr\text{-}ft^2\text{-}R$)
h_{fg}	-	Latent Heat of Vaporization (Btu/lb_m)
Heat Balance	-	1st Law Energy Balance for Chiller (kW)
Heat Balance%	-	1st Law Energy Balance for Chiller (%)
HX	-	Heat Exchanger
k	-	Thermal Conductivity (Btu/hr-ft-R)
kW/ton	-	Compressor Efficiency

$\dot{m}$	-	Mass Flow Rate (lb_m/hr)
μ	-	Viscosity (lb_m/ft-hr)
NTU	-	Number of Transfer Units
NU_D	-	Nusselt Number
P	-	Pressure (psia)
P_lift	-	Pressure Lift Across Compressor (psia)
PO_feed	-	Pressure of Oil Feed (psig)
PO_net	-	Net Oil Pressure (psia)
Pr	-	Prandtl Number
PRC	-	Pressure of Refrigerant in Condenser (psig)
PRE	-	Pressure of Refrigerant in Evaporator (psig)
$\dot{Q}$	-	Heat Transfer Rate (Btu/hr)
q''	-	Heat Flux (Btu/ft^2-hr)
$\dot{Q}_{ct,tons}$	-	Predicted Condenser Heat Transfer Rate (tons)
$\dot{Q}_{et,tons}$	-	Predicted Evaporator Heat Transfer Rate (tons)
Re_D	-	Reynolds Number
ρ	-	Density (lb_m/ft^3)
RLA%	-	Percent of Maximum Rated Load Amps (%)
Shared Cond Tons	-	Shared Condenser HX Heat Transfer (tons)
Shared Evap Tons	-	Shared Evaporator HX Heat Transfer (tons)
T	-	Temperature (F)
T_suc	-	Refrigerant Suction Temperature (F)
TBI	-	Temperature of Building Water In (F)
TBO	-	Temperature of Building Water Out (F)
TCA	-	Condenser Approach Temperature (F)
TCI	-	Temperature of Condenser Water In (F)
TCO	-	Temperature of Condenser Water Out (F)
TEA	-	Evaporator Approach Temperature (F)
TEI	-	Temperature of Evaporator Water In (F)
TEO	-	Temperature of Evaporator Water Out (F)
THI	-	Temperature of Hot Water In (F)
THO	-	Temperature of Hot Water Out (F)
TO_feed	-	Temperature of Oil Feed (F)
TO_sump	-	Temperature of Oil in Sump (F)

Tolerance%	-	Heat Balance Tolerance (%)
TR_dis	-	Refrigerant Discharge Temperature (F)
TRC_sub	-	Liquid-line Refrigerant Subcooling from Condenser (F)
Tsh_dis	-	Refrigerant Discharge Superheat Temperature (F)
Tsh_suc	-	Refrigerant Suction Superheat Temperature (F)
TSI	-	Temperature of Shared HX Water In (F)
TSO	-	Temperature of Shared HX Water Out (F)
TWCI	-	Temperature of Condenser Water In (F)
TWCO	-	Temperature of Condenser Water Out (F)
TWEI	-	Temperature of Evaporator Water In (F)
TWEO	-	Temperature of Evaporator Water Out (F)
TWI	-	Temperature of City Water In (F)
TWO	-	Temperature of City Water Out (F)
u	-	Uncertainty
UA	-	Overall Heat Transfer Conductance (Btu/hr-R)
V	-	Velocity (ft/hr)

Additional subscripts

c	-	Condenser
e	-	Evaporator
g	-	Gas
i	-	Inside
l	-	Liquid
o	-	Outside
r	-	Refrigerant
s	-	Surface
sat	-	Saturated
sc	-	Subcooling
sh	-	Superheating
t	-	Total
w	-	Water
v	-	Vapor

ABSTRACT

Comstock, Matthew, C., M.S.M.E., Purdue University, December, 1999. Development of Analysis Tools for the Evaluation of Fault Detection and Diagnostics in Chillers. Major Professor: Dr. James E. Braun, School of Mechanical Engineering.

An experimental study was conducted on a 90-ton centrifugal chiller to produce a database that will be used in the development and evaluation of Fault Detection and Diagnostic (FDD) methods applied to chillers. The chiller was tested at 27 different operating states under both normal and faulty conditions. The fault conditions were tested at different levels of severity to aid in determining the sensitivity of future FDD methods.

The data collected includes both transient and steady state conditions for the following faults: loss of water flow in the condenser, loss of water flow in the evaporator, refrigerant leakage, refrigerant overcharge, presence of excess oil, condenser fouling, presence of non-condensables in the refrigerant, and faulty expansion valve.

A simple steady state heat exchanger model was developed to check the thermodynamic integrity of the collected data. Moreover, a fault survey was conducted among major American chiller manufacturers to determine the most frequently occurring and costly faults for screw and centrifugal chillers.

1.0 INTRODUCTION

1.1 Background

Although there is a large body of literature on fault detection and diagnostics (FDD) for applications in critical processes, relatively little exists for application to chillers or other vapor compression equipment. The benefits of applying FDD to chillers include less expensive repairs, timely maintenance, and shorter downtimes.

It is common for chillers manufactured today to contain a wealth of sensor information. They also usually contain a microprocessor for control and to detect simple faults such as high condenser pressure, high discharge temperature, and low evaporator pressure. With the increased instrumentation of chillers, the interest in FDD systems for chillers is rapidly growing.

Moreover, many chillers can now be fitted with modems or network cards that allow connection to the Internet, permitting measurements to be distributed anywhere in the world. Within a few years it will be possible to plan maintenance of chillers solely through information collected online, even before the building's occupants are aware that a problem is developing. Such preventative maintenance is one of the key advantages to utilizing FDD methods in chillers.

1.2 Literature Review

An exhaustive literature review of fault detection and diagnostics was performed by Comstock et al. (1999b). The review of presently available literature demonstrated the lack of experimental data that can be used to develop FDD methods in chillers. Only a handful of papers have been published on chillers and many have one or more of the following shortcomings: testing at only one loading condition, testing at only one fault

level (often at a catastrophic level), testing of only a few types of faults, or using a chiller not directly applicable to most building installations. The following subsections contain the most relevant literature reviews to this project.

1.2.1 Bailey

Bailey (1998) trained a neural network using normal and faulty data from a screw chiller to directly classify normal and faulty performance. The faults simulated were refrigerant loss and overcharge, oil loss and overcharge, air-cooled condenser fouling, and the loss of an air-cooled condenser fan. Experimental data were collected from a 70-ton air-cooled screw chiller using R-22 as a refrigerant. Two independent variables—fault degree and chiller load—were varied to study the following dependent variables: energy consumption, chilled water supply control temperature, superheat and subcooling temperatures, suction pressure, and discharge pressure. Another study focused on the effects of outdoor air temperature (an uncontrollable independent variable) on the same dependent variables.

The chiller tests were conducted over a two-month period. A distinct test was run each day, with the chiller started at a minimum load that was increased throughout the day. Refrigerant charge testing started at –60% of design charge and was increased 5% each day until a +30% charge was reached. Oil charge was started at –50% of design levels and increased to +35% over the course of five days. Air-cooled condenser fouling was simulated at five different levels by covering the air intake screens, first at 22% coverage, and concluding with a test at 67% coverage. The air-cooled condenser fan loss was simulated by turning off the fan that affected the first and third stages, then by turning off the fan that affected the second and third stages (as the cooling load increased, the number of active fans was increased through staging—as opposed to using a variable frequency drive).

Although the data collection process appears to have been thorough, the sensitivity of the measured variables to the faults introduced was not given. Moreover, the ability of the neural network to classify the faults is difficult to deduce from the

results. The best model that was presented—with a valid training data set—had a misclassification rate of 20%.

1.2.2 Grimmelius, Woud, and Been

Grimmelius et al. (1995) used residuals (differences between measured values and expected values) and expert knowledge for detecting and diagnosing chiller faults. Experimental data were collected from a 77-ton reciprocating chiller. A total of about 20 measurements were taken—temperatures, pressures, power consumption, and compressor oil level—during an undisclosed test period. Initially 58 possible steady-state failure modes were identified, but many were combined to yield a symptom matrix with 37 failure modes. Only five failure modes were published: increased flow resistance in the compressor suction and discharge, increased flow resistance in the condenser cooling water, increased resistance in the liquid line, loose thermal expansion valve bulb, and increased flow resistance in the chilled water through the evaporator.

During the chiller testing, the chilled water inlet temperature and condenser cooling water inlet temperatures were varied. The authors commented that the faults were introduced at levels below those that would cause alarms in the preexisting facility (they did not comment on what levels the faults were introduced at or whether multiple fault levels were tested). They also mentioned that the FDD method tended to conclude that a fault had occurred without many symptoms being found. The model was not designed to detect faults during transient behavior.

1.2.3 Peitsman and Bakker

Peitsman and Bakker (1996) used both autoregressive (ARX) and artificial neural network (ANN) models to generate residuals for a FDD method applied to a laboratory chiller. Models were used at the system level for fault detection and at the component level to isolate the fault. Input parameters for the models included: condenser supply water temperature, evaporator supply glycol temperature, instantaneous compressor

power, and the flow rate of cooling water entering the condenser (ANN only). A total of 14 process output variables were estimated from these inputs, consisting of various refrigerant temperatures, refrigerant pressures, refrigerant mass flow rate, and outlet water temperatures. Both the ARX and ANN models demonstrated a reliability of nearly 97% in predicting the outputs based on the given input parameters (as long as the training data is robust with healthy dynamic changes). The authors commented that the ANN performed slightly better than the ARX due to the nonlinearity of the system.

Only one fault was demonstrated (at an unidentified level)—detecting air in the refrigerant using the discharge refrigerant pressure.

1.2.4 Stylianou and Nikanpour

Gordon and Ng (1995) developed a thermodynamic model for COP and capacity of chillers that could be used to generate characteristic quantities for use within a fault detection method. Stylianou and Nikanpour (1996) and Stylianou (1997) used this model as part of their FDD approach applied to a reciprocating chiller. This model was used solely for fault detection (not diagnosis) during steady state operation of the chiller. Diagnostics were performed in a manner similar to that presented by Grimmelius et al. (1995) using the information contained in Table 1.1. The 5-ton reciprocating chiller used in the study was tested at a range of condenser and evaporator water entering temperatures. A total of 17 measurements were taken over an unidentified test period.

The faults simulated in the study were: refrigerant leak, refrigerant line restriction (to represent a plugged filter-drier), condenser water flow restriction and evaporator water flow restriction (both to represent fouling or a pump fault). The diagnostic fault table with corresponding changes in measured variables is shown in Table 1.1.

Table 1.1: Fault pattern of Stylianou and Nikanpour's chiller diagnostic module.

	Discharge Temp.	Discharge Pressure	High Pressure Liquid Line Temp.	Low Pressure Liquid Line Temp.	Suction Line Temp.	Suction Pressure	Condenser Water Temp. Difference	Evaporator Water Temp. Difference
Fault								
Liquid Line Restriction	+	-	-	-	+	-	-	+
Refrigerant Leak	+	-	-	-	+	-	-	+
Reduced Condenser Water Flow Rate	+	+	+	-	-	-	+	-
Reduced Evaporator Water Flow Rate	+	-	-	-	-	-	-	-

The plus (+) signs indicate an increase in the measured variable and minus (-) signs correspond to a decrease. When the residuals (differences between the measured and model predicted variables) match a pattern indicated above, then that particular fault is diagnosed. Among the faults tested, the liquid line restriction was introduced at two levels and was characterized as a pressure drop. However, no information was presented on how the other faults were characterized. Hence, it is not even known whether the other faults were tested at multiple levels of severity.

1.2.5 Stylianou

Stylianou (1997) extended the work done of Stylianou and Nikanpour (1996) to include a statistical pattern recognition algorithm (SPRA) to evaluate the model residuals in order to improve the ability of the method in diagnosing faults. The experimental data appear to be reused from Stylianou and Nikanpour (1996). An overall misclassification rate of 4.7% was given, as well as some sensitivity thresholds for the faults studied. When the refrigerant charge was 85% of the design charge, the method correctly

determined the cause in 88.7% of the samples. A 25% reduction in the water flow rates was shown to be sufficient to detect those corresponding faults. And finally, an 11-psi pressure drop across a liquid line restriction was adequate to trigger an alarm.

1.2.6 Rossi and Braun

Rossi and Braun (1997) presented an FDD method for packaged air-conditioners using nine temperature measurements and a humidity measurement to detect and diagnose five faults: refrigerant leakage, liquid line restriction, compressor valve leakage, fouled condenser coil, and dirty evaporator coil. The FDD technique used a steady state model to predict temperatures in a normally operating unit in order to generate residuals for both the fault detection and diagnostic classifiers. The magnitudes of the residuals are statistically evaluated to perform fault detection and are compared with a set of rules based on directional changes in order to classify those faults.

1.2.7 Breuker and Braun

Breuker and Braun (1998b) evaluated the method proposed by Rossi and Braun (1997). A 3-ton rooftop air-conditioner was instrumented to obtain normal and faulty operating data. A total of 96 transient tests were performed with fault tests run at four to five different fault levels. For each fault, the FDD performance was quantified according to:

- The minimum level at which the fault can first be diagnosed
- The minimum level at which the fault can be diagnosed at all steady state points
- The percentage of the total operating points where the fault can be diagnosed
- The degradation in the cooling capacity at the diagnosable fault level
- The degradation in COP at the diagnosable fault level

Based on the results shown in Table 1.2, it is possible to detect some faults very early (Table 1.2 is constructed using the best results for detecting all tested fault levels

from both Breuker's low- and high-cost models). Breuker and Braun (1998a) also presented results from an analysis of a database of service records for a HVAC (Heating, Ventilating, and Air-Conditioning) service company. Most of the stores that were serviced used direct expansion rooftop air-conditioning units. The database contained 6000 separate repair cases from 1989 to 1995 and included repairs resulting from component failures, comfort complaints, and regular maintenance. The repairs were analyzed according to frequency of occurrence and total costs of repairs. Approximately 60% of the faults leading to poor comfort conditions were related to electrical and control failures, while 40% were attributed to mechanical problems. Although compressor failures accounted for only 5% of the service calls, they were the most costly failure for unitary air-conditioners, representing about 25% of the total service costs within the database analyzed by Breuker and Braun (1998a).

Table 1.2: Performance of Breuker and Braun's FDD model.

	Refrigerant Leakage	Liquid Line Restriction	Compressor Valve Leak	Condenser Fouling	Evaporator Fouling
Fault Level %	<12.5	4.1	7.0	17.4	20.3
% Loss Capacity	7.1	3.4	7.3	3.5	11.5
% Loss COP	4.1	2.5	7.9	5.1	10.3

1.2.8 Stouppe and Lau

Stouppe and Lau (1989) performed the most comprehensive study into HVAC system failures. They summarized the causes of 15,760 failures that led to insurance claims during an eight-year period from 1980 to 1987. In hermetic air-conditioning and refrigeration units, 76.6% of the failures were electrical, 18.9% were mechanical, and 4.5% were traced to the refrigeration system. The most common failure for centrifugal compressors was loss of bearing lubrication, resulting in 55% of the failures in hermetic

compressors and 69% of the failures in non-hermetic compressors. The most likely age for mechanical damage to occur to a large hermetic centrifugal compressor is after 15 years.

1.3 Research Objectives

The main goal of this research project was to produce a database of transient and steady state measurements of a chiller under different loading and fault conditions. The test stand developed and used in this study is described in Chapter 3. The faults studied—loss of water flow in the condenser, loss of water flow in the evaporator, refrigerant leakage, refrigerant overcharge, presence of excess oil, condenser fouling, presence of non-condensables in the refrigerant, and faulty expansion valve—are fully presented in Chapter 4.

A secondary goal of the project was to compile a survey of common faults in chillers and rank them according to frequency of occurrence and cost to repair. The major American chiller manufacturers participated in this survey, which is the first of its kind in the industry. The results of the survey are presented in Chapter 2.

Chapter 5 discusses some of the unique trends and sensitivity of the collected data for each of the faults studied. With this information, future researchers will be able to determine which measurements can be best used to detect the faults examined in this work.

The research done for this thesis is actually the first of a two-phase project sponsored by ASHRAE (American Society of Heating, Refrigerating, and Air-Conditioning Engineers). The results obtained here will be used in the development and evaluation of FDD methods applied to chillers. These methods include various statistical approaches, fuzzy logic rule-based systems, and artificial neural networks. Chapter 6 explains additional work done to construct heat exchanger models used in assisting the development of a dynamic chiller model. Moreover, data obtained in this work will be used to tune the dynamic model used to evaluate proposed FDD methods.

2.0 CHILLER FAULT SURVEY

No study on detecting and diagnosing faults in chillers would be complete without a survey of the most important faults that occur in chillers. The major American chiller manufacturers were surveyed to determine the most likely and costly faults associated with centrifugal and screw chillers. This chapter explains how the survey was constructed, contains the results of the survey, and concludes with how the faults were chosen for the experimental work performed for this project.

2.1 Fault Survey

The primary source of information used to determine the kinds of faults that occur in chillers are the technicians that service them. This expert knowledge provided many possible kinds of faults; some caused by normal wear and tear, some by poor installation, and others by human error during servicing.

The information gathered from the service technicians and design engineers was used to develop a fault survey for chillers. The fault survey included all possible kinds of faults that occur in chillers. The survey form had five major categories:

- Type of Equipment
- Reason for Service
- Fault
- Action
- Cost

The complete survey form is shown in Table 2.1 and is followed by explanations of all the terms. Only one survey form was filled out for each fault condition; therefore,

chillers with multiple faults occurring at the same time are not included (to limit possible confounding of cost and frequency information).

Table 2.1: Fault survey form.

Type of Equipment		Reason for Service		Fault		Action		$ (Cost)
1	Centrifugal Chiller	1	Mechanical Failure			1	Replace	
2	Screw Chiller, water cooled	2	Electrical Failure	A	**System Level**	2	Repair	
3	Screw Chiller, air cooled	3	Loss of Capacity	1	Non-condensables in refrigerant	3	Recharge	
		4	Loss of Performance	2	Refrigerant leak	4	Clean	
		5	Routine Maintenance	3	Too much oil in evaporator			
				B	**Lubrication**			
				1	Oil Cooler			
				2	Lube Box			
				3	Oil Pump			
				4	Low oil pressure			
				5	High oil flow			
				C	**Control Box / Starter**			
				D	**Screw Compressor**			
				1	Screw / Gate valve			
				2	Capacity Control System			
				3	Motor Temperature			
				4	Bearings			
				5	Motor Burnout			
				E	**Centrifugal Compressor**			
				1	Impeller / Vanes			
				2	Capacity Control System			
				3	Motor temperature			
				4	Bearings			
				5	Motor Burnout			
				F	**Piping**			
				1	Liquid line			
				2	Motor cooling			
				3	Expansion device			
				4	Filter drier			
				G	**Evaporator**			
				1	Water flow loss			
				2	Other			
				H	**Condenser**			
				1	Water flow loss			
				2	Fouling			
				3	Fan motor			
				4	Other			

The first category, type of equipment, indicates the kinds of chillers surveyed. Chillers with reciprocating and scroll compressors are not included in this survey. The size of the chiller is not recorded; neither is its age. Since many smaller screw chillers are available with either water-cooled or air-cooled condensers, the survey is able to maintain that distinction.

The second category, reason for service, seeks to determine why service was sought for the chiller. The options were chosen to cover most circumstances:

- Mechanical failure refers to any physical damage or wear.
- Electrical failure refers to the power supply, motor, or internal electronics.
- Loss of capacity is a customer complaint about the chiller's inability to maintain desired comfort levels (because of a fault, not due to a misapplication).
- Loss of performance is based on excessive energy demands to achieve desired comfort levels (because of a fault, not due to a misapplication).
- Routine maintenance covers service calls done in a regular manner as part of a service contract.

The third category, fault, is used to define the specific type of problem that was identified by the technician. The faults are organized according to location within the chiller, with further detailed conditions contained within each area. System level faults include:

- Non-condensables in refrigerant, usually introduced during improper servicing
- Refrigerant leak
- Too much oil in evaporator, caused by adding excess oil to compressor

The system level faults are not strictly confined to a specific location within the chiller. The lubrication faults refer to the entire system that keeps the bearings lubricated:

- Oil cooler; which may use either refrigerant, condenser water supply, or air
- Lube box, the distribution mechanism that supplies oil to the bearings
- Oil pump, can be either a separate unit or integrated with the compressor drive
- Low oil pressure
- High oil flow

The 'Control Box / Starter' fault encompasses all the faults related to power supply, microprocessor control system, switches, and relays. The next two fault areas are nearly

identical; the one chosen depends on the type of compressor used in the chiller. For a chiller with a screw compressor, the following faults may be indicated:

- Screw / Gate valve, used for a mechanical problem with the compressor itself
- Capacity control system, a mechanical or electrical problem associated with the slider used to adjust cooling load
- Motor temperature, an electrical or mechanical failure in the motor
- Bearings, a mechanical failure associated with the main drive system
- Motor burnout, a catastrophic failure of the motor requiring a complete system cleaning and motor replacement

If the chiller has a centrifugal compressor, then the following faults are used:

- Impeller / Vanes, used for a mechanical problem with the compressor itself
- Capacity control system, a mechanical or electrical problem associated with the vanes used to adjust cooling load
- Motor temperature, an electrical or mechanical failure in the motor
- Bearings, a mechanical failure associated with the main drive system
- Motor burnout, a catastrophic failure of the motor requiring a complete system cleaning and motor replacement

Piping faults are to be limited to the refrigerant lines linking the major system components:

- Liquid line connecting the condenser to evaporator
- Motor cooling, a separate liquid line siphoned off to cool the motor cavity
- Expansion device, either a fixed orifice or expansion valve
- Filter drier, primarily checked for blockage

Both the evaporator and condenser faults include problems with the water flow rate. In addition, the condenser is much more likely to experience fouling. If the condenser is air-cooled, then the possibility exists for problems with the cooling fans. Any other problems are categorized generically as ‘other’.

The fourth category, action, further clarifies the fault by showing what corrective action was taken during the service call. Choices include replacing a component,

repairing it, recharging or filtering the refrigerant and oil, and cleaning tubes in the condenser or evaporator. And finally, the last category records the cost of the service call.

2.2 Survey Results

Five domestic chiller manufacturers filled out the surveys. The information collected is normally kept confidential, thus the names of the contributing companies will be kept anonymous. There were some deviations in how the different companies filled out the survey forms. In particular, one company provided a large number of service records, but the organization of their database was incompatible with the fault survey in a few categories. Furthermore, this same survey data lacks cost information; therefore, this data was kept separate from those that contain cost information.

A total of 170 service records for centrifugal chillers with cost information were collected (three companies), along with an additional 1000 records without cost information (one company). 228 service records of water-cooled screw chillers were collected with cost information (four companies), along with an additional 1000 records without cost information (one company). And a total of 111 service records of air-cooled screw chillers were collected with cost information (four companies). The service records with the cost information are always kept separate from those without cost information, even when only frequency data is presented. This was done because the data without the cost records was not as detailed (the method of sorting the data was not as accurate in determining the correct fault condition).

The survey of centrifugal chillers is most pertinent to the experimental work performed for this project. Figure 2.1 shows the normalized frequency results from the 170 service records detailing the various kinds of faults that occur in centrifugal chillers. The most common fault recorded dealt with a problem in the control box or starter. These kinds of faults are typically easy to detect and fix, but are a nuisance because of the downtime they cause. The high frequency of refrigerant leakage is surprising, but is relatively simple to correct. Nevertheless, environmental regulations warrant the

detection of refrigerant leakage as soon as possible. Approximately 56% of the faults have the potential to affect the thermodynamic states of the chiller. The results are similar to those reported by Breuker (1997) for rooftop air-conditioners (when adjusting for the differences in construction).

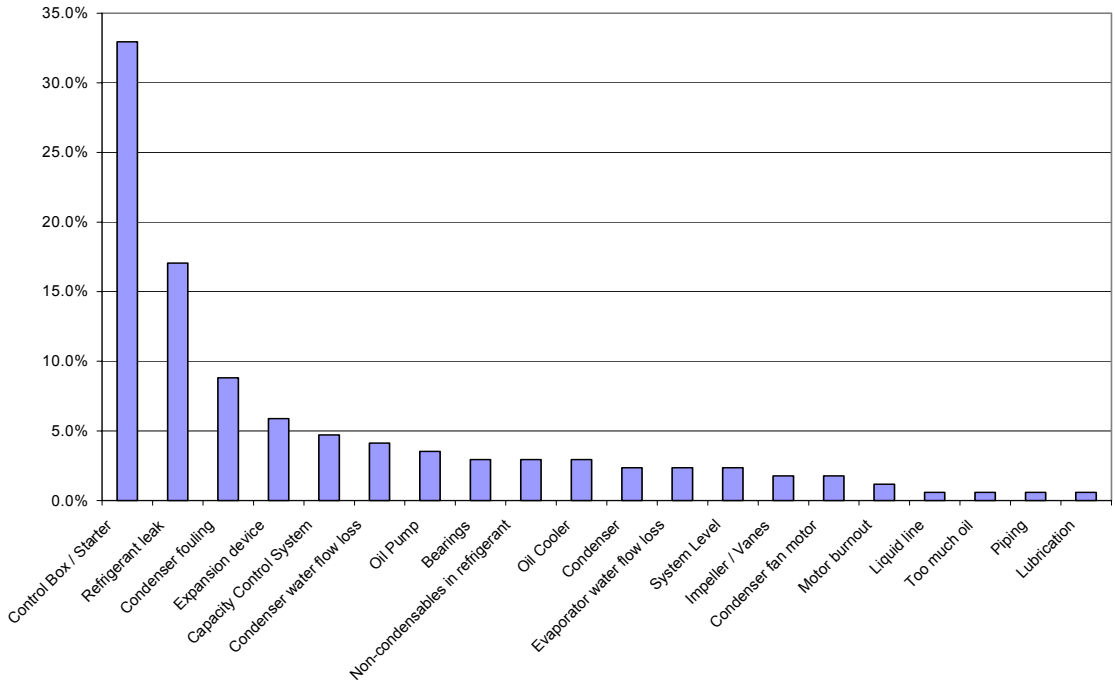

Figure 2.1: Centrifugal chiller detailed survey results normalized by frequency.

The survey data used to construct Figure 2.1 was then sorted according to cost and the results are presented in Figure 2.2. The one condition that shows a dramatic shift is related to motor burnout, which occurs very infrequently but is by far the most expensive repair. Compressor and electrical problems account for 64% of the total cost of repair. Breuker found that the distribution of repair costs were similar for rooftop air-conditioners, with one major exception—the cost to correct a chiller's refrigerant leak is several times greater than for an air-conditioner (when the cost data is normalized). Breuker also mentioned that many compressor failures result from overloading the motor,

thus suggesting the possibility that detecting other faults early could reduce the frequency of compressor failures.

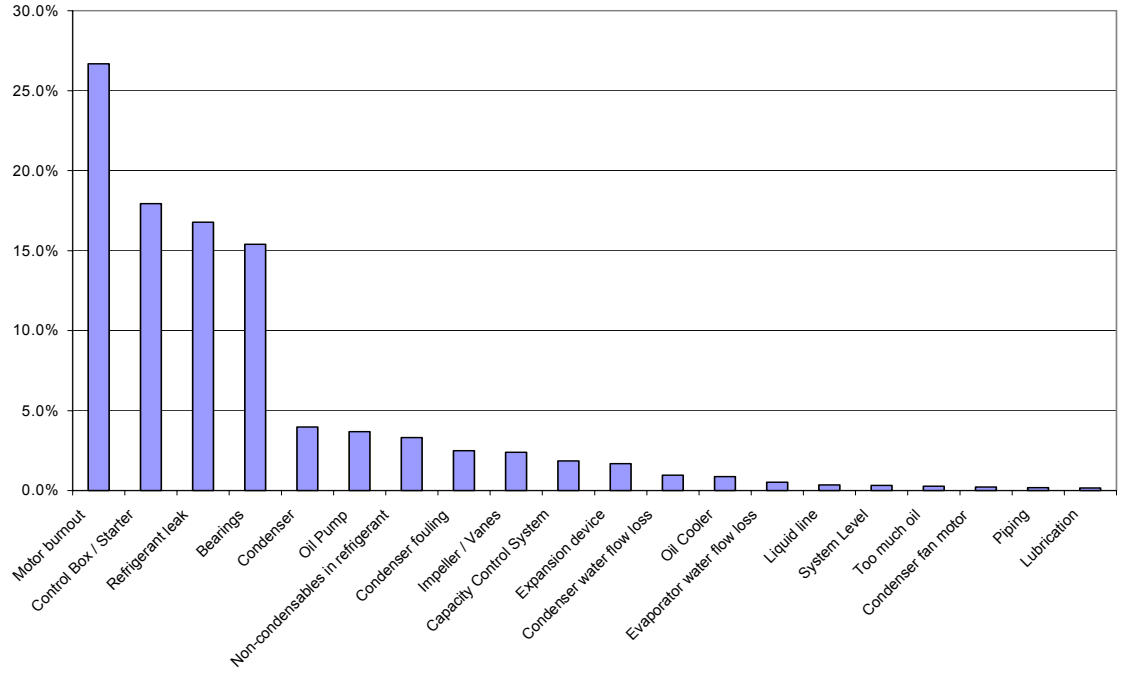

Figure 2.2: Centrifugal chiller detailed survey results normalized by cost.

The results of the centrifugal chiller survey were then condensed into just the seven major fault areas and are presented in Figure 2.3 with both normalized frequency and cost information. In general, the cost to repair a particular fault is directly associated to the fault's frequency of occurrence. The only exception is the faults related to the compressor, which closely matches the trends seen by Breuker.

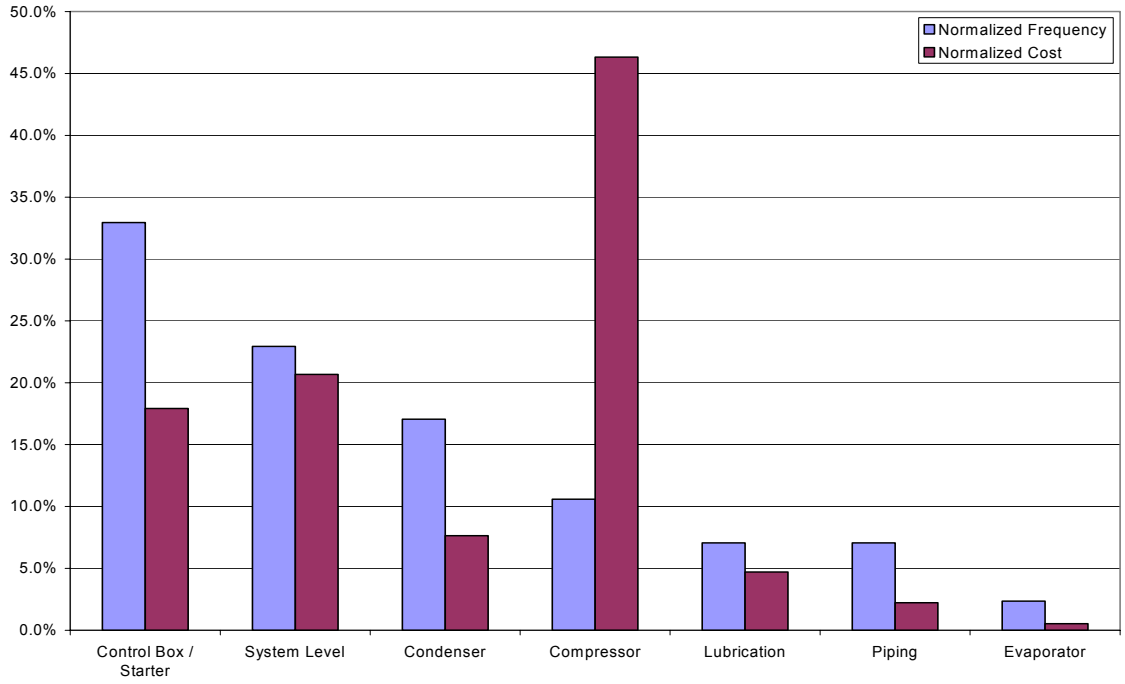

Figure 2.3: Centrifugal chiller condensed survey results.

The remaining centrifugal chiller survey results are shown in Figure 2.4. The most notable change relates to the relatively infrequent classification of a fault to either the condenser or evaporator. This leaves the information somewhat suspect, since condenser fouling would normally be serviced in more than 0.2% of the service calls (the primary reason why the data from this company was kept separate from the rest).

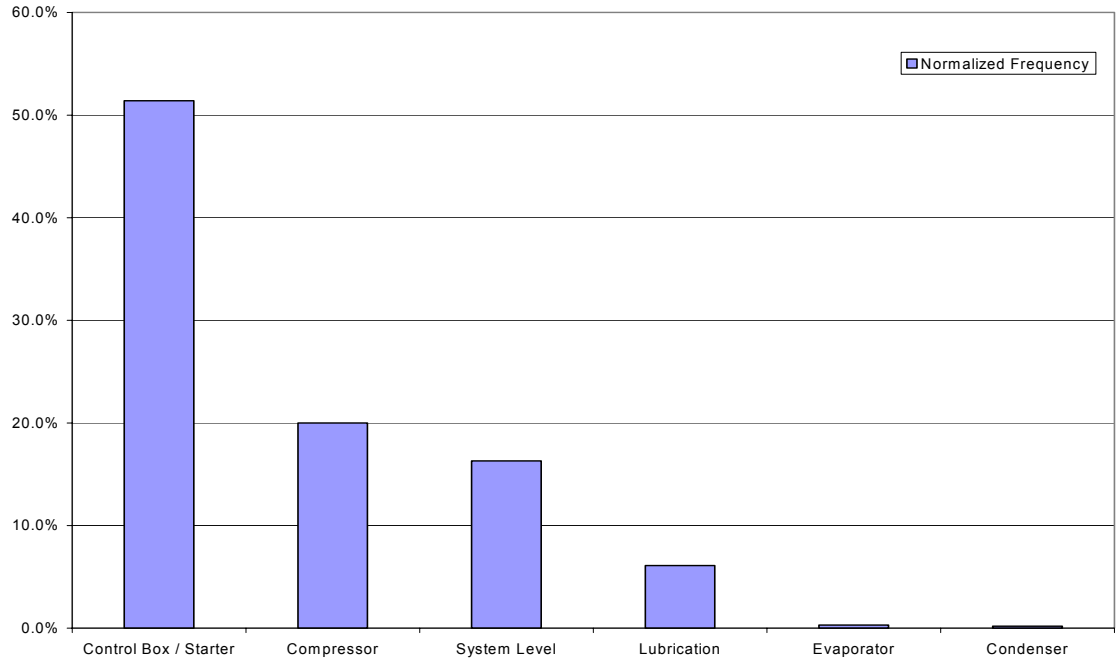

Figure 2.4: Centrifugal chiller additional survey results without cost data.

In addition to collecting information on centrifugal chillers, service records for screw chillers were also surveyed. Although centrifugal chillers have been in service for more than 30 years, many applications requiring smaller capacities are now utilizing screw chillers. Moreover, the smaller capacity of screw chillers permits the use of air-cooled condensers. Therefore, the service records for water-cooled and air-cooled screw chillers were recorded separately.

The 228 service records for water-cooled screw chillers were sorted by frequency and the normalized results are shown in Figure 2.5. The same results were then sorted by cost, which are presented in Figure 2.6. The results from screw chillers are remarkably similar to centrifugal chillers. In general, screw chillers seem to have fewer problems with the compressor, but more in the piping system. Of particular interest is the significant frequency and cost associated with a refrigerant leak. Screw chillers also do not seem to have problems with bearing failure, which is a significant fault for centrifugal compressors. The condensed fault results are given in Figure 2.7.

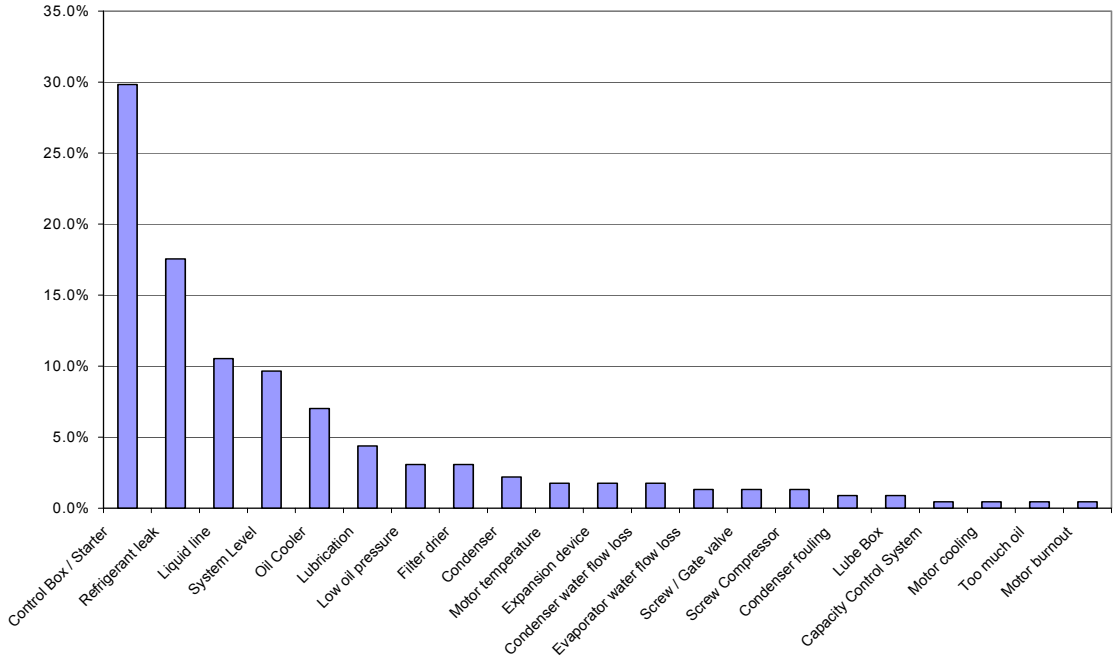

Figure 2.5: Water-cooled screw chiller detailed survey results normalized by frequency.

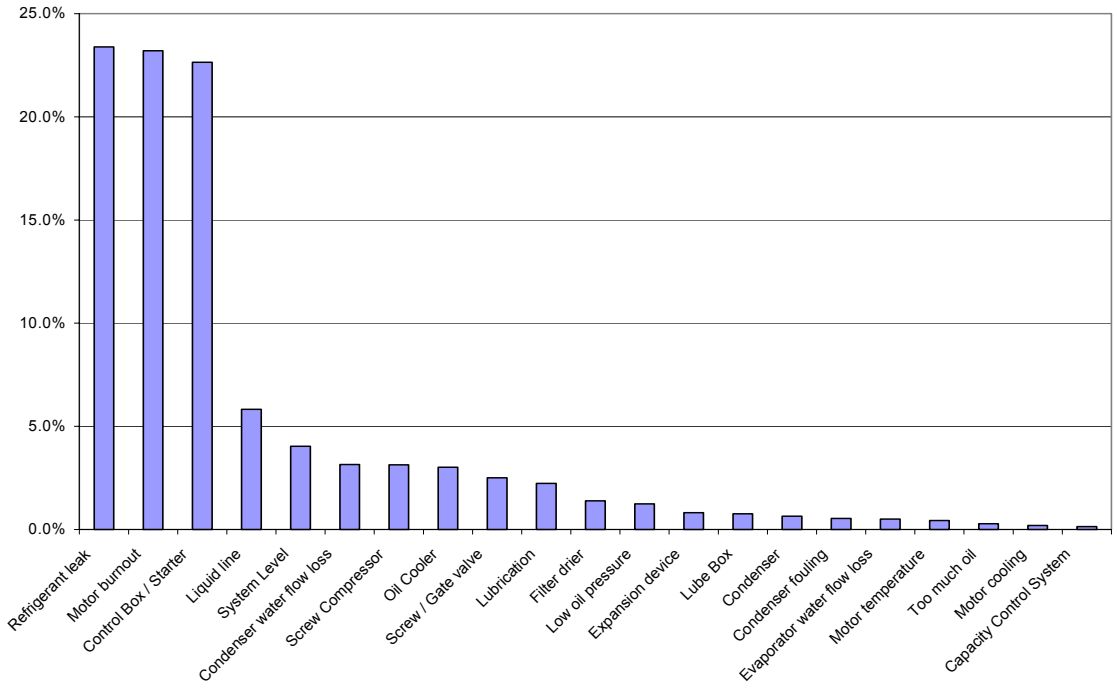

Figure 2.6: Water-cooled screw chiller detailed survey results normalized by cost.

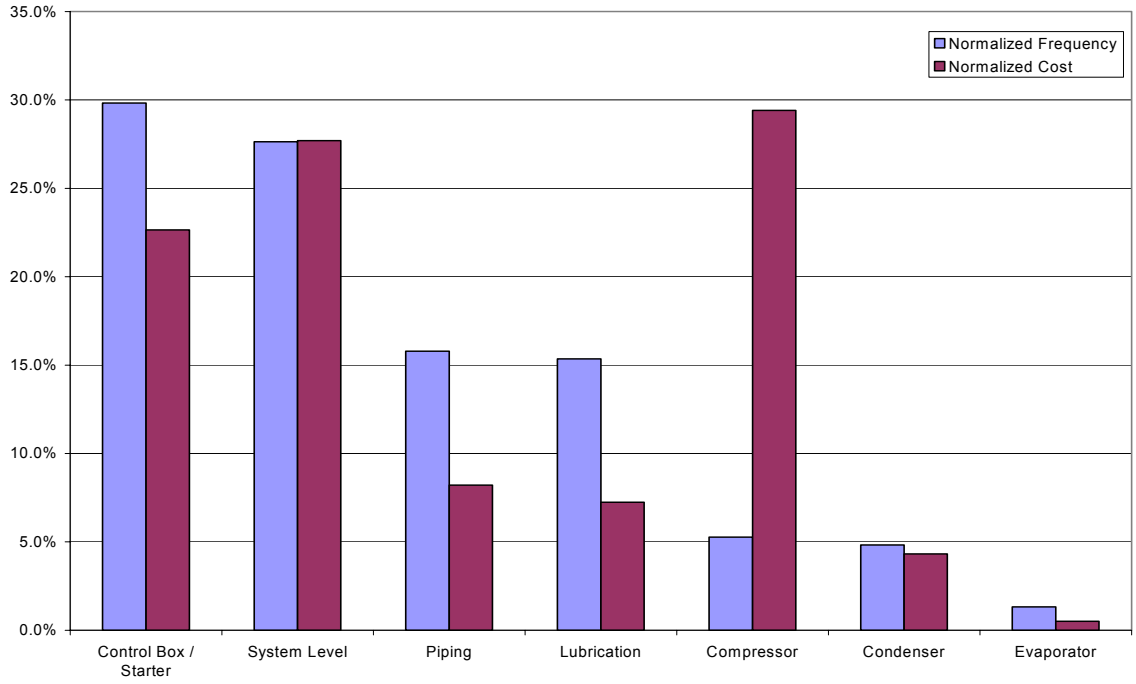

Figure 2.7: Water-cooled screw chiller condensed survey results.

Just as with the additional non-cost survey data for centrifugal chillers, the screw chiller data without cost information was kept separate. The distribution of results given in Figure 2.8 matches closely with those in Figure 2.4—very few condenser or evaporator faults. The increase in system level faults seen between Figures 2.1 and 2.5 is also apparent between Figures 2.4 and 2.8. However, for some unknown reason, no faults were assigned to the piping fault classification (which had a substantial 16% assigned in the more detailed survey results).

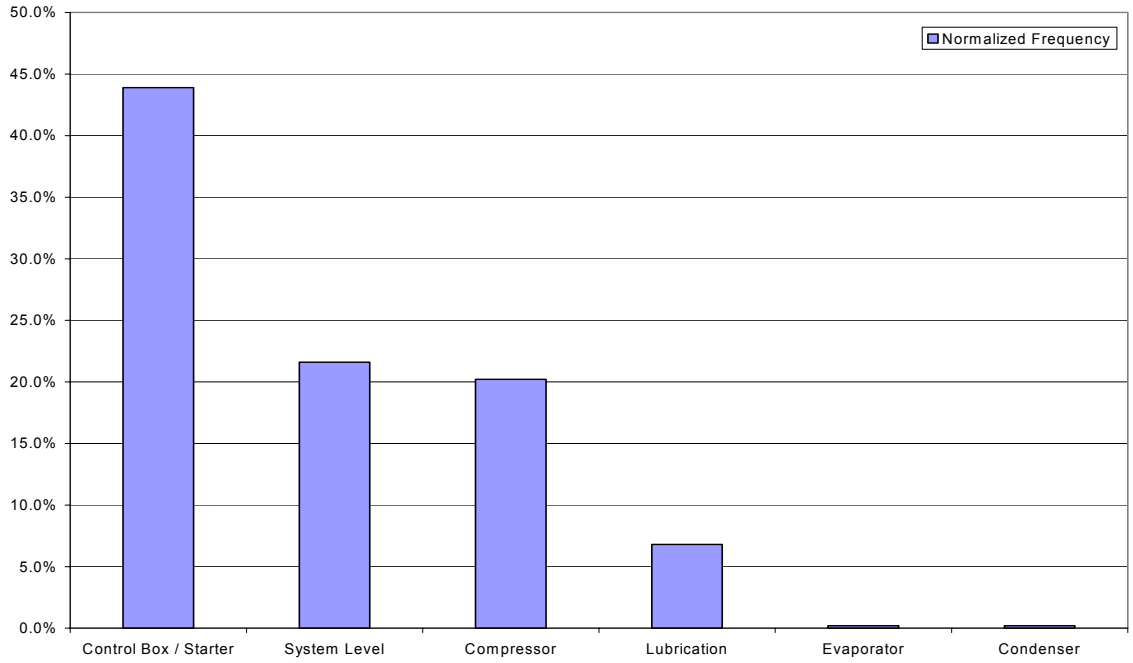

Figure 2.8: Water-cooled screw chiller additional survey results without cost data.

The final group of chillers surveyed was the air-cooled screw chillers. A total of 111 service records were used to compile the normalized frequency and cost graphs shown in Figures 2.9 and 2.10. However, no additional non-cost survey data was available. It is also likely that the smaller size of the air-cooled screw chillers was responsible for halving the cost of repairing a motor burnout compared to the other chiller types despite having about the same frequency of occurrence. The condensed fault survey results are given in Figure 2.11.

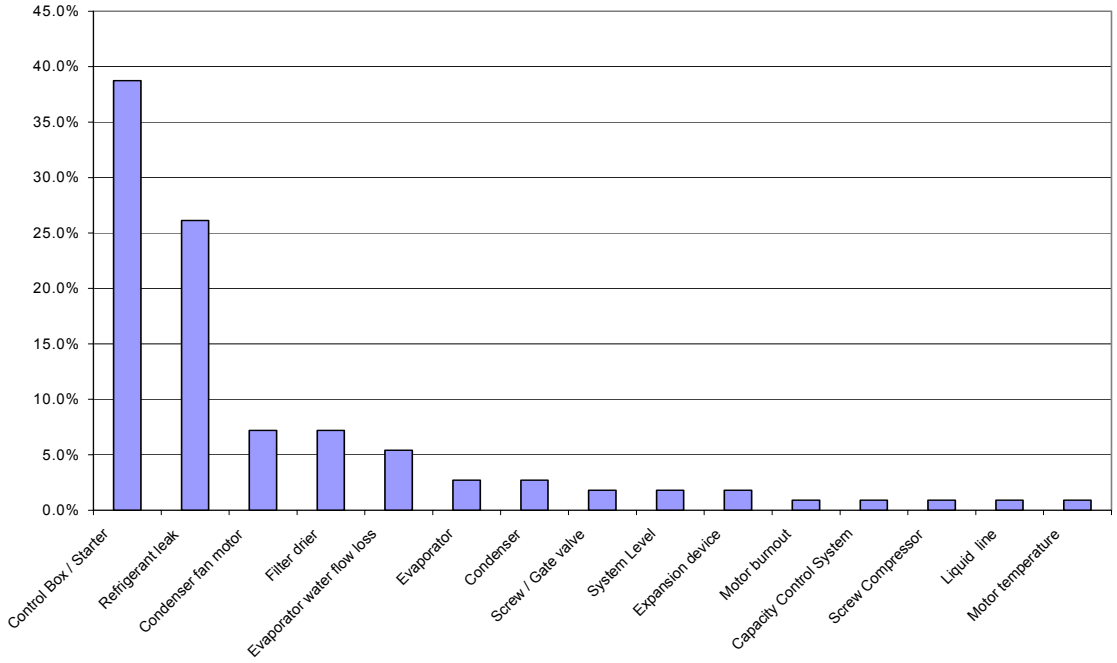

Figure 2.9: Air-cooled screw chiller detailed results normalized by frequency.

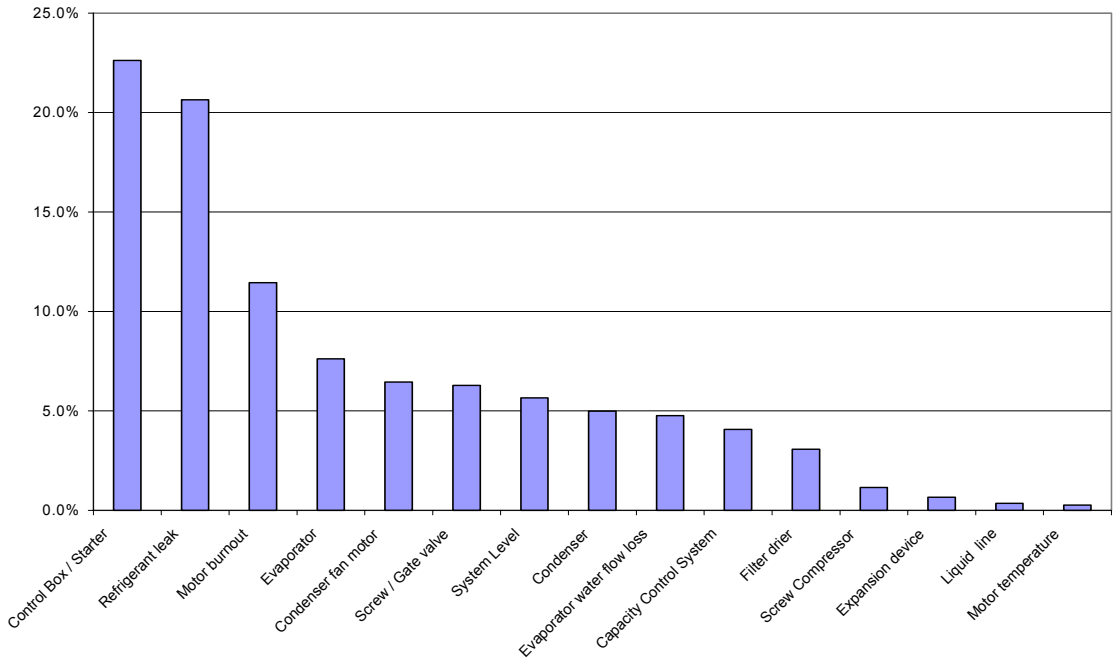

Figure 2.10: Air-cooled screw chiller detailed survey results normalized by cost.

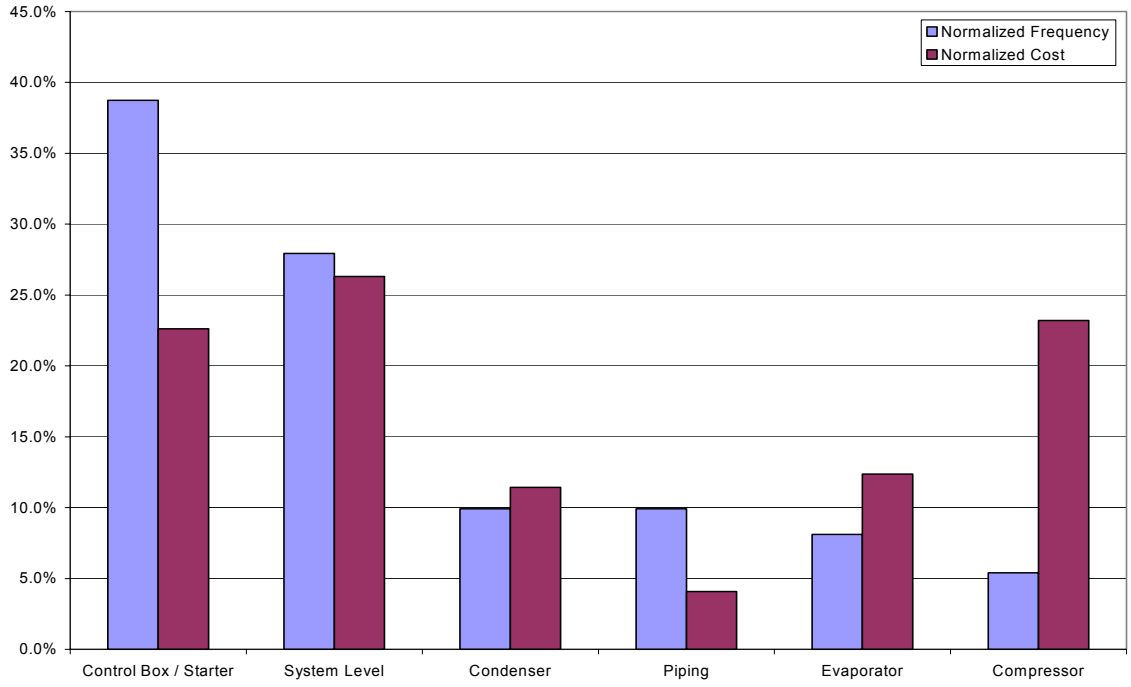

Figure 2.11: Air-cooled screw chiller condensed survey results.

The final three figures contain the combined information from all the service records for centrifugal and screw chillers, representing a total of 509 distinct records. Figure 2.12 gives the frequency sorted and normalized results, Figure 2.13 gives the cost sorted and normalized results, and Figure 2.14 presents the condensed fault classification graph for the combined survey records. The detailed compressor information is combined according to logical pairings, which lead to a new classification where 'Impeller / Vanes' is combined with 'Screw /Gate'.

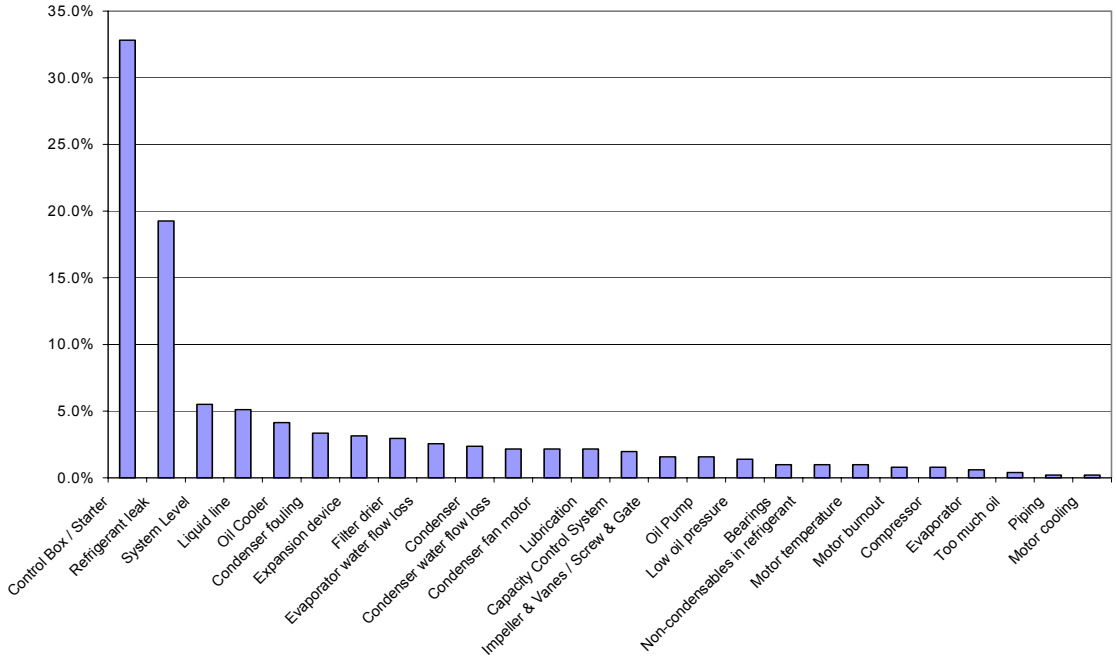

Figure 2.12: Detailed survey results for all chiller types normalized by frequency.

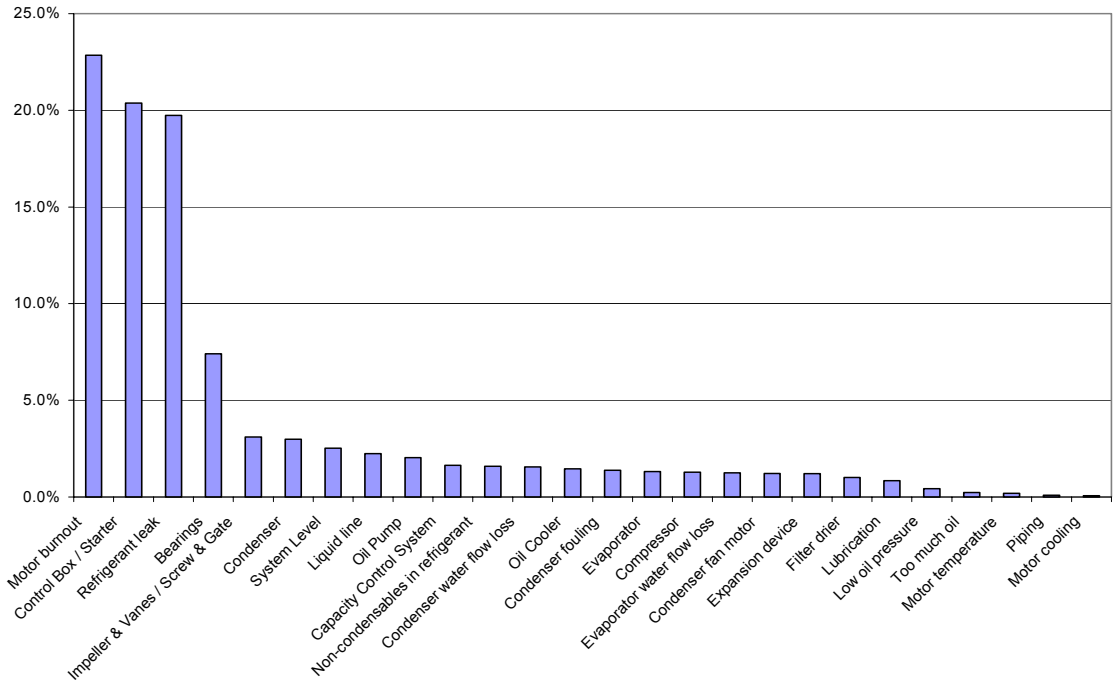

Figure 2.13: Detailed survey results for all chiller types normalized by cost.

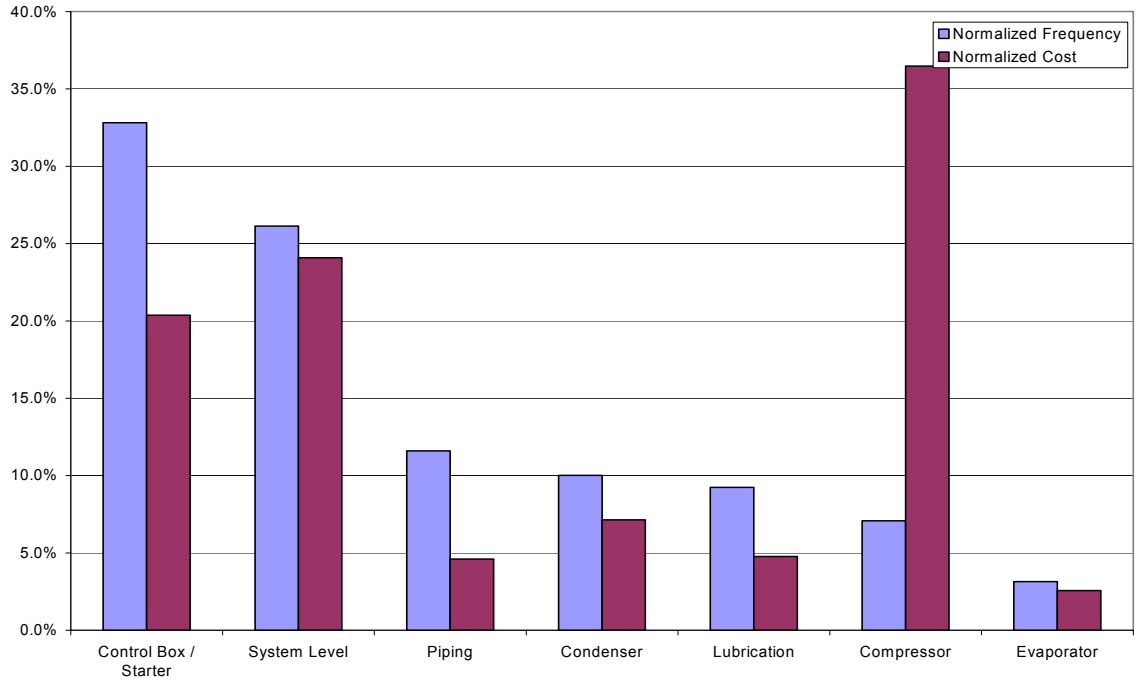

Figure 2.14: Condensed survey results for all compressor types.

2.3 Conclusion

A large number of possible faults and failures were identified in this study. However, not all of them would be practical for further examination as part of the fault detection and diagnostics scheme. For example, most electrical and compressor failures do not need sophisticated detection methods, since their presence is obvious (e.g. motor burnout). Most failures can be easily detected with simple—albeit sometimes expensive—equipment. Degradation faults, on the other hand, generally lead to a loss of performance, but are otherwise not easily detected (since the chiller is often still operational) and cannot normally be detected with a single sensor. Consequently, the faults chosen for experimental study were:

- Reduced condenser water flow
- Reduced evaporator water flow
- Refrigerant leak/undercharge

- Refrigerant overcharge
- Excess oil
- Condenser fouling
- Non-condensables in the refrigerant
- Defective expansion valve

It was known that some of these conditions do not occur that frequently; however, cumulatively they account for 42% of the service calls made and 26% of the repair cost. The only fault not listed among those studied was the refrigerant overcharge fault (which was not on the survey form, but was tested since it is a fault that can theoretically occur due to improper servicing).

One of the faults not studied was a blockage in the liquid line, normally associated with the filter drier. This fault was omitted from testing because the filter drier on the test chiller was not located in the main liquid line. Furthermore, to properly introduce the fault would have required another valve in series with the main valve (which could not be artificially restricted). The infrequent occurrence and low expense of liquid line faults did not warrant the extensive modification to the chiller required for such testing.

It was expected that the faults chosen for experimental testing could be detected by monitoring the thermodynamic states of the chiller. Moreover, according to Breuker's research, it is possible that many of the thermodynamically detectable faults may serve as a warning sign for potential failures that can occur later if the fault is not treated.

3.0 EXPERIMENTAL CHILLER TEST FACILITY

One of the downsides of fault testing is the lack of suitable testing sites. It is rare to find a building where the occupants or equipment can tolerate the dramatic change in conditions required for adequate fault testing. Therefore, the test stand developed in this project uses a simulated building to load the chiller.

3.1 Design Goals

One of the primary goals of the project was to obtain normal and fault data for a chiller that is representative of many chillers in service today. A 90-ton centrifugal chiller proved small enough for a research test stand while also being representative of chillers used in larger installations. The chiller was installed indoors with a nearly constant ambient temperature of 72°F.

A goal in the design of the test stand was to meet many of the specifications of ARI (Air-Conditioning and Refrigeration Institute) Standard 550 for Centrifugal and Rotary Screw Water-Chilling Packages. For example, the chiller test facility follows ARI guidelines on condenser and evaporator water flow rates. According to ARI Standard 550, the evaporator water loop should have a flow rate of 2.4 gpm/ton and the condenser water loop a flow rate of 3.0 gpm/ton. Therefore, the water flow rate for a 90-ton chiller would be 216 gpm in the evaporator and 270 gpm in the condenser.

3.2 Simulated Building

This section provides an overview of the test stand, which was used to load the chiller as a building typically would load a chiller. For detailed information consult

Appendices A and B. The initial construction of the test stand took the following factors into account:

- The condenser water circuit must be a closed loop to limit unintentional fouling
- The evaporator water circuit must be a closed loop to limit unintentional fouling
- The steam heating system used to load the chiller cannot be at direct risk of contamination

To allow the possibility for making ice with this system (requiring the addition of glycol to the evaporator water loop), it was necessary to add another closed loop water circuit between the evaporator water loop and the steam heating. This additional water circuit is referred to as the hot water loop. To reduce the demand on steam heating and condenser cooling water, an additional heat exchanger was added between the evaporator and condenser water circuits. This shared heat exchanger allows heat to transfer between the condenser water and the evaporator water loops.

Figure 3.1 depicts the important equipment contained within the chiller test facility as well as indicating their approximate relative locations. The abbreviation 'HX' stands for 'heat exchanger'. The test stand utilizes the following equipment:

- Three water-to-water heat exchangers
- One steam-to-water heat exchanger
- One electronically actuated 3-way valve
- Six electronically actuated 2-way valves
- Three water pumps
- Two vortex flow meters

Figure 3.1 accurately displays the water inlets and outlets to each heat exchanger and valve. A single valve in the figure represents two of the steam valves mounted in parallel in the actual system. However, it is not necessary to know the exact physical construction of the test facility in order to understand its design philosophy. Figure 3.2 shows a simplified layout of the water flow paths.

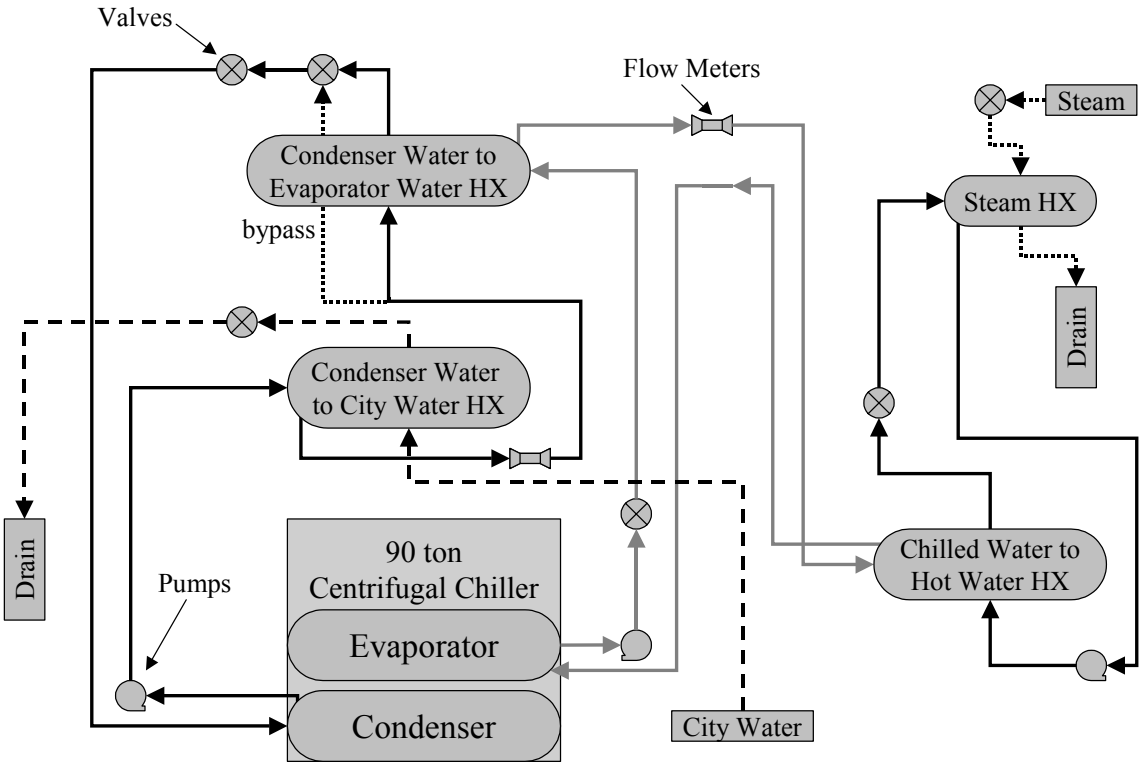

Figure 3.1: Schematic of chiller test facility showing approximate locations of components.

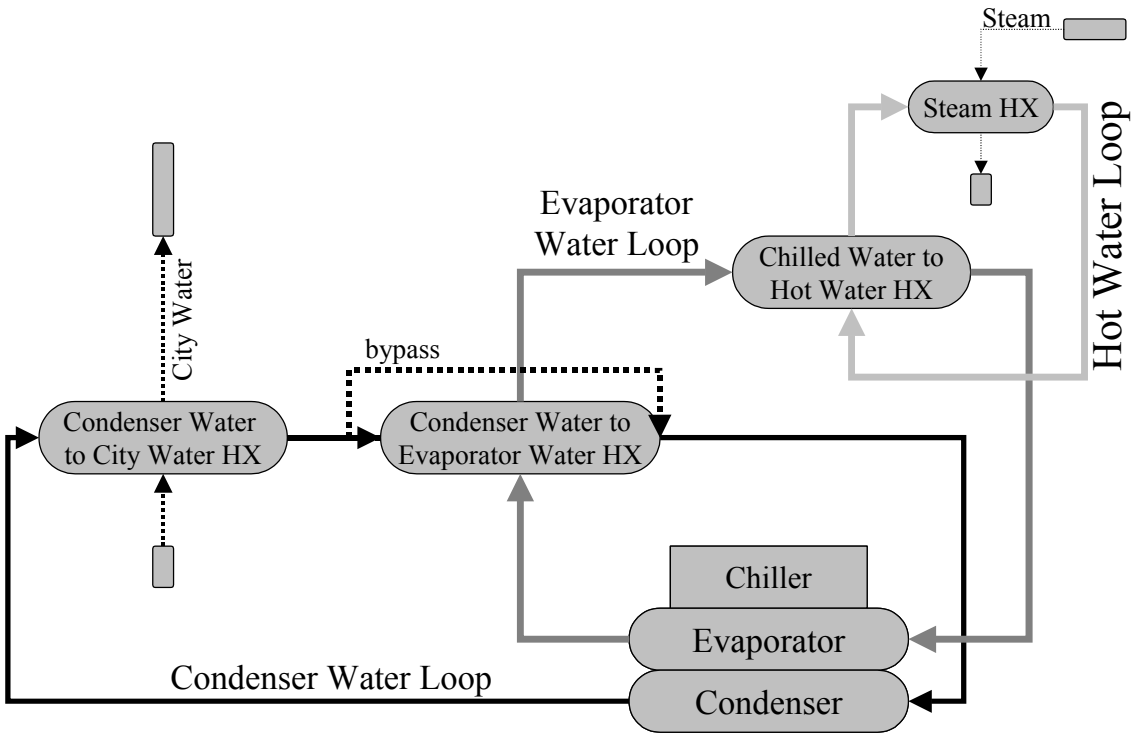

Figure 3.2: Simplified layout to emphasize water flow circuits.

A total of five flow paths are present in the chiller test facility:

1. Evaporator water circuit
2. Condenser water circuit
3. Hot water circuit
4. City water supply
5. Steam supply

Both the city water and steam pass through their respective heat exchangers without ever directly mixing with the three internal water circuits. Nearly 70-80% of the chiller load comes from the shared heat exchanger between the evaporator and condenser water loops. A 3-way valve in the condenser water loop redirects water around the shared heat exchanger in order to reduce the load on the chiller. Changes in the 3-way valve position impact both the condenser water and evaporator water temperature. The city water is used to remove the additional heat generated by the compressor motor and water pumps as well as providing precise control over the condenser water temperature without

compromising the stability of the evaporator water temperature. Likewise, the steam heating is used for small adjustments in chiller loading without affecting the condenser water temperature. The hot water loop exists solely to isolate the steam from the evaporator water loop.

The ordering of the heat exchangers in the condenser and evaporator water circuits ensures the largest temperature differences across each one. For the evaporator water loop, the shared heat exchanger is placed first because a lower temperature ensures greater heat transfer from the condenser water loop. Moreover, the hot water loop is always capable of achieving a high enough temperature to ensure heat transfer to the evaporator water. For the condenser water loop it was necessary to place the city water heat exchanger first, since the city water temperature is always higher than the evaporator water temperature. Even after the city water cools the condenser water by a few degrees, the evaporator entering water temperature is always much cooler than the condenser water entering temperature to the shared heat exchanger.

3.3 Chiller

The refrigerant flow path in the chiller is essentially the same as most vapor compression equipment. Refrigerant vapor is compressed in the compressor and discharged into the condenser (shell and tube design, with refrigerant in the shell), where it is condensed into a subcooled liquid. The liquid drains from the bottom of the condenser and passes through an expansion valve, thus reducing the pressure and temperature. The low-pressure two-phase mixture next enters the evaporator (also a shell and tube design, with refrigerant in the shell) and boils off into a superheated vapor that is then pulled into the compressor to repeat the cycle.

In addition to this main refrigerant cycle, there are two additional refrigerant flow paths that run parallel to the main liquid line as shown in Figure 3.3: the motor cooling liquid line and the pilot valve liquid line. The motor cooling line is used to absorb all excess heat generated by the motor and compressor (the motor is well insulated and does not interact with the surroundings). The motor cooling line also contains the filter drier.

The main valve position is controlled by the flow of refrigerant through the secondary line, which in turn is regulated by the pilot valve (a thermal expansion valve which has a sensing bulb in the evaporator). Both of the ancillary liquid lines return to the main liquid line before the refrigerant enters the evaporator.

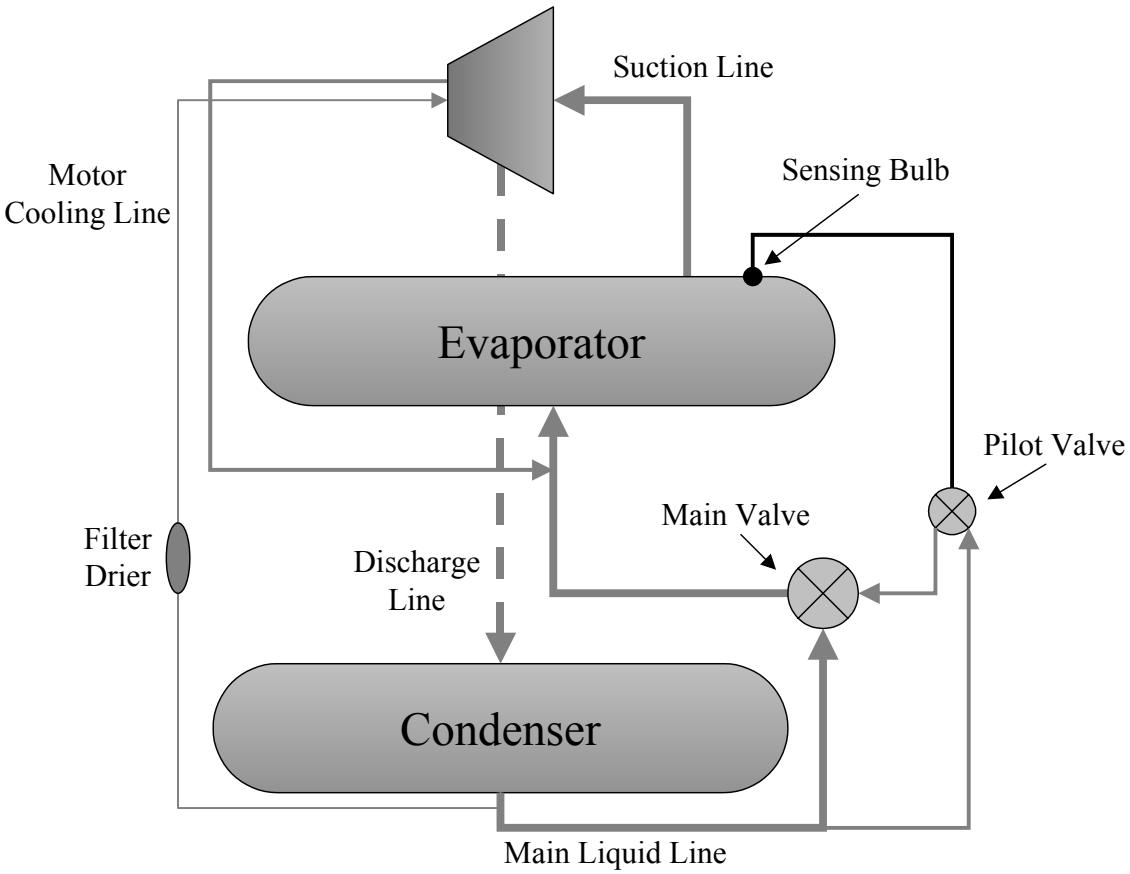

Figure 3.3: Chiller refrigerant flow paths according to approximate physical locations.

The compressor uses an impeller to achieve the desired pressure lift within the system. Capacity control is possible by using adjustable inlet vanes to the impeller. The onboard chiller controller (MicroTech controller) hydraulically regulates the vane position to achieve the chilled water setpoint temperature; however, the vane position is not monitored. In addition, power consumption to the compressor can be artificially restricted by the MicroTech controller, which in turn inhibits the opening of the vanes,

and can cause the chiller to be unable to meet the chilled water setpoint unless the load is reduced.

3.4 Data Acquisition and Control

A comprehensive suite of sensor information is collected by the MicroTech controller mounted on the chiller as part of its typical installation package. Data are relayed to the PC from the MicroTech controller through a RS-232 connection to COM Port 2. The test stand is controlled by a group of three Johnson Controls Inc. Air Handling Unit (JCI AHU) controllers on an N2 bus (RS-485 network), which in turn is connected to the PC through COM Port 1 via a RS-485 to RS-232 converter as shown in Figure 3.4 (also refer to Appendices A.1.3 and A.1.4).

Both the MicroTech and JCI AHU controllers are interfaced on the PC via VisSim—a visual simulation software package with customizable features that allow various communication protocols to be enabled simultaneously. The program developed within VisSim collects all the data gathered by the controllers and exports it to a tab delimited text file. This program also imports data used to automatically control the test sequence and operating conditions. VisSim samples the data and makes control adjustments at 10-second intervals (further information is available in Appendices A.2.1 and A.2.2).

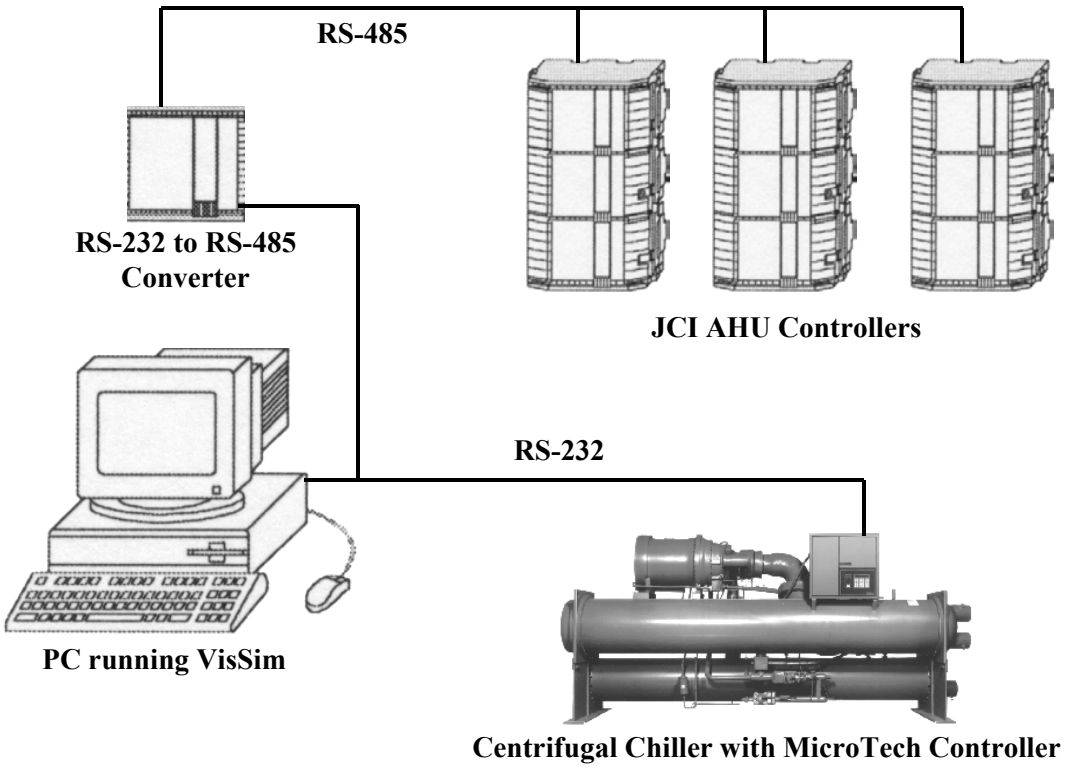

Figure 3.4: Schematic showing chiller test stand control interface.

The MicroTech controller was able to control evaporator water outlet temperature and other internal chiller operations. The JCI AHU controllers were used to control the water pumps and valve positions. The valve positions had a direct influence on the water temperatures within the system, including the evaporator water outlet temperature. A full explanation of how the valves were controlled to meet the desired operating conditions is contained in Appendix A.2.

The MicroTech controller mounted on the chiller was able to provide all the necessary measurements for this project except the instantaneous compressor power input and water flow rates. The test stand contains additional sensors used to help measure the magnitude of introduced faults and assists in general troubleshooting. These sensors are interfaced to the JCI AHU controllers. A few test stand sensors supplement the MicroTech sensors that measure the entering and leaving water temperatures for the evaporator and condenser. All the sensor information was compiled in VisSim using

special communication protocols to communicate through the two controller networks. The following tables and figures provide some additional information on the data acquired through the MicroTech and JCI AHU controllers. Table 3.1 lists the equipment directly controlled by the JCI AHU controllers, while Figures 3.5 and 3.6 show their placement within the test stand. Further equipment specifications are listed in Appendix A.1, and measurement accuracy is presented later in this chapter.

Table 3.1: Explanation of designations used with JCI AHU controllers.

Designation	Description
TCI	Temperature of Condenser Water In
TCO	Temperature of Condenser Water Out
TEI	Temperature of Evaporator Water In
TEO	Temperature of Evaporator Water Out
TSI	Temperature of Shared HX Water In
TSO	Temperature of Shared HX Water Out
TBI	Temperature of Building Water In
TBO	Temperature of Building Water Out
THI	Temperature of Hot Water HX In
THO	Temperature of Hot Water HX Out
FWC	Flow Rate of Condenser Water
FWE	Flow Rate of Evaporator Water
VC	Electronic Valve in Condenser Water Loop
VM	Electronic 3-way Mixing Valve
VW	Electronic Valve for City Water Supply
VE	Electronic Valve in Evaporator Water Loop
VH	Electronic Valve in Hot Water Loop
VSS	Small Electronic Valve for Steam Supply
VSL	Large Electronic Valve for Steam Supply
PWC	Condenser Water Pump
PWE	Evaporator Water Pump
PWH	Hot Water Pump
WATT	Watt Transducer Measuring Instantaneous Power

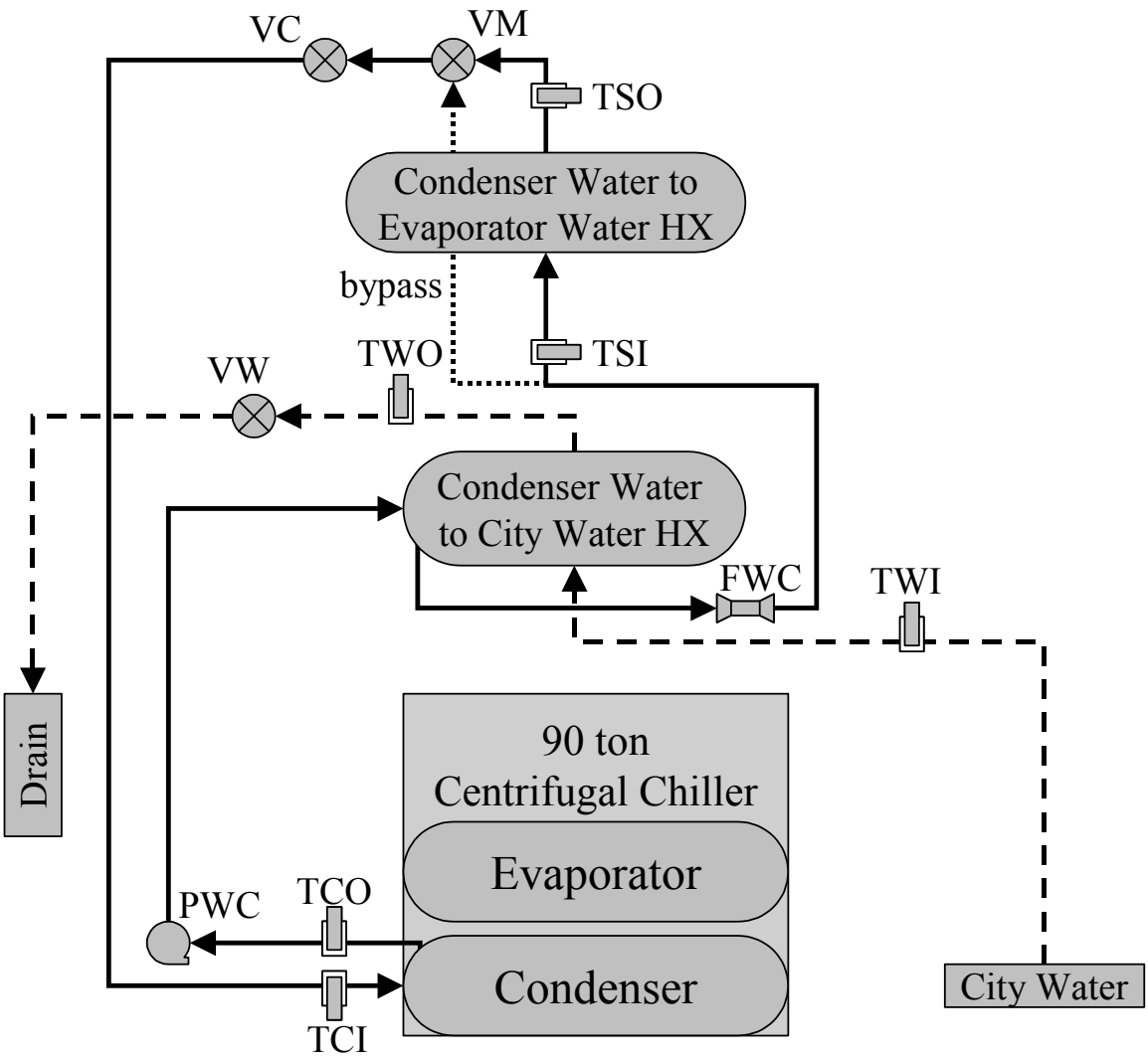

Figure 3.5: Sensors mounted in condenser water circuit and city water supply.

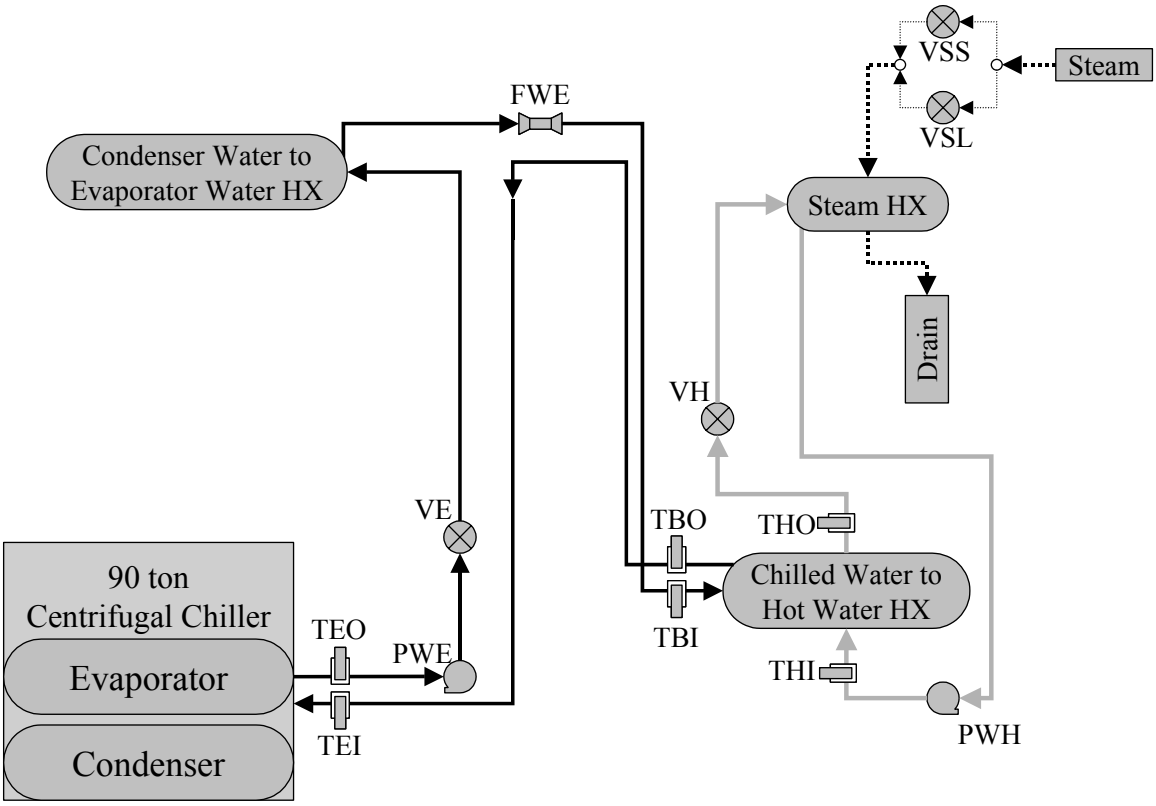

Figure 3.6: Sensors mounted on evaporator water circuit and steam supply.

3.5 Measured and Calculated Variables

The VisSim program used to collect the data and operate the test stand also performs real time calculations that are exported along with the measured sensor data. All the exported information is contained in Table 3.2. A calculated quantity is indicated when the source lists 'VisSim'; however, the MicroTech controller also internally performs some calculations using measurements (i.e. evaporator temperature, condenser temperature, superheat, subcooling, approach temperatures, etc.).

Table 3.2: Exported data from experimental test runs.

Designation	Source	Description	Units
Time	VisSim	Real time counter	Seconds
TWE_set	MicroTech	Chilled water setpoint—control variable	F
TEI	JCI AHU (RTD)	Temperature of Evaporator Water In	F
TWEI	MicroTech (Thermistor)	Temperature of Evaporator Water In	F
TEO	JCI AHU (RTD)	Temperature of Evaporator Water Out	F
TWEO	MicroTech (Thermistor)	Temperature of Evaporator Water Out	F
TCI	JCI AHU (RTD)	Temperature of Condenser Water In	F
TWCI	MicroTech (Thermistor)	Temperature of Condenser Water In	F
TCO	JCI AHU (RTD)	Temperature of Condenser Water Out	F
TWCO	MicroTech (Thermistor)	Temperature of Condenser Water Out	F
TSI	JCI AHU (RTD)	Temperature of Shared HX Water In (in Condenser Water Loop)	F
TSO	JCI AHU (RTD)	Temperature of Shared HX Water Out (in Condenser Water Loop)	F
TBI	JCI AHU (RTD)	Temperature of Building Water In (in Evaporator Water Loop)	F
TBO	JCI AHU (RTD)	Temperature of Building Water Out (in Evaporator Water Loop)	F
Cond Tons	VisSim	Calculated Condenser Heat Rejection Rate	Tons
Cooling Tons	VisSim	Calculated City Water Cooling Rate	Tons
Shared Cond Tons	VisSim	Calculated Shared HX Heat Transfer (only valid with no water bypass)	Tons
Cond Energy Balance	VisSim	Calculated 1st Law Energy Balance for Condenser Water Loop (only valid with no water bypass)	Tons
Evap Tons	VisSim	Calculated Evaporator Cooling Rate	Tons
Shared Evap Tons	VisSim	Calculated Shared HX Heat Transfer (should equal Shared Cond Tons with no water bypass)	Tons
Building Tons	VisSim	Calculated Steam Heating Load	Tons
Evap Energy Balance	VisSim	Calculated 1st Law Energy Balance for Evaporator Water Loop	Tons
kW	JCI AHU	Watt Transducer Measuring Instantaneous Compressor Power	kW
COP	VisSim	Calculated Coefficient of Performance	--
kW/ton	VisSim	Calculated Compressor Efficiency	kW/ton
FWC	JCI AHU	Flow Rate of Condenser Water	GPM
FWE	JCI AHU	Flow Rate of Evaporator Water	GPM
TEA	MicroTech	Evaporator Approach Temperature (TWEO-TRE)	F
TCA	MicroTech	Condenser Approach Temperature (TRC-TWCO)	F
TRE	MicroTech	Saturated Refrigerant Temperature in Evaporator	F

Table 3.2: Continued.

Designation	Source	Description	Units
PRE	MicroTech	Pressure of Refrigerant in Evaporator	PSIG
TRC	MicroTech	Saturated Refrigerant Temperature in Condenser	F
PRC	MicroTech	Pressure of Refrigerant in Condenser	PSIG
TRC_sub	MicroTech	Liquid-line Refrigerant Subcooling from Condenser	F
T_suc	MicroTech	Refrigerant Suction Temperature	F
Tsh_suc	MicroTech	Refrigerant Suction Superheat Temperature	F
TR_dis	MicroTech	Refrigerant Discharge Temperature	F
Tsh_dis	MicroTech	Refrigerant Discharge Superheat Temperature	F
P_lift	MicroTech	Pressure Lift Across Compressor	PSI
Amps	MicroTech	Current Draw Across One Leg of Motor Input	Amps
RLA%	MicroTech	Percent of Maximum Rated Load Amps	%
Heat Balance (kW)	VisSim	Calculated 1st Law Energy Balance for Chiller	kW
Heat Balance%	VisSim	Calculated 1st Law Energy Balance for Chiller	%
Tolerance%	VisSim	Calculated Heat Balance Tolerance (ARI 550 defined as allowable test tolerance on heat balance)	%
Unit Status	MicroTech	Consult Table B.4 in Appendix	0 – 27
Active Fault	MicroTech	Consult Table B.3 in Appendix	0 – 44
TO_sump	MicroTech	Temperature of Oil in Sump	F
TO_feed	MicroTech	Temperature of Oil Feed	F
PO_feed	MicroTech	Pressure of Oil Feed	PSIG
PO_net	MicroTech	Oil Feed minus Oil Vent Pressure	PSI
TWCD	MicroTech	Condenser Water Temperature Difference (TWCO-TWCI)	F
TWED	MicroTech	Evaporator Water Temperature Difference (TWEI-TWEO)	F
VSS	JCI AHU	Small Steam Valve Position	% Open
VSL	JCI AHU	Large Steam Valve Position	% Open
VH	JCI AHU	Hot Water Valve Position	% Open
VM	JCI AHU	3-way Mixing Valve Position	% Mix
VC	JCI AHU	Condenser Valve Position	% Open
VE	JCI AHU	Evaporator Valve Position	% Open
VW	JCI AHU	City Water Valve Position	% Open
TWI	JCI AHU (RTD)	Temperature of City Water In	F
TWO	JCI AHU (RTD)	Temperature of City Water Out	F
THI	JCI AHU (RTD)	Temperature of Hot Water In	F
THO	JCI AHU (RTD)	Temperature of Hot Water Out	F
FWW	VisSim	Calculated City Water Flow Rate	GPM
FWH	VisSim	Calculated Hot Water Flow Rate	GPM
FWB	VisSim	Calculated Condenser Water Bypass Flow Rate	GPM

Within the VisSim environment the following calculations were made (consult Table 3.2 for explanation of the nomenclature):

$$\text{Evap Tons} = \frac{\text{FWE} * (\text{TEI} - \text{TEO})}{24} \tag{3.1}$$

$$\text{Shared Evap Tons} = \frac{\text{FWE} * (\text{TBI} - \text{TEO})}{24} \tag{3.2}$$

$$\text{Building Tons} = \frac{\text{FWE} * (\text{TBO} - \text{TBI})}{24} \tag{3.3}$$

$$\text{Evap Energy Balance} = \text{Evap Tons} + \text{Shared Evap Tons} + \text{Building Tons} \tag{3.4}$$

$$\text{Cond Tons} = \frac{\text{FWC} * (\text{TCO} - \text{TCI})}{24} \tag{3.5}$$

$$\text{Cooling Tons} = \frac{\text{FWC} * (\text{TCO} - \text{TSI})}{24} \tag{3.6}$$

$$\text{Shared Cond Tons} = \frac{\text{FWC} * (\text{TSO} - \text{TSI})}{24} \tag{3.7}$$

$$\text{Cond Energy Balance} = \text{Cond Tons} + \text{Cooling Tons} + \text{Shared Cond Tons} \tag{3.8}$$

$$\text{COP} = \frac{\text{Evap Tons} * 12000}{\text{kW} * 3413} \tag{3.9}$$

$$\text{kW/Ton} = \frac{\text{kW}}{\text{Evap Tons}} \tag{3.10}$$

$$\text{Heat Balance} = \frac{\text{Evap Tons} * 12000}{3413} + \text{kW} - \frac{\text{Cond Tons} * 12000}{3413} \tag{3.11}$$

$$\text{Heat Balance\%} = \text{Heat Balance} * \frac{3413}{\text{Cond Tons} * 12000} * 100 \tag{3.12}$$

$$\text{Tolerance\%} = 10.5 - 0.07 * \text{RLA\%} + \left(\frac{1500}{11.75 * \text{RLA\%}} \right) \tag{3.13}$$

$$\text{FWW} = \text{FWC} * \frac{(\text{TCO} - \text{TSI})}{(\text{TWI} - \text{TWO})} \tag{3.14}$$

$$\text{FWH} = \text{FWE} * \frac{(\text{TBO} - \text{TBI})}{(\text{THI} - \text{THO})} \tag{3.15}$$

$$\text{FWB} = \text{FWC} - \frac{\text{Shared Evap Tons} * 24}{(\text{TSI} - \text{TSO})} \tag{3.16}$$

The above calculations have had the temperature differentials rearranged so that positive numbers are calculated. However, the convention used within VisSim had outlet temperature always subtracted from inlet temperature (absolute values were used in plots or for exported data, with the exception of energy balances). The conversion factors used are 1 Ton = 12000 Btu/hr and 1 kW = 3413 Btu/hr (a thermal ton is the amount of energy required to freeze/melt one ton of water in 24 hours). Equation (3.13) is adapted from ARI Standard 550. The use of RLA% replaces %FL (percent full load tons) since for many of the fault tests the full load tons at a given operating condition were not known in advance. The 11.75 term is the change in chilled water temperature (F) across the evaporator at full load (nominally it would be 10 degrees F, however the larger number was chosen to compensate for potential effects from certain faults). Ultimately, the relevance of this index for fault testing is open to debate and its inclusion was only for comparison purposes.

3.6 Stability and Accuracy of Measured Data

All the onboard chiller sensors were retained for use in the data collection process, since they would normally be available for fault detection and diagnostics. The downside to this choice was the inability to calibrate many of those sensors. Since the condenser and evaporator water leaving and entering temperatures are important for load calculations, those measurements were duplicated by the test stand to ensure greater accuracy. All the sensors on the test stand were calibrated immediately before testing began, whereas only the pressure transducers on the chiller could be calibrated.

Initially the RTDs (Resistance Temperature Detectors) measuring the water temperatures were calibrated with an ice water bath; however, it was soon realized that absolute accuracy in measurements was not as important as precision (fault conditions are determined by deviation from normal behavior). Consequently, each RTD in a water flow circuit was calibrated to read the same temperature as the other RTDs when there was no heat transfer occurring (all the water loops are coupled together with heat exchangers). Moreover, the temperatures of the RTDs were matched to the average reading of the MicroTech's thermistors at ambient conditions and no load (nomenclature explained in Table 3.2):

- (TWEI+TWEO)/2 = TEI = TEO = TBI = TBO = THI = THO
- (TWCI+TWCO)/2 = TCI = TCO = TSI = TSO

The RTDs' readings were based on the thermistors' readings simply because the thermistors could not be calibrated. The averages of the MicroTech thermistors were used because they tended to randomly fluctuate by about ± 0.2°F (the inlet relative to the outlet temperature) whereas the RTDs could be repeatedly tuned to about ± 0.05°F. The display resolution of the RTDs is ± 0.01°F; however, their true resolution is approximately ± 0.04°F. The thermistors' display and actual resolution are ± 0.1°F and ± 0.2°F respectively. To illustrate the repeatability of temperature measurements, Table 3.3 shows actual data taken during various low load situations.

Table 3.3: Sample measurements taken at the end of a test run after the chiller has been turned off and during a quasi-static test run.

Designation	Temperatures soon after chiller turned off	Temperatures 10 minutes later	Special Steady State Test	Special Steady State Test--2 minutes later
TEI	47.99	56.18	98.76	98.76
TWEI	48.2	56.5	98.8	98.6
TEO	41.34	56.12	98.74	98.74
TWEO	41	56.3	98.2	98.4
TCI	60.64	56.54	98.23	98.27
TWCI	61.2	56.5	98	98
TCO	66.57	56.87	98.31	98.35
TWCO	67.2	56.5	97.9	98.2
TSI	65.85	56.76	98.16	98.16
TSO	60.57	56.48	98.28	98.32
TBI	48.05	56.19	98.69	98.69
TBO	48.2	56.31	98.64	98.64
TWI	55.77	56.06	--	--
TWO	61.84	56.4	--	--
THI	48.42	56.44	98.58	98.58
THO	48.36	56.51	98.52	98.52

The first and second columns of data belong to the same test run, separated in time by 10 minutes, during which the temperatures were approaching steady state. The city water supply was still running and the entering water temperature designated by TWI indicates the true steady state temperature (it would take about 30 minutes for all temperatures to reach TWI within ± 0.1°F). The measurements taken shortly after the chiller was turned off are consistent with those taken 10 minutes later. For example, TEO was lower than TEI, indicating that the evaporator shell was still extracting heat from the water (a very small amount). Likewise, TCO was higher than TCI, showing that the condenser shell was still rejecting heat. The evaporator water loop was still cooler than the condenser water loop; therefore, heat was still being transferred across the shared heat exchanger (TSO lower than TSI on the condenser side and TBI higher than TEO on the evaporator water side—refer to Figures 3.5 and 3.6 for sensor placement).

During operation, the majority of temperature sensor readings deviate as much as 30°F from the calibrating temperature at ambient conditions (about 72°F). Therefore, to check whether the entire temperature span of each sensor was consistent with the other sensors, another test was run to see if the temperatures would still match after undergoing

a slow heating process. The third and fourth columns of data in Table 3.3 were taken during a special test run to check the accuracy of sensors under quasi-static conditions (the TWI and TWO temperatures are omitted because no city water was supplied during this test). The water pumps slowly heated the water circuits, which reached steady state conditions after an elapsed time of about 14 hours. The purpose of showing two time segments is to demonstrate that the RTD measurements are stable, whereas the thermistors' readings are not. Although load calculations use the RTD measurements, it is important to remember that the internal MicroTech calculations do not (superheat, subcooling, etc.).

The pressure transducers on the chiller were calibrated with a laboratory grade pressure gauge. The display resolution of the pressure transducers is ± 0.1 psi; although the evaporator pressure transducer often fluctuates by ± 0.3 psi and the condenser pressure transducer oscillates by ± 0.5 psi. The MicroTech controller uses these pressure readings to predict the saturation temperatures within the condenser and evaporator shells, which are then used in further calculations of subcooling, superheat, and approach temperatures. While the unit is not running, the pressures in the evaporator and condenser equalize and the pressure transducers reflect this by indicating pressures that match within ± 0.8 psi (exceptionally good considering that each pressure gauge was independently calibrated during operation and the combined uncertainty is nearly ± 0.8 psi). Moreover, while the chiller is off, the predicted saturation temperature within the shell matches the water temperature in the tubes to within ± 0.8°F (this can cause errors up to 12% for calculations such as the overall heat transfer coefficient at low loads).

The watt transducer measuring the power input has an overall accuracy of ± 1.5% full scale, including the current transformers used in the measurement process. With the present configuration, the maximum power reading is 120 kW, thus the accuracy is ± 1.8 kW. The 'Amp' measurement made by the MicroTech controller was not used in any power calculations, since it merely indicates the current drawn from just one of three power legs leading to the compressor motor.

The vortex flow meters used to measure the condenser and evaporator water flow rates were factory calibrated (traceable to NIST) and are accurate to ± 1% full scale. The

condenser flow meter has a maximum reading of 276 gpm; therefore, its accuracy is ± 2.8 gpm. The evaporator flow meter has a maximum reading of 221 gpm and a subsequent accuracy of ± 2.2 gpm.

The additional MicroTech sensor readings pertain to the oil temperatures and pressures, whose accuracy could not be verified. Nevertheless, experimental data was used to determine the repeatability of these measurements.

An uncertainty analysis was performed for all the calculated quantities in Table 3.2 and the results are contained in Table 3.4 (the uncertainty of the internal MicroTech measurements could only be inferred). The uncertainty calculation for the evaporator heat transfer rate is given below as an example (Fox and McDonald, 1992):

$$u_{\text{Evap Tons}} = \pm\left[\left(\frac{\text{FWE}}{\text{Evap Tons}}\cdot\frac{\partial\text{Evap Tons}}{\partial\text{FWE}}\cdot u_{\text{FWE}}\right)^2 + \left(\frac{\text{(TEI - TEO)}}{\text{Evap Tons}}\cdot\frac{\partial\text{Evap Tons}}{\partial\text{(TEI - TEO)}}\cdot u_{\text{(TEI-TEO)}}\right)^2\right]^{1/2} \quad (3.17)$$

where the uncertainties are designated by a 'u' with a descriptive subscript and are dimensionless. By substituting Equation (3.01) into (3.17), the uncertainty in the calculation of the evaporator load is:

$$u_{\text{Evap Tons}} = \pm\left[u_{\text{FWE}}^2 + u_{\text{(TEI-TEO)}}^2\right]^{1/2} \quad (3.18)$$

As mentioned earlier, the error associated with the evaporator water flow rate is ± 2.2 gpm and the uncertainty can be calculated using:

$$u_{\text{FWE}} = \frac{\pm 2.2\ \text{gpm}}{\text{FWE}} \quad (3.19)$$

This translates into an uncertainty of ± 0.01 (or ± 1%) when the flow rate is 216 gpm. The uncertainty in the chilled water temperature difference takes a little more effort and is calculated using:

$$u_{\text{(TEI-TEO)}} = \pm\left[\left(\frac{\text{TEI}}{\text{TEI - TEO}}\cdot\frac{\partial\text{(TEI - TEO)}}{\partial\text{TEI}}\cdot u_{\text{TEI}}\right)^2 + \left(\frac{\text{TEO}}{\text{TEI - TEO}}\cdot\frac{\partial\text{(TEI - TEO)}}{\partial\text{TEO}}\cdot u_{\text{TEO}}\right)^2\right]^{1/2} \quad (3.20)$$

After evaluating the partial derivatives, Equation (3.20) simplifies to:

$$u_{(TEI-TEO)} = \pm\left[\left(\frac{TEI}{TEI - TEO}\cdot u_{TEI}\right)^2 + \left(\frac{- TEO}{TEI - TEO}\cdot u_{TEO}\right)^2\right]^{1/2} \tag{3.21}$$

The individual uncertainties are calculated according to the relations:

$$u_{TEI} = \frac{\pm 0.05\ ^\circ F}{TEI} \tag{3.22}$$

$$u_{TEO} = \frac{\pm 0.05\ ^\circ F}{TEO} \tag{3.23}$$

Consequently, the overall uncertainty of the temperature difference will simplify to:

$$u_{(TEI-TEO)} = \frac{\pm 0.07\ ^\circ F}{(TEI - TEO)} \tag{3.24}$$

The chilled water temperature difference varies from about three to ten degrees F, which leads to uncertainties of ± 0.023 at low load and ± 0.007 at full load. When these results are used in Equation (3.18), the overall uncertainty of the evaporator heat transfer rate calculation is ± 0.025 (± 2.5%) at low load and ± 0.012 (± 1.2%) at full load. The corresponding absolute uncertainty in the calculation is therefore approximately ± 0.75 tons at low load and ± 1.08 tons at full load.

Table 3.4: Complete listing of measured and calculated variables with corresponding absolute uncertainties.

Designation	Source	Full Load Uncertainty	Low Load Uncertainty	Units
TEI	JCI AHU (RTD)	±0.05	±0.05	F
TWEI	MicroTech (Thermistor)	±0.2	±0.2	F
TEO	JCI AHU (RTD)	±0.05	±0.05	F
TWEO	MicroTech (Thermistor)	±0.2	±0.2	F
TCI	JCI AHU (RTD)	±0.05	±0.05	F
TWCI	MicroTech (Thermistor)	±0.2	±0.2	F
TCO	JCI AHU (RTD)	±0.05	±0.05	F
TWCO	MicroTech (Thermistor)	±0.2	±0.2	F
TSI	JCI AHU (RTD)	±0.05	±0.05	F
TSO	JCI AHU (RTD)	±0.05	±0.05	F
TBI	JCI AHU (RTD)	±0.05	±0.05	F
TBO	JCI AHU (RTD)	±0.05	±0.05	F
Cond Tons	VisSim	±1.32	±0.7	Tons
Cooling Tons	VisSim	±0.9	±0.85	Tons
Shared Cond Tons	VisSim	±1.32*	±0.7*	Tons
Cond Energy Balance	VisSim	±2.07*	±1.3*	Tons
Evap Tons	VisSim	±1.08	±0.75	Tons
Shared Evap Tons	VisSim	±1.08	±0.75	Tons
Building Tons	VisSim	±0.63	±1.05	Tons
Evap Energy Balance	VisSim	±1.65	±1.49	Tons
kW	JCI AHU	±1.8	±1.8	kW
COP	VisSim	±0.117	±0.153	--
kW/ton	VisSim	±0.026	±0.071	--
FWC	JCI AHU	±2.8	±2.8	GPM
FWE	JCI AHU	±2.2	±2.2	GPM
TEA	MicroTech	±0.3	±0.3	F
TCA	MicroTech	±0.5	±0.5	F
TRE	MicroTech	±0.3	±0.3	F
PRE	MicroTech	±0.3	±0.3	PSIG
TRC	MicroTech	±0.3	±0.3	F
PRC	MicroTech	±0.5	±0.5	PSIG
TRC_sub	MicroTech	±0.54	±0.54	F
T_suc	MicroTech	±0.2	±0.2	F
Tsh_suc	MicroTech	±0.36	±0.36	F
TR_dis	MicroTech	±0.2	±0.2	F
Tsh_dis	MicroTech	±0.54	±0.54	F
P_lift	MicroTech	±0.6	±0.6	PSI
Amps	MicroTech	±5	±5	Amps
RLA%	MicroTech	±4	±4	%
Heat Balance (kW)	VisSim	±12.4	±6.72	kW
Heat Balance%	VisSim	±3.1	±5.6	%

Table 3.4: Continued.

Designation	Source	Full Load Uncertainty	Low Load Uncertainty	Units
Tolerance%	VisSim	±5.7	±5.7	%
TO_sump	MicroTech	±0.2	±0.2	F
TO_feed	MicroTech	±0.2	±0.2	F
PO_feed	MicroTech	±0.5	±0.5	PSIG
PO_net	MicroTech	±0.5	±0.5	PSI
TWCD	MicroTech	±0.6	±0.6	F
TWED	MicroTech	±0.4	±0.4	F
TWI	JCI AHU (RTD)	±0.05	±0.05	F
TWO	JCI AHU (RTD)	±0.05	±0.05	F
THI	JCI AHU (RTD)	±0.05	±0.05	F
THO	JCI AHU (RTD)	±0.05	±0.05	F
FWW	VisSim	±4.5	±7.0	GPM
FWH	VisSim	±3.5	±25	GPM
FWB	VisSim	±4.9	±7.3	GPM

* denotes a calculation whose results are unreliable if any condenser water is bypassed around shared heat exchanger

The values given in Table 3.4 are the absolute uncertainties for each measurement, to find the uncertainty it is necessary to divide by the measurement. Important measurements with the highest uncertainties are:

- Suction superheat with an uncertainty of 5 to 25%
- Liquid subcooling with an uncertainty of 5 to 15%
- Evaporator approach temperature with an uncertainty of 4 to 10%
- Condenser approach temperature with an uncertainty of 8 to 25%
- kW/ton with an uncertainty of 4 to 5%

Differences in uncertainties occur because of significant changes in the measurements at various operating conditions.

3.7 Test Matrix

Soon after commissioning the chiller test stand, tests were run at various temperature and loading extremes to determine the operating envelope of the chiller. ARI Standard 550 recommends testing at a chilled water temperature of 44°F (TEO) and a condenser water entering temperature of 85°F (TCI) for standard rating conditions.

Moreover, ARI 550 also recommends testing at chilled water temperatures of 40-48°F and condenser water entering temperatures of 60-105°F for operational rating conditions.

Based on the earlier test results, chilled water temperatures of 40°F, 45°F, and 50°F were easily achievable and determined to be good testing points. However, limitations of the cooling water supply made condenser water entering temperatures of 60°F nearly impossible, although 65°F was realistically attainable in seven out of nine low temperature tests. The most severe limitation was placed on the upper limit of the condenser water entering temperature. The chiller was unable to accept condenser water entering temperatures above 90°F without being precariously close to its surge limit. (In a centrifugal compressor, surge occurs when the refrigerant flow reverses direction because the pressure lift between the evaporator and condenser becomes too high at a particular loading condition. A large pressure lift is often caused by high condenser water temperatures that elevate the condenser pressure). To provide a buffer between the testing conditions and the surge limit, the maximum condenser water entering temperature was chosen to be 85°F. This also compensates for the unpredictable impact of faults, which tend to lower the surge limit.

Since fault testing relies on comparisons of different test runs, the test sequence was constructed in a manner that was consistent for all the faults tested. Therefore, once the test sequence was selected, it was kept unmodified for all the tests performed. The three control variables chosen were the chilled water temperature, the condenser water entering temperature, and the chiller cooling load. Using these three variables each at three levels resulted in a 3x3x3 test matrix of 27 tests for each fault level as shown in Table 3.5. The column titled ‘Capacity%’ indicates the percent of capacity the actual cooling load was able to reach. A range is given, since the cooling load cannot be directly controlled.

Table 3.5: Test sequence of desired operating conditions.

TEO	TCI	Capacity%
50	85	90-100
50	85	50-60
50	85	25-40
50	75	90-100
50	75	50-60
50	75	25-40
50	70	70-80
50	65	45-50
50	62	25-35
45	85	90-100
45	85	50-60
45	85	25-40
45	75	90-100
45	75	50-60
45	75	25-40
45	70	70-90
45	62	45-50
45	62	25-35
40	80	90-100
40	80	50-60
40	80	25-40
40	70	90-100
40	70	50-60
40	70	25-40
40	65	70-80
40	62	45-50
40	62	25-35

Another goal of the test sequence was to capture both steady state and transient behavior. Based on earlier observations, steady state is usually reached within 5 to 15 minutes after a change in operating setpoints. Changes in the chilled water setpoint led to the slowest response to reach steady state; therefore, the test matrix was designed so that this variable was changed the least frequently. Each of the 27 tests were allowed at least 30 minutes to reach steady state, with 45 minutes being allocated to those tests where the chilled water setpoint was changed. This provided between 15 and 25 minutes of steady state operation for each test case. Results of an actual test run at normal conditions are shown in Figure 3.7—each data point on this graph is the actual measurement reading at two-minute intervals. The water flow rates were at ARI conditions; the evaporator water

leaving temperature (TEO) was initially set for 50°F, then stepped down to 45°F and 40°F; the condenser water entering temperature (TCI) varied between high to low temperature for each chilled water temperature; the evaporator cooling load varied between high to low with the greatest frequency and compressor power was also plotted to show increases in efficiency when the condenser water temperature was reduced (refer to Table 3.2 for a complete definition of terms).

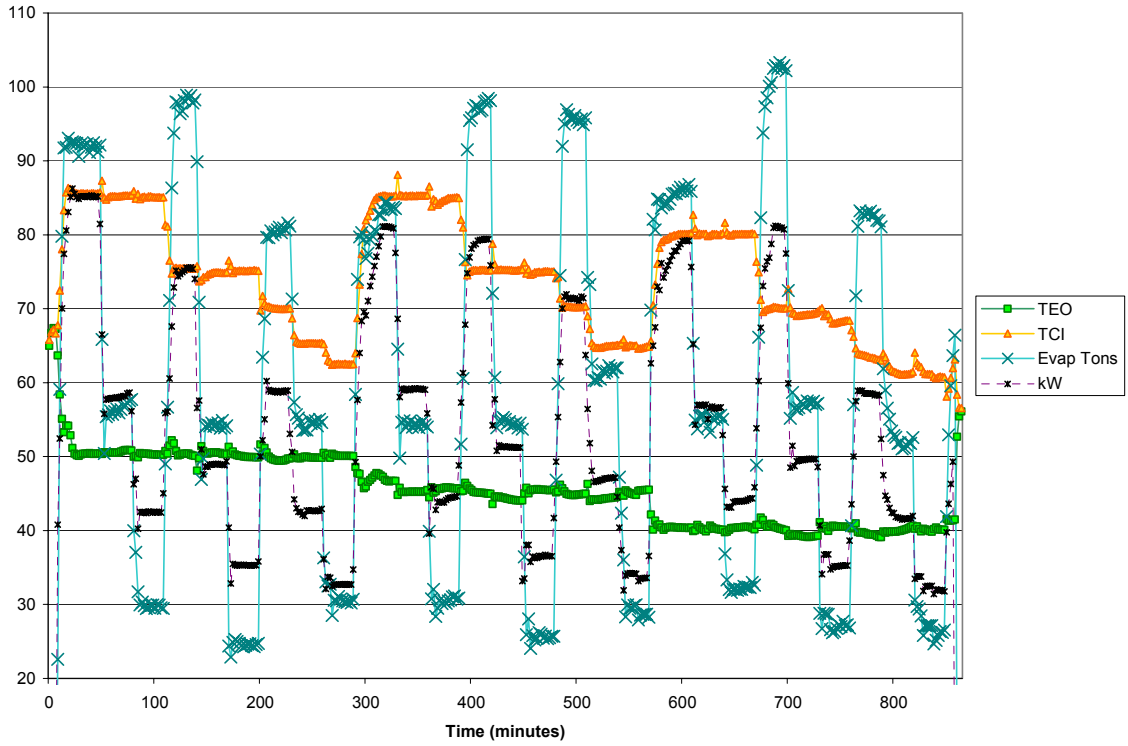

Figure 3.7: Data from an actual test run meeting all 27 operating conditions.

The reason for fixing the length of the test runs instead of implementing a steady state trigger was to allow easier comparison between different test runs at every instant in time as well as to simplify the data analysis.

The data from 'Normal 1' was also used to produce Figures 3.8 through 3.10, which show transients for the condenser pressure (PRC), evaporator pressure (PRE), and power input. Three different time segments are shown; Figure 3.8 shows the start-up

from about 150 to 1000 seconds, Figure 3.9 shows the first operating setpoint change from test 1 to test 2 at 2,500 to 3,700 seconds, and Figure 3.10 shows the shut-down procedure of the test run from 50,500 to 51,900 seconds.

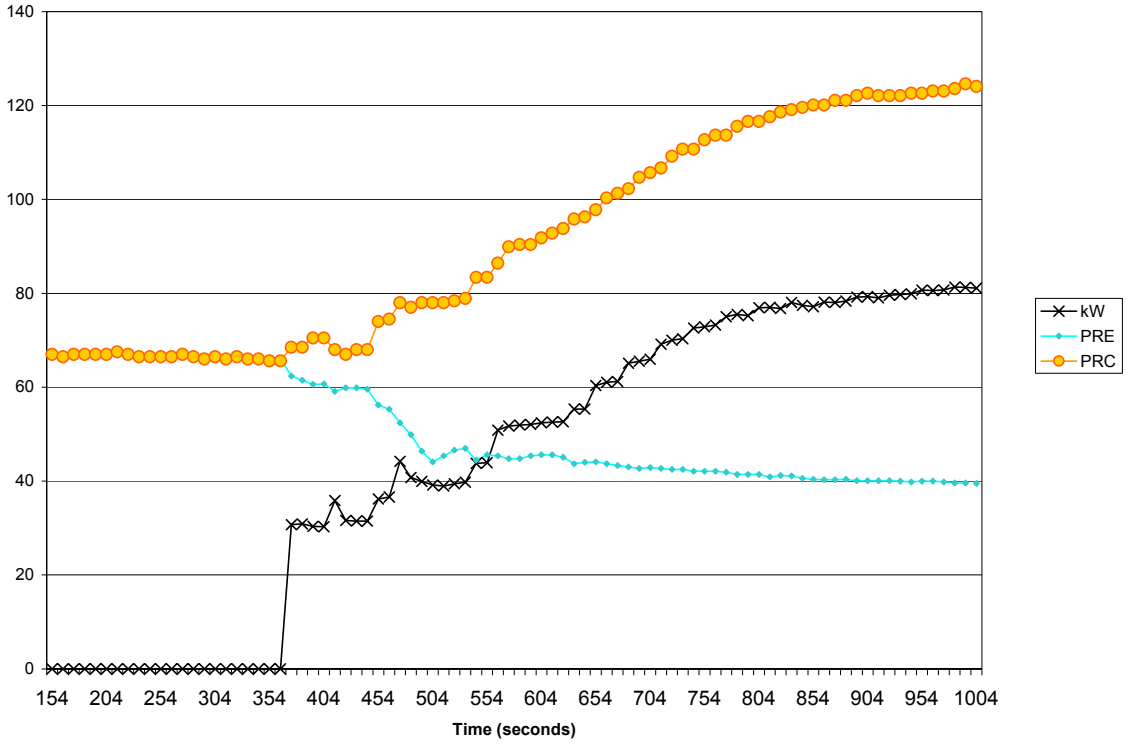

Figure 3.8: Sample of transient data during start-up.

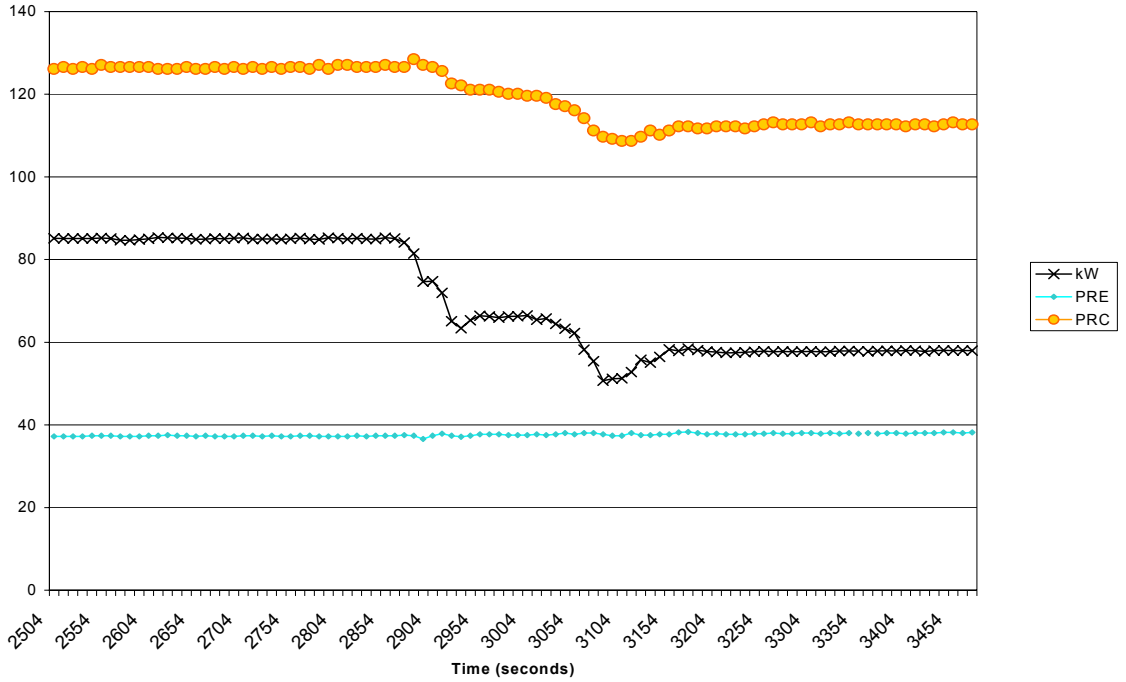

Figure 3.9: Sample of transient data during operating setpoint change.

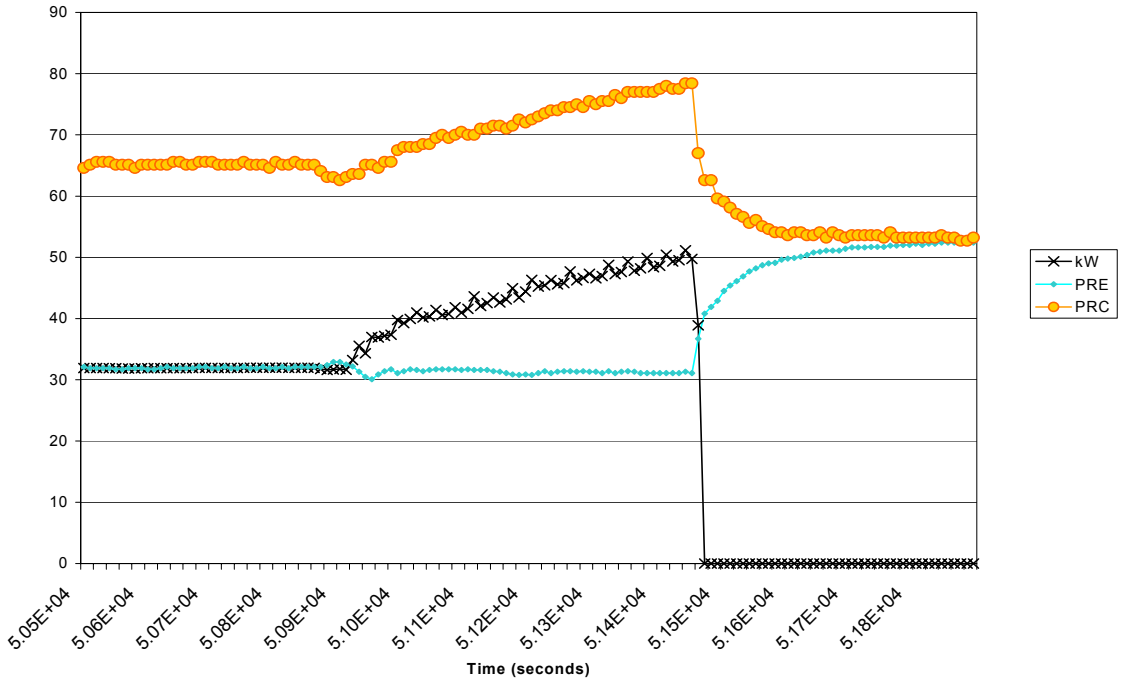

Figure 3.10: Sample of transient data during shut-down procedure.

To make sure that the test sequence did not introduce any unanticipated errors into the data collection process, the sequence was reversed and tested. A comparison with other tests under the same steady state operating conditions showed that the results were identical. The chiller test stand was able to create a wide range of operating conditions as shown in Figure 3.11. However, the test stand was unable to effectively load the chiller when the evaporator and condenser water temperatures were close together. Figure 3.11 shows data taken from a normal test run. The individual points are grouped according to the difference between the condenser and evaporator water leaving temperatures (F), which are good indicators of the pressure lift across the compressor. At the highest temperature differences there is an increased risk of inducing surge within the compressor (as shown by the dotted line). The one operating condition beyond the maximum capacity limit can be accounted for through measurement uncertainty.

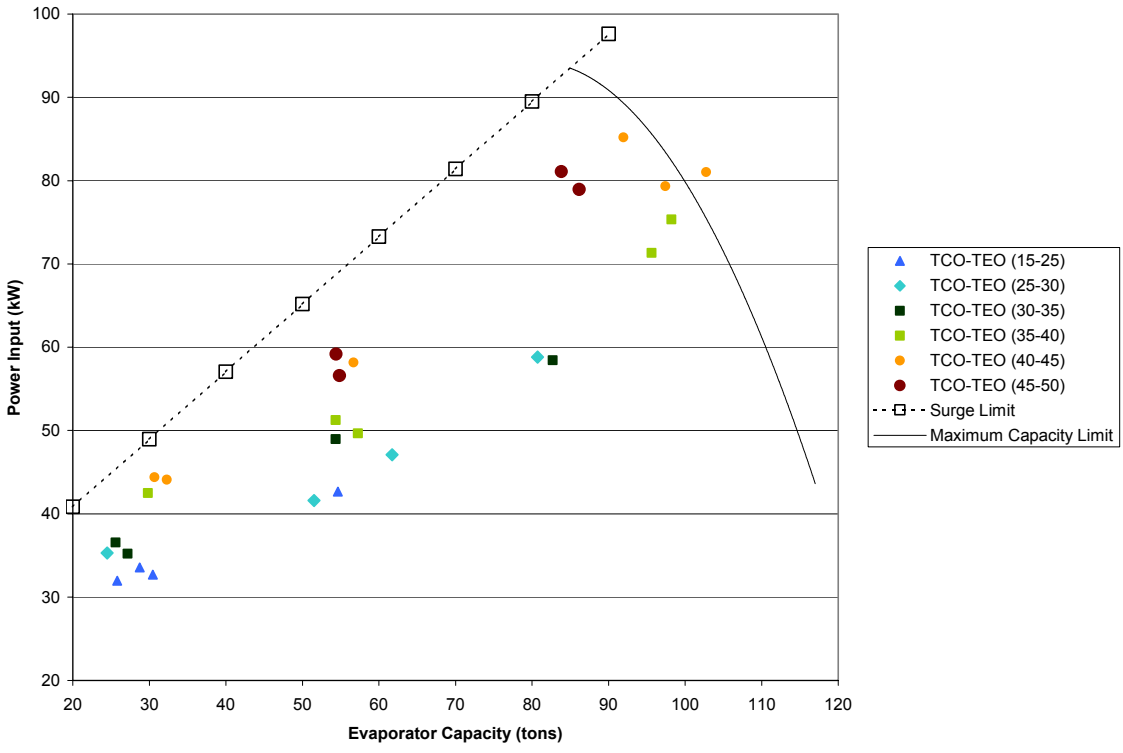

Figure 3.11: Distribution of actual test conditions within possible operating envelope.

4.0 FAULT IMPLEMENTATION AND CHARACTERIZATION

This chapter discusses the primary focus of this project; namely, which faults were implemented, how they were simulated, and how they were measured. The order in which these faults are presented is the same sequence in which they were tested—the only exception is the defective pilot valve fault (consult the companion report on the experimental data prepared by Comstock and Braun (1999a) for more detailed information). Table 4.1 from the supplementary report is provided to show the exact order and timing of tests. The names of these files will occasionally be used in Chapters 4 and 5. Between each of the fault tests there was at least one test performed under normal conditions. Moreover, the few fault tests that did not satisfactorily meet the desired operating conditions were repeated. The fault tests were run in order of least intrusive to most intrusive with the exception of the defective pilot valve, which was already present when testing began. The condenser water pump was also replaced in the midst of the reduced condenser water flow rate tests. The following subsections of this chapter will provide more detail on the faults and how they were implemented.

Table 4.1: Sequence of experimental tests and file names.

File name	Date of Test	Comments
Defective Pilot Valve	8/19/99	The last test before the pilot valve was replaced; condenser water flow rate was not corrected
Normal DPV	8/25/99	The first test where the new pilot valve was properly adjusted; condenser water flow rate was not corrected
FWC30	9/2/99	Condenser water flow rate reduced by 30%; was able to perform test with old pump
FWC40	9/3/99	Condenser water flow rate reduced by 40%; was able to perform test with old pump (last test with smaller condenser pump)
Near Normal3	9/9/99	The worst of the corrected condenser water flow rate tests; hence it was numbered #3 even though it was the first

Table 4.1: Continued.

File name	Date of Test	Comments
Near Normal1	9/10/99	Test run under normal conditions; however, not all the desired operating conditions were met satisfactorily
Near Normal2	9/11/99	Test run under normal conditions; however, not all the desired operating conditions were met satisfactorily
Normal	9/12/99	The first test run where all operating conditions were met
FWC10	9/13/99	Condenser water flow rate reduced by 10%
FWC20 alt	9/14/99	Condenser water flow rate reduced by 20%; not all operating conditions met satisfactorily
FWC20	9/15/99	Condenser water flow rate reduced by 20%
Normal1	9/16/99	Another test under normal conditions; became the reference standard by meeting all the operating conditions exceptionally well
FWE10	9/17/99	Evaporator water flow rate reduced by 10%
FWE20 alt	9/18/99	Evaporator water flow rate reduced by 20%; test number 5 never reached steady state
FWE20	9/18/99	Evaporator water flow rate reduced by 20%; test performed all day long immediately after overnight test run FWE20 alt
FWE30	9/19/99	Evaporator water flow rate reduced by 30%
FWE40 alt	9/20/99	Evaporator water flow rate reduced by 40%; test number 8 never reached steady state
FWE40	9/21/99	Evaporator water flow rate reduced by 40%
Normal2	9/21/99	Another test under normal conditions created for comparison purposes
FWE20FWC20	9/22/99	Evaporator and Condenser water flow rates reduced by 20%; a compound fault
RL40 alt	9/24/99	Refrigerant charge 40% less than nominal; 5 of the 27 tests did not reach steady state
RL40	9/25/99	Refrigerant charge 40% less than nominal
RL30	9/26/99	Refrigerant charge 30% less than nominal
RL20	9/27/99	Refrigerant charge 20% less than nominal
RL10	9/28/99	Refrigerant charge 10% less than nominal
Normal R	9/29/99	Refrigerant charge at nominal (300 lbs)
RO10	9/30/99	Refrigerant charge 10% more than nominal
RO20	10/1/99	Refrigerant charge 20% more than nominal
RO30	10/2/99	Refrigerant charge 30% more than nominal
RO40	10/3/99	Refrigerant charge 40% more than nominal
Normal R1	10/5/99	Refrigerant charge at nominal (300 lbs)
Normal EO	10/6/99	Changed control program to improve ability to reach desired operating conditions
Normal B	10/7/99	Control program reversed so that tests were run in opposite sequence; data compares favorably to other normal test runs but is normally excluded from analysis because test sequence numbers do not match and may therefore cause confusion
EO14	10/8/99	Oil charge 14% more than nominal (added 3.25 lbs of oil, bringing total charge to 25 pounds)
EO32	10/9/99	Oil charge 32% more than nominal (added 4 lbs of oil, bringing total charge to 29 pounds)
EO50	10/10/99	Oil charge 50% more than nominal (added 4 lbs of oil, bringing total

		charge to 33 pounds)

Table 4.1: Continued.

File name	Date of Test	Comments
Aborted EO86	10/11/99	Oil charge 86% more than nominal (added 8 lbs of oil, bringing total charge to 41 pounds); chiller stopped in middle of third test
EO73 alt	10/12/99	Oil charge 73% more than nominal (removed 3 lbs of oil, bringing total charge to 38 pounds); first test never reached steady state
EO68	10/13/99	Oil charge 68% more than nominal (removed 1 lb of oil, bringing total charge to 37 pounds); first test never reached steady state
Normal CF	10/14/99	Oil charge back to normal (21 pounds, 1 less than before); oil pressure regulator turned CW ($1/8^{th}$ turn) boosting oil pressures
CF6	10/15/99	Plugged 10 tubes in the condenser (out of 164)
CF12	10/16/99	Plugged 20 tubes in the condenser
CF20	10/19/99	Plugged 33 tubes in the condenser
CF30	10/20/99	Plugged 49 tubes in the condenser
Normal CF2	10/21/99	Unplugged all the tubes
Normal CF3	10/22/99	Another normal test run; 16th test had about a 5% reduction in condenser water flow
Normal CF4	10/23/99	Another normal test run
Normal CF5	10/24/99	Another normal test run; started soon after the previous one had finished (starting water temperatures were therefore cooler)
Normal CF6	10/25/99	Another normal test run; the fifth in a row
CF45	10/26/99	Plugged 74 tubes in the condenser
Normal NC	10/27/99	Unplugged all the tubes
Aborted NC	10/29/99	Too much Nitrogen (even after trying to purge some); stopped after 10th test due to surge
Modified NC	10/31/99	Modified low load tests to determine if complete test sequence could be completed by eliminating the surge-prone low load tests
NC5	11/3/99	Approximately 0.54 lbs Nitrogen (displacing about 5.6% of the volume at room temperature); could not reach all desired operating conditions
NC3	11/4/99	Approximately 0.22 lbs Nitrogen (displacing about 2.4% of the volume at room temperature)
NC2	11/6/99	Approximately 0.16 lbs Nitrogen (displacing about 1.8% of the volume at room temperature)
NC1	11/7/99	Approximately 0.10 lbs Nitrogen (displacing about 1.0% of the volume at room temperature)
NC Trace	11/8/99	Trace amount of Nitrogen present
NC Trace 2	11/9/99	Trace amount of Nitrogen present (some purged after previous test)

Each of these faults (except the defective pilot valve) was introduced at four different levels of severity so that the sensitivity of future detection methods can be determined. The least intrusive fault was labeled Fault Level 1; the most severe was called Fault Level 4. Each of the fault tests went through the same operating conditions described in Section 3.7.

4.1 Regression Analysis

Although each test run was designed to repeat the same operating and driving conditions, there will always be some minor fluctuations between test runs. In order to compare data from different test runs, a simple regression analysis was performed.

The inputs to the regression models included the evaporator water leaving temperature (TEO), the condenser water entering temperature (TCI), and the evaporator heat transfer rate (Evap Tons). Several models of different orders and cross terms were evaluated. Higher order models provide better fits to the data, but the fit is not as smooth between the points used by the regression analysis. The goal was to find the lowest order regression model without sacrificing much accuracy. The most effective regression model with the least number of inputs was found to be in the form:

$$\begin{aligned} y = a_0 + a_1 \cdot TEO + a_2 \cdot TCI + a_3 \cdot EvapTons \\ + a_4 \cdot TEO \cdot EvapTons + a_5 \cdot TCI \cdot EvapTons + a_6 \cdot EvapTons^2 \end{aligned} \tag{4.1}$$

where ‘y’ is any measurement from the chiller system and ‘a’ is a coefficient determined from the regression analysis.

A regression analysis was performed on 15 different variables as shown later in Table 4.3. A fixed sequence of the input parameters—values of TEO, TCI, and ‘Evap Tons’ that would not require extrapolation from the actual operating conditions (listed in Table 4.2)—was then fed into the regression models. The outputs of the regression models for normal and fault tests were then compared to obtain the results presented in the following subsections.

Table 4.2: Operating conditions used for regression comparison.

TEO (F)	TCI (F)	Evap Tons
40	60	30
40	60	40
40	60	50
40	60	60
40	60	70
40	70	30
40	70	40
40	70	50
40	70	60
40	70	70
40	70	80
40	70	90
40	80	30
40	80	40
40	80	50
40	80	60
40	80	70
40	80	80
40	80	90
45	65	30
45	65	40
45	65	50
45	65	60
45	65	70
45	75	30
45	75	40
45	75	50
45	75	60
45	75	70
45	75	80
45	75	90
45	85	30
45	85	40
45	85	50
45	85	60
45	85	70
45	85	80
45	85	90
50	65	30
50	65	40
50	65	50
50	65	60
50	65	70

Table 4.2: Continued.

TEO (F)	TCI (F)	Evap Tons
50	75	30
50	75	40
50	75	50
50	75	60
50	75	70
50	75	80
50	75	90
50	85	30
50	85	40
50	85	50
50	85	60
50	85	70
50	85	80
50	85	90

4.2 FDD Benchmarking

All the data from the faults tested would be useless without benchmark data. Therefore, each fault test performed was specifically linked to a test run under normal conditions. It was necessary to repeat these normal tests because of the difficulty in getting the chiller exactly back to the same condition it was in before certain faults were introduced. These normal test runs were usually conducted before the fault tests.

In addition to running normal tests for use as benchmarks, other normal tests were run in order to determine the experimental uncertainty of particular measurements. The results from those tests confirm the findings from the uncertainty analysis done in Chapter 3 and are presented in Table 4.3 along with those measured variables that were specifically singled out for FDD analysis. The variables chosen for study were generally thought to be useful in characterizing the thermodynamic performance of the chiller.

The final four measurements pertain to oil temperatures and pressures. It was discovered in the literature review that some researchers had tried to correlate chiller fault detection and diagnosis with oil measurements. Since the data were already available, it took minimal effort to evaluate how these measurements responded to different faults.

The ranges of uncertainty given in Table 4.3 are based on a regression analysis of data taken from two different series of normal tests. One group of normal tests was done before any faults had been implemented; the other group was taken after numerous refrigerant charge changes. The uncertainty range corresponds to differences in time between the tests. The first number indicates the repeatability for tests performed in quick succession with few modifications being made, the second number gives an upper range of repeatability over an indefinite time period (assuming no manual adjustments were made on the chiller). The uncertainty in Table 4.3 takes into account the errors of the regression analysis (shown as a R^2 value in the table) as well as the measurement uncertainty.

Table 4.3: Measurements and uncertainty for FDD analysis.

Measurement	Description	Experimental Uncertainty	Regression R^2 Value
kW	Instantaneous input power	± 1-1.5%	0.998-0.999
PRE	Evaporator Pressure	± 1-2%	0.987-0.993
PRC	Condenser Pressure	± 1-2%	0.997-0.999
TRC_sub	Subcooling	± 7-20%	0.972-0.983
Tsh_suc	Suction Superheat	± 10-25%	0.956-0.985
Tsh_dis	Discharge Superheat	± 2-3%	0.994-0.998
TEA	Evaporator Approach Temperature	± 6-10%	0.975-0.990
TCA	Condenser Approach Temperature	± 10-30%	0.941-0.980
TEI-TEO	Evaporator Water Temperature Difference	± 0.3-0.6%	0.999
TCO-TCI	Condenser Water Temperature Difference	± 1-2%	0.999
kW/ton	Chiller efficiency	± 1-2.5%	0.992-0.995
TO_sump	Oil Sump Temperature	± 0.5-1%	0.970-0.985
TO_feed	Oil Feed Temperature	± 0.3-1.5%	0.948-0.971
PO_feed	Oil Feed Pressure	± 1-7%	0.785-0.943
PO_net	Oil Net Pressure	± 1-7%	0.801-0.993

Each of the fault sections in this chapter contains a table similar to Table 4.4. Table 4.4 shows each of the FDD tracking variables along with its average deviation

from the corresponding benchmark test. It is necessary to show an average deviation since the individual deviations vary under different operating conditions (and presenting deviations for over 50 different operating conditions is space prohibitive). The benchmark test in Table 4.4 is a normal test performed a day before the 'Normal CF3' test. 'Normal CF6' is a test run three days after the 'Normal CF3' test and four days after the benchmark test. The 'Normal 1' test was performed about two months earlier, with substantial refrigerant charge changes having taken place in the meantime (but actual testing charge within ± 3% of the other tests). The 'Normal R' test was done about a month earlier, with several fault tests having taken place in the meantime. The oil pressure setting was increased just before the 'Normal CF' tests were run, which explains why the earlier 'Normal 1' and 'Normal R' tests show such a large deviations from the benchmark.

Table 4.4: Average deviations from benchmark data set.

	Normal CF3	Normal CF6	Normal 1	Normal R
kW	-0.2%	0.0%	0.2%	0.1%
PRE	-0.5%	-0.1%	0.5%	0.2%
PRC	0.0%	0.2%	0.2%	0.8%
TRC_sub	1.2%	0.7%	1.0%	8.8%
Tsh_suc	6.1%	1.5%	1.4%	7.9%
Tsh_dis	0.2%	0.4%	0.4%	0.2%
TEA	3.5%	0.7%	-2.8%	-0.4%
TCA	1.5%	1.9%	3.4%	16.8%
TEI-TEO	-0.2%	-0.1%	-0.2%	-0.4%
TCO-TCI	-0.1%	0.1%	-1.0%	-1.4%
kW/ton	-0.4%	0.0%	0.0%	-0.3%
TO_sump	-0.1%	-0.1%	0.6%	0.8%
TO_feed	-0.1%	0.0%	1.2%	1.0%
PO_feed	-0.4%	-0.2%	-13.3%	-15.6%
PO_net	-0.5%	0.1%	-17.5%	-20.3%

By comparing the results contained in Table 4.4 with Table 4.3 it is easily shown that the uncertainty in the tracking variables is much smaller when averaging the deviations across all the operating conditions. Although the deviations presented cannot be used in an FDD method as they are presented here, they do provide the simplest means of indicating the trends that develop when introducing different faults. In order to

convey some of the impact that the operating conditions have on these tracking variables, a few figures will be shown in each of the following sections for those variables that are greatly influenced by the given fault. Each figure follows the same format, showing the impact of different fault levels at a constant evaporator water leaving temperature (TEO) of 45°F and three different condenser water entering temperatures (TCI) of approximately 65°F, 75°F, and 85°F. To gauge the impact of a particular fault on system performance, kW/ton was also tracked.

4.3 Reduced Condenser Water Flow

An electronic valve regulated the water flow rate in the condenser by changing the head pressure across the water pump. The base water flow rate was 270 gpm and each fault level reduced the water flow rate by 10% as shown in Table 4.5. The uncertainty of the fault level depends on the condenser water flow rate measurement, which has an uncertainty of ± 2.8 gpm.

Table 4.5: Fault levels for reduced condenser water flow.

Case	Desired Condition	Actual Flow Range
Normal Operation	270 gpm	264-270 gpm
Fault Level 1	10% reduction in flow (243 gpm)	234-250 gpm
Fault Level 2	20% reduction in flow (216 gpm)	209-219 gpm
Fault Level 3	30% reduction in flow (189 gpm)	187-190 gpm
Fault Level 4	40% reduction in flow (162 gpm)	159-166 gpm

As the severity of the fault increased, several noticeable trends developed as shown in Table 4.6. Since evaporator heat transfer rate is one of the inputs to the regression model, it is not directly possible to determine the effect on capacity. However, since the compressor power is actually limited at full load, it can be deduced that capacity is diminishing when the kW or kW/ton measurements are increasing.

Unlike the other fault tests, there was a brief delay between running the tests at Fault Levels 1 and 2, and those at Fault Levels 3 and 4. This occurred because the condenser water pump was replaced (Fault Levels 3 and 4 were run first with a smaller pump, followed by those at Fault Levels 1 and 2). The replacement of the pump required some modifications to the expansion valve settings, hence larger than expected deviations between the two groups of test runs occurred for the superheat measurements, which also had an effect on the approach temperatures. These deviations; however, are minor when compared to the uncertainties involved in these measurements and the insensitivity these measurements displayed in the presence of this fault.

The trends in condenser pressure (PRC), condenser water temperature difference (TCO-TCI), and power consumption (kW) were expected for this fault. Reducing the condenser water flow rate at a constant condenser entering water temperature raises the leaving water temperature. Hence the condenser temperature and pressure are higher, causing the compressor to work harder and draw more power. An unexpected trend was an increase in the condenser approach temperature (TCA). The condenser pressure increase apparently was large enough to cause the condenser approach temperature to increase, even though the lower flow rate would naturally tend to reduce the approach temperature.

An additional effect of reducing the condenser water flow rate was a large increase in the subcooling (TRC_sub). This occurs because the temperature difference between the water and condensing refrigerant is greater (higher condenser pressure and temperature at constant water entering temperature), thus increasing the driving potential for heat transfer. Therefore, less area is needed for condensing, thereby providing more area for subcooling.

Table 4.6: Average deviations for reduced condenser water flow.

	Fault Level 1	Fault Level 2	Fault Level 3	Fault Level 4
kW	0.8%	2.7%	3.9%	7.0%
PRE	1.0%	0.2%	2.7%	1.7%
PRC	1.6%	3.6%	5.7%	9.5%
TRC_sub	10.5%	24.4%	33.9%	61.5%
Tsh_suc	-7.5%	1.4%	-21.2%	-10.1%
Tsh_dis	-1.3%	-0.1%	-3.7%	-0.3%
TEA	-7.6%	-0.3%	-19.9%	-11.7%
TCA	5.8%	9.1%	7.6%	21.7%
TEI-TEO	-0.1%	-0.1%	-0.3%	-0.1%
TCO-TCI	12.4%	26.5%	45.3%	70.2%
kW/ton	0.8%	2.5%	3.2%	6.1%
TO_sump	0.5%	0.7%	1.4%	2.3%
TO_feed	0.4%	0.5%	1.2%	1.6%
PO_feed	0.3%	0.3%	-3.9%	-4.0%
PO_net	0.4%	0.4%	-6.2%	-5.2%

Figures 4.1 to 4.5 contain detailed information from approximately a third of the operating conditions that were compared (only one chilled water temperature is plotted). Each figure contains a tracking variable chosen because of its sensitivity to the introduced fault. In general, each fault becomes more noticeable at higher cooling loads because the chiller is unable to compensate for the debilitating effects of the fault when the evaporator and condenser are being more fully used. Some figures may also show slightly unusual behavior, which can normally be explained by the uncertainties involved in the measured data and in the regression analysis. However, the improved performance seen in Figure 4.5 for medium cooling loads is not caused by experimental uncertainty. Apparently several design parameters are interacting in such a way as to minimize performance loss under certain operating conditions even when a severe fault condition is present.

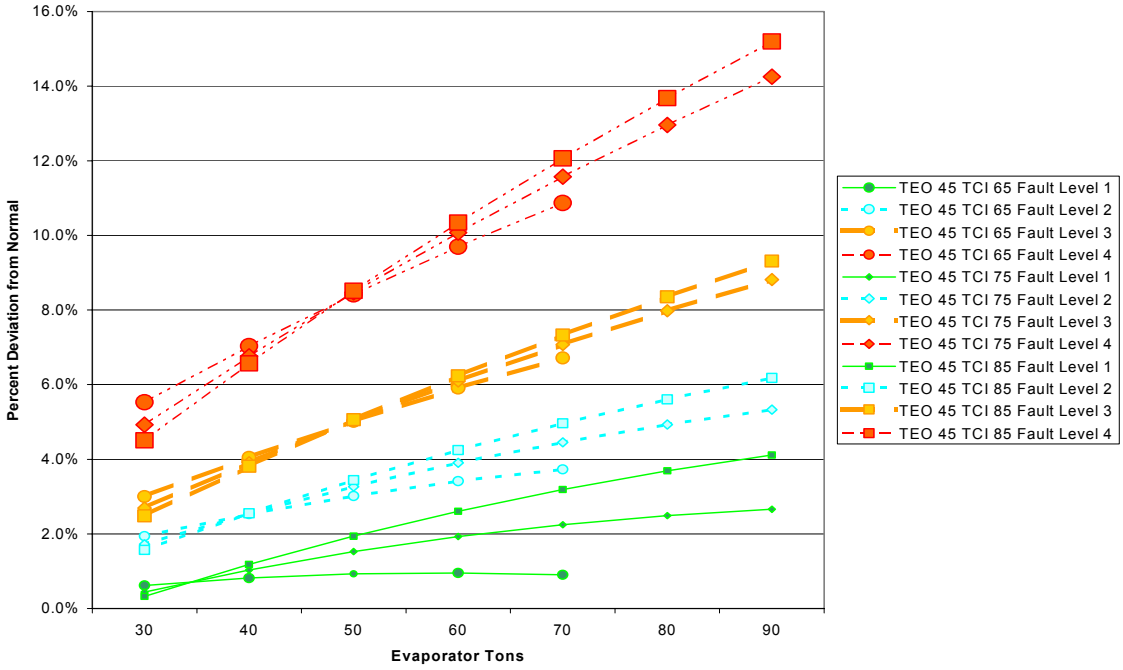

Figure 4.1: Deviation in condenser pressure for reduced condenser water flow.

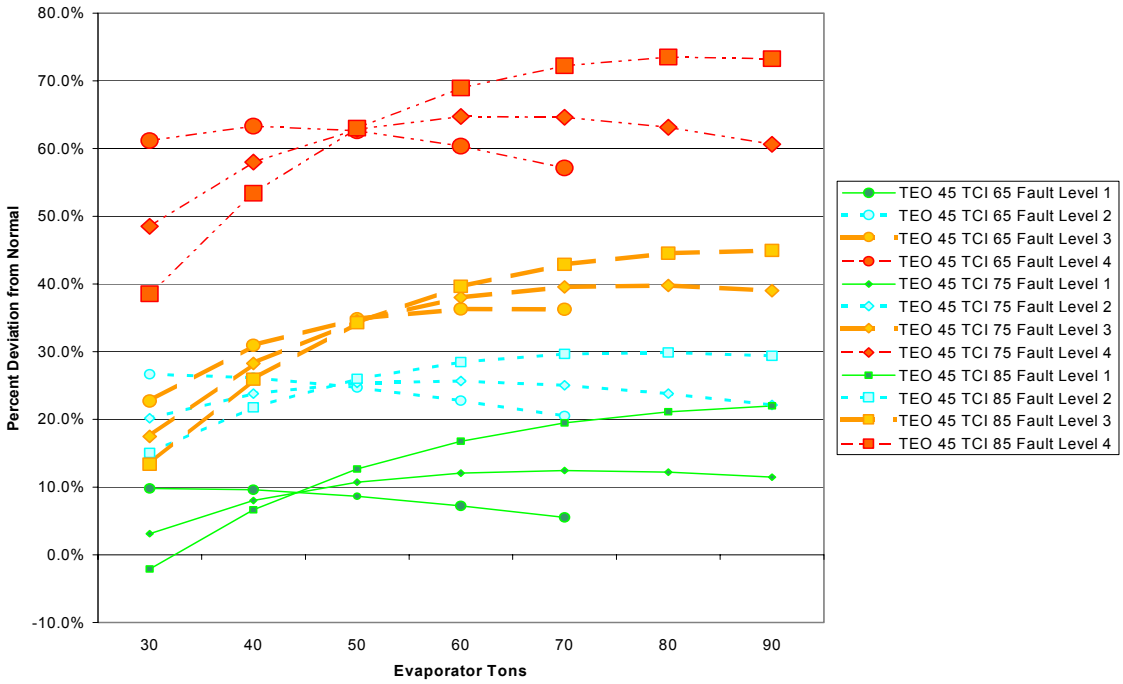

Figure 4.2: Deviation in subcooling for reduced condenser water flow.

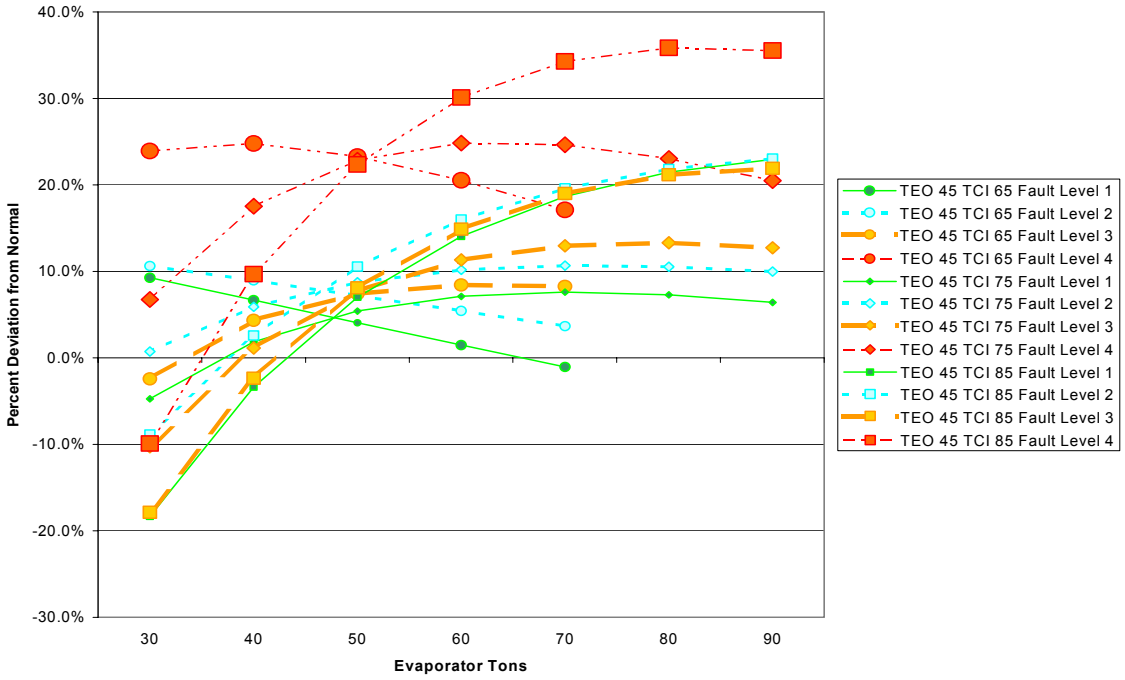

Figure 4.3: Deviation in condenser approach temperature for reduced condenser water flow.

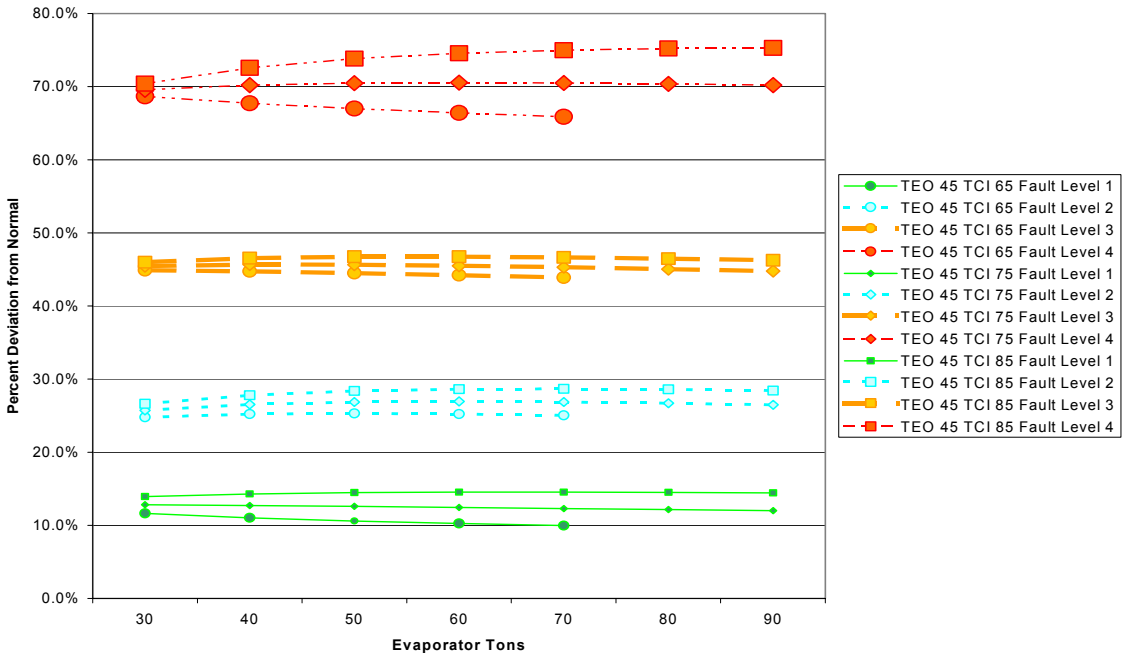

Figure 4.4: Deviation in condenser water temperature difference for reduced condenser water flow.

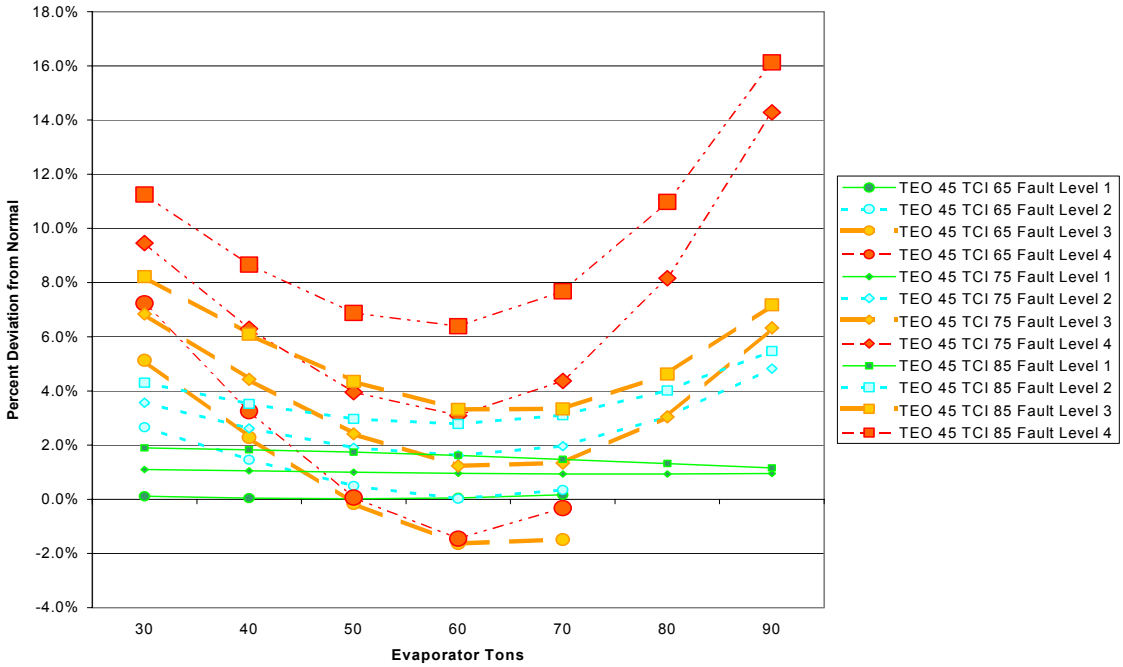

Figure 4.5: Deviation in kW/ton for reduced condenser water flow.

4.4 Reduced Evaporator Water Flow

An electronic valve regulated the water flow rate in the evaporator by changing the head pressure across the water pump. The base water flow rate was 216 gpm and each fault level reduced the water flow rate by about 10% as shown in Table 4.7. The accuracy of the fault level depends on the evaporator water flow rate measurement, which has an uncertainty of ± 2.2 gpm.

Due to difficulties in fine-tuning the valve position, the actual flow rate was more difficult to obtain at lower flow rates. Consequently it can be seen that the actual reduction in flow for Fault Level 2 was 19%, for Fault Level 3 it was 28%, and for Fault Level 4 it was 36%.

Table 4.7: Fault levels for reduced evaporator water flow.

Case	Desired Condition	Actual Flow Range
Normal Operation	216 gpm	214-216 gpm
Fault Level 1	10% reduction in flow (194 gpm)	194-196 gpm
Fault Level 2	20% reduction in flow (173 gpm)	175-177 gpm
Fault Level 3	30% reduction in flow (151 gpm)	155-156 gpm
Fault Level 4	40% reduction in flow (130 gpm)	137-141 gpm

As shown in Table 4.8, the trends are not as clear in the evaporator as in the condenser. This occurs in large part because of the expansion valve which helps regulate the evaporator pressure and temperature. The slight decrease in evaporator pressure (PRE) is important since the expansion valve was attempting to keep it nearly constant. The trends in evaporator approach temperature (TEA) and evaporator water temperature difference (TEI-TEO) were expected for this fault. Reducing the evaporator water flow rate increases the evaporator water temperature difference.

Table 4.8: Average deviations for reduced evaporator water flow.

	Fault Level 1	Fault Level 2	Fault Level 3	Fault Level 4
kW	0.0%	0.4%	0.4%	0.5%
PRE	-0.1%	-0.9%	-1.4%	-1.6%
PRC	-0.1%	0.6%	0.2%	0.1%
TRC_sub	-0.3%	1.2%	1.5%	2.9%
Tsh_suc	-3.3%	1.2%	-1.4%	-12.1%
Tsh_dis	-1.1%	-1.6%	-1.2%	-3.0%
TEA	1.5%	6.5%	10.1%	13.0%
TCA	-1.4%	2.8%	2.1%	2.5%
TEI-TEO	10.2%	22.3%	38.8%	55.8%
TCO-TCI	1.0%	1.5%	1.6%	1.7%
kW/ton	-0.2%	0.5%	1.5%	2.4%
TO_sump	-0.1%	-0.1%	0.0%	0.5%
TO_feed	0.0%	-0.1%	0.1%	0.5%
PO_feed	-0.1%	-0.4%	-0.5%	-0.6%
PO_net	0.2%	0.3%	0.3%	0.1%

Figures 4.6 through 4.10 are presented similarly to those from the reduced condenser water flow fault; however, some of the plotted variables have been changed to

show those that are sensitive to the introduction of the evaporator water flow fault. Keep in mind that some of the unusual trends seen with regard to Figures 4.6, 4.7, and 4.8 are due to automatic adjustments made in the expansion valve. Recall that the evaporator approach temperature has a high degree of uncertainty, which is why Figure 4.8 has overlapping deviations for the different fault levels. The performance shows little degradation at medium loads at most operating conditions, but is severely penalized at high loads as shown in Figure 4.10.

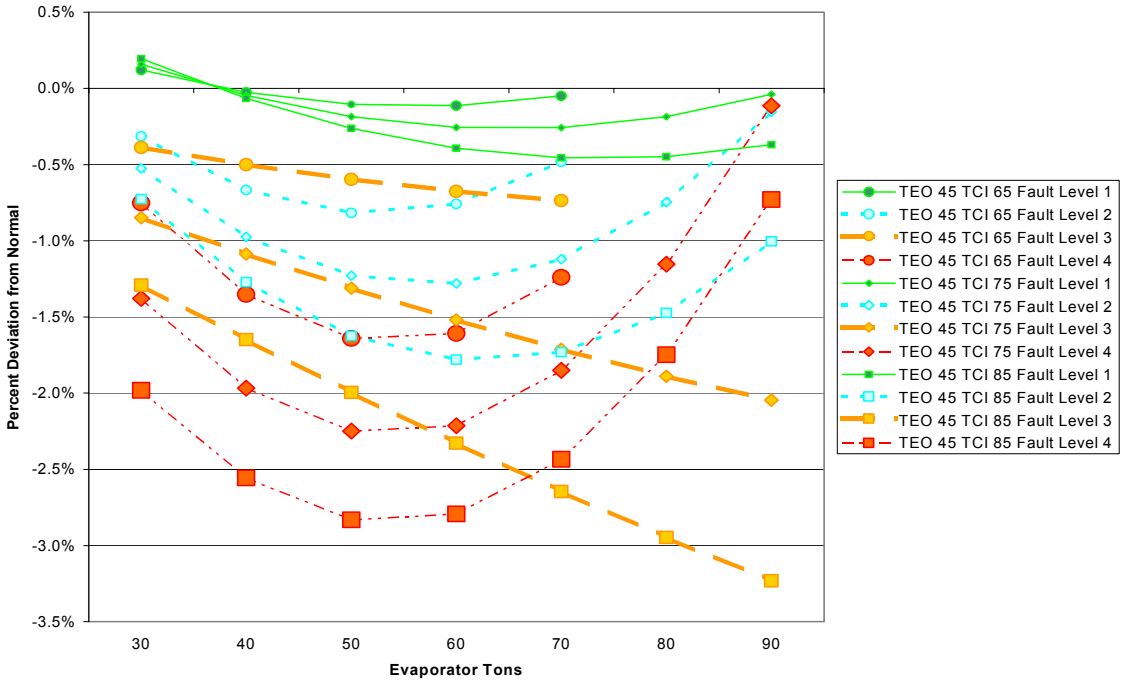

Figure 4.6: Deviation in evaporator pressure for reduced evaporator water flow.

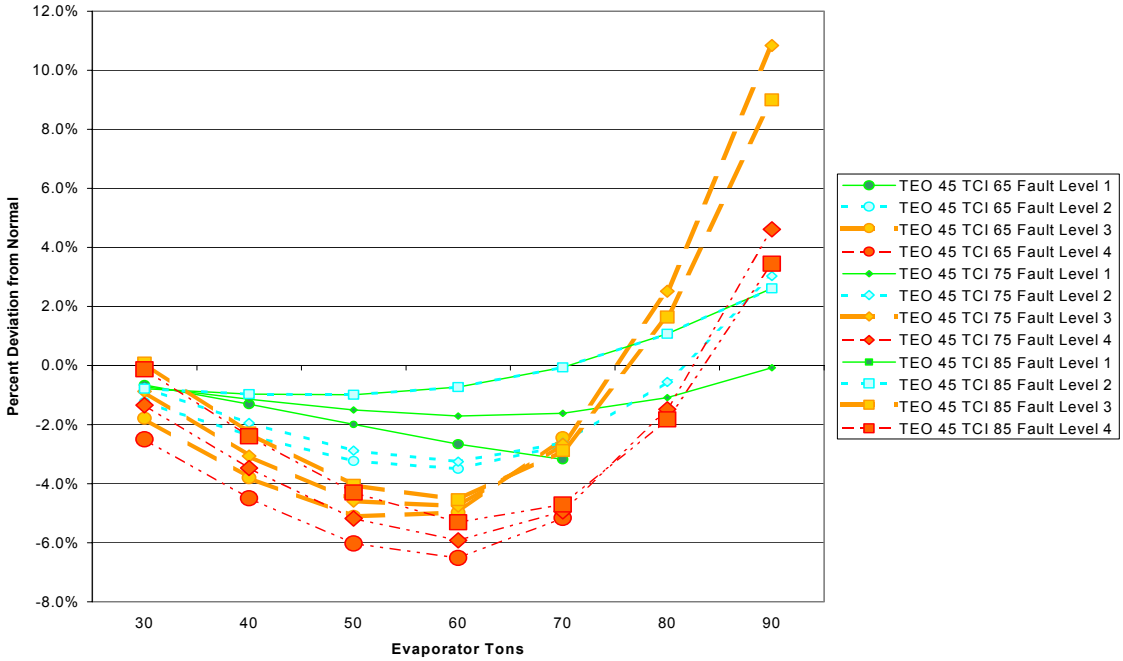

Figure 4.7: Deviation in discharge superheat for reduced evaporator water flow.

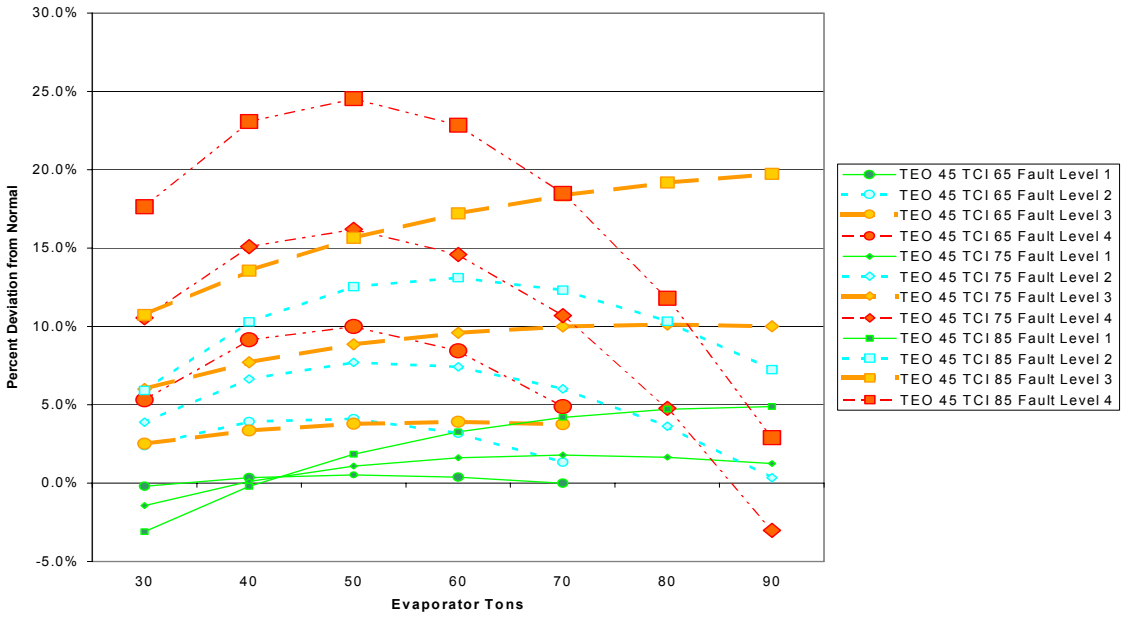

Figure 4.8: Deviation in evaporator approach temperature for reduced evaporator water flow.

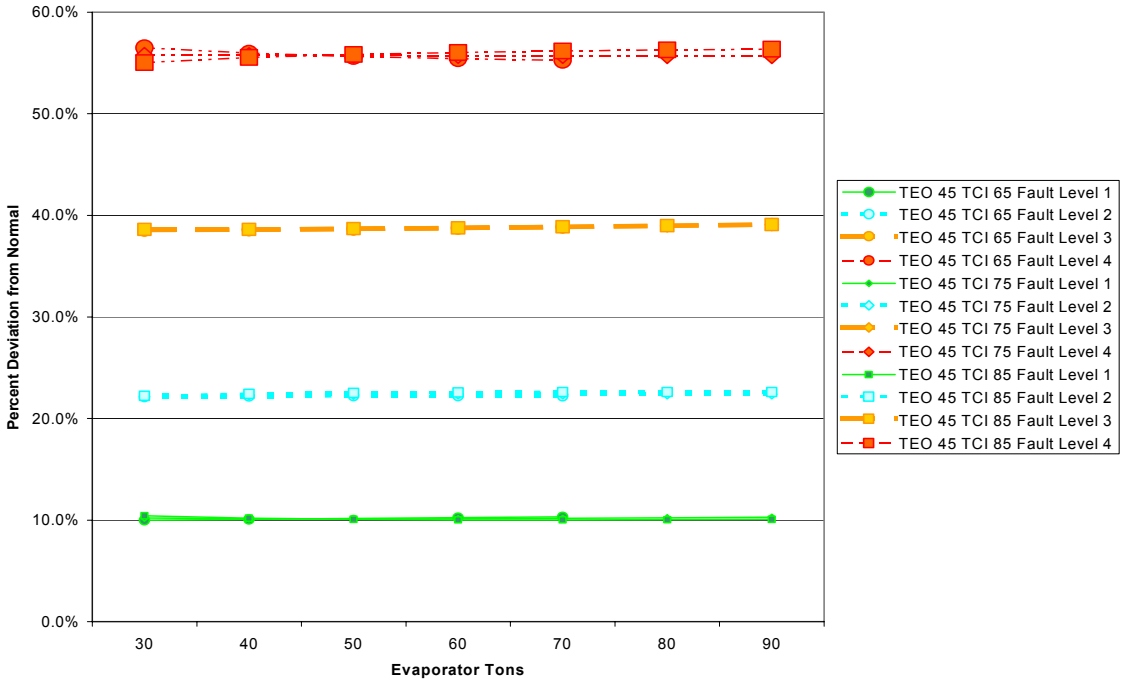

Figure 4.9: Deviation in evaporator water temperature difference for reduced evaporator water flow.

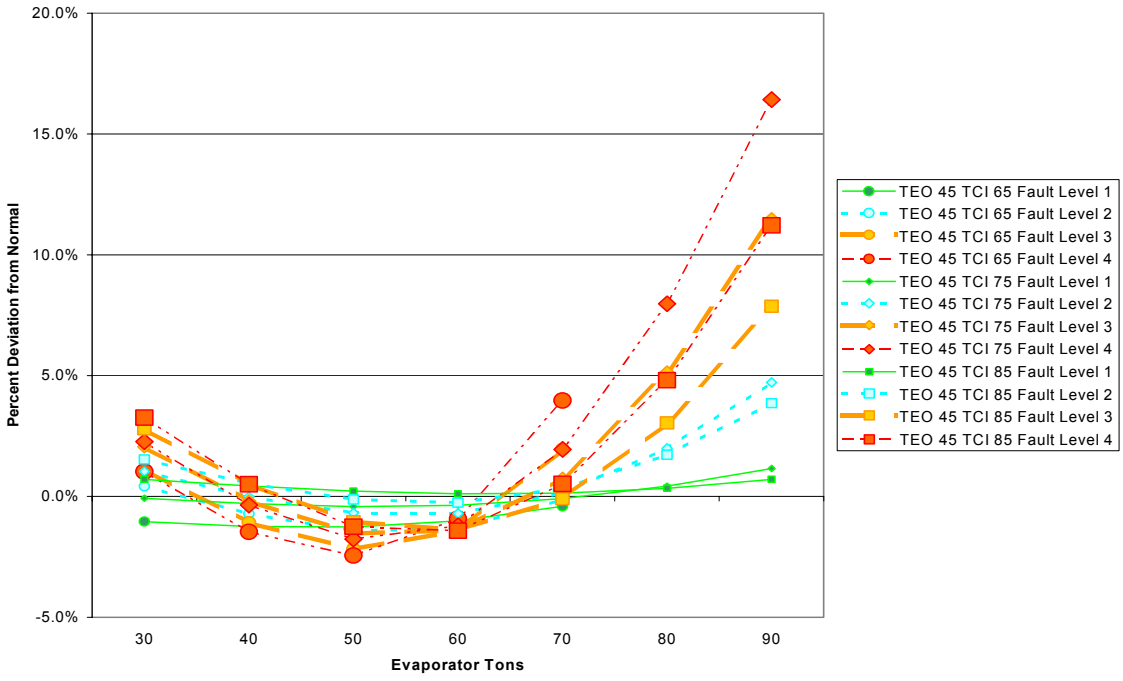

Figure 4.10: Deviation in kW/ton for reduced evaporator water flow.

4.5 Refrigerant Leak

Removing refrigerant from the system simulated the refrigerant leak. The base refrigerant charge in the system was 300 pounds (manufacturer recommended). Each fault level reduced the refrigerant charge by 10% as shown in Table 4.9. The system was initially brought to a vacuum before charging it to 180 pounds (Fault Level 4). The fault tests were run in reverse order, with each successive test adding 30 pounds of refrigerant. The amount of refrigerant added was weighed on an industrial scale with an uncertainty of ± 0.5 pounds.

The error in the actual charge is less than 1%. Each additional 30 pounds of refrigerant was measured from the same recovery tank. Thus the actual amount of refrigerant added was based on a single reference point, rather than on the last charge level.

Table 4.9: Fault levels for refrigerant leak.

Case	Desired Condition	Actual Charge
Normal Operation	300 lbs refrigerant	300 lbs
Fault Level 1	10% reduction in charge	270 lbs
Fault Level 2	20% reduction in charge	240 lbs
Fault Level 3	30% reduction in charge	210 lbs
Fault Level 4	40% reduction in charge	180 lbs

As listed in Table 4.10, the trends in condenser pressure (PRC), refrigerant subcooling (TRC_sub), and condenser approach temperature (TCA) were expected; however, no noticeable trends were found for evaporator pressure (PRE), suction superheat (Tsh_suc), or evaporator approach temperature (TEA). Less refrigerant in the system will naturally cause both the condenser and evaporator pressures to be lower; nevertheless, the expansion valve was able to compensate to maintain a constant pressure in the evaporator. The lower condenser pressure caused a lower saturation temperature, thus reducing the subcooling potential. Moreover, the condenser approach temperature is

lower because both the water and refrigerant temperatures are closer together at the inlet (water temperature held constant while refrigerant temperature was lower).

One surprising outcome of this testing was the increase in cooling capacity by as much as 10% (as directly observed from the test results). Apparently the design charge has a significant factor of safety built-in; moreover, the expansion valve was able to compensate by continuing to open further. At some point, the expansion valve would no longer be able to compensate for refrigerant loss and the evaporator pressure would drop and the superheat would increase. Chillers that use a fixed orifice would exhibit a performance penalty at smaller refrigerant charges.

Table 4.10: Average deviations for refrigerant leak.

	Fault Level 1	Fault Level 2	Fault Level 3	Fault Level 4
kW	0.6%	0.4%	-0.9%	-0.5%
PRE	-0.5%	-1.1%	-0.5%	-1.1%
PRC	0.4%	-0.4%	-2.2%	-3.0%
TRC_sub	0.9%	-4.7%	-35.5%	-66.0%
Tsh_suc	6.1%	12.5%	6.6%	8.9%
Tsh_dis	0.3%	0.3%	-1.1%	-1.3%
TEA	3.6%	9.2%	5.8%	10.4%
TCA	8.3%	-6.1%	-37.2%	-53.0%
TEI-TEO	-0.1%	0.1%	0.0%	0.1%
TCO-TCI	-0.4%	-0.6%	-0.1%	-0.1%
kW/ton	0.4%	0.2%	-1.2%	-0.8%
TO_sump	0.2%	0.1%	-0.1%	0.0%
TO_feed	0.1%	0.3%	0.3%	0.5%
PO_feed	4.7%	4.7%	4.2%	4.3%
PO_net	7.0%	6.6%	5.8%	6.1%

Detailed results are presented in Figures 4.11 to 4.14. Although the trends in Figure 4.14 are barely above the noise level in the measurements, it is possible to see an improvement in the performance of the chiller at reduced charge levels. The trends in Figure 4.14 suggest a possible optimum charge at about 210 pounds of refrigerant (strictly from a performance perspective).

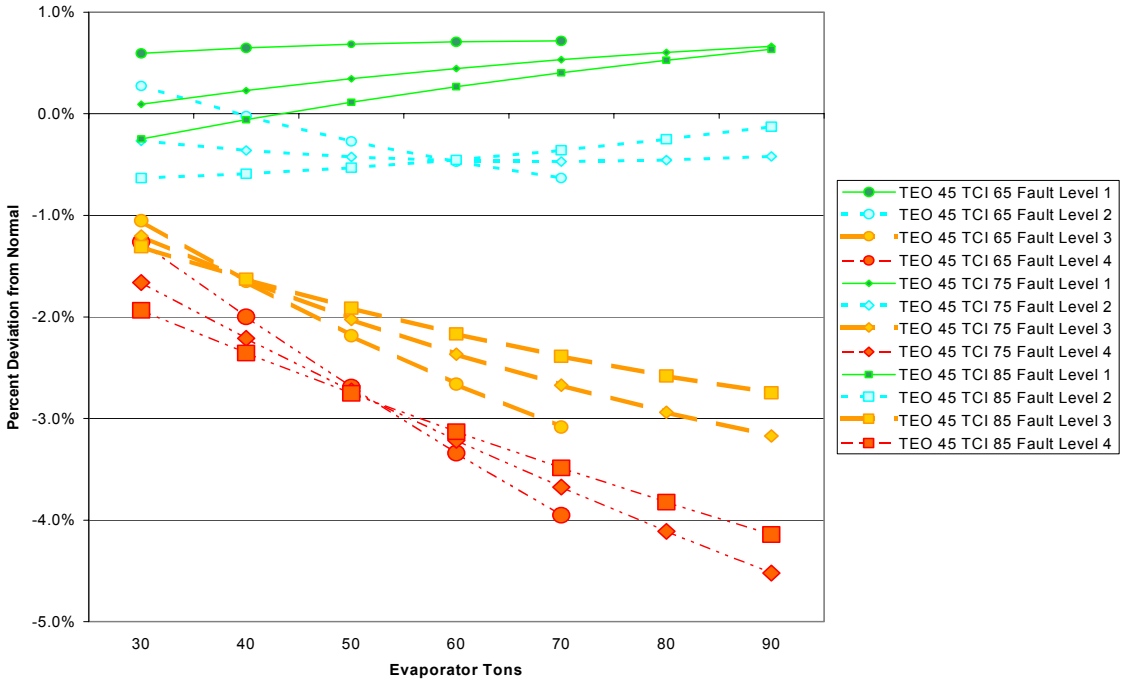

Figure 4.11: Deviation in condenser pressure for refrigerant leak.

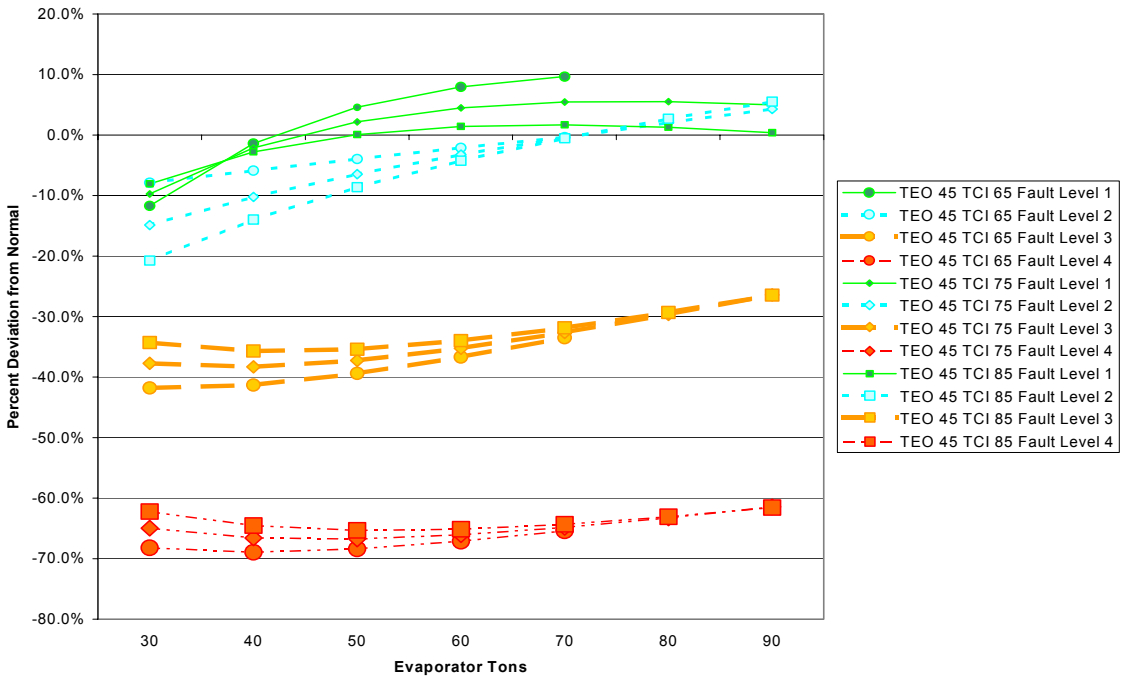

Figure 4.12: Deviation in subcooling for refrigerant leak.

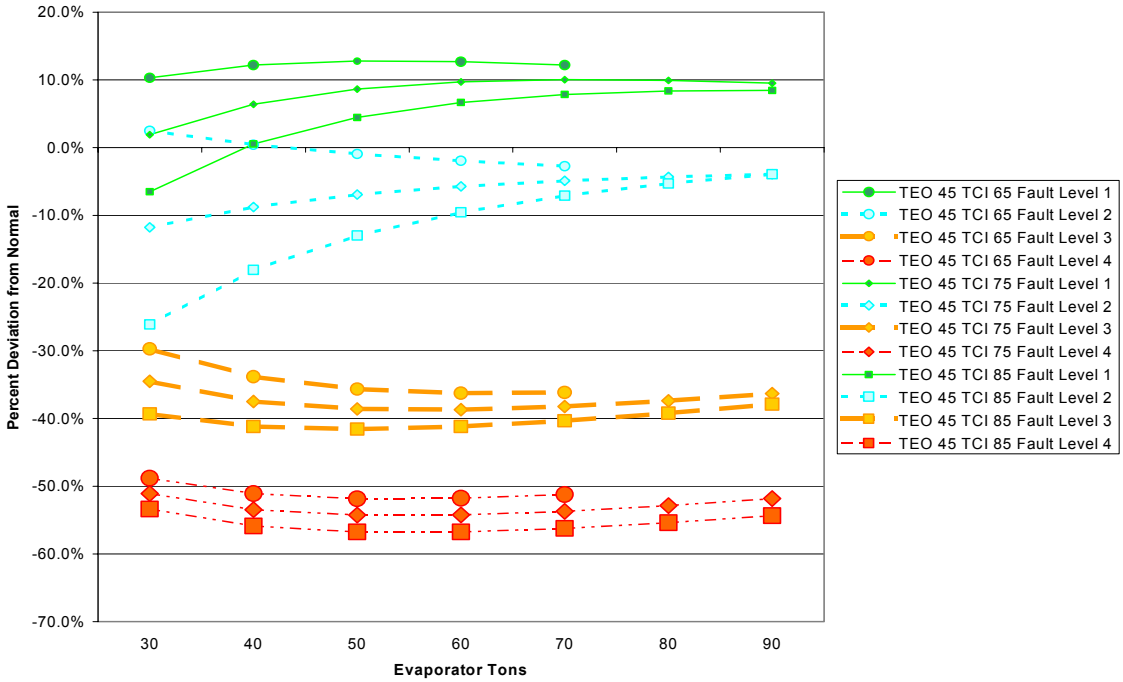

Figure 4.13: Deviation in condenser approach temperature for refrigerant leak.

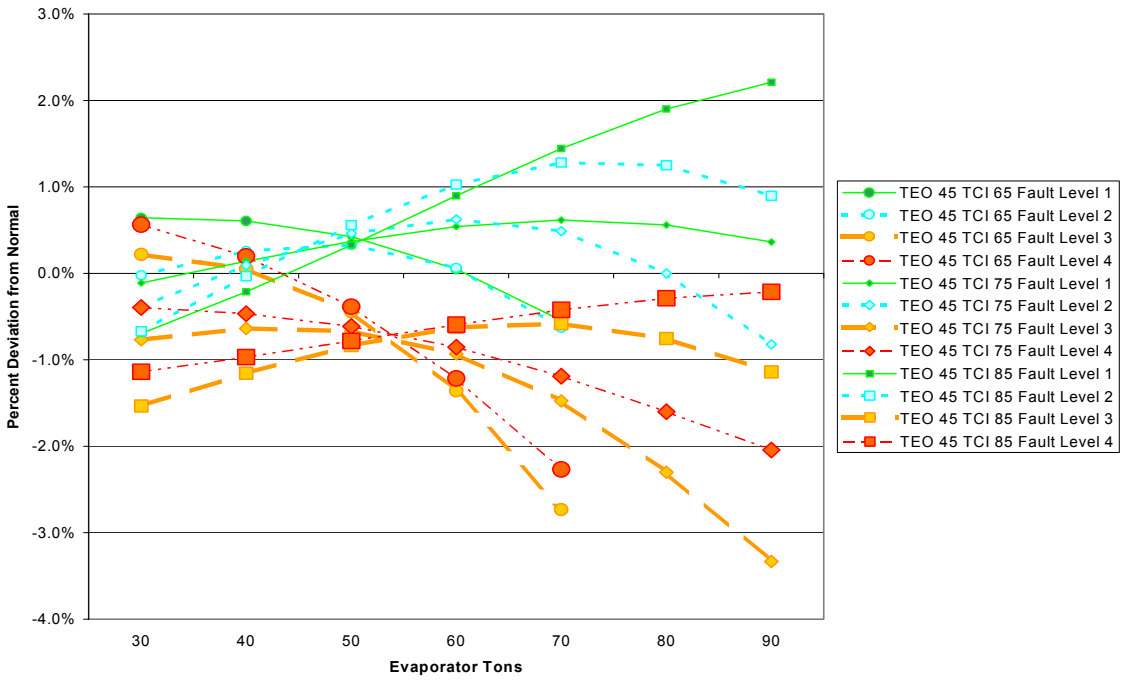

Figure 4.14: Deviation in kW/ton for refrigerant leak.

4.6 Refrigerant Overcharge

Adding refrigerant to the system simulated the refrigerant overcharge condition. The base refrigerant charge in the system was 300 pounds. Each fault level increased the refrigerant charge by 10% as shown in Table 4.11. These fault tests were a natural continuation of the refrigerant leak testing done earlier, with each successive test adding 30 pounds of refrigerant. The amount of refrigerant added was weighed on a laboratory scale with an uncertainty of ± 0.1 pounds.

The error in the actual charge is less than 1%. Each additional 30 pounds of refrigerant was added from a 30-pound net weight non-reusable canister. Thus the actual amount of refrigerant added was based on a moving reference point, with the final charge having an uncertainty equaling the accumulated uncertainty of the previous measurements (± 0.5 pounds).

Table 4.11: Fault levels for refrigerant overcharge.

Case	Desired Condition	Actual Charge
Normal Operation	300 lbs refrigerant	300 lbs
Fault Level 1	10% increase in charge	330 lbs
Fault Level 2	20% increase in charge	360 lbs
Fault Level 3	30% increase in charge	390 lbs
Fault Level 4	40% increase in charge	420 lbs

As shown in Table 4.12, the trends in condenser pressure (PRC), refrigerant subcooling (TRC_sub), and condenser approach temperature (TCA) were expected; however, no noticeable trends were found for evaporator pressure (PRE), suction superheat (Tsh_suc), or evaporator approach temperature (TEA). More refrigerant in the system will naturally cause both the condenser and evaporator pressures to be higher; nevertheless, the expansion valve was able to compensate to maintain a constant pressure in the evaporator. The higher condenser pressure caused a higher saturation temperature, thus increasing the subcooling potential. Moreover, the condenser approach temperature is higher because both the water and refrigerant temperatures are further apart at the inlet (water temperature held constant while refrigerant temperature was higher). The higher

condenser pressure created a greater pressure lift for the compressor to overcome, and thus caused a reduction in capacity and efficiency.

The trends for refrigerant overcharge are the opposite of those seen for the refrigerant leak testing. Likewise, the expansion valve was able to compensate for greater refrigerant charge by restricting refrigerant flow, thus keeping the evaporator pressure constant (lower than it would naturally be). Again, those chillers that use a fixed orifice would notice a performance penalty earlier.

Table 4.12: Average deviations for refrigerant overcharge.

	Fault Level 1	Fault Level 2	Fault Level 3	Fault Level 4
kW	1.9%	2.4%	4.8%	8.5%
PRE	-1.0%	-1.5%	-1.3%	-1.0%
PRC	2.3%	2.9%	6.4%	11.3%
TRC_sub	25.7%	32.2%	68.9%	113.1%
Tsh_suc	10.9%	14.2%	12.7%	10.0%
Tsh_dis	1.2%	2.3%	3.3%	5.1%
TEA	9.1%	12.8%	10.9%	7.3%
TCA	39.5%	44.1%	79.0%	129.3%
TEI-TEO	0.0%	0.0%	0.0%	0.1%
TCO-TCI	0.0%	0.7%	4.8%	10.2%
kW/ton	1.8%	2.5%	4.9%	9.0%
TO_sump	0.4%	0.3%	1.2%	2.1%
TO_feed	0.1%	0.0%	0.6%	1.1%
PO_feed	4.8%	4.8%	5.1%	5.6%
PO_net	6.8%	7.3%	7.1%	7.8%

Figures 4.15 through 4.18 more clearly show that the lower fault levels had little impact on the system; however, beyond a 20% overcharge the system performance dropped significantly.

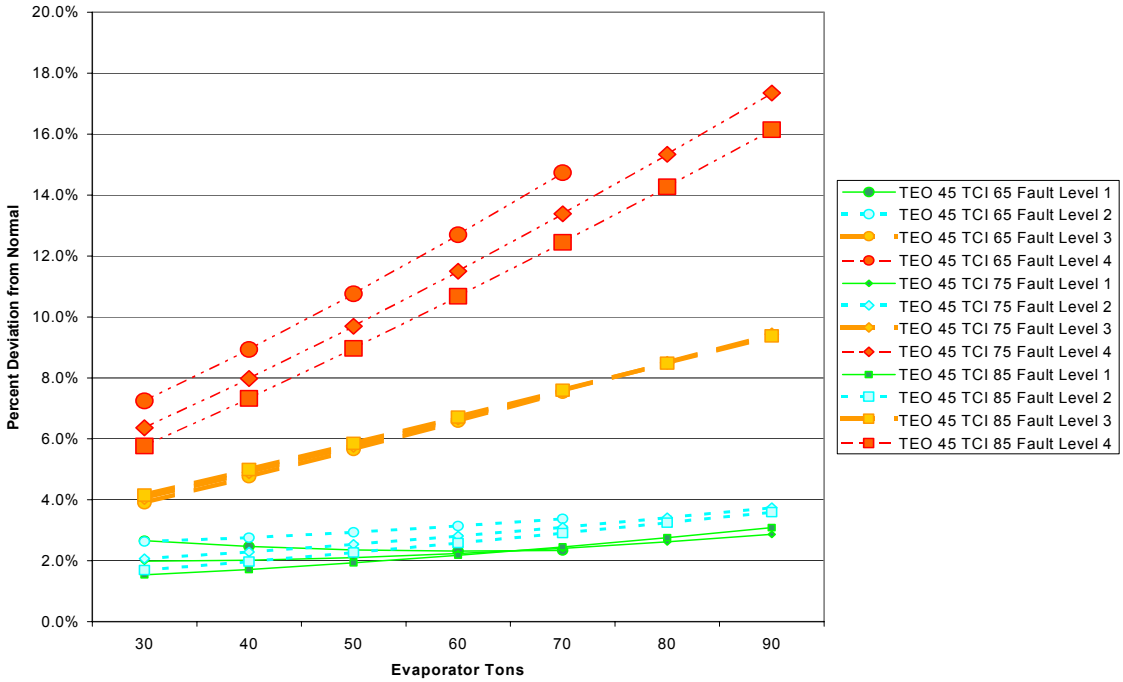

Figure 4.15: Deviation in condenser pressure for refrigerant overcharge.

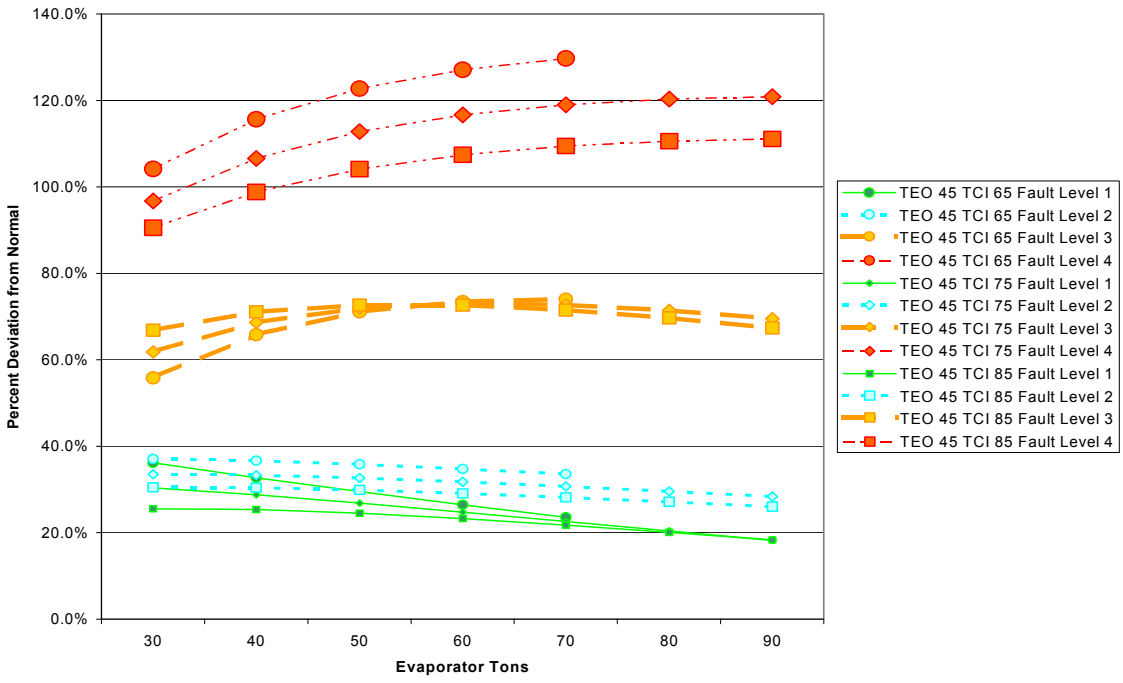

Figure 4.16: Deviation in subcooling for refrigerant overcharge.

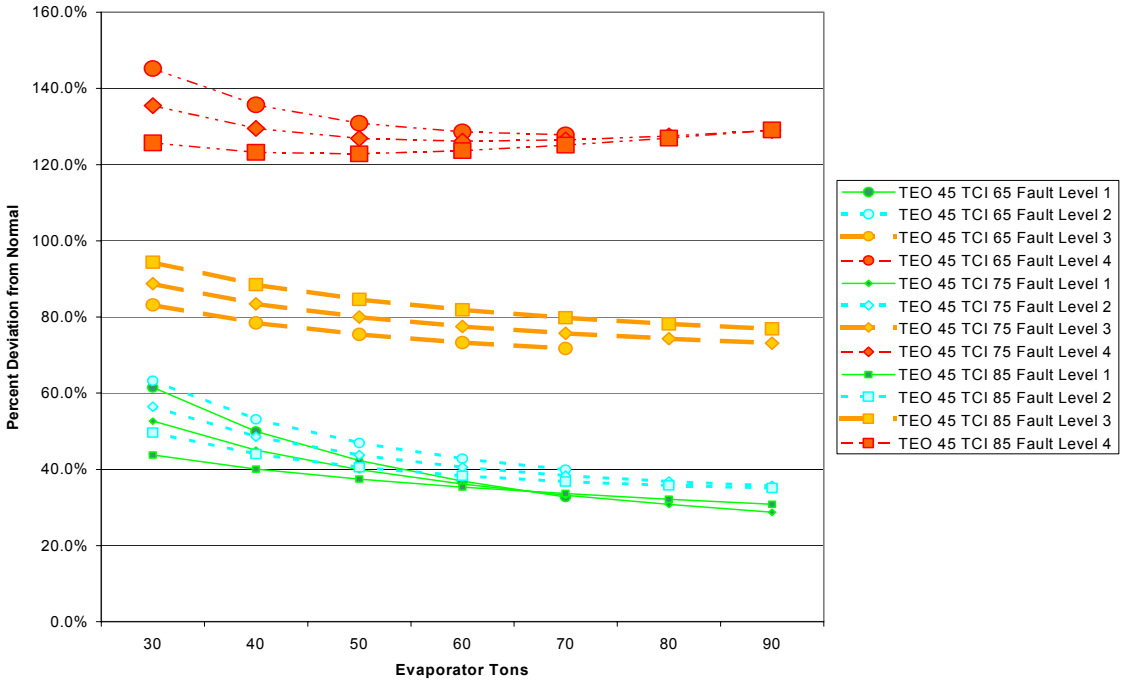

Figure 4.17: Deviation in condenser approach temperature for refrigerant overcharge.

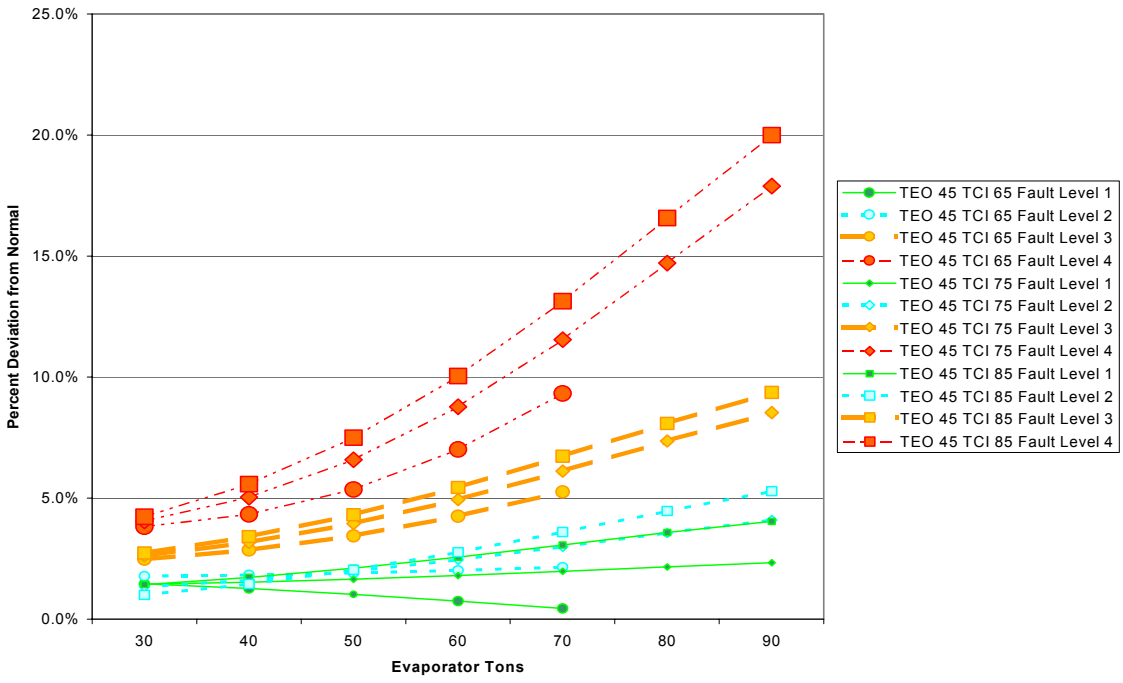

Figure 4.18: Deviation in kW/ton for refrigerant overcharge.

4.7 Excess Oil

Adding oil to the system simulated the excess oil condition. The base oil charge in the system was 22 pounds. Each fault level increased the oil charge by varying amounts as shown in Table 4.13. The amount of oil added was weighed on a laboratory scale with an uncertainty of ± 0.1 pounds.

The base oil charge of 22 pounds is based on specifications provided by the chiller manufacturer. In an attempt to determine the actual oil charge, about 13 pounds of oil were recovered (the rest presumably was trapped in various locations, some could be seen through the sight glass near one of the oil pumping reservoirs). The remaining trapped oil was assumed to be approximately 9 pounds—this could not be experimentally verified, since the only way to remove all the oil would have been to dismantle the compressor. Hence the uncertainty in the base oil charge is unknown (theoretically could be as high as ± 5 pounds), but the amount of excess oil charged into the system is known to within an error of less than 2%.

Table 4.13: Fault levels for excess oil.

Case	Desired Condition	Actual Charge
Normal Operation	22 lbs oil (2.75 gallons)	22 lbs
Fault Level 1	14% increase in charge	25 lbs
Fault Level 2	32% increase in charge	29 lbs
Fault Level 3	50% increase in charge	33 lbs
Fault Level 4	68% increase in charge	37 lbs

The excess oil fault was introduced with the expectation that it would migrate into the evaporator and inhibit heat transfer; however, these experimental studies show that no oil migrated from the compressor. It is possible that migration may occur over time, but that is beyond the scope of this study.

Consequently, all the added oil simply filled up the compressor cavity and submerged some of the gearing. The viscous effects caused by the excess oil lead to increased mechanical losses in the compressor. The only visible trends as shown in

Table 4.14 are an increase in compressor power and oil temperatures (TO_feed and TO_sump).

After introducing this fault, it was determined that the oil pressure measurements were useless for fault detection and diagnosis. The oil pressure is independently regulated and usually does not correlate well with any of the input variables. The oil temperatures are also independently regulated, but can be influenced by the system. In this case the oil was heated through frictional losses caused by excessive oil in the gearing.

Although excess oil was studied in this project, loss of oil was not. The reason is that loss of oil is a much more severe fault. Consequently, chiller manufacturers already monitor for insufficient oil by checking oil pressure. A loss of oil pressure results in an immediate compressor shut down.

Table 4.14: Average deviations for excess oil.

	Fault Level 1	Fault Level 2	Fault Level 3	Fault Level 4
kW	0.7%	1.4%	2.7%	5.2%
PRE	-0.8%	-0.1%	-0.1%	-0.8%
PRC	0.1%	0.2%	0.2%	0.7%
TRC_sub	1.6%	2.3%	2.6%	6.2%
Tsh_suc	8.3%	2.6%	3.7%	1.9%
Tsh_dis	0.7%	0.3%	0.5%	1.7%
TEA	6.7%	1.3%	1.5%	3.0%
TCA	2.3%	3.8%	4.7%	10.8%
TEI-TEO	0.0%	-0.1%	-0.1%	-0.1%
TCO-TCI	-0.3%	-0.4%	-0.5%	1.2%
kW/ton	0.7%	1.3%	2.8%	5.8%
TO_sump	2.2%	6.6%	10.3%	16.0%
TO_feed	1.8%	4.5%	7.5%	13.9%
PO_feed	2.8%	2.1%	1.3%	2.4%
PO_net	4.0%	2.9%	1.6%	3.7%

Figures 4.19 to 4.21 show the trends in the most important measured variables at some of the different operating conditions.

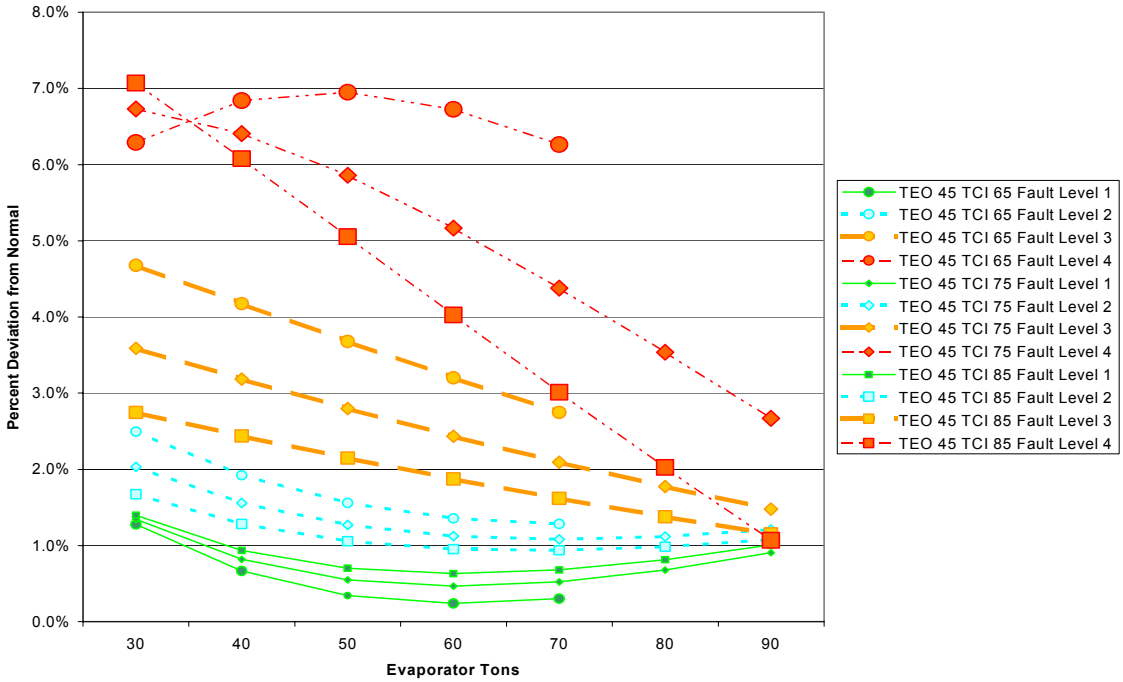

Figure 4.19: Deviation in kW for excess oil.

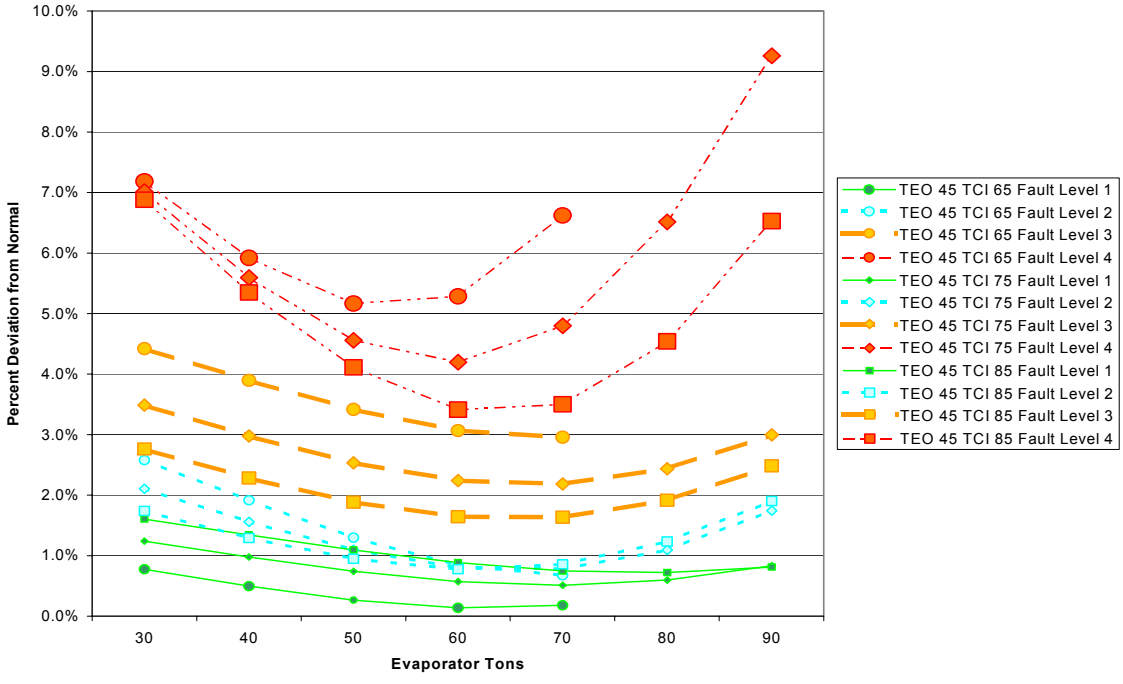

Figure 4.20: Deviation in kW/ton for excess oil.

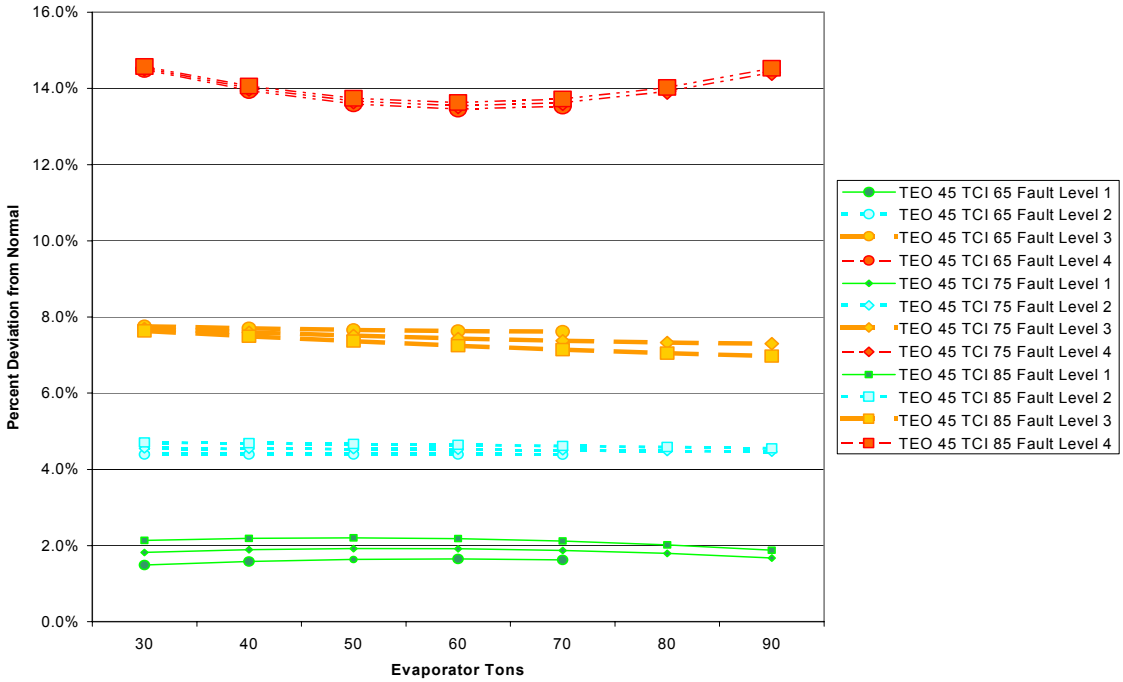

Figure 4.21: Deviation in oil feed temperature for excess oil.

4.8 Condenser Fouling

Tubes were plugged in the condenser to simulate condenser fouling. The condenser contains 164 tubes; approximately half are used in the first pass and the remaining tubes for the second pass. Each fault level reduced the number of available tubes as shown in Table 4.15. The blocked tubes were evenly distributed between the two passes in a spread-out pattern as shown in Figure 4.22.

Among prior investigations into condenser fouling simulations, some researchers have attempted different methods to simulate condenser fouling (including reducing the condenser water flow rate). The decision to block tubes was made because it lowers the effective heat transfer coefficient (the actual heat transfer coefficient remains nearly constant, but the surface area is reduced) and affects the water flow rate in a manner consistent with true condenser fouling (a 45% reduction in tube area resulted in a 5% drop in condenser water flow rate).

Table 4.15: Fault levels for condenser fouling.

Case	Desired Condition	Actual Condition
Normal Operation	164 unblocked tubes	No blocked tubes
Fault Level 1	12% reduction in tubes	20 blocked tubes
Fault Level 2	20% reduction in tubes	33 blocked tubes
Fault Level 3	30% reduction in tubes	49 blocked tubes
Fault Level 4	45% reduction in tubes	74 blocked tubes

Figure 4.22: Plug pattern for condenser fouling fault level 3.

The trends given in Table 4.16 for condenser pressure (PRC), condenser approach temperature (TCA), and power consumption (kW) were expected. With less surface area available for heat transfer—simulating lower heat transfer coefficients—the condenser pressure increased. This in turn increased the pressure lift and made the compressor operate less efficiently. However, the expansion valve once again corrected for the lost condenser area and maintained a relatively constant superheat (Tsh_suc) and evaporator pressure (PRE). The subcooling (PRC_sub) remained moderately constant since the total heat rejection and refrigerant flow did not change much. By blocking tubes in the condenser, the available cross sectional area for water flow is reduced. Thus the water passes through the condenser at a higher velocity and has less time to reach thermal equilibrium with the refrigerant, resulting in a higher condenser approach temperature.

The increase in condenser water temperature difference is significant, but can be explained by the slight loss in condenser water flow.

The important measured variables are once again presented in several figures following Table 4.16. In Figures 4.23 and 4.26 the second fault level shows some noisy behavior in the compressor power input, but the deviation is still within the uncertainty of the measurement and regression analysis. The same can be said of the first fault level in Figure 4.25.

Table 4.16: Average deviations for condenser fouling.

	Fault Level 1	Fault Level 2	Fault Level 3	Fault Level 4
kW	0.6%	0.7%	1.9%	3.9%
PRE	-1.1%	0.7%	0.2%	0.0%
PRC	1.0%	1.3%	2.3%	4.5%
TRC_sub	4.1%	0.1%	4.9%	1.2%
Tsh_suc	11.6%	-6.1%	-5.3%	-0.9%
Tsh_dis	1.0%	-0.6%	-0.2%	0.8%
TEA	8.3%	-4.6%	-2.4%	0.3%
TCA	14.8%	14.9%	28.1%	53.8%
TEI-TEO	-0.2%	-0.2%	-0.1%	-0.1%
TCO-TCI	0.4%	2.5%	2.8%	6.4%
kW/ton	0.8%	0.9%	1.9%	4.1%
TO_sump	0.1%	0.2%	0.3%	0.7%
TO_feed	0.3%	0.5%	0.2%	0.5%
PO_feed	0.0%	-0.5%	-0.2%	-0.3%
PO_net	0.3%	-1.2%	-0.3%	-0.3%

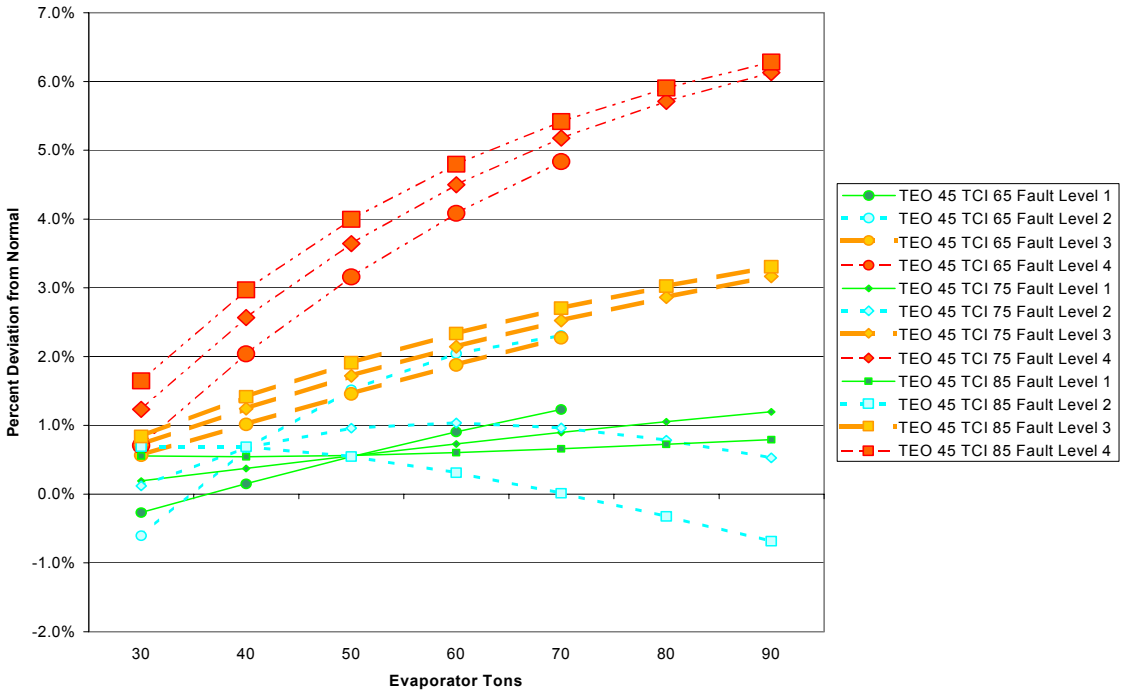

Figure 4.23: Deviation in kW for condenser fouling.

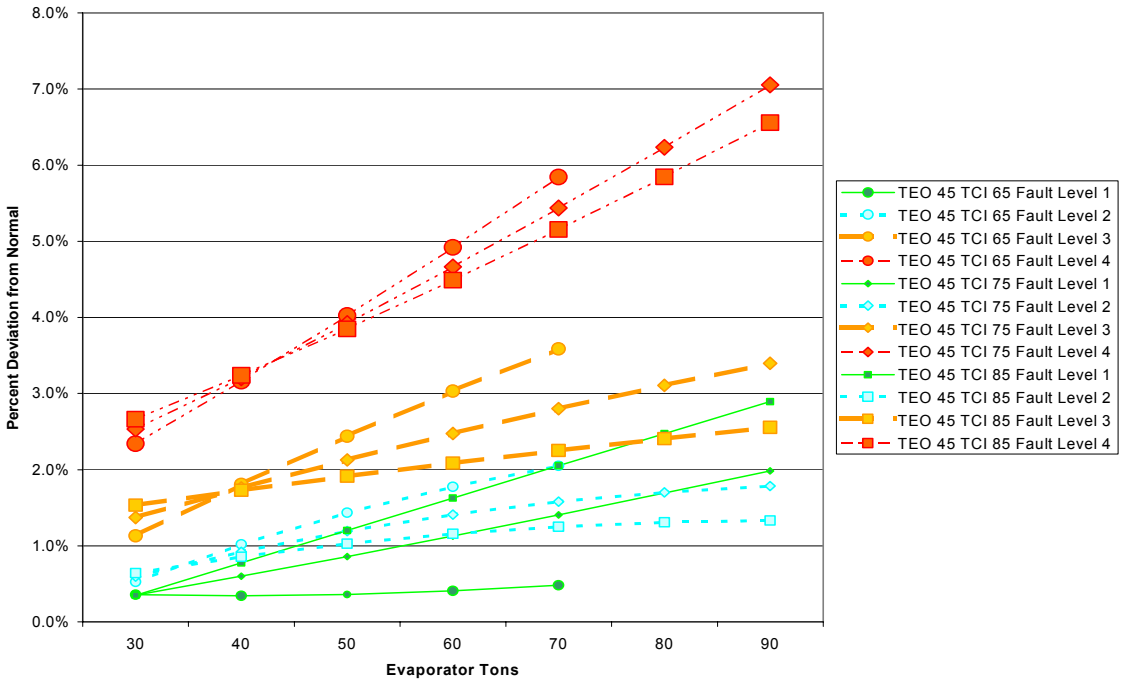

Figure 4.24: Deviation in condenser pressure for condenser fouling.

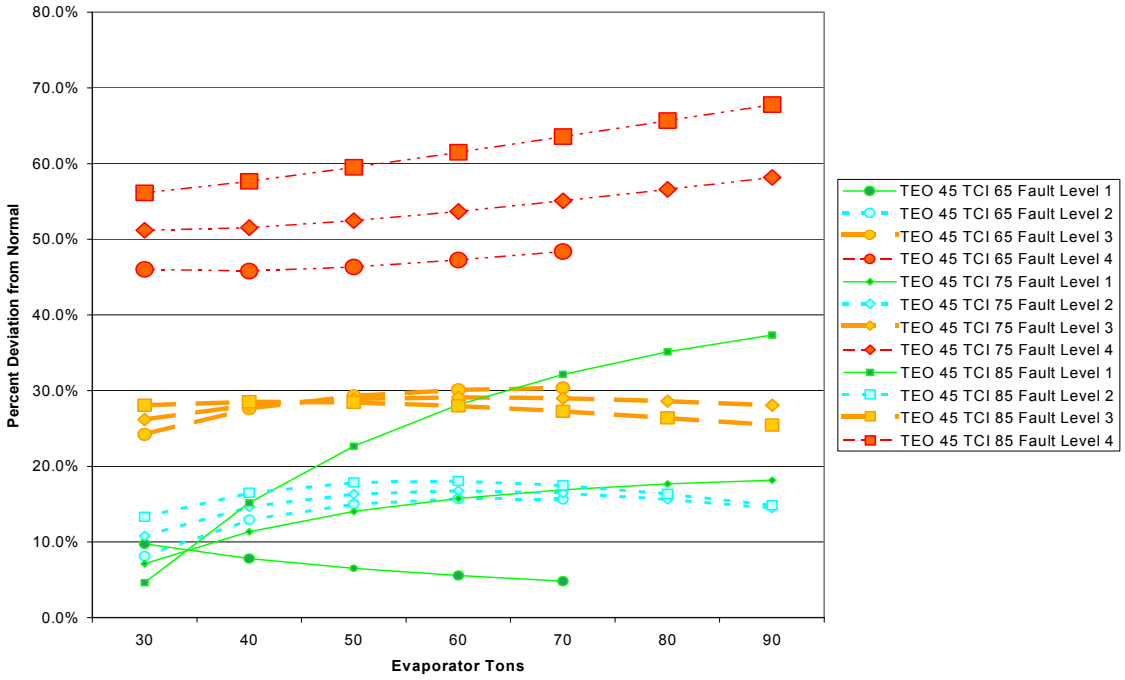

Figure 4.25: Deviation in condenser approach temperature for condenser fouling.

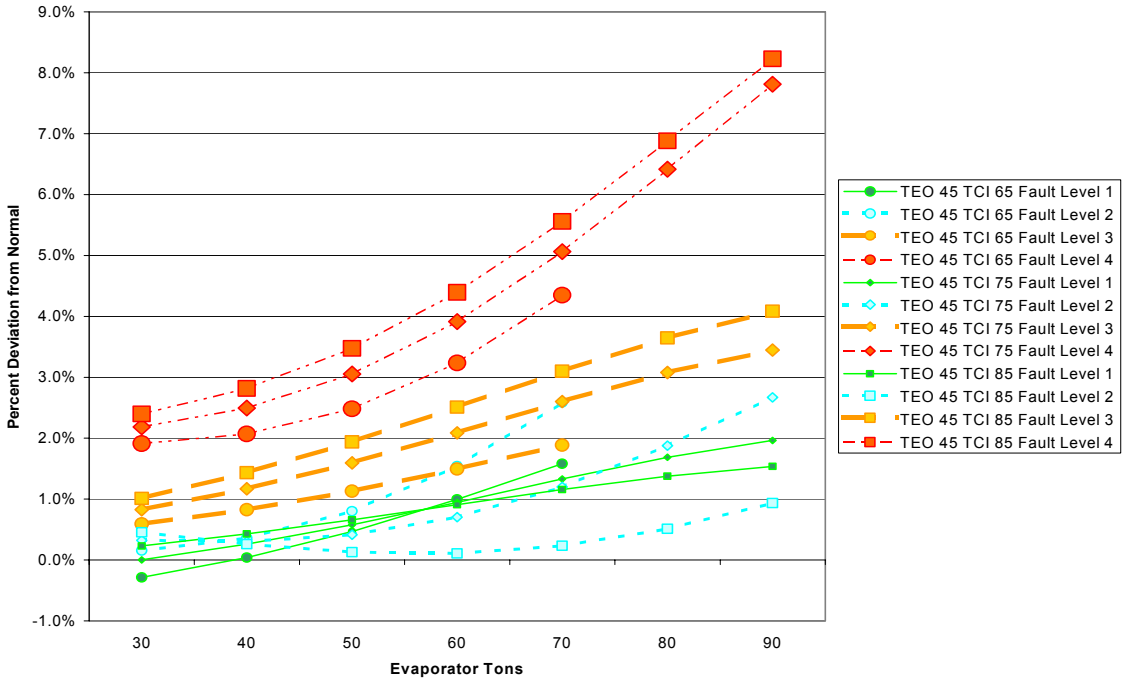

Figure 4.26: Deviation in kW/ton for condenser fouling.

4.9 Non-Condensables in Refrigerant

Nitrogen was added to the system to simulate non-condensables in the refrigerant. The amount of nitrogen present in the system for each of the fault levels is shown in Table 4.17. The fault level testing was run in reverse order, with the most severe fault tested first (further explained in Appendix B.5). Each subsequent fault was then tested after purging some nitrogen out of the system. The actual amount of nitrogen in the system for each fault case was determined using Dalton's law of additive pressures. The uncertainty in the calculation was ± 0.05 pounds (or about ± 0.5% by volume when calculated at a temperature of 72°F). The error in characterizing this fault is significant; nevertheless, it arises because it takes very little nitrogen to develop some adverse responses from the chiller. Even the mildest fault level is easily detected.

Non-condensables are normally just air that is accidentally introduced into the refrigerant during servicing. For this study, laboratory grade nitrogen was chosen in order to avoid the risk of moisture contamination associated with introducing air into the system. The substitution is validated by the fact that air is about 79% nitrogen, and the molecular weight of nitrogen is only 2% less than that of air.

Table 4.17: Fault levels for non-condensables in refrigerant.

Case	Desired Condition	Actual Condition
Normal Operation	No Nitrogen	No Nitrogen
Fault Level 1	1% by volume Nitrogen	0.10 pounds (1.0%)
Fault Level 2	2% by volume Nitrogen	0.16 pounds (1.7%)
Fault Level 3	3% by volume Nitrogen	0.22 pounds (2.4%)
Fault Level 4	5% by volume Nitrogen	0.54 pounds (5.7%)

Based on physical observations, nitrogen is trapped solely in the condenser during operation. The first trap is the liquid refrigerant at the bottom of the condenser; it is not logically possible for the nitrogen (a low density gas) to infiltrate the refrigerant (a high

density liquid) below it. On the contrary, the lighter nitrogen naturally tends to migrate upwards but is turned away by the second trap, the constant inrush of refrigerant vapor from the compressor.

System performance was more sensitive to the presence of non-condensables in the refrigerant than to any of the other faults tested (as shown in Table 4.18). The presence of just 1% by weight non-condensables rendered the chiller completely unusable. Yet it is also the easiest fault to detect—sometimes detectable when the chiller is turned off, since pressure readings are artificially inflated (over saturation pressure) when non-condensables are present in the refrigerant.

The following calculations are based on pressure measurements:

- Evaporator temperature derived from pressure using saturation tables
- Condenser temperature derived from pressure using saturation tables
- Suction superheat (Tsh_suc) calculated from suction line temperature minus evaporator temperature
- Discharge superheat (Tsh_dis) calculated from discharge temperature minus condenser temperature
- Liquid subcooling (TRC_sub) calculated from condenser temperature minus liquid line temperature
- Condenser approach temperature (TCA) calculated from condenser temperature minus leaving condenser water temperature
- Evaporator approach temperature (TEA) calculated from leaving evaporator water temperature minus evaporator temperature

Since non-condensables settle in the condenser during operation, the condenser pressure (PRC) is increased substantially, but the actual temperature increases by only a small amount. Therefore, the derived condenser temperature is higher than the actual temperature, thus causing the condenser approach temperature and subcooling temperature to be extraordinarily overstated.

Moreover, the higher condenser pressure increases the pressure lift across the compressor and results in severe capacity and efficiency penalties. As the amount of nitrogen in the system increases, the pressure lift becomes high enough to cause

surging—first at low loads with high condenser water temperatures, then eventually affecting all the operating conditions.

The one unexpected trend was the increase in the discharge superheat measurement. The nitrogen in the condenser would artificially inflate the condenser temperature measurement, thus diminishing the discharge superheat reading. However, the increase in the discharge temperature was even larger than the increase in the estimated condenser temperature. Therefore, the true discharge superheat increased by as much as 30% at the worst fault level.

Table 4.18: Average deviations for non-condensables in refrigerant.

	Fault Level 1	Fault Level 2	Fault Level 3	Fault Level 4
kW	4.8%	6.3%	7.8%	15.0%
PRE	0.9%	1.1%	1.6%	1.0%
PRC	8.3%	10.5%	12.6%	20.6%
TRC_sub	74.9%	93.9%	110.5%	177.7%
Tsh_suc	3.0%	-0.3%	-2.8%	3.2%
Tsh_dis	1.6%	1.9%	3.0%	7.5%
TEA	-4.8%	-6.6%	-9.5%	-6.1%
TCA	134.7%	166.0%	195.4%	315.8%
TEI-TEO	0.1%	0.0%	0.1%	-0.1%
TCO-TCI	1.3%	1.7%	2.7%	4.1%
kW/ton	4.7%	6.5%	8.1%	14.7%
TO_sump	0.5%	0.9%	2.0%	3.1%
TO_feed	0.2%	0.6%	1.4%	1.9%
PO_feed	-7.4%	-8.7%	-8.8%	-5.2%
PO_net	-10.1%	-11.8%	-12.0%	-7.2%

In addition to the fault levels presented here, there were a couple tests performed with trace amounts of nitrogen in the system. The results of these tests are contained in Table 4.19. The amount of nitrogen in the system could not be determined for these tests; however, some nitrogen was purged after the first test labeled ‘Trace’. The minimal amount of nitrogen in the ‘Trace2’ test did not affect performance, but was detectable in the subcooling and condenser approach temperature measurements.

Table 4.19: Average deviations for trace amounts of non-condensables in refrigerant.

	Trace2	Trace
kW	0.2%	0.4%
PRE	0.7%	0.3%
PRC	1.3%	2.4%
TRC_sub	13.1%	22.3%
Tsh_suc	3.4%	5.6%
Tsh_dis	-0.3%	0.0%
TEA	-4.2%	-1.4%
TCA	26.4%	42.8%
TEI-TEO	0.2%	0.1%
TCO-TCI	-0.8%	-0.5%
kW/ton	0.0%	0.6%
TO_sump	-0.4%	-0.3%
TO_feed	-0.2%	-0.5%
PO_feed	-3.6%	-4.5%
PO_net	-5.3%	-6.3%

As can be seen in Figures 4.29 and 4.30, the subcooling and condenser approach temperatures have enormous deviations that diminish at higher loads. This occurs because the offset caused by the non-condensables is nearly constant, whereas the measured variable increases at higher loads.

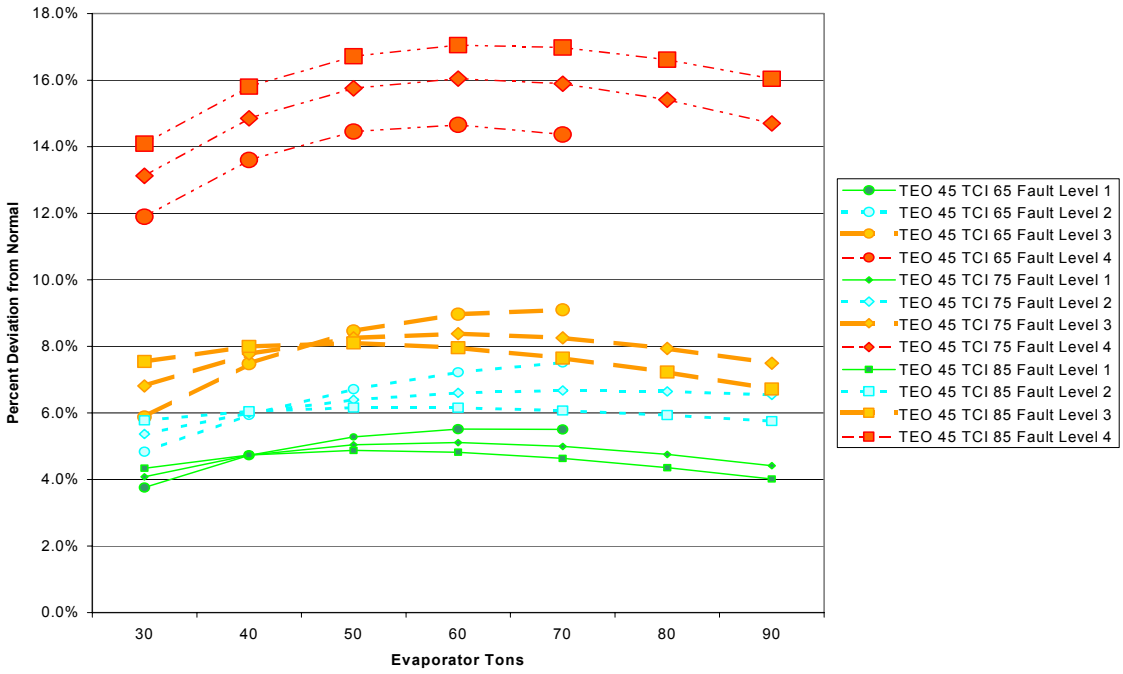

Figure 4.27: Deviation in kW for non-condensables in refrigerant.

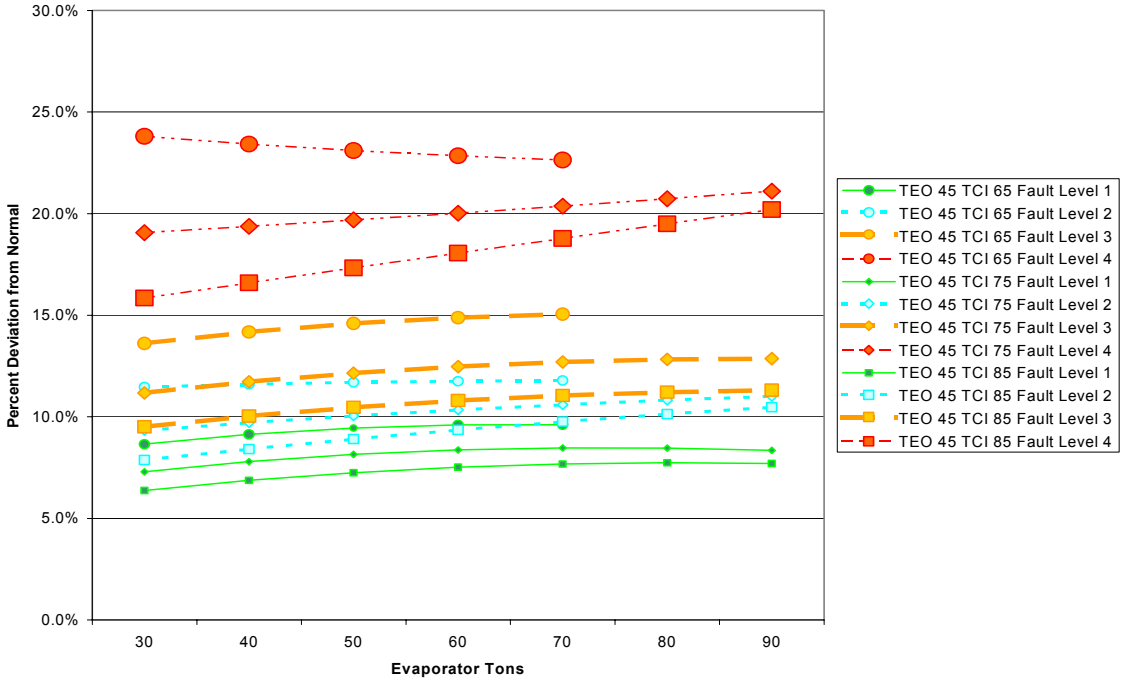

Figure 4.28: Deviation in condenser pressure for non-condensables in refrigerant.

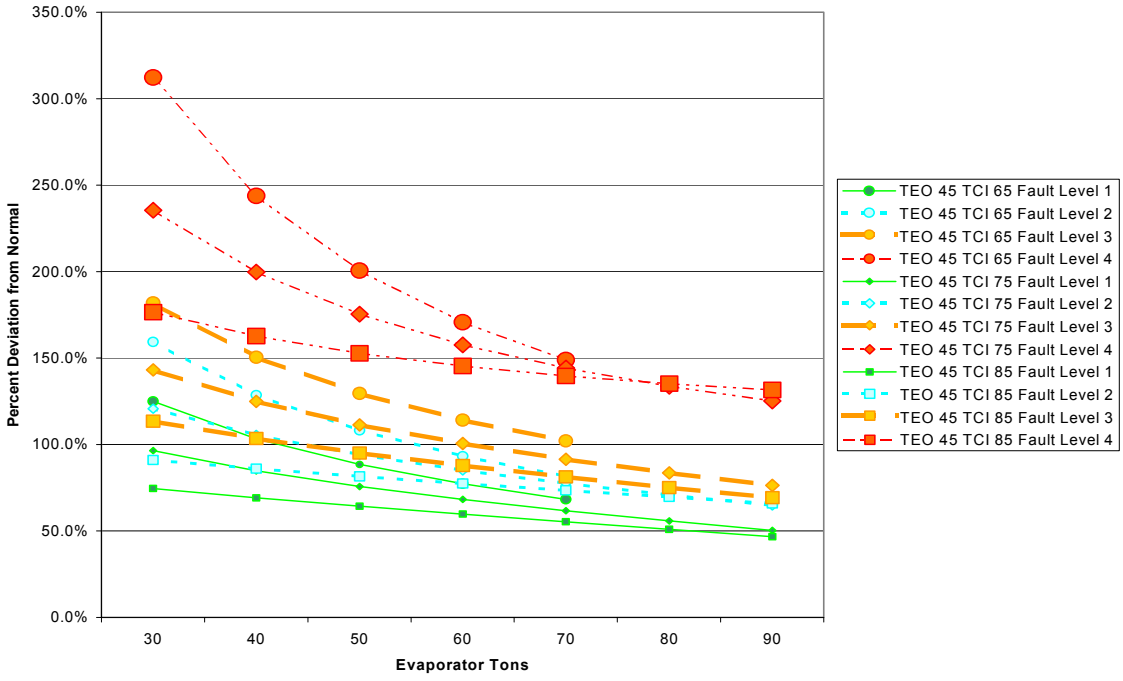

Figure 4.29: Deviation in subcooling for non-condensables in refrigerant.

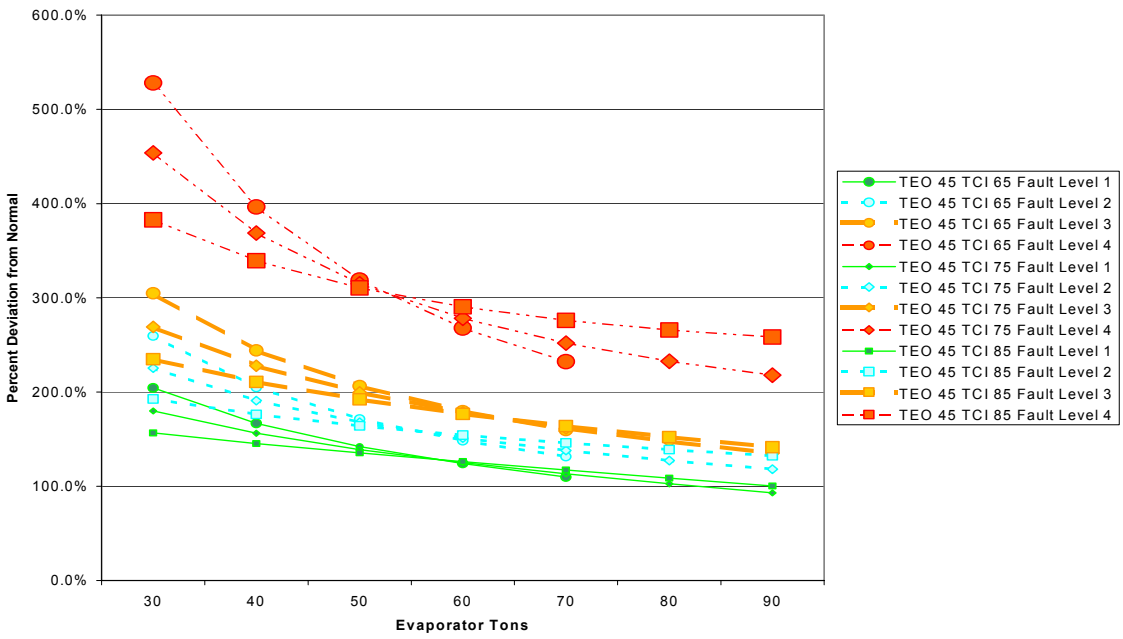

Figure 4.30: Deviation in condenser approach temperature for non-condensables in refrigerant.

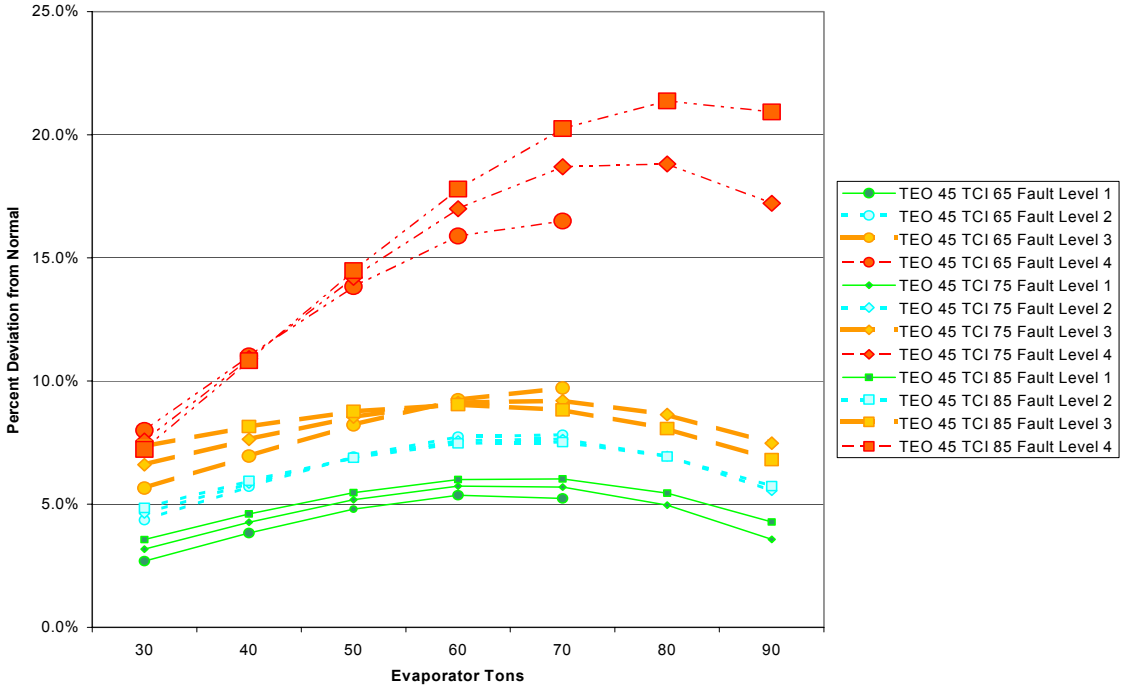

Figure 4.31: Deviation in kW/ton for non-condensables in refrigerant.

4.10 Defective Pilot Valve

The defective pilot valve was the only preexistent fault tested in the chiller. The fault was suspected during the commissioning phase of the chiller test facility, when the superheat could not be properly adjusted. Once the pilot valve was replaced, a substantial improvement in the superheat control as well as overall capacity confirmed the suspicion.

The pilot valve is a simple thermal expansion valve with a sensing bulb in the evaporator. It regulates refrigerant flow in a small liquid line that runs parallel to the main liquid line. This 'siphoned' refrigerant is then returned to the main liquid line via the main valve. The main valve position is controlled by the amount of refrigerant entering it via the liquid line controlled by the pilot valve.

Although data were collected before the pilot valve was replaced, there was one drawback—the condenser water flow was not yet up to specifications (its average flow rate was 20% lower than ARI standards, and its flow rate varied by as much as ± 10% during a test run). These problems were eventually solved, yet the fault data still needed to be compared to a normal test case under similar flow conditions. Therefore, the benchmark data set was selected from a test run completed a few days after the pilot valve replacement (it took a few days to properly adjust the superheat settings for all the operating conditions).

The average deviations for the defective pilot valve are presented in Table 4.20; however, in this case the averages are not meaningful (many of the individual deviations vary between negative to positive depending on the operating conditions).

Table 4.20: Average deviations for defective pilot valve.

	DPV
kW	0.4%
PRE	0.3%
PRC	-0.4%
TRC_sub	-4.1%
Tsh_suc	-8.2%
Tsh_dis	0.1%
TEA	-3.9%
TCA	-10.7%
TEI-TEO	-0.1%
TCO-TCI	0.8%
kW/ton	1.7%
TO_sump	0.0%
TO_feed	0.0%
PO_feed	0.4%
PO_net	0.3%

The greatest influence on the pilot valve was from the evaporator temperature, which is a function of the evaporator water leaving temperature (TEO). Therefore, some of the following figures are presented differently than the others to illustrate this effect. The first four figures are presented as two pairs, with each pair plotting the same variable against two different evaporator water leaving temperatures (the first one at 50°F, and the second at 40°F). The first pair of figures shows the effect of evaporator water leaving temperature on subcooling (TRC_sub; Figures 4.32 and 4.33). The second pair of figures shows the effect of evaporator water leaving temperature on discharge superheat (Tsh_dis; Figures 4.34 and 4.35). Note that the deviation in subcooling is much greater at the lower evaporator temperature, likewise so is the deviation in discharge superheat. Figures 4.36 and 4.37 show how certain measurements deviate differently at different condenser temperatures and chiller loads. Finally, Figure 4.38 shows that the performance was only seriously impacted at high loading conditions.

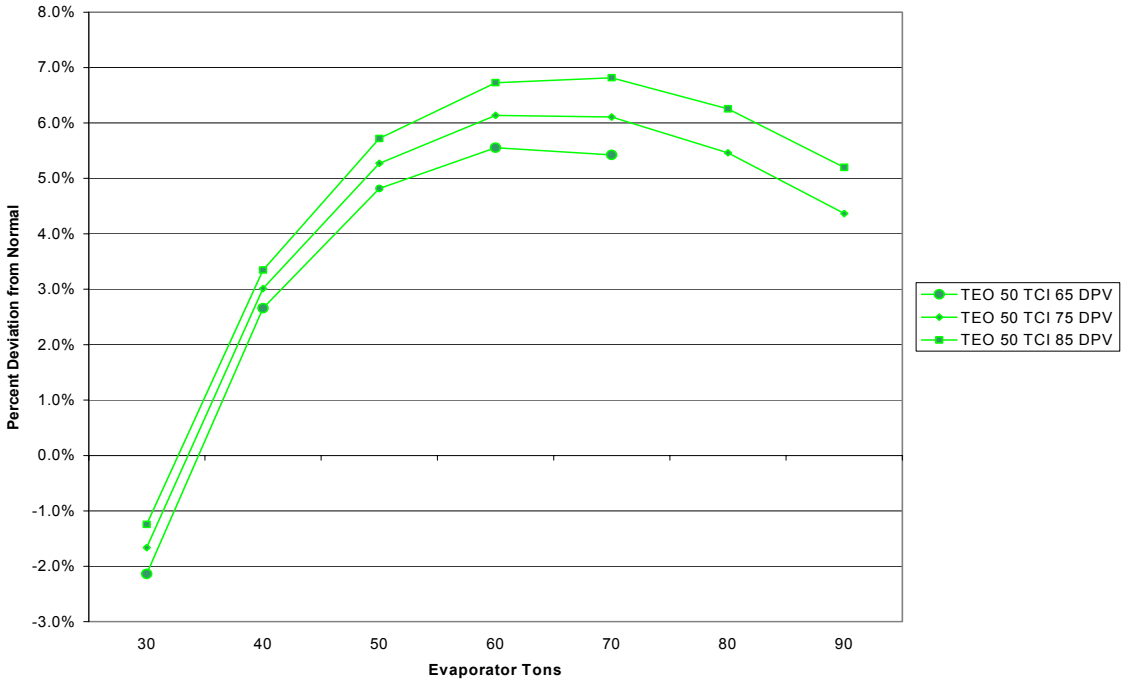

Figure 4.32: Deviation in subcooling for defective pilot valve.

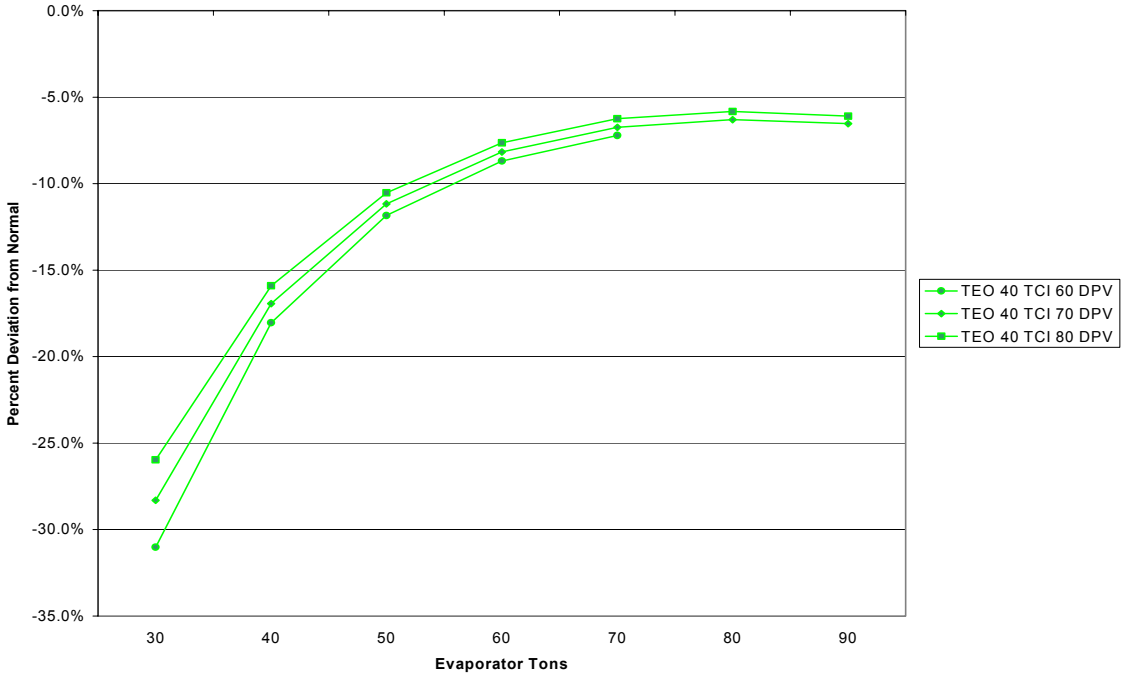

Figure 4.33: Deviation in subcooling for defective pilot valve (at lower evaporator temperature).

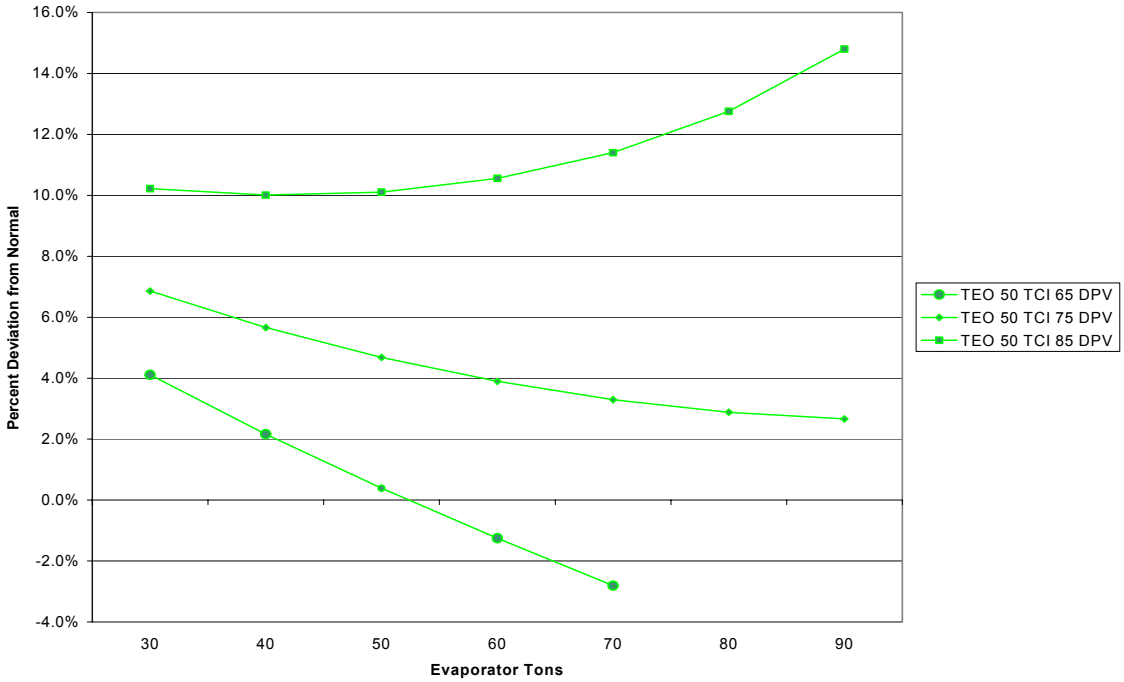

Figure 4.34: Deviation in discharge superheat for defective pilot valve.

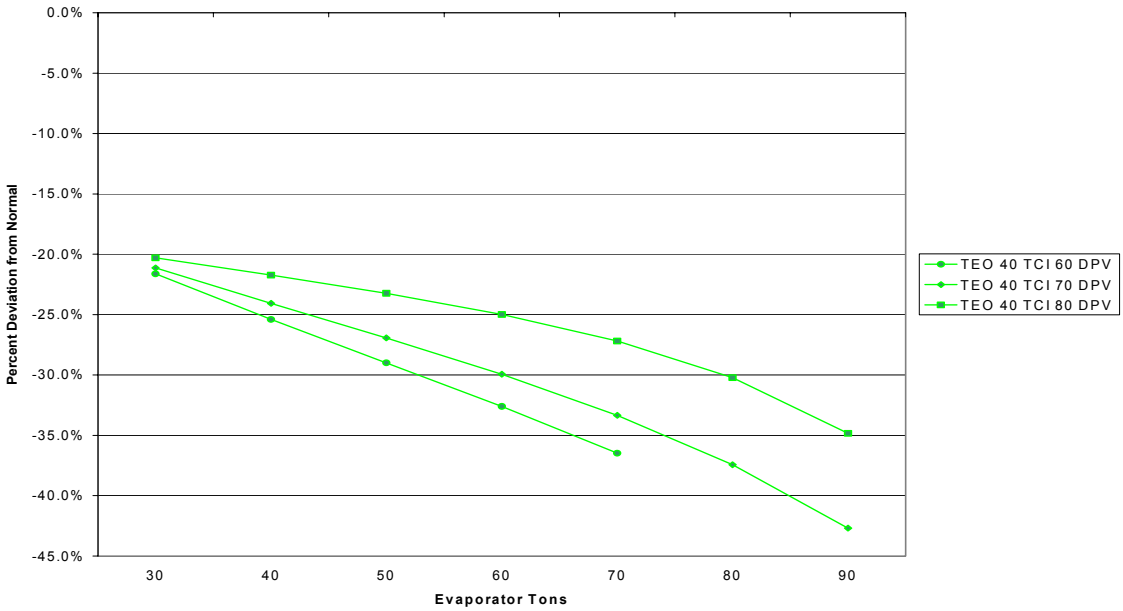

Figure 4.35: Deviation in discharge superheat for defective pilot valve (at lower evaporator temperature).

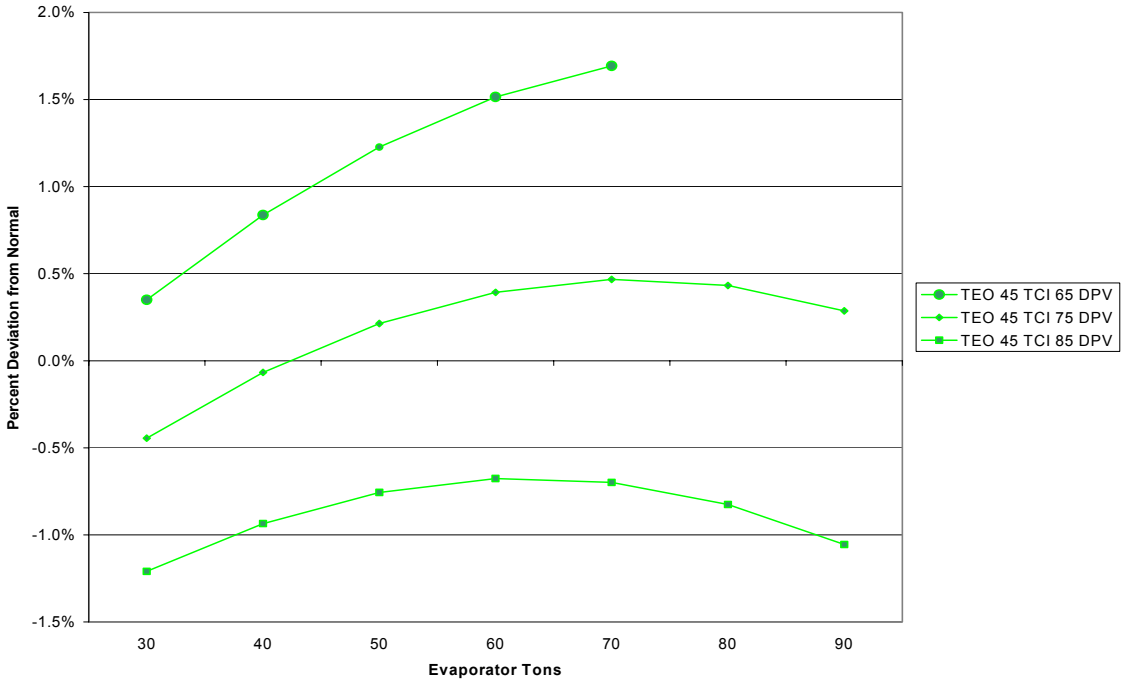

Figure 4.36: Deviation in evaporator pressure for defective pilot valve.

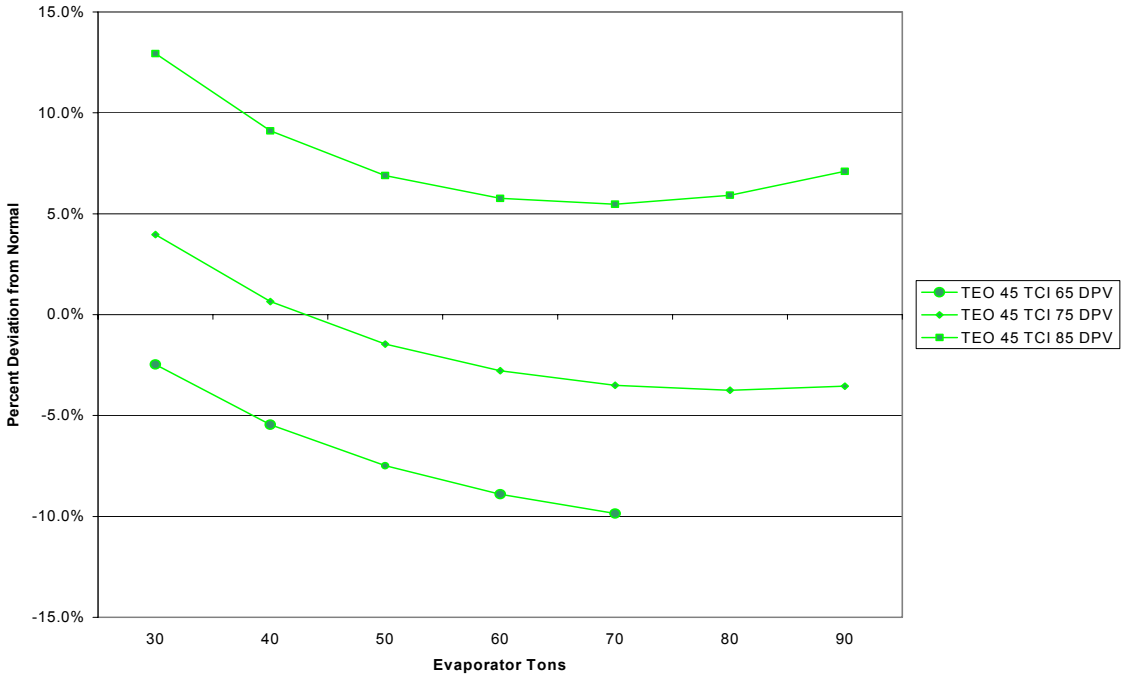

Figure 4.37: Deviation in evaporator approach temperature for defective pilot valve.

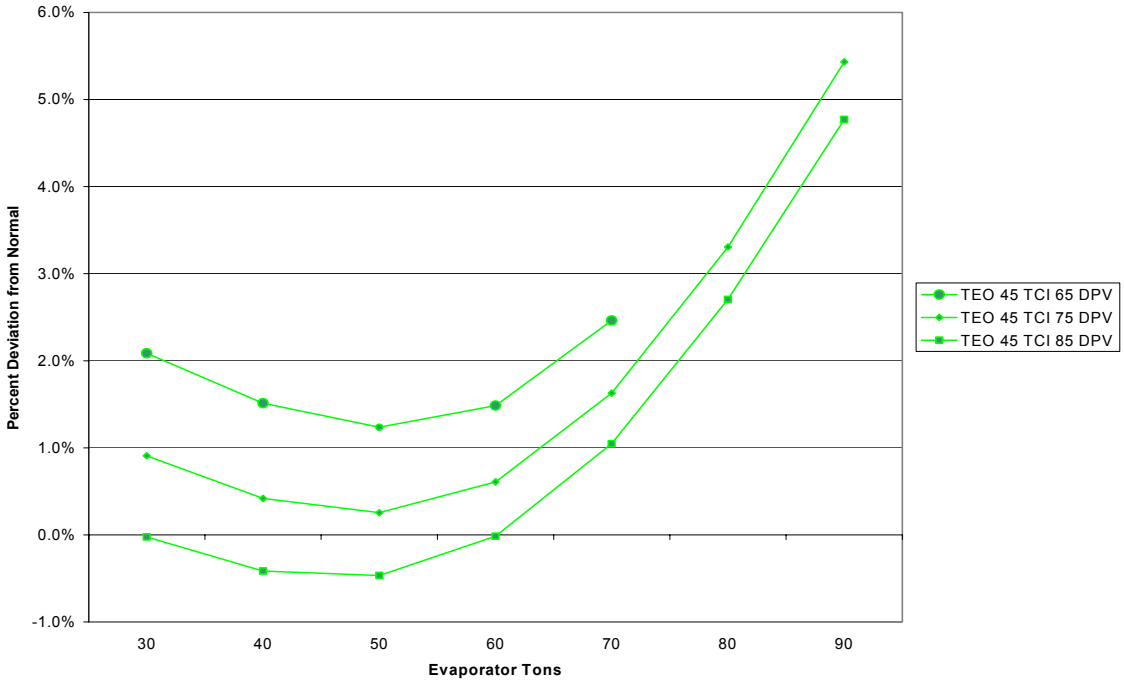

Figure 4.38: Deviation in kW/ton for defective pilot valve.

The performance differences before and after the pilot valve was replaced suggest that the valve was too restrictive at higher evaporator temperatures (i.e. the bulb was less sensitive at higher temperatures).

4.11 Multiple Faults

Since the defective pilot valve occurred early in the commissioning phase of the project, it was not possible to isolate it as well as the other faults that were deliberately introduced. Although it was possible to compare the defective pilot valve fault with a benchmark test under the same operating conditions, both sets of tests still suffered from a reduced condenser water flow rate.

This prompted the question of whether multiple faults present simultaneously would produce the same result as if both faults were present separately then added

together. Other possible outcomes from adding faults could lead to magnifying or diminishing the effects of the other faults present.

The possible combinations of multiple faults are staggering and are not within the scope of this research project. However, the effect of multiple faults involving the condenser water flow rate is relevant to settle the question as to the reliability of the defective pilot valve test data.

Since the defective pilot valve had an impact on the evaporator, it was decided to create a fault where the condenser and evaporator water flow rates were each reduced by 20%. Recall that the uncertainty of the condenser water flow measurement is ± 2.8 gpm and for the evaporator water flow it is ± 2.2 gpm. Table 4.21 shows the designations given to the different fault situations. The last fault case simply added the deviations from the individual faults introduced earlier, whereas the third case (FWC20FWE20) represents the new test run that had both faults introduced simultaneously.

Table 4.21: Multiple fault comparison.

Case	Desired Condition	Actual Flow Range
Normal Operation	270 gpm in condenser 216 gpm in evaporator	264-270 gpm 214-216 gpm
FWC20	20% reduction in condenser flow (216 gpm)	209-219 gpm
FWE20	20% reduction in evaporator flow (173 gpm)	175-177 gpm
FWC20FWE20	20% reduction in condenser flow (216 gpm) 20% reduction in evaporator flow (173 gpm)	210-218 gpm 177-178 gpm
FWC20+FWE20	20% reduction in condenser flow (216 gpm) 20% reduction in evaporator flow (173 gpm)	209-219 gpm 175-177 gpm

Comparing the last two columns of Table 4.22 reveals that multiple faults involving the condenser water flow rate contain no synergistic effects. In other words, the individual impact of each fault on the measured variables can be added together to determine the effect when both faults are present at the same time.

Table 4.22: Average deviations for reduced condenser and evaporator water flow.

	FWC20	FWE20	FWC20FWE20	FWC20+FWE20
kW	2.7%	0.4%	3.0%	3.1%
PRE	0.2%	-0.9%	-1.0%	-0.7%
PRC	3.6%	0.6%	3.6%	4.2%
TRC_sub	24.4%	1.2%	23.6%	25.6%
Tsh_suc	1.4%	1.2%	4.2%	2.6%
Tsh_dis	-0.1%	-1.6%	0.9%	-1.8%
TEA	-0.3%	6.5%	8.3%	6.1%
TCA	9.1%	2.8%	6.4%	11.9%
TEI-TEO	-0.1%	22.3%	21.5%	22.2%
TCO-TCI	26.5%	1.5%	27.7%	28.0%
kW/ton	2.5%	0.5%	3.3%	3.0%
TO_sump	0.7%	-0.1%	0.8%	0.6%
TO_feed	0.5%	-0.1%	0.5%	0.4%
PO_feed	0.3%	-0.4%	-0.6%	-0.1%
PO_net	0.4%	0.3%	-0.3%	0.7%

Figure 4.39 illustrates this synergistic effect, since both faults contribute a portion of the performance penalty seen when both faults are present at the same time. Most of the other measured variables are largely only affected by one fault or the other, as demonstrated in Figures 4.40 through 4.43.

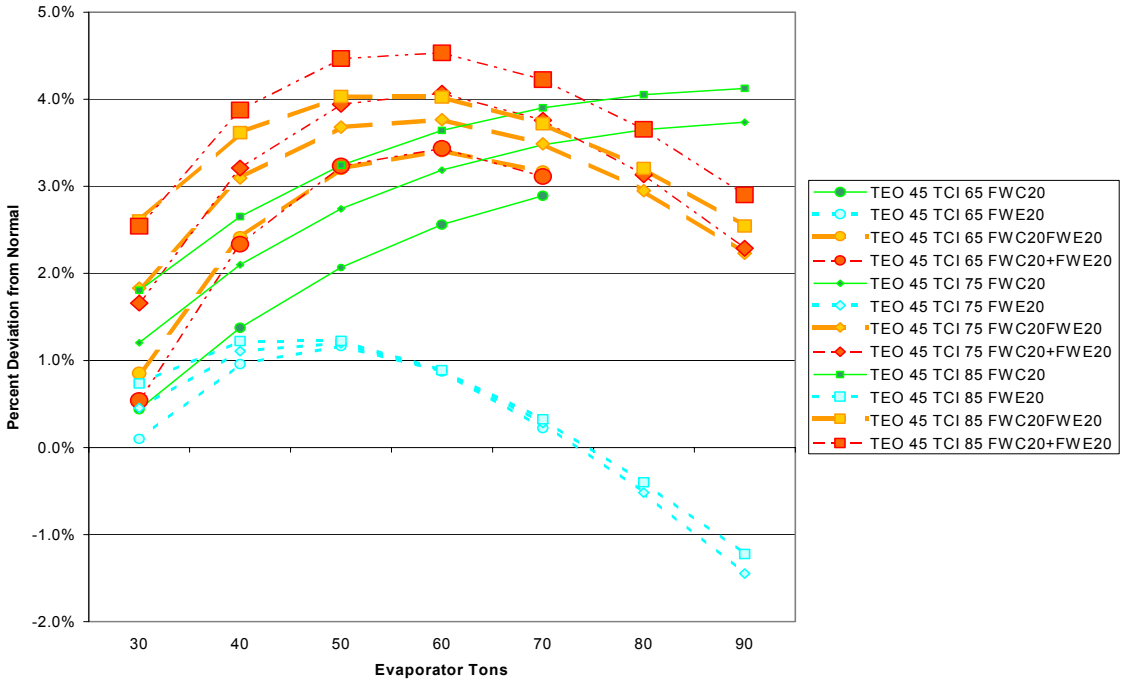

Figure 4.39: Deviation in kW for reduced condenser and evaporator water flow.

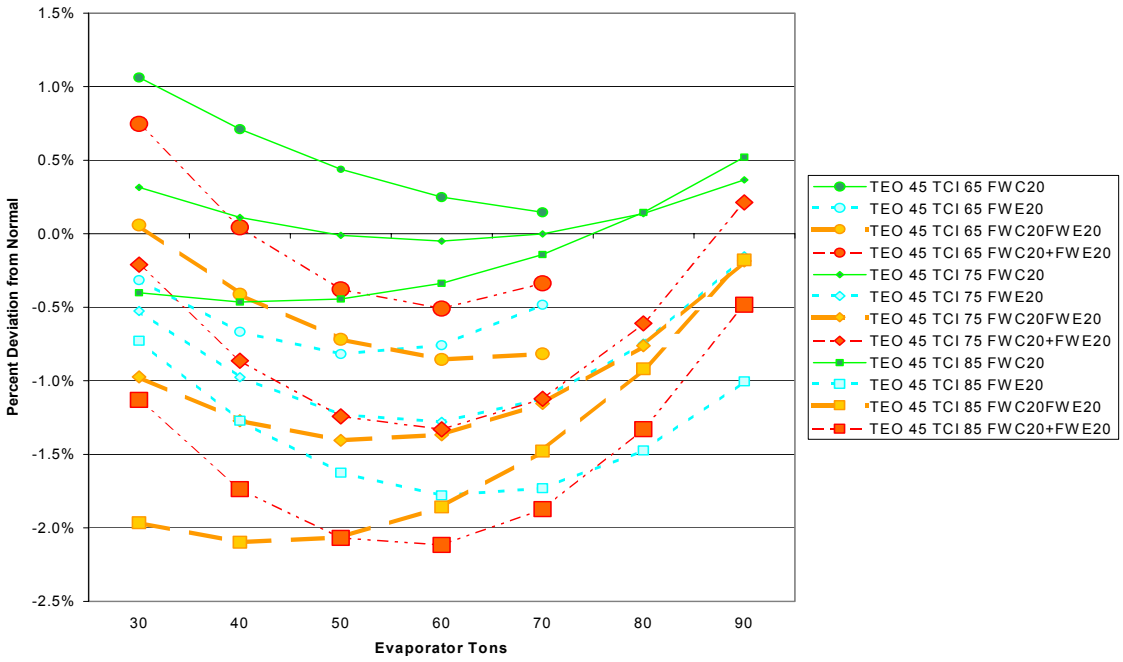

Figure 4.40: Deviation in evaporator pressure for reduced condenser and evaporator water flow.

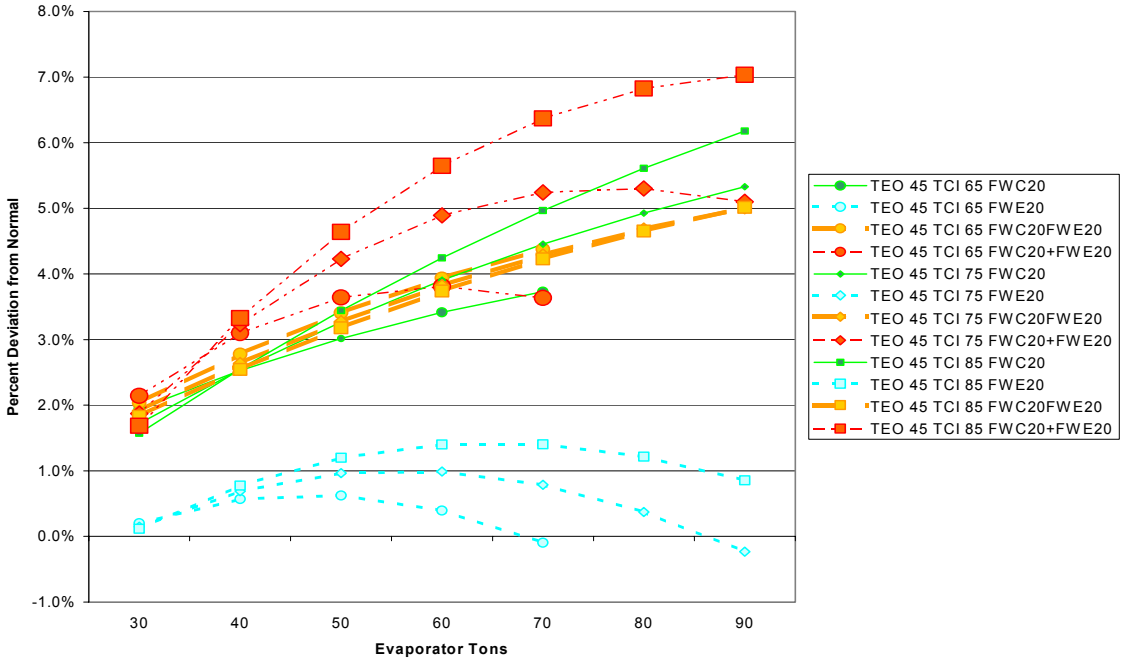

Figure 4.41: Deviation in condenser pressure for reduced condenser and evaporator water flow.

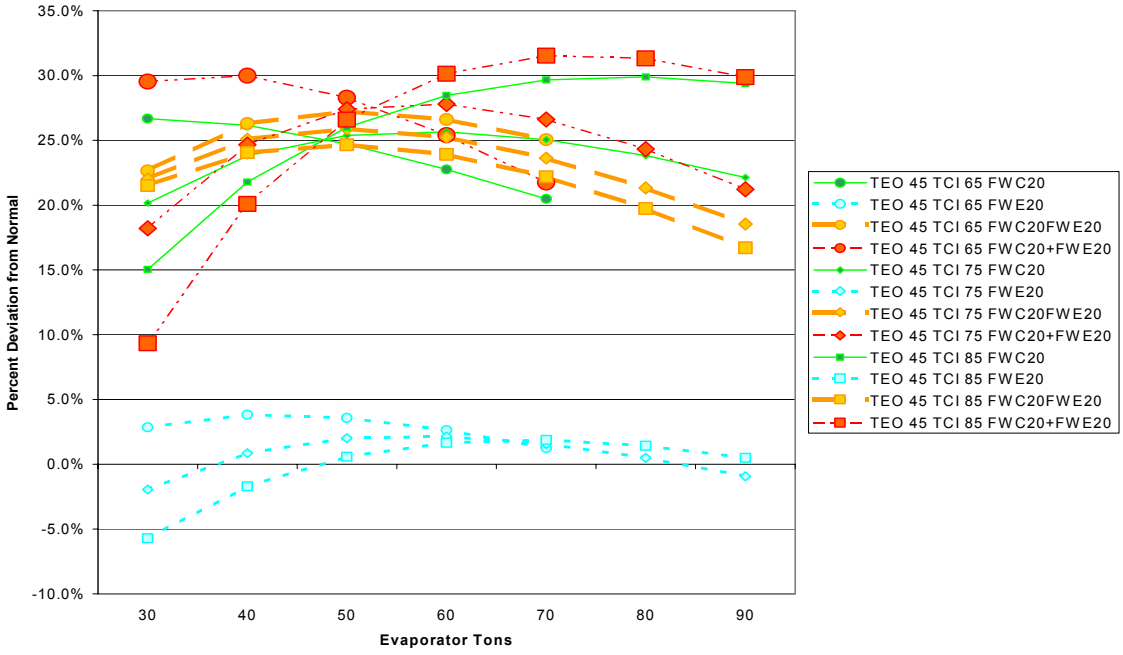

Figure 4.42: Deviation in subcooling for reduced condenser and evaporator water flow.

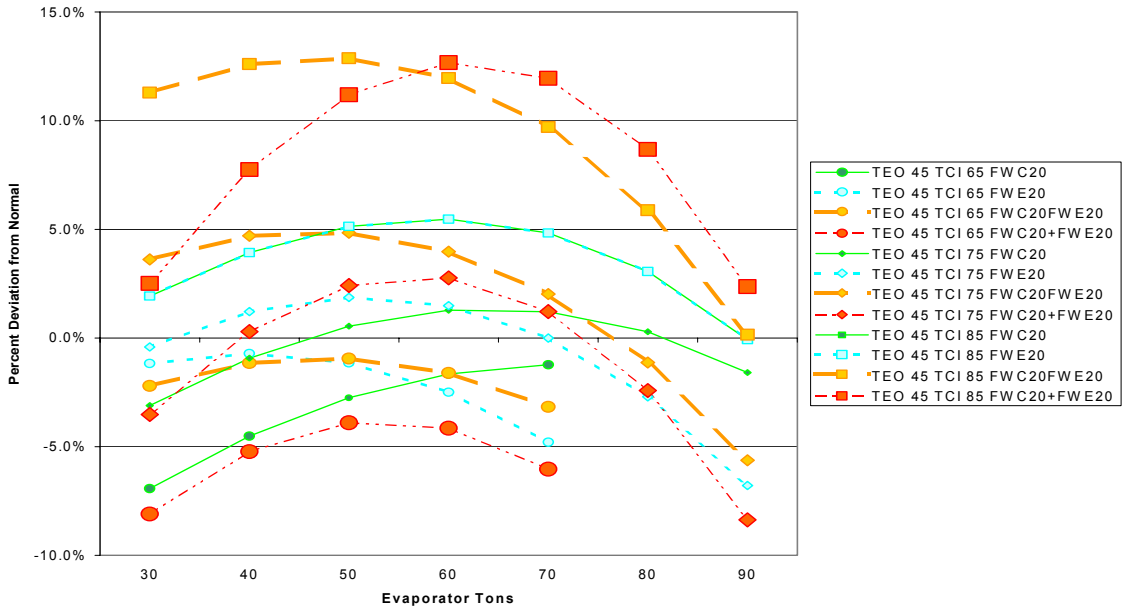

Figure 4.43: Deviation in suction superheat for reduced condenser and evaporator water flow.

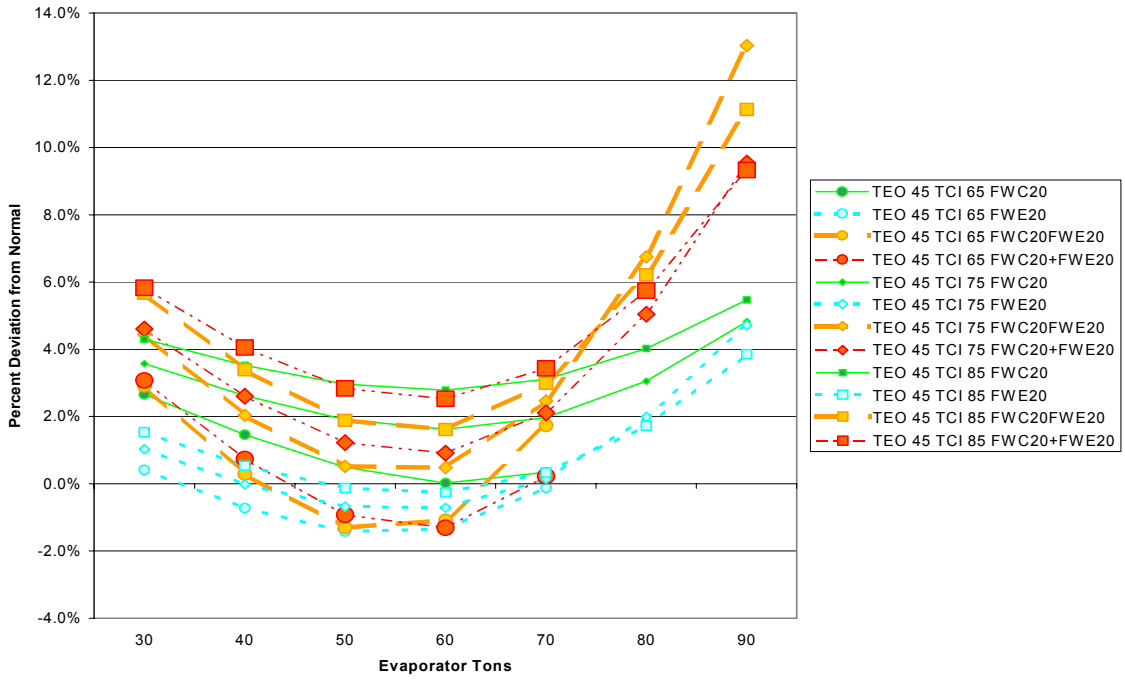

Figure 4.44: Deviation in kW/ton for reduced condenser and evaporator water flow.

5.0 EVALUATION OF FAULT DATA

The purpose of this chapter is to sift through the data collected from the experimental testing explained in Chapter 4. This chapter will answer the following questions:

- How close to steady state did each of the 27 operating conditions get during each fault test?
- Which variables are sensitive to the faults introduced?
- How can the faults be diagnosed from the measured variables?

This chapter will lay the foundation upon which future studies into chiller FDD methods may be supported.

5.1 Steady-State Analysis

The purpose of the test matrix developed for the experimental chiller testing was to provide both steady state and transient data (Section 3.7). The transient data are ensured by the abrupt changes in the operating setpoints, as well as the start-up and shut-down sequences. On the other hand, steady state is reached indirectly by providing enough time (theoretically) to arrive at steady state conditions; however, this does not guarantee that steady state was actually reached. This section will survey the test data to determine whether each of the 27 test conditions adequately reached steady state for each test run performed.

There are many variables to choose from in determining whether steady state was reached. Due to space constraints, only one variable can be presented here; therefore, the heat transfer rate in the condenser was chosen. The condenser heat transfer captures information from both the evaporator heat transfer as well as the input power to the

compressor motor. The following tables contain the rate of change in the condenser heat transfer rate (the units are tons per minute). The calculation is based on the last ten minutes of the test; therefore, a small rate of change indicates that steady state was achieved at least ten minutes before the end of the test. A high number doesn't mean steady state was never reached, it simply indicates that steady state was not reached ten minutes before the end of the test.

Each table is structured so that each of the 27 tests per test run can be checked. The first column contains the original benchmark data set intended for use in the fault analysis. The following four columns contain the fault data sets. Some faults have multiple benchmark tests available to them. If the original benchmark test contains some flaws, then additional benchmark tests may be listed after the faults. These alternate benchmark tests were occasionally used instead of the original benchmark test when comparing the fault data. The file names given to each of the test runs can be found at the beginning of Chapter 4.

The benchmark test labeled 'Normal 1' is a suitable benchmark for the reduced condenser and evaporator water flow faults. There are many more benchmark tests available (Normal, Normal 2, Near Normal 1, Near Normal 2, and Near Normal 3), 'Normal 1' was chosen because it was the closest to the ideal test conditions. The uncertainty in the rate calculation is about 0.25 tons/minute. Among all the reduced condenser water flow tests shown in Table 5.1, none indicated a rate of change exceeding 0.5 tons/minute (approximately 0.5% per minute), which should satisfy the steady state criteria of most researchers.

Table 5.1: Rate of change for condenser heat transfer (in tons/minute) in reduced condenser water flow tests.

Test	Normal 1	FWC10	FWC20	FWC30	FWC40
1	0.08	-0.06	-0.01	-0.10	0.14
2	0.00	0.07	0.38	0.17	0.03
3	-0.05	0.07	-0.03	-0.10	0.04
4	0.09	0.06	-0.09	-0.09	0.05
5	-0.10	-0.37	0.04	-0.25	-0.07
6	-0.13	-0.07	0.03	0.02	0.00
7	0.09	-0.08	0.12	-0.17	0.20
8	0.03	-0.02	-0.05	-0.04	-0.15
9	-0.01	-0.03	0.06	-0.02	-0.11
10	0.11	-0.01	-0.06	0.12	0.01
11	-0.07	0.01	-0.03	-0.05	-0.01
12	0.12	0.07	0.03	0.03	0.06
13	-0.03	-0.07	-0.06	0.13	-0.15
14	0.01	-0.02	0.03	-0.20	0.01
15	0.00	-0.10	-0.02	0.05	-0.03
16	-0.05	0.05	-0.16	0.03	0.19
17	-0.02	0.01	0.13	0.10	0.09
18	-0.19	0.07	0.02	0.06	0.04
19	0.43	0.18	-0.09	-0.10	0.02
20	0.26	0.25	-0.10	0.09	0.05
21	0.01	-0.07	-0.09	-0.01	0.15
22	0.21	0.36	-0.02	0.04	0.02
23	-0.08	-0.03	0.05	-0.09	0.18
24	-0.09	0.13	0.06	0.07	-0.06
25	0.05	-0.15	-0.22	0.20	0.18
26	-0.13	-0.10	-0.26	-0.02	0.09
27	-0.19	0.00	-0.41	-0.01	-0.01

The benchmark tests suitable for reduced condenser water flow are also suitable for reduced evaporator water flow. None of these tests listed in Table 5.2 indicated a rate of change exceeding 0.5 tons per minute.

Table 5.2: Rate of change for condenser heat transfer (in tons/minute) in reduced evaporator water flow tests.

Test	Normal 1	FWE10	FWE20	FWE30	FWE40
1	0.08	0.04	0.14	0.28	0.08
2	0.00	0.27	0.20	0.05	0.12
3	-0.05	0.05	0.00	0.11	0.25
4	0.09	0.16	-0.18	0.05	-0.05
5	-0.10	-0.05	0.06	0.01	0.25
6	-0.13	-0.18	-0.02	0.10	0.01
7	0.09	-0.01	0.00	0.02	0.14
8	0.03	-0.08	-0.01	0.05	-0.14
9	-0.01	0.01	-0.18	-0.13	0.16
10	0.11	-0.05	0.07	0.22	0.24
11	-0.07	-0.03	-0.03	-0.09	0.09
12	0.12	0.01	0.00	-0.04	-0.07
13	-0.03	-0.09	0.00	0.02	0.07
14	0.01	0.04	-0.01	0.02	-0.44
15	0.00	0.07	-0.24	-0.06	0.06
16	-0.05	0.13	0.10	0.16	0.16
17	-0.02	-0.09	0.03	0.07	-0.04
18	-0.19	-0.02	0.13	-0.08	-0.04
19	0.43	-0.04	0.33	0.16	-0.03
20	0.26	-0.10	0.03	-0.01	-0.20
21	0.01	0.00	-0.14	0.04	-0.04
22	0.21	0.05	0.20	0.04	0.02
23	-0.08	-0.11	-0.25	0.07	-0.14
24	-0.09	-0.07	0.21	0.01	-0.06
25	0.05	0.01	0.10	-0.05	0.02
26	-0.13	0.01	0.06	-0.03	0.09
27	-0.19	-0.22	-0.05	0.06	0.15

The 'Normal R' benchmark test was taken immediately after the refrigerant leak tests; the 'Normal R1' benchmark test was taken immediately after the refrigerant overcharge tests. Both sets can be used with confidence; however, the 'Normal R1' set achieved better steady state conditions. Within the refrigerant leak tests, there were a few tests that exceeded the arbitrarily defined 0.5 tons per minute threshold as shown in Table 5.3. One test in the 10% undercharge case (RL10 test 16) exceeded 1.0 ton per minute, although appeared to approach steady state within the last few minutes.

Table 5.3: Rate of change for condenser heat transfer (in tons/minute) in refrigerant leak tests.

Test	Normal R	RL10	RL20	RL30	RL40	Normal R1
1	0.12	0.19	-0.07	0.06	0.09	0.36
2	0.05	-0.06	0.10	0.11	0.22	-0.26
3	-0.05	-0.04	-0.06	0.06	-0.05	0.05
4	0.06	-0.04	-0.05	-0.15	0.04	0.11
5	-0.05	-0.03	-0.04	0.03	0.20	-0.09
6	-0.09	0.05	0.09	-0.06	-0.07	-0.04
7	0.01	-0.01	0.05	0.09	0.01	0.00
8	-0.04	-0.04	-0.12	-0.04	-0.05	0.11
9	-0.14	-0.04	-0.16	-0.04	-0.02	0.00
10	-0.01	0.20	0.06	-0.01	0.13	0.12
11	-0.07	-0.05	0.10	0.14	-0.04	-0.03
12	-0.05	-0.22	0.01	-0.09	-0.19	-0.12
13	0.60	0.71	0.33	0.21	-0.05	0.53
14	-0.16	0.06	-0.08	0.00	-0.19	0.07
15	0.01	0.10	-0.08	0.00	-0.08	0.02
16	0.90	1.05	0.73	0.45	-0.03	0.07
17	0.25	0.10	0.01	-0.14	0.12	0.04
18	-0.23	-0.25	0.06	0.42	-0.01	0.32
19	0.24	0.01	0.50	-0.01	0.19	-0.02
20	-0.31	-0.03	0.04	-0.01	0.13	0.06
21	0.05	-0.11	-0.09	-0.07	0.05	0.11
22	0.86	0.39	0.38	0.20	0.24	0.15
23	0.14	0.07	-0.01	-0.01	-0.14	0.09
24	-0.06	-0.03	0.00	0.09	-0.01	0.00
25	0.19	0.04	-0.04	0.04	0.03	0.07
26	-0.15	0.15	0.10	-0.06	0.07	0.01
27	-0.03	-0.04	0.10	-0.02	-0.07	0.07

The 'Normal R' benchmark test was performed before the refrigerant overcharge tests; the 'Normal R1' benchmark test was done immediately after the refrigerant overcharge tests. Either benchmark data set may be used; however, the 'Normal R1' tests reached steady state more frequently. A couple tests in the 10% overcharge case (RO10) exceeded 0.5 tons per minute (refer to Table 5.4); all the remaining tests were below 0.5 tons per minute. It is interesting to note that in each of the test runs, test 13 consistently had the highest rate of change compared to any of the other tests (indicating the chiller took longer to reach steady state for that particular operating condition).

Table 5.4: Rate of change for condenser heat transfer (in tons/minute) in refrigerant overcharge tests.

Test	Normal R	RO10	RO20	RO30	RO40	Normal R1
1	0.12	0.04	0.10	0.03	0.10	0.36
2	0.05	0.01	0.09	-0.10	0.21	-0.26
3	-0.05	-0.19	-0.13	-0.08	-0.08	0.05
4	0.06	0.11	0.16	0.19	0.39	0.11
5	-0.05	-0.07	-0.08	0.03	0.08	-0.09
6	-0.09	-0.01	0.00	-0.07	-0.02	-0.04
7	0.01	-0.13	-0.05	0.10	-0.50	0.00
8	-0.04	-0.08	-0.04	0.00	0.09	0.11
9	-0.14	-0.08	-0.06	-0.01	-0.03	0.00
10	-0.01	0.18	0.12	-0.05	0.00	0.12
11	-0.07	0.00	-0.08	0.05	-0.10	-0.03
12	-0.05	0.02	-0.08	0.02	-0.14	-0.12
13	0.60	0.63	0.40	0.49	0.26	0.53
14	-0.16	-0.20	-0.06	-0.19	-0.05	0.07
15	0.01	0.05	-0.17	-0.04	-0.07	0.02
16	0.90	0.31	-0.02	0.46	0.41	0.07
17	0.25	-0.02	-0.01	0.01	-0.11	0.04
18	-0.23	-0.11	0.03	0.04	0.18	0.32
19	0.24	0.16	0.19	-0.02	0.07	-0.02
20	-0.31	0.01	0.04	0.06	-0.15	0.06
21	0.05	0.14	0.07	0.07	0.03	0.11
22	0.86	0.61	0.06	0.07	0.15	0.15
23	0.14	0.04	-0.11	-0.17	-0.09	0.09
24	-0.06	-0.05	0.20	0.00	-0.12	0.00
25	0.19	0.09	-0.09	0.05	0.14	0.07
26	-0.15	-0.02	-0.03	-0.01	-0.11	0.01
27	-0.03	-0.03	-0.02	-0.28	-0.33	0.07

The 'Normal EO' benchmark test was performed immediately before the excess oil tests. The 'Normal R1' test was performed just before the 'Normal EO' test (thus also making it a suitable candidate for the refrigerant fault tests). The 'Normal R1' test showed a tendency to reach steady state faster than the 'Normal EO' test. A few tests exceeded a rate of change of 0.5 tons per minute as given in Table 5.5. The chiller had greater difficulty reaching steady state during the excess oil tests because of problems with the vane control. Test 1 from EO73 did not reach steady state and was one of the few tests excluded from the analysis contained in Chapter 4 (data from Tests 2 through 27 were still used, even though the operating conditions in tests 10, 13, 19, and 22 were still slowly drifting).

Table 5.5: Rate of change for condenser heat transfer (in tons/minute) in excess oil tests.

Test	Normal EO	EO14	EO28	EO50	EO73	Normal R1
1	-0.03	0.44	0.46	0.23	1.04	0.36
2	0.04	0.09	-0.04	0.02	0.01	-0.26
3	0.03	-0.01	0.05	0.05	0.12	0.05
4	0.41	0.04	0.07	0.15	0.50	0.11
5	0.19	-0.12	-0.15	-0.12	0.05	-0.09
6	0.06	0.06	-0.24	0.00	0.02	-0.04
7	-0.13	-0.04	0.03	0.01	0.02	0.00
8	-0.04	-0.07	0.01	-0.01	0.11	0.11
9	-0.05	0.12	-0.06	-0.09	-0.02	0.00
10	-0.01	0.43	0.19	0.28	0.30	0.12
11	0.06	0.02	-0.04	-0.14	0.00	-0.03
12	0.02	0.01	0.02	0.02	0.00	-0.12
13	0.24	0.79	0.49	0.09	0.22	0.53
14	-0.10	-0.09	0.05	0.04	-0.02	0.07
15	-0.05	0.07	-0.08	-0.04	0.07	0.02
16	-0.69	-0.01	-0.60	-0.11	0.69	0.07
17	0.06	0.04	-0.01	0.10	0.02	0.04
18	0.07	-0.02	-0.02	0.09	0.03	0.32
19	-0.11	0.10	-0.16	0.24	0.29	-0.02
20	-0.51	0.02	0.00	0.04	0.03	0.06
21	0.13	0.06	0.07	-0.15	0.02	0.11
22	0.74	0.41	-0.09	-0.06	0.86	0.15
23	0.05	0.08	-0.10	-0.06	-0.18	0.09
24	-0.21	-0.01	-0.12	-0.01	0.07	0.00
25	-0.01	-0.01	-0.03	0.01	0.64	0.07
26	0.10	-0.17	0.04	0.06	-0.22	0.01
27	-0.07	-0.11	0.00	0.06	0.07	0.07

The condenser fouling tests contain a wealth of benchmark data sets. 'Normal CF' was performed before any of the condenser fouling tests; 'Normal CF2' through 'Normal CF6' were performed between the CF30 and CF45 fault tests; CF45 was subsequently followed by the 'Normal NC' test. As shown in Table 5.6, the 'Normal CF2' test 16 may have reached steady state at the very end, but should probably be excluded from most analyses. Among the condenser fouling tests, both CF12 and CF20 test 16 had the same problem, but more conclusively reached steady state at the end of their respective tests.

Table 5.6: Rate of change for condenser heat transfer (in tons/minute) in condenser fouling tests.

Test	Normal CF2	CF12	CF20	CF30	CF45	Normal CF4
1	-0.03	0.07	0.24	-0.04	0.06	0.08
2	0.00	-0.02	-0.03	0.05	-0.08	-0.05
3	-0.02	-0.02	-0.02	0.07	0.06	0.01
4	0.13	0.10	0.26	0.07	0.10	0.06
5	0.13	0.04	0.01	-0.01	-0.02	-0.11
6	-0.01	-0.11	0.03	0.03	-0.04	0.20
7	-0.26	-0.09	-0.38	0.04	0.05	0.01
8	-0.05	-0.10	-0.04	0.00	0.01	-0.02
9	-0.07	-0.05	-0.05	-0.08	-0.12	0.01
10	0.05	0.13	0.06	0.07	0.10	0.12
11	0.01	-0.08	-0.09	0.02	0.11	-0.15
12	-0.32	0.09	-0.04	0.00	0.02	0.00
13	0.21	-0.06	0.04	0.15	0.38	0.16
14	0.04	0.02	-0.04	0.13	0.05	0.01
15	0.06	0.01	0.01	0.04	0.02	-0.07
16	-1.00	-0.74	-0.68	0.06	-0.13	-0.06
17	0.16	0.01	-0.04	-0.34	0.02	-0.06
18	0.00	0.03	-0.24	-0.02	-0.26	-0.02
19	-0.03	-0.02	0.00	0.17	0.01	-0.06
20	0.05	0.02	0.10	0.01	0.02	-0.15
21	0.15	0.09	-0.30	0.18	-0.05	0.05
22	0.14	0.49	0.14	0.46	0.23	0.05
23	-0.07	0.12	0.03	0.07	-0.03	0.12
24	0.03	-0.16	-0.03	0.09	0.08	-0.09
25	0.04	0.00	0.06	-0.31	-0.10	-0.06
26	-0.21	-0.04	0.03	0.02	-0.03	0.05
27	0.01	0.03	0.04	0.22	0.07	-0.11

The 'Normal NC' test was conducted immediately before nitrogen was introduced into the system. However, the entire series of 'Normal CF' tests are also applicable, and 'Normal CF6' was chosen as the benchmark for the results presented in Chapter 4. A few of the non-condensable fault tests showed unusual behavior (refer to Table 5.7), such as NC1 test 8, NC2 test 12, and NC3 test 12 (these tests should probably be excluded from steady state analyses). At the higher fault levels the performance was severely affected, to the point where the operating conditions did not always reach the desired conditions, such as NC3 test 19 (where it took the entire 45 minutes to reach the desired evaporator water leaving temperature).

Table 5.7: Rate of change for condenser heat transfer (in tons/minute) in non-condensables in refrigerant tests.

Test	Normal NC	NC1	NC2	NC3	NC5	Normal CF6
1	0.06	0.06	0.26	0.13	0.03	0.27
2	0.12	-0.07	-0.05	0.01	0.11	-0.14
3	0.00	0.01	-0.04	-0.05	-0.03	-0.04
4	0.21	0.06	0.19	0.65	-0.05	0.35
5	-0.36	0.14	0.05	0.01	0.05	-0.08
6	0.01	-0.01	0.03	-0.03	0.06	-0.08
7	0.05	-0.05	-0.19	0.07	0.01	-0.01
8	-0.01	-0.23	0.00	-0.01	0.14	0.19
9	-0.21	-0.20	-0.10	-0.04	0.19	-0.01
10	0.17	-0.01	0.20	0.05	0.04	0.26
11	-0.04	-0.10	-0.03	0.11	0.04	0.04
12	0.07	-0.05	-0.78	-0.83	0.04	-0.30
13	0.79	0.46	0.51	0.01	0.11	-0.05
14	-0.08	0.01	-0.09	0.05	-0.15	0.05
15	-0.08	0.00	-0.02	0.05	-0.11	-0.04
16	-0.45	-0.26	0.01	-0.31	0.25	-0.14
17	0.01	-0.07	-0.08	0.04	0.02	0.03
18	0.03	0.10	-0.24	-0.03	0.02	-0.05
19	0.13	-0.05	0.03	0.22	0.11	0.06
20	0.00	0.05	0.00	-0.13	-0.12	0.08
21	0.02	0.02	0.00	0.11	-0.13	0.15
22	-0.20	0.65	0.41	0.59	0.09	0.09
23	-0.16	0.12	0.02	0.10	0.05	0.02
24	0.00	-0.04	0.03	0.00	0.04	-0.01
25	0.06	0.03	0.06	-0.16	-0.36	0.01
26	-0.14	0.10	0.33	0.02	-0.01	-0.08
27	0.35	-0.10	0.06	-0.04	0.11	0.04

The 'Normal DPV' benchmark data set was obtained a few days after the fault state was tested. According to Table 5.8, DPV fault test 22 may not have reached steady state (slight chance it reached it at the end). In addition, 'Normal DPV' test 19 didn't reach the desire operating condition and should be excluded from steady state analysis.

Table 5.8: Rate of change for condenser heat transfer (in tons/minute) in defective pilot valve tests.

Test	Normal DPV	DPV
1	0.19	-0.05
2	0.13	-0.02
3	0.02	0.01
4	-0.07	0.10
5	-0.04	0.06
6	-0.05	-0.01
7	0.03	0.10
8	0.22	-0.11
9	-0.14	-0.21
10	0.29	0.34
11	0.03	0.02
12	0.02	-0.22
13	0.10	-0.10
14	0.02	0.19
15	-0.36	-0.02
16	0.21	0.50
17	-0.18	-0.35
18	0.09	0.31
19	0.22	-0.29
20	0.03	-0.10
21	-0.06	-0.19
22	0.15	0.92
23	0.22	-0.21
24	-0.04	0.05
25	0.24	0.15
26	-0.32	-0.27
27	0.06	-0.05

5.2 Sensitivity Analysis

This section and the next will focus on the usefulness of the measurements taken for fault detection and diagnosis. This section will largely be a review of the important information contained in Chapter 4. In addition, the measurements useful for detecting each fault will be assessed, as well as how severely the fault impacted system performance. Table 5.9 is provided as a review of the measured parameters introduced in Chapter 4.

Table 5.9: Measurements and uncertainty for FDD analysis.

Measurement	Description	Experimental Uncertainty
kW	Instantaneous input power	± 1-1.5%
PRE	Evaporator Pressure	± 1-2%
PRC	Condenser Pressure	± 1-2%
TRC_sub	Subcooling	± 7-20%
Tsh_suc	Suction Superheat	± 10-25%
Tsh_dis	Discharge Superheat	± 2-3%
TEA	Evaporator Approach Temperature	± 6-10%
TCA	Condenser Approach Temperature	± 10-30%
TEI-TEO	Evaporator Water Temperature Difference	± 0.3-0.6%
TCO-TCI	Condenser Water Temperature Difference	± 1-2%
kW/ton	Chiller efficiency	± 1-2.5%
TO_sump	Oil Sump Temperature	± 0.5-1%
TO_feed	Oil Feed Temperature	± 0.3-1.5%
PO_feed	Oil Feed Pressure	± 1-20%
PO_net	Oil Net Pressure	± 1-20%

For each of the faults studied, a table will present the most sensitive measurements. The sensitivity is calculated from the maximum average deviation for the worst fault case divided by the maximum experimental uncertainty for that particular measurement (the worst case uncertainty is used from Table 5.9 and is not based on an averaged uncertainty):

$$\text{Sensitivity} = \frac{\text{Average Deviation of Given Measurement at Fault Level 4 (\%)}}{\text{Maximum Experimental Uncertainty of Given Measurement (\%)}} \quad (5.1)$$

Therefore, the sensitivity value will be a ratio analogous to signal-to-noise. Due to the method in calculating the sensitivity, the value will be extremely conservative.

For the reduced condenser water flow rate, the parameters sensitive to the introduction of the fault were: compressor input power, condenser pressure, subcooling temperature, condenser approach temperature, and condenser water temperature difference. The results are given in Table 5.10. The data further indicate that when the condenser water flow rate is reduced by 20%, it will begin to have a noticeable effect on system performance.

Table 5.10: Measurement sensitivity for reduced condenser water flow rate.

Measurement	Sensitivity
KW	4.67
PRC	4.75
TRC_sub	3.08
TCA	0.72
TCO-TCI	35.1
kW/ton	2.44

For the reduced evaporator water flow rate, the parameters sensitive to the introduction of the fault were: evaporator pressure, discharge superheat, evaporator approach temperature, and evaporator water temperature difference. The results are given in Table 5.11. The data suggests that when the evaporator water flow rate is reduced by about 28%, the system performance will deteriorate by a noticeable margin (at higher loads). Many of the sensitivities are low because some trends go both negative and positive depending on the operating conditions (thus the effect is negated when all the values are averaged together).

Table 5.11: Measurement sensitivity for reduced evaporator water flow rate.

Measurement	Sensitivity
PRE	0.8
Tsh_dis	1.0
TEA	1.3
TEI-TEO	93
kW/ton	0.96

For a refrigerant leak, the parameters sensitive to a loss of refrigerant charge were: condenser pressure, subcooling temperature, and condenser approach temperature. The results are given in Table 5.12. With a refrigerant leak, the system performance improved slightly; however, difficulty in controlling the chiller during the experimental testing suggests that the chiller's ability to quickly reach steady state or reach certain operating conditions may be adversely affected.

Table 5.12: Measurement sensitivity for refrigerant leak.

Measurement	Sensitivity
PRC	1.5
TRC_sub	3.3
TCA	1.77
kW/ton	0.32

During refrigerant overcharge, the sensitive parameters were: compressor input power, condenser pressure, subcooling temperature, discharge superheat, condenser approach temperature, and condenser water temperature difference. The results are given in Table 5.13. Refrigerant overcharge will begin to have a noticeable effect on system performance when the system is about 26% overcharged.

Table 5.13: Measurement sensitivity for refrigerant overcharge.

Measurement	Sensitivity
kW	5.67
PRC	5.65
TRC_sub	5.65
Tsh_dis	1.7
TCA	4.31
TCO-TCI	5.1
kW/ton	3.6

For excess oil, the sensitive parameters were: compressor input power, oil sump temperature, and oil feed temperature. The results are given in Table 5.14. A decrease in system performance can be detected when the oil is overcharged by approximately 50%.

Table 5.14: Measurement sensitivity for excess oil.

Measurement	Sensitivity
kW	3.47
TO_sump	16.0
TO_feed	9.27
kW/ton	2.32

For condenser fouling, the parameters sensitive to the introduction of the fault were: compressor input power, condenser pressure, condenser approach temperature, and condenser water temperature difference. The results are given in Table 5.15. Condenser fouling causes a detectable drop in system performance when fouling has effectively eliminated 40% of the heat transfer area.

Table 5.15: Measurement sensitivity for condenser fouling.

Measurement	Sensitivity
kW	2.6
PRC	2.25
TCA	1.79
TCO-TCI	3.2
kW/ton	1.64

Non-condensables in the refrigerant affect the following parameters: compressor input power, condenser pressure, subcooling temperature, discharge superheat, condenser approach temperature, and condenser water temperature difference. The results are given in Table 5.16. Anything beyond trace amounts of non-condensables (greater than 0.05 pounds) will negatively affect system performance at a level that can be easily detected.

Table 5.16: Measurement sensitivity for non-condensables in refrigerant.

Measurement	Sensitivity
kW	10.0
PRC	10.3
TRC_sub	8.89
Tsh_dis	2.5
TCA	10.52
TCO-TCI	2.05
kW/ton	5.88

For the defective pilot valve, the sensitivity parameters were not as clear and are heavily dependent on the operating conditions. Evaporator pressure tended to be higher at lower evaporator temperatures and lower at higher evaporator temperatures (sensitivities in the range of 1 to 1.5). Subcooling was lower at lower evaporator temperatures and approached normal behavior at higher evaporator temperatures (sensitivity peaking at about 1.3). Suction superheat was also abnormally low at lower evaporator temperatures (sensitivity of about 1.5) as well as discharge superheat (sensitivity approaching 2); however discharge superheat began to deviate to the high

side at higher evaporator temperatures. Finally, the evaporator and condenser approach temperatures were lower at low evaporator temperatures (sensitivity around 1).

The defective pilot valve had an effect on system performance at higher loads, but was virtually unnoticeable when the cooling load was at about half capacity.

5.3 Pattern Analysis

The information in the previous section indicated which measurements were useful for detecting the faults. This section continues by analyzing whether there are unique trends in the measurements that can help in differentiating the faults tested.

Based on the literature review, it was found that many prior researchers presented their fault data in a table similar to Table 5.17. The table lists all the faults tested as well as the important parameters for detecting those faults. The purpose of this table is to show the trends in all the measurements. Differences found in the patterns can subsequently be used to diagnose the fault. A dot is used when no discernable trend in the measurement was found. Triangles pointing upwards indicate a trend for the measurement to increase with an increasing fault severity (with more triangles demonstrating stronger confidence in that trend). Downward pointing triangles are used for those parameters that decrease when the fault becomes more severe (with more triangles being used to indicate a stronger confidence). Triangles pointing both up and down in the same box indicate deviations which trend both positive and negative depending on the operating conditions.

Table 5.17: Trends in measurement deviation for fault diagnosis.

	kW	PRE	PRC	TRC_sub	Tsh_suc	Tsh_dis	TEA	TCA	TEI-TEO	TCO-TCI	kW/ton	TO_sump	TO_feed
Reduced Condenser Water Flow	▲▲	▲	▲▲	▲▲	▼	·	▼	▲▲	·	▲▲▲	▲▲	▲	▲
Reduced Evaporator Water Flow	▲	▼	·	▲▼	▼	▲▼	▼	·	▲▲▲	·	▲▲	·	·
Refrigerant Leak	▼	·	▼▼	▼▼▼	·	·	·	▼▼	·	·	▼	·	·
Refrigerant Overcharge	▲▲	▼	▲▲	▲▲▲	·	▲	·	▲▲	·	▲	▲▲	▲	▲
Excess Oil	▲▲	·	·	▲	·	·	·	▲	·	·	▲▲	▲▲▲	▲▲▲
Condenser Fouling	▲▲	·	▲▲	·	·	·	·	▲▲	·	▲	▲▲	·	·
Non-condensables in Refrigerant	▲▲▲	▲	▲▲▲	▲▲▲▲	·	▲▲	▼	▲▲▲▲	·	▲	▲▲▲	▲	▲
Defective Pilot Valve	▲	▲▼	·	▲▼	▲▼	▲▼	▲▼	▼	·	·	▲▲	·	·

There is a clear distinction between the faults presented, except for non-condensables in the refrigerant and refrigerant overcharge. For those two faults there are some weak trends that deviate, but for the most part the strong trends are identical. It may be possible to separate them based on the differences in the magnitude of those strong trends, but future researchers will have to explore that possibility with their FDD methods. Another solution would be to add a temperature measurement inside the condenser shell for comparison with the saturation temperature calculated from the pressure measurement. The defective pilot valve generally did not have strong trends, with evaporator pressure trending higher and lower depending on the operating

conditions. Some of the other parameters trended lower, but only at certain operating conditions. Moreover, some of these trends were not visible until the evaporator load increased beyond 50% of its capacity. The excess oil fault may also present a problem for those who do not have the oil temperature readings available. It does have a serious impact on power consumption, but few of the other parameters are affected.

6.0 PRELIMINARY HEAT EXCHANGER MODELING

As part of the overall project sponsored by ASHRAE, some simple steady state modeling of the condenser and evaporator was done to help prepare for future work on the development of a dynamic chiller model. This chapter gives an introductory explanation of how to model the experimental chiller's heat exchangers. The actual code written using EES (Klein and Alvarado, 1999) is provided in Appendix C.

6.1 Condenser Modeling

The condenser is a shell and tube design with refrigerant in the shell and water flowing through the tubes. The water makes two passes—the first pass is at the bottom of the condenser, and the return pass is closer to the top of the condenser. There are a total of 164 tubes—74 are in the first pass and the remaining 90 in the second. During the condenser fouling tests, the end cap to the condenser shell was removed; a picture of the tube pattern can be seen in Section 4.8. The important known physical parameters of the condenser are listed in Table 6.1.

Table 6.1: Condenser physical dimensions.

Parameter	Dimension	Units
Tube outside diameter	0.75	inches
Tube inside diameter	0.612	inches
Tube length	8	feet
Shell volume	~10	cubic feet

Since the refrigerant is within the shell, the pressure drop through the condenser is almost negligible (can be approximated by about a 1 psi drop from the compressor

discharge). Superheated refrigerant from the compressor discharge enters the condenser at the top of the shell and condenses on the myriad of water-cooled tubes. The condensed refrigerant then pools on the bottom of the condenser shell, where it is subcooled. The subcooled refrigerant then leaves the bottom of the shell and enters the main liquid line.

To more accurately model the condenser, it was necessary to partition it into two sections. The first section dealt only with the condensing refrigerant (and the small amount of superheated vapor), the second section dealt only with the subcooled refrigerant. Each section was assumed to be in counterflow and the appropriate water-side and refrigerant-side heat transfer coefficients in the condenser were estimated using relations from Incropera and Dewitt (1996).

The total heat transfer rate in the condenser was found by summing the individual heat transfer rates from each section:

$$\dot{Q}_{\text{c,total}} = \dot{Q}_{\text{condensing}} + \dot{Q}_{\text{subcool}} \tag{6.1}$$

where the individual heat transfer rates were found using:

$$\dot{\text{Q}}_{\text{condensing}} = \varepsilon_c \cdot C_{\min,c}\left(T_c - T_{w,mid}\right) \tag{6.2}$$

$$\dot{\text{Q}}_{\text{subcool}} = \varepsilon_{sc} \cdot C_{\min,sc}\left(T_c - T_{w,in}\right) \tag{6.3}$$

where $\dot{Q}$ is the heat transfer rate, ε is the effectiveness, C_{min} is the minimum heat capacity rate, T_c is the condensing saturation temperature, $T_{w,mid}$ is the intermediate water entering temperature (to the condensing section), and $T_{w,in}$ is the water inlet temperature (to the subcooled section). The effectiveness and heat capacity rates were calculated by:

$$\varepsilon = 1 - e^{-\left[\frac{UA}{C_{\min}}\right]} \tag{6.4}$$

$$C_{\min} = \dot{m} \cdot c_p \tag{6.5}$$

For the condensing section, $\dot{m}$ is the condenser water mass flow rate and c_p is the water specific heat. For the subcooled section, $\dot{m}$ is the refrigerant mass flow rate and c_p is the subcooled refrigerant specific heat. The counterflow effectiveness relation was

approximated with Equation (6.4) since the ratio of the minimum heat capacity rate to the maximum heat capacity rate is nearly zero for both sections of the condenser. The only difference is that the water-side capacity rate is a minimum in the condensing section and a maximum in the subcooled section.

When calculating the overall heat transfer conductance, the fouling factor was tuned to a level about two times higher than what is typically associated with acceptable fouling (according to ARI guidelines). The overall heat transfer conductance was calculated for each section by using the following equations:

$$\frac{1}{UA_c} = \frac{1}{h_{r,c}A_{o,c}} + \frac{1}{h_w A_{i,c}} + \frac{ff_c}{A_{i,c}} \tag{6.6}$$

$$\frac{1}{UA_{sc}} = \frac{1}{h_{r,sc}A_{o,sc}} + \frac{1}{h_w A_{i,sc}} + \frac{ff_c}{A_{i,sc}} \tag{6.7}$$

where UA is the overall heat transfer conductance, h_r is the refrigerant-side heat transfer coefficient, A_o is the outside tube surface area, h_w is the water-side heat transfer coefficient, A_i is the inside tube surface area, and ff is the fouling factor.

The water-side heat transfer coefficient in the condenser was calculated using:

$$h_w = C_{w,f} \cdot \frac{k_w}{D_w} \cdot Nu_{w,D} \tag{6.8}$$

where C_f is a tube enhancement correction factor, k is the thermal conductivity of the water, D is the inside diameter of the tube, and Nu is the Nusselt number. The correction factor was tuned by using heat transfer data supplied by the manufacturer. Nu is calculated from:

$$Nu_{w,D} = \frac{(f/8)Re_D\,Pr}{1.07 + 12.7(f/8)^{1/2}\left(Pr^{2/3} - 1\right)} \tag{6.9}$$

where f is the friction factor, Re is the Reynolds number ($10^4 < Re < 5e10^6$), and Pr is the Prandtl number ($0.5 < Pr < 2000$). The friction factor was calculated using the following correlation:

$$f = \left(0.790\ln\left(\mathrm{Re}_D - 1.64\right)\right)^{-2} \tag{6.10}$$

The Reynolds number ($3000 < Re < 5e10^6$) was calculated by:

$$\mathrm{Re}_D = \frac{\rho_w \cdot V_w \cdot D_w}{\mu_w} \tag{6.11}$$

where ρ is the water density, V is the water velocity, D is the inside tube diameter, and μ is the water viscosity.

The condensing heat transfer coefficient was calculated from the following expression:

$$h_c = C_{c,f} \cdot 0.729 \cdot \left[\frac{g_c \rho_{c,l}\left(\rho_{c,l} - \rho_{c,v}\right) k_{c,l}^3 h'_{c,fg}}{\mu_{c,l}\left(T_{sat} - T_s\right) D_c}\right]^{1/4} \tag{6.12}$$

where C_f is an enhanced surface correction factor (tuned with data supplied by the manufacturer), g_c is the gravitational constant, ρ is the refrigerant density, the subscript l is for saturated liquid and v for saturated vapor, k is the refrigerant conductivity, μ is the refrigerant viscosity, T_{sat} is the refrigerant saturation temperature, T_s is the tube surface temperature, D is the inside tube diameter, and h'_{fg} is a modified form of the latent heat calculated from:

$$h'_{c,fg} = \left(h_{c,g} - h_{c,f}\right) + 0.68 \cdot c_{p,l} \cdot \left(T_{sat} - T_s\right) \tag{6.13}$$

where h_g is the saturated vapor enthalpy, h_f is the saturated liquid enthalpy, and $c_{p,l}$ is the specific heat of the liquid refrigerant.

The subcooled refrigerant heat transfer coefficient was calculated using a correlation for flow across a bank of tubes:

$$h_{sc} = C_{sc,f} \cdot \frac{k_{sc}}{D_{sc}} \cdot \mathrm{Nu}_{sc,D} \tag{6.14}$$

where C_f is a tube enhancement correction factor (tuned with experimental data), k is the thermal conductivity of the refrigerant, D is the outside diameter of the tube, and the Nusselt number is found from:

$$Nu_{sc,D} = 1.13 \cdot C_1 \cdot Re^{1/2} \, Pr^{1/3} \tag{6.15}$$

where C_1 is a constant determined from the tube arrangement (~0.5). This correlation is good for $2000 < Re < 40000$ and $Pr \geq 7$.

The remainder of the condenser model is used to determine the area of the tubes exposed to the condensing refrigerant and the area in contact with the subcooled refrigerant. The surface area of the tubes required to condense all the refrigerant is determined from Equation (6.16) in conjunction with Equation (6.2):

$$\dot{Q}_{condensing} = \dot{m}_r \cdot \left(h_{c,i} - h_{c,f} \right) \tag{6.16}$$

where $\dot{Q}$ is the condensing heat transfer rate, $\dot{m}_r$ is the refrigerant mass flow rate, $h_{c,i}$ is the condenser inlet enthalpy, and $h_{c,f}$ is the saturated liquid enthalpy.

The inputs to the computer model include: condenser water flow rate, inlet condenser water temperature, condenser pressure, entering refrigerant temperature, and refrigerant mass flow rate. The outputs are: condenser heat transfer rate, condenser water outlet temperature, condensing surface area, and refrigerant outlet enthalpy and subcooling.

The condenser model was able to accurately predict the actual heat transfer rate given inputs determined from measurements, such as the refrigerant mass flow rate:

$$\dot{m}_r = \frac{\dot{m}_{w,c} \cdot c_p \cdot \left(TCO - TCI \right)}{h_{c,i} - h_{c,o}} \tag{6.17}$$

where $\dot{m}_{w,c}$ is the mass flow rate of water in the condenser, c_p is the specific heat of the water, 'TCO-TCI' is the temperature difference of the water through the condenser, and '$h_{c,i}$-$h_{c,o}$' is the enthalpy difference of the refrigerant through the condenser. Figure 6.1 shows a plot of the predicted condenser heat transfer rate against the actual heat transfer rate. $\dot{Q}_{ct,tons}$ is the predicted heat transfer rate in tons, and $Cond_{tons}$ is the actual heat transfer rate. The data are from the 'Normal 1' benchmark test.

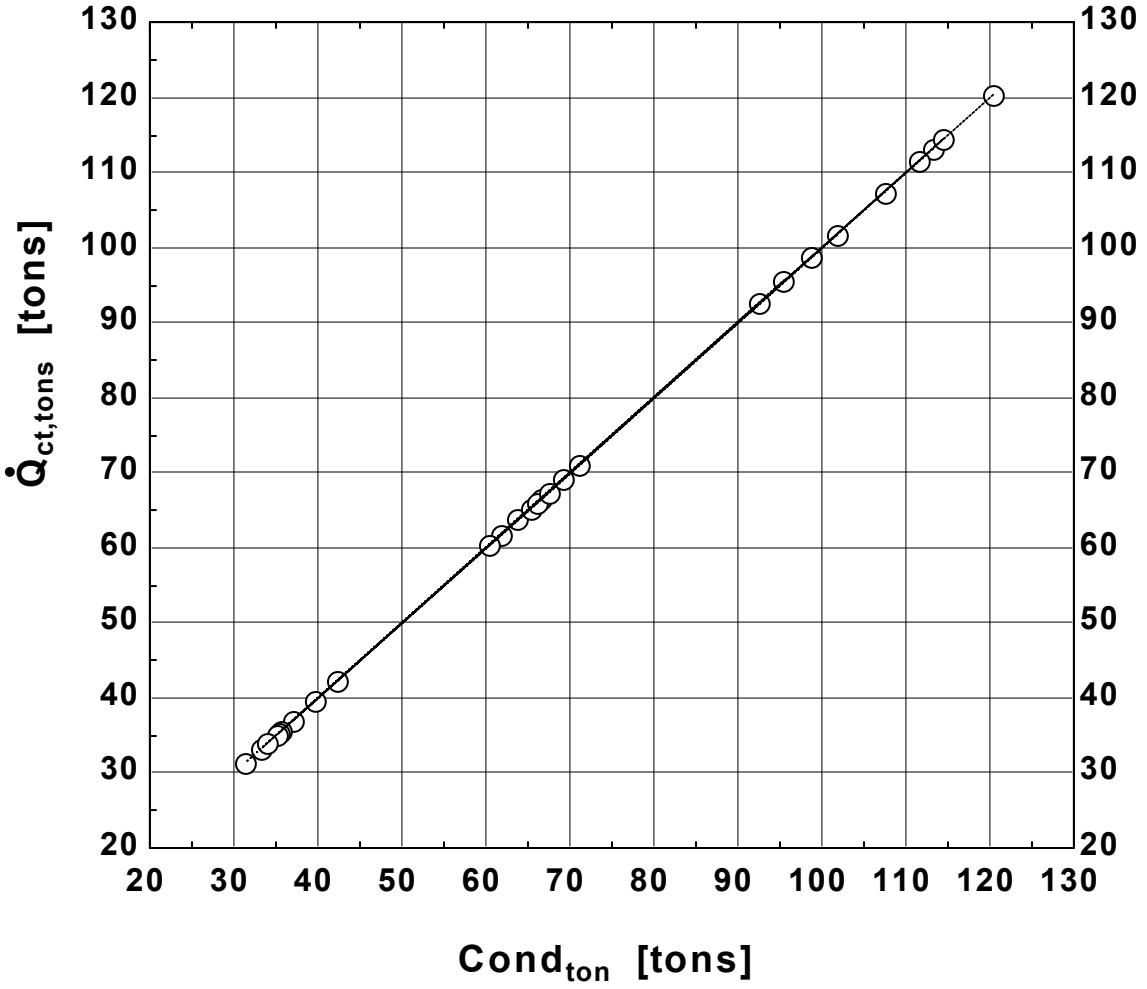

Figure 6.1: Predicted condenser heat transfer rate plotted against the actual heat transfer rate.

When the subcooling is specified as an input into the model, the condenser pressure is predicted as shown in Figure 6.2. PRC is the actual measured pressure and P_c is the estimated condenser pressure (both in psia).

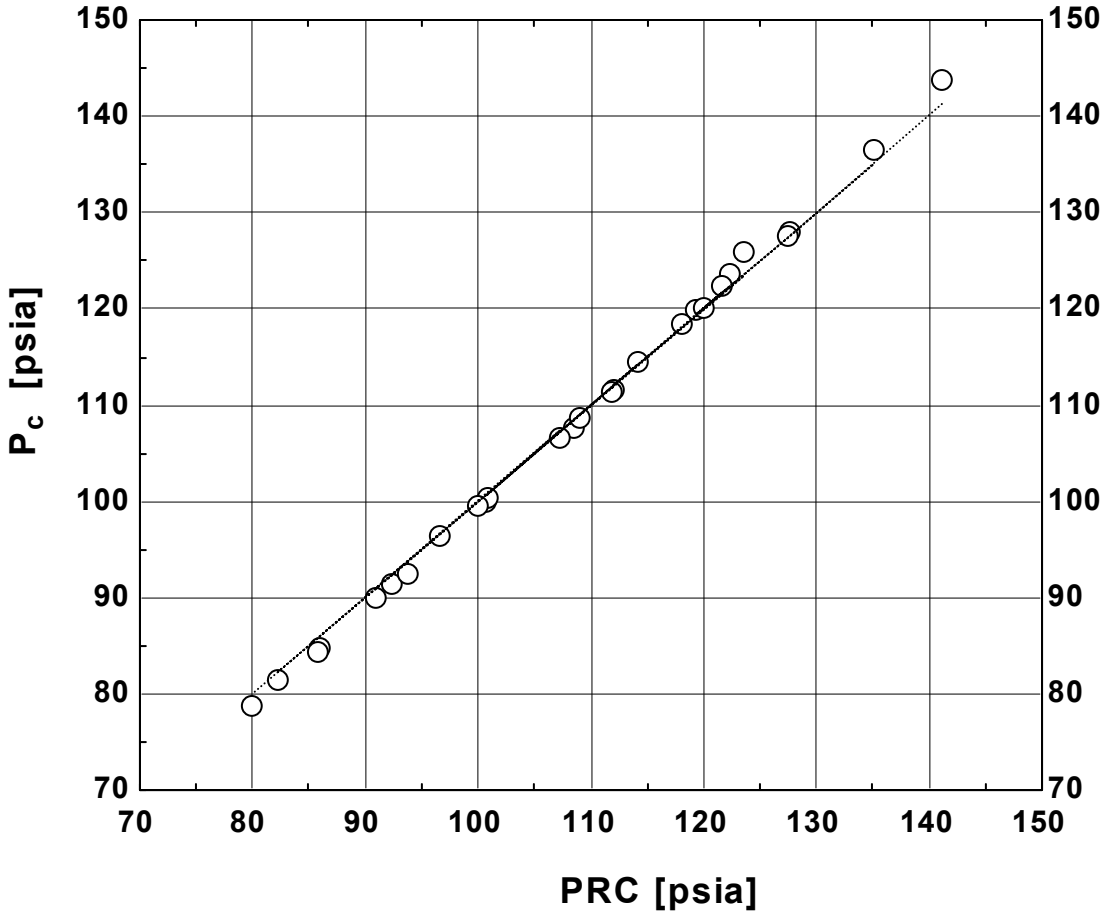

Figure 6.2: Predicted condenser pressure plotted against actual condenser pressure.

When condenser pressure is specified as an input to the model, the subcooling is estimated using:

$$\dot{Q}_{\text{subcooling}} = \dot{m}_r \cdot c_{p,c} \cdot \left(T_c - T_{liquid}\right) \tag{6.18}$$

where 'T_c-T_{liquid}' is the subcooling (difference between condensing temperature and subcooled temperature). Figure 6.3 shows a plot of the predicted subcooling against the actual measured subcooling. TRC_{sub} is the measured subcooling and T_{sc} is the predicted subcooling (both in degrees F). The one data point that was severely under-predicted belongs to 'Normal 1' test 19.

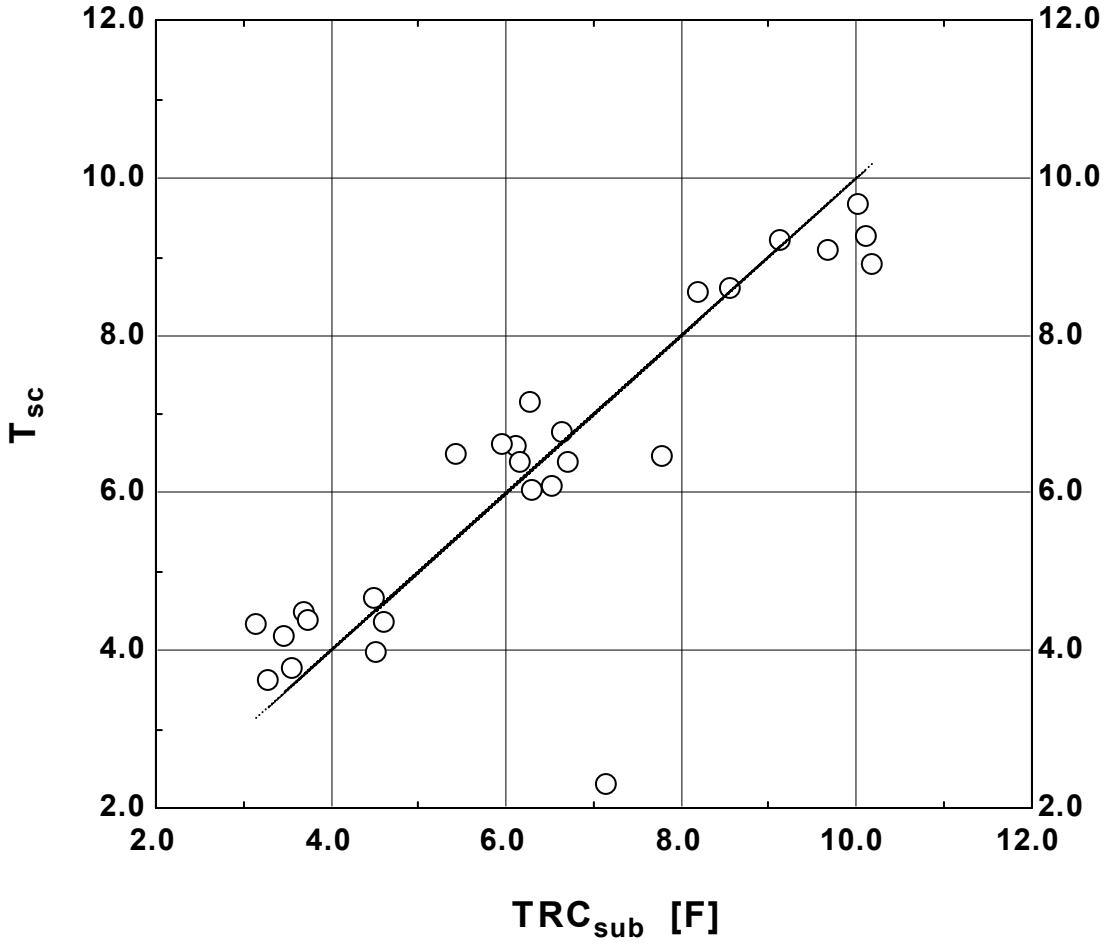

Figure 6.3: Predicted subcooling plotted against actual subcooling.

6.2 Evaporator Modeling

The evaporator is also a shell and tube design with refrigerant in the shell and water flowing through the tubes. The water makes two passes—the first pass is at the bottom of the evaporator, with the return pass closer to the top of the evaporator (not a logical design since coolest water is in contact with warmest refrigerant). There are a total of 149 tubes, with 74 in the first pass and 80 in the second pass. The important known physical parameters of the evaporator are listed in Table 6.2.

Table 6.2: Evaporator physical dimensions.

Parameter	Dimension	Units
Tube outside diameter	~0.77	inches
Tube inside diameter	~0.632	inches
Tube length	8	feet
Shell volume	~10	cubic feet

Since the refrigerant is within the shell, the pressure drop through the evaporator is almost negligible (can be approximated by about a 1 psi drop from the evaporator shell to the compressor inlet). Liquid refrigerant enters the evaporator at the bottom of the shell. The pool of refrigerant then boils off from the tube surfaces containing the water, thus cooling the water that is in turn used to condition air throughout an entire building. The boiled off refrigerant is superheated at the top of the evaporator shell before being pulled into the compressor (mounted above the evaporator).

The modeling of the heat transfer in the evaporator is nearly identical to that in the condenser. The evaporator was partitioned into two sections. The first section dealt only with the boiling refrigerant, the second interacted only with the superheated refrigerant. Each section was assumed to be in counterflow and the appropriate water-side and refrigerant-side heat transfer coefficients in the evaporator were estimated using relations from Incropera and Dewitt (1996).

The total heat transfer rate in the evaporator was found by summing the individual heat transfer rates from each section:

$$\dot{Q}_{\text{e,total}} = \dot{Q}_{\text{evaporating}} + \dot{Q}_{\text{superheat}} \tag{6.19}$$

where the individual heat transfer rates were found using:

$$\dot{\text{Q}}_{\text{evaporating}} = \varepsilon_e \cdot C_{e,\min}\left(T_{w,in} - T_e\right) \tag{6.20}$$

$$\dot{\text{Q}}_{\text{superheat}} = \varepsilon_{sh} \cdot C_{sh,\min}\left(T_{w,med} - T_e\right) \tag{6.21}$$

where $\dot{Q}$ is the heat transfer rate, ε is the effectiveness, C_{min} is the minimum heat capacity rate, T_e is the evaporating saturation temperature, $T_{w,in}$ is the water inlet temperature (to the evaporating section), and $T_{w,mid}$ is the intermediate water entering

temperature (to the superheated section). The effectiveness and heat capacity rates were calculated by:

$$\varepsilon = 1 - e^{-\left[\frac{UA}{C_{\min}}\right]} \tag{6.22}$$

$$C_{\min} = \dot{m} \cdot c_p \tag{6.23}$$

For the evaporating section, $\dot{m}$ is the evaporator water mass flow rate and c_p is the water specific heat. For the superheated section, $\dot{m}$ is the refrigerant mass flow rate and c_p is the superheated refrigerant specific heat. The counterflow effectiveness relation was approximated with Equation (6.22) since the ratio of the minimum heat capacity rate to the maximum heat capacity rate is nearly zero for both sections of the evaporator. The only difference is that the water-side capacity rate is a minimum in the evaporating section and a maximum in the superheated section.

When calculating the overall heat transfer conductance, the fouling factor was tuned to a level about equal to what is typically associated with acceptable fouling in the evaporator (according to ARI guidelines). The overall heat transfer conductance was calculated for each section by using the following equations:

$$\frac{1}{UA_e} = \frac{1}{h_{r,e}A_{o,e}} + \frac{1}{h_w A_{i,e}} + \frac{ff_e}{A_{i,e}} \tag{6.24}$$

$$\frac{1}{UA_{sh}} = \frac{1}{h_{r,sh}A_{o,sh}} + \frac{1}{h_w A_{i,sh}} + \frac{ff_e}{A_{i,sh}} \tag{6.25}$$

where UA is the overall heat transfer conductance, h_r is the refrigerant-side heat transfer coefficient, A_o is the outside tube surface area, h_w is the water-side heat transfer coefficient, A_i is the inside tube surface area, and ff is the fouling factor.

The water-side heat transfer coefficient in the evaporator was calculated using the same relations as those used in the condenser. The only difference was a slight modification to the tube enhancement correction factor and different property states due to the lower temperatures.

The evaporating heat transfer coefficient was calculated from the following expression:

$$h_e = C_{e,1} + C_{e,2} \cdot q''_e \tag{6.26}$$

where C_1 and C_2 are constants and q'' is the boiling heat flux. A book correlation could not be used since there were too many unknown factors associated with the refrigerant and tube surface interface. Equation (6.26) is a simplified correlation that approximates a confidential correlation experimentally determined by the manufacturer.

The superheated refrigerant heat transfer coefficient was calculated using:

$$h_{sh} = C_{sh,f} \cdot \frac{k_{sh}}{D_{sh}} \cdot Nu_{sh,D} \tag{6.27}$$

where C_f is a tube enhancement correction factor (tuned with experimental data), k is the thermal conductivity of the refrigerant, D is the outside diameter of the tube, and the Nusselt number is found from the same correlation for flow across a bank of tubes given in Equation (6.15).

The remainder of the evaporator model is used to determine the area of the tubes exposed to the evaporating refrigerant and the area in contact with the superheated refrigerant. The surface area of the tubes required to evaporate all the refrigerant is determined from using Equation (6.28) in conjunction with Equation (6.20):

$$\dot{Q}_{evaporating} = \dot{m}_r \cdot \left(h_{e,g} - h_{e,i}\right) \tag{6.28}$$

where $\dot{Q}$ is the evaporating heat transfer rate, $\dot{m}_r$ is the refrigerant mass flow rate, $h_{e,g}$ is the saturated vapor enthalpy, and $h_{e,i}$ is the evaporator inlet enthalpy. The superheated surface area is determined based on the known total evaporator surface area and the area required for evaporating the refrigerant.

The inputs to the computer model include: evaporator water flow rate, inlet evaporator water temperature, evaporator pressure, refrigerant mass flow rate, and entering refrigerant enthalpy. The outputs are: evaporator heat transfer rate, evaporator

water outlet temperature, evaporating surface area, and refrigerant outlet enthalpy and superheat.

The evaporator model was also able to accurately predict the actual heat transfer given inputs determined from data. The evaporator inlet enthalpy was calculated using:

$$h_{e,i} = h_{e.o} - \frac{\dot{m}_{w,e} \cdot c_p \cdot (TEI - TEO)}{\dot{m}_r} \tag{6.29}$$

where $h_{e,o}$ is the evaporator outlet enthalpy, $\dot{m}_{w,e}$ is the mass flow rate of water in the evaporator, c_p is the specific heat of the water, and 'TEI-TEO' is the temperature difference of the water through the evaporator. Figure 6.4 shows a plot of the predicted evaporator heat transfer rate against the actual heat transfer rate. $\dot{Q}_{et,tons}$ is the predicted heat transfer rate in tons, and $Evap_{tons}$ is the actual heat transfer rate. The data is from the 'Normal 1' benchmark test.

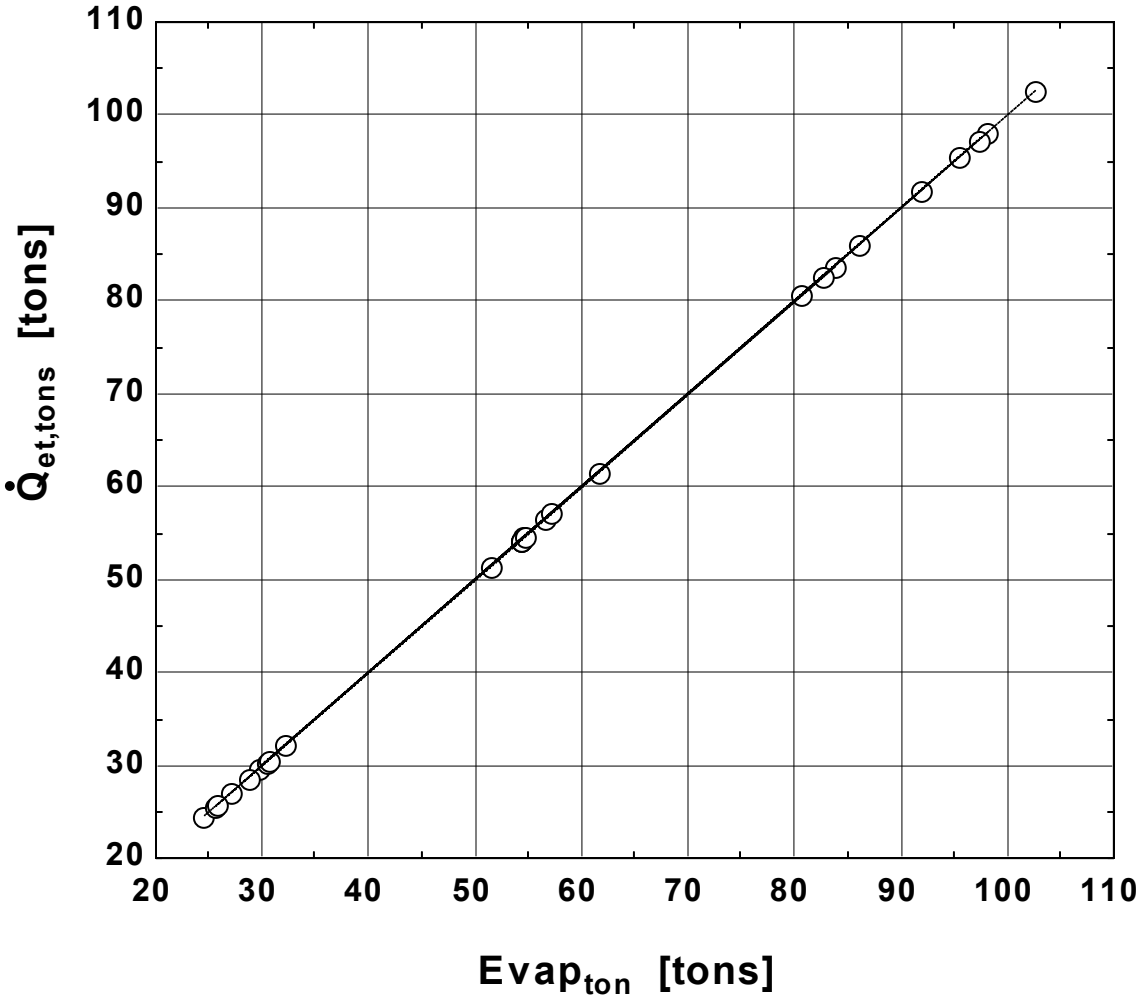

Figure 6.4: Predicted evaporator heat transfer rate plotted against the actual heat transfer rate.

When the superheat is specified as an input into the model, the evaporator pressure is predicted as shown in Figure 6.5. PRE is the actual measured pressure and P_e is the estimated evaporator pressure (both in psia).

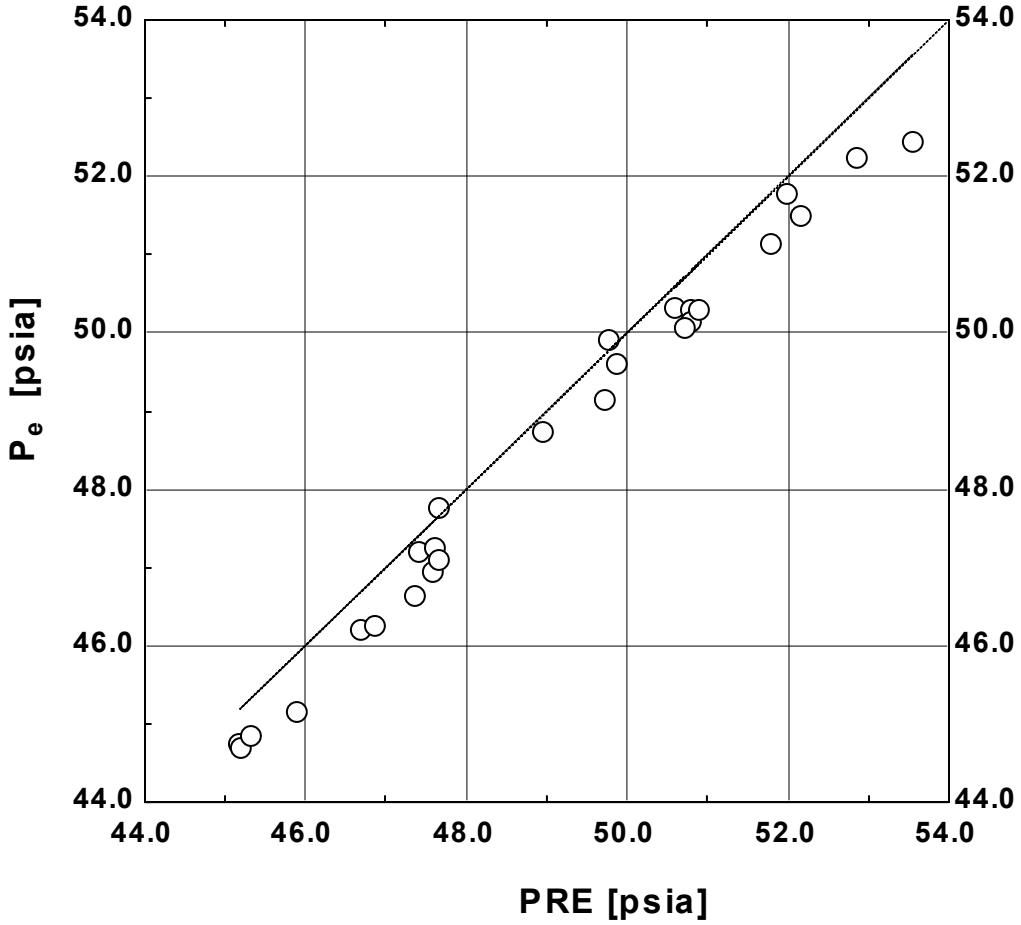

Figure 6.5: Predicted evaporator pressure plotted against actual evaporator pressure.

When evaporator pressure is specified as an input to the model, the superheat is estimated using:

$$\dot{Q}_{\text{superheat}} = \dot{m}_r \cdot c_{p,e} \cdot \left(T_{suction} - T_e\right) \tag{6.30}$$

where '$T_{suction}$-T_e' is the superheat (difference between suction temperature and evaporator temperature). Figure 6.6 shows a plot of the predicted superheat against the actual measured superheat. Tsh_{suc} is the measured superheat and T_{sh} is the predicted superheat (both in degrees F).

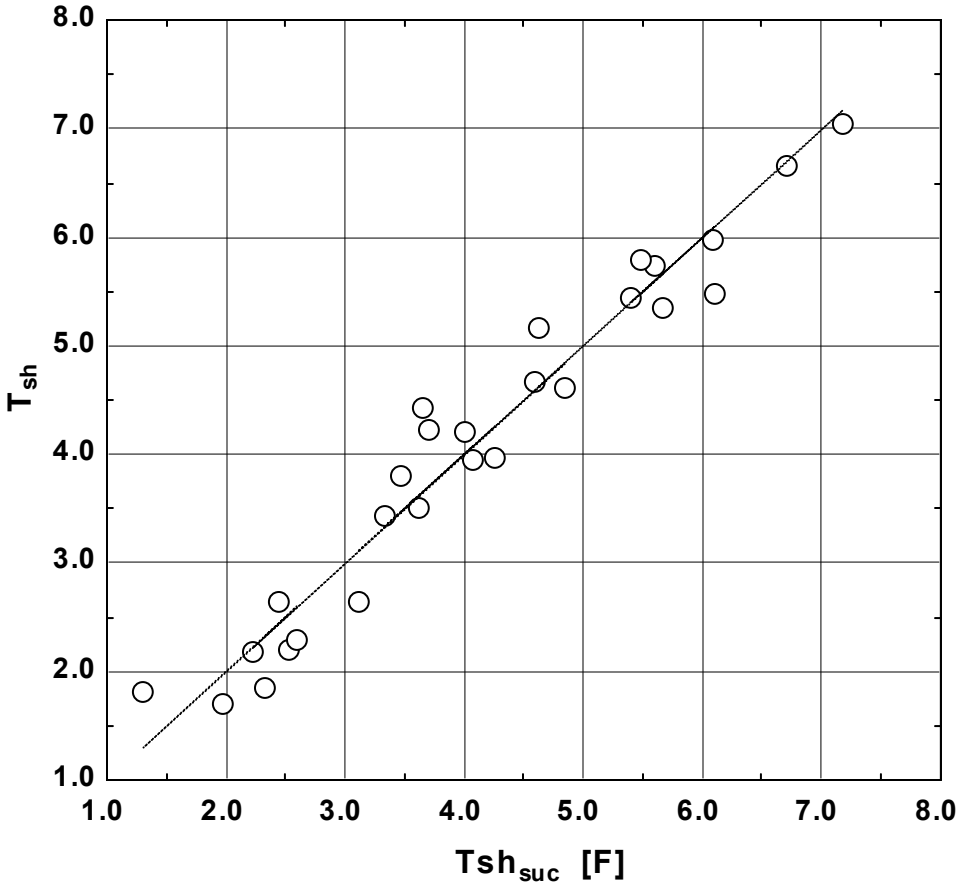

Figure 6.6: Predicted superheat plotted against actual superheat.

6.3 Fault Modeling

The heat exchanger models from the previous sections used a wealth of input data to predict the condenser and evaporator heat transfer rates. The results shown earlier are from test data without any faults present. When modeling faults, no modifications are necessary for the heat exchanger models in most instances.

One exception was for the condenser fouling tests. The model was adjusted to reflect the number of tubes that were blocked during the experimental testing. Figure 6.7 shows the predicted condenser heat transfer rate during the condenser fouling test with 30% of the tubes blocked (both in the computer model and in the experimental testing).

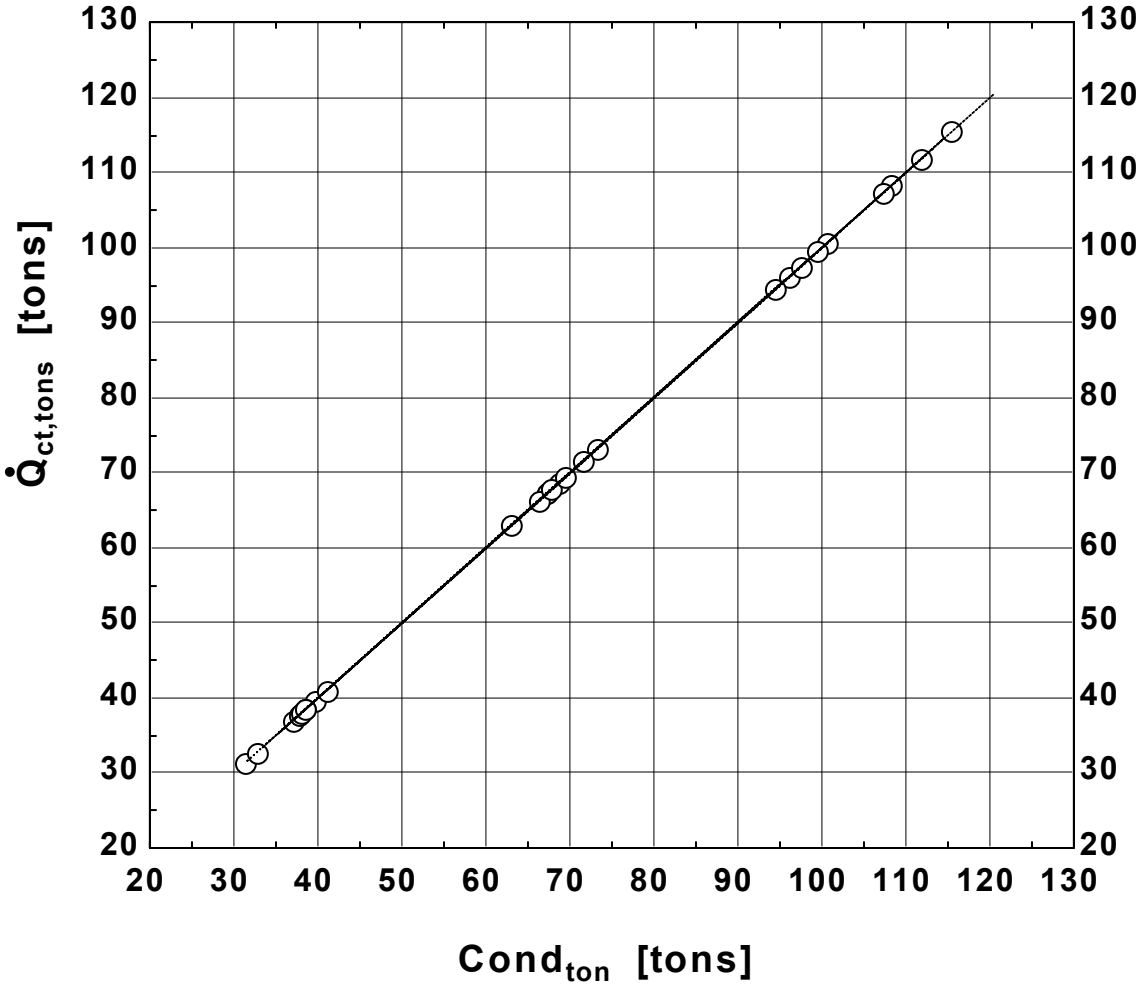

Figure 6.7: Predicted condenser heat transfer rate plotted against actual heat transfer rate using condenser fouling test data.

Figure 6.8 shows the predicted condenser pressure plotted against the actual pressure (both in psia) when subcooling is used as an input. The results show that the condenser pressure is slightly over-predicted (beyond the already inflated pressures caused by condenser fouling).

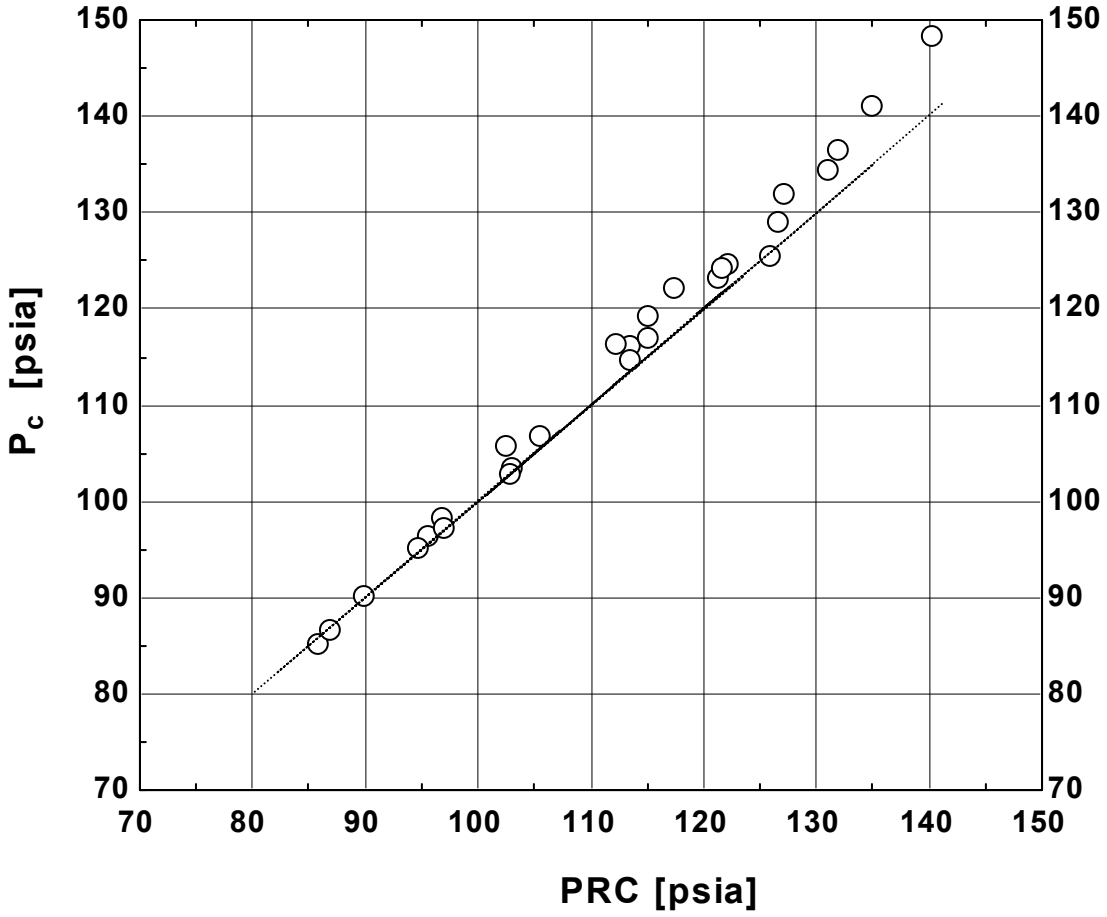

Figure 6.8: Predicted condenser pressure plotted against actual pressure using condenser fouling test data.

Figure 6.9 shows the predicted subcooling plotted against the actual subcooling (in degrees F) when condenser pressure is used as an input. The results show a substantial under-prediction of the subcooling.

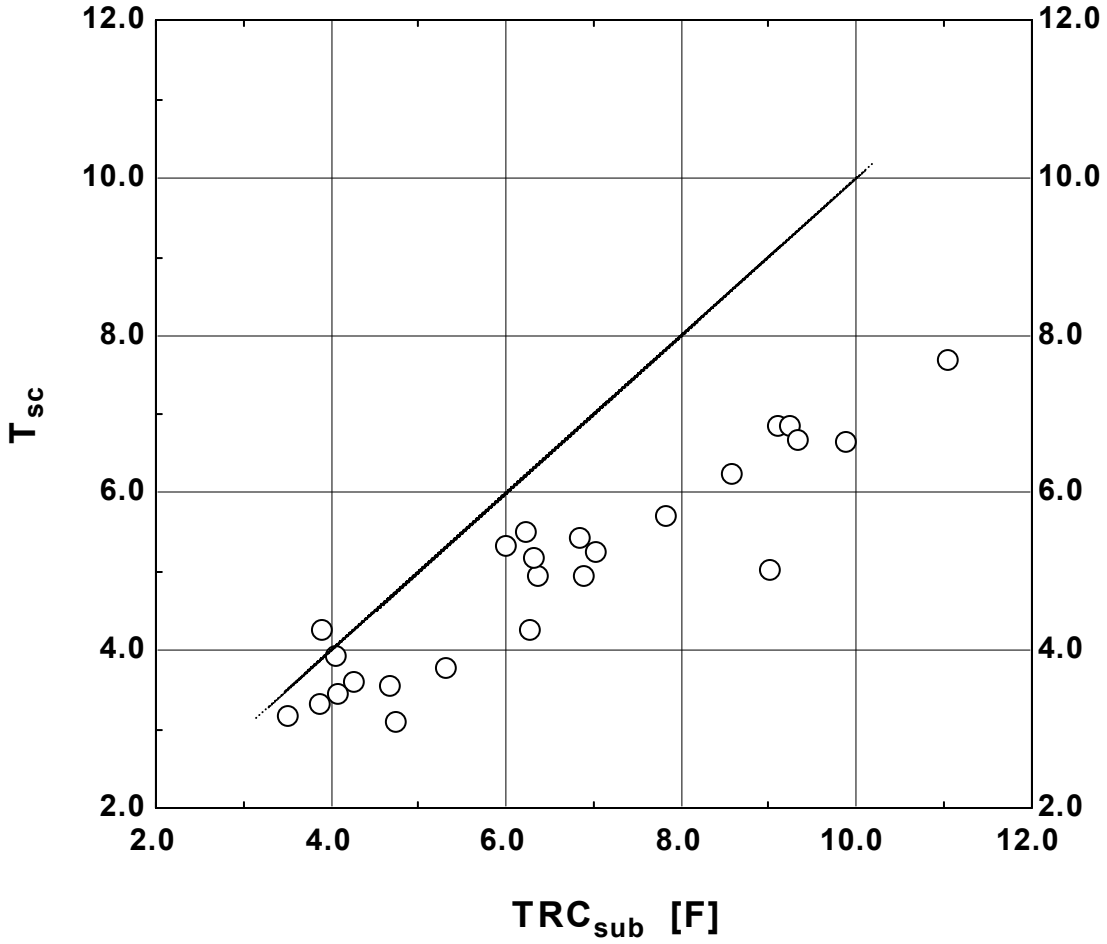

Figure 6.9: Predicted subcooling plotted against actual subcooling using condenser fouling test data.

In general, the fault data will prove very useful in tuning future system models that attempt to keep track of refrigerant charge, water flow rates, and superheat settings.

7.0 CONCLUSIONS AND RECOMMENDATIONS

7.1 Conclusions

The literature review performed at the beginning of this project demonstrated a lack of experimental data that can be used to develop FDD methods in chillers. Interviews with service technicians and an industry wide fault survey of service records indicated that the best faults to study were: loss of water flow in the condenser, loss of water flow in the evaporator, refrigerant leakage, refrigerant overcharge, presence of excess oil, condenser fouling, presence of non-condensables in the refrigerant, and a faulty expansion valve.

These faults were studied on a 90-ton centrifugal chiller at 27 different operating states to determine which of the measured thermodynamic properties were sensitive to each of the faults studied. The faults were tested at four levels of severity so that the data may be used to determine the sensitivity of future FDD methods (a separate report was prepared by Comstock and Braun (1999a) to help explain how to use the data, which is contained on CD-ROM). The data were sampled at a rate that allows dynamic analysis and includes both the start-up and shut down transients in addition to the changes in the operating conditions. Furthermore, the chiller was held at each operating condition long enough to reach steady state. Simple steady state models were developed for the condenser and evaporator, which were used to check the consistency of the measured data. In addition, the data were reviewed to ensure that steady state was reached during the vast majority of tests.

The results of the experimental testing revealed that all eight faults are detectable using simple temperature and pressure measurements already available in nearly all

chiller installations of the past 10 years. Excess oil proved to be the most difficult fault to detect, since the measurements with the strongest sensitivity are the least likely to be accurately monitored—compressor input power and oil temperature. Moreover, the defective pilot valve only impacted system performance at certain operating states, thus it would only be detectable in those conditions. The experimental testing also showed that it would be possible to differentiate between many of the faults tested, thus allowing accurate diagnosis. Only two faults displayed nearly identical measurement trends, refrigerant overcharge and non-condensables in the refrigerant. Nevertheless, differences in the magnitudes of the deviations as well as the responses of less sensitive measurements should still be adequate for accurate diagnosis.

7.2 Recommendations

This project was part of the first phase of an ASHRAE sponsored project. The remaining work necessary for the first phase of this project includes a complete dynamic chiller model. Some of the modeling performed for this thesis may prove useful in developing the dynamic model. In particular, the modeling of the heat transfer coefficients should be completely transferable to a dynamic model. More importantly, a vast assortment of experimental data is available for tuning the dynamic model. When using the experimental data, researchers should take care only to use the direct measurements and avoid relying on the calculations made within VisSim (detailed in Table 3.2)—primarily because VisSim did not have access to accurate property data.

The second phase of the ASHRAE project will involve the development of FDD methods. These methods may rely either on the dynamic model or on the actual experimental data. Researchers will find Chapters 4 and 5 particularly useful in determining the best approach to take in developing an FDD method.

The fault survey discussed in Chapter 2 is one of the most far reaching to date. Getting the cooperation of multiple manufacturers to release confidential information is difficult at best. Nevertheless, the information collected could still be improved. Future surveys could seek to record information on actual chiller capacity and age. Moreover, it

may be worth the effort to track the likely cause of field failures in order to determine whether there are any useful measurements that can be used to prevent such failures (i.e. find a small problem before it becomes a big problem).

The test chiller uses an expansion valve in the main liquid line between the condenser and evaporator; however, many commercial chillers use a fixed orifice as the expansion device. Since the system behavior would be different if using a fixed orifice, it is recommended that a chiller with a fixed orifice expansion device be tested in the future. Moreover, manual changes in the current expansion valve setting of the existing test chiller will be useful in determining its effect on certain measurements and system performance.

Finally, some researchers may be disappointed with the uncertainty inherent in the measured experimental data. As mentioned earlier, the purpose of this research was to explore a feasible means of introducing an FDD method in chillers with the minimum of additional sensors. If further research determines that more accurate instrumentation is either required or made feasible in commercial applications using FDD, then upgrading the chiller's instrumentation to run further tests would be warranted.

LIST OF REFERENCES

LIST OF REFERENCES

ARI Standard 550, 1992, *Centrifugal and Rotary Screw Water-Chilling Packages*, Air-Conditioning & Refrigeration Institute, Arlington, VA.

Bailey, M.B., 1998, *The Design and Viability of a Probabilistic Fault Detection and Diagnosis Method for Vapor Compression Cycle Equipment*, Ph.D. Thesis, School of Civil Engineering, University of Colorado.

Breuker, M.S., 1997, *Evaluation of a Statistical, Rule-Based Fault Detection and Diagnostics Method for Vapor Compression Air Conditioners*, Master Thesis, School of Mechanical Engineering, Purdue University.

Breuker, M.S. and J.E. Braun, 1998, "Common Faults and their Impacts for Rooftop Air Conditioners," *International Journal of Heating, Ventilating, and Air Conditioning and Refrigerating Research*, Vol. 4, No. 3, pp. 303-318.

Breuker, M.S. and J.E. Braun, 1998, "Evaluating the Performance of a Fault Detection and Diagnostic System for Vapor Compression Equipment," *International Journal of Heating, Ventilating, and Air Conditioning and Refrigerating Research*, Vol. 4, No. 4, pp. 401-425.

Comstock, M.C. and J.E. Braun, 1999, *Experimental Data from Fault Detection and Diagnostic Studies on a Centrifugal Chiller*, Purdue University, Ray W. Herrick Laboratories, Report # HL99-18.

Comstock, M.C., J.E. Braun, and B. Chen, 1999, *Literature Review for Application of Fault Detection and Diagnostic Methods to Vapor Compression Cooling Equipment*, Purdue University, Ray W. Herrick Laboratories, Report # HL99-19.

Fox, R.W. and A.T. McDonald, 1992, *Introduction to Fluid Mechanics*, 4th Edition, John Wiley and Sons, New York.

Grimmelius, H.T., J.K. Woud, and G. Been, 1995, "On-line Failure Diagnosis for Compression Refrigeration Plants," *International Journal of Refrigeration*, Vol. 18, No. 1, pp. 31-41.

Incropera, F.P. and D.P. DeWitt, 1996, *Fundamentals of Heat and Mass Transfer*, 4th Edition, John Wiley and Sons, New York.

Klein, S.A. and F.L. Alvarado, (1992-1999), *Engineering Equation Solver (EES) Version 5.028*, F-Chart Software, 4406 Fox Bluff Road, Middletown, WI 53562.

McQuay International, 1995, *200-Series MicroTech Control Panel For Centrifugal Chillers: Installation and Maintenance Data*, Bulletin No. IM 616.

McQuay International, 1996, *200-Series MicroTech Control Panel: Operations and Maintenance Data*, Bulletin No. OM 125.

McQuay International, 1995, *MicroTech Unit Controller: Installation and Maintenance Data*, Bulletin No. IM 403.

McQuay International, 1995, *MicroTech Chiller System Controller: Installation and Maintenance Data*, Bulletin No. IM 618.

McQuay International, 1995, *MicroTech Chiller System Controller For Centrifugal, Reciprocating, and Screw Chillers: Operation Manual*, Bulletin No. OM 127.

McQuay International, 1996, *Single/Dual Compressor Centrifugal Chillers: Operating and Maintenance Manual*, Bulletin No. OM 307-5.

McQuay International, 1995, *Starters For Use With McQuay Centrifugal Units: Installation and Maintenance Data*, Bulletin No. IM 322-3.

McQuay International, 1995, *Wye-Delta Wiring: Engineering Data*, Bulletin No. 8002.

Peitsman, H. and V. Bakker, 1996, "Application of Black-Box Models to HVAC Systems for Fault Detection," *ASHRAE Transactions*, Vol. 102, Pt. 1, pp. 628-640.

Rossi, T.M. and J.E. Braun, 1993, "Classification of Fault Detection and Diagnostic Methods," *International Energy Agency Building Optimisation and Fault Diagnosis System Concept*. Published by the Technical Research Centre of Findland, Laboratory of Heating and Ventilation.

Rossi, T.M., 1995, *Detection, Diagnosis, and Evaluation of Faults in Vapor Compression Cycle Equipment*, Ph.D. Thesis, School of Mechanical Engineering, Purdue University.

Rossi, T.M. and J.E. Braun, 1996, "Minimizing Operating Costs of Vapor Compression Equipment with Optimal Service Scheduling," *International Journal of Heating, Ventilating, and Air Conditioning and Refrigerating Research*, Vol. 2, No. 1, pp. 3-26.

Rossi, T.M. and J.E. Braun, 1997, "A Statistical, Rule-Based Fault Detection and Diagnostic Method for Vapor Compression Air Conditioners," *International Journal of Heating, Ventilating, and Air Conditioning and Refrigerating Research*, Vol. 3, No. 1, pp. 19-37.

Stouppe, D.E. and Y.S. Lau, 1989, "Air Conditioning and Refrigeration Equipment Failures," *National Engineer*, Vol. 93, No. 9, pp. 14-17.

Stylianou, M. and D. Nikanpour, 1996, "Performance Monitoring, Fault Detection, and Diagnosis of Reciprocating Chillers," *ASHRAE Transactions*, Vol. 102, Pt. 1, pp. 615-627.

Stylianou, M. P., 1997, "Application of Classification Functions to Chiller Fault Detection and Diagnosis," *ASHRAE Transactions*, Vol. 103, Pt. 1, pp. 645-656.

Wark Jr., K., 1988, *Thermodynamics*, 5th Edition, McGraw-Hill Inc., New York.

ADDITIONAL REFERENCES

ADDITIONAL REFERENCES

Anderson, S.A. and Joseph C. Dieckert, 1990, "On-site Chiller Testing," *ASHRAE Journal*, Vol. 32, April, pp. 54-60.

Austin, S.B., 1991, "Optimum Chiller Loading," *ASHRAE Journal*, Vol. 33, July, pp. 40-43.

Basseville, M., 1988, "Detecting Changes in Signals and Systems—A Survey," *Automatica*, Vol. 24, No. 3, pp. 309-326.

Brambley, M., R. Pratt, D. Chassin, S. Katipamula, and D. Hatley, 1998, "Diagnostics for Outdoor Air Ventilation and Economizers," *ASHRAE Journal*, Vol. 40, October, pp. 49-55.

Browne, M.W. and P.K. Bansal, 1998, "Challenges in Modeling Vapor-Compression Liquid Chillers," *ASHRAE Transactions*, Vol. 104, Pt. 1a, pp. 474-486.

Brownell, K.A., S.A. Klein, and D.T. Reindl, 1999, "Refrigerator System Malfunctions," *ASHRAE Journal*, Vol. 41, No. 2, pp. 40-47.

Buecker, B., 1995, "Beware of Condenser Fouling," *Chemical Engineering*, Vol. 102, April, pp. 108-112.

Bultman, D.H., L.C. Burmeister, V. Bortone, and P.W. TenPas, 1993, "Vapor-compression refrigerator performance degradation due to condenser air flow blockage," *American Society of Mechanical Engineers (Paper)*, 93-HT-34, pp. 1-13.

Chen, J. and R.J. Patton, 1999, *Robust Model-Based Fault Diagnosis for Dynamic Systems*, Kluwer Academic Publishers, Boston.

Culp, C., 1989, "Expert Systems in Preventative Maintenance and Diagnostics," *ASHRAE Journal*, Vol. 31, No. 8, pp. 25-27.

Dexter, A.L., 1995, "Fuzzy Model Based Fault Diagnosis," *IEE Proc.-Control Theory Appl*., Vol. 142, Pt. D, No. 6, pp. 545-550.

Dexter, A.L. and M. Benouarets, 1996, "A Generic Approach to Identifying Faults in HVAC Plants," *ASHRAE Transactions*, Vol. 102, Pt. 1, pp. 550-556.

Dexter, A.L. and M. Benouarets, 1997, "Model-Based Fault Diagnosis Using Fuzzy Matching," *IEEE Transactions on Systems, Man, and Cybernetics*, Vol. 27, No. 5, Pt. A, pp. 673-682.

Dialynas, E.N., A.V. Machias, and J.L. Souflis, 1987, "Reliability and Fault Diagnosis Methods of Power System Components." In S. Tzafestas, M. Singh, and G. Schmidt (Ed.), *System Fault Diagnostics, Reliability and Related Knowledge-Based Approaches* (Vol. 1, pp. 327-341). Dordrecht, Holland: D. Reidel Publishing Company.

Eppelheimer, D.M., 1996, "Variable Flow—The Quest for System Energy Efficiency," *ASHRAE Transactions*, Vol. 102, Pt. 2. pp. 673-678.

Farzad, M. and D.L. O'Neal, 1993, "Influence of the Expansion Device on Air-Conditioning System Performance Characteristics Under a Range of Charging Conditions," *ASHRAE Transactions*, Vol. 99, Pt. 1, pp. 3-13.

Fasolo, P.S. and D.E. Seborg, 1995, "Monitoring and Fault Detection for an HVAC Control System," *International Journal of Heating, Ventilating, and Air-Conditioning and Refrigerating Research*, Vol. 1, No. 3, pp. 177-193.

Frank, P.M., 1987, "Fault Diagnosis in Dynamic Systems via State Estimation: A Survey." In S. Tzafestas, M. Singh, and G. Schmidt (Ed.), *System Fault Diagnostics, Reliability and Related Knowledge-Based Approaches* (Vol. 1, pp. 35-98). Dordrecht, Holland: D. Reidel Publishing Company.

Frank, P.M., 1990, "Fault Diagnosis in Dynamic Systems Using Analytical and Knowledge-Based Redundancy – A Survey and Some New Results," *Automatica*, Vol. 26, No. 3, pp. 459-474.

Gertler, J.J., 1988, "Survey of Model-Based Failure Detection and Isolation in Complex Plants," *IEEE Control Systems Magazine*, Vol. 8, No. 6, pp. 3-11.

Gertler, J.J., 1998, *Fault Detection and Diagnosis in Engineering Systems*, Marcel Dekker Inc., New York.

Glass, A.S., P. Gruber, M. Roos, and J. Tödtli, 1995, "Qualitative Model-Based Fault Detection in Air-Handling Units," *IEEE Control Systems Magazine*, Vol. 15, No. 4, pp. 11-22.

Gordon, J.M. and K.C. Ng, 1995, "Predictive and diagnostic aspects of a universal thermodynamic model for chillers," *International Journal of Heat and Mass Transfer*, Vol. 38, No. 5, pp. 807-818.

Hartman, T.B., 1996, "Design Issues of Variable Chilled-Water Flow Through Chillers," *ASHRAE Transactions*, Vol. 102, Pt. 2. pp. 679-683.

Haves, P., T. Salsbury, and J.A. Wright, 1996, "Condition Monitoring in HVAC Subsystems Using First Principles Models," *ASHRAE Transactions*, Vol. 102, Pt. 1, pp. 519-527.

Houghton, D., 1997, "Operating and Maintaining Rooftop Air Conditioners", *ASHRAE Journal*, Vol. 39, December, pp. 50-54.

Howell, J., 1994, "Model-based Fault Detection in Information Poor Plants," *Automatica*, Vol. 30, No. 6, pp. 929-943.

Hyvärinen, J. and S. Kärki (Ed.), 1996, *International Energy Agency Building Optimisation and Fault Diagnosis Source Book*. Published by the Technical Research Centre of Findland, Laboratory of Heating and Ventilation.

Inatsu, H., H. Matsuo, K. Fujiwara, K. Yamada, and K. Nishizawa, 1992, "Development of Refrigerant Monitoring Systems for Automotive Air-Conditioning Systems," *Society of Automotive Engineers*, SAE Paper No. 920212.

Isermann, R., 1984, "Process Fault Detection Based on Modeling and Estimation – A Survey," *Automatica*, Vol. 20, No. 4, pp. 387-404.

Isermann, R., 1987, "Experiences with Process Fault Detection Methods via Parameter Estimation." In S. Tzafestas, M. Singh, and G. Schmidt (Ed.), *System Fault Diagnostics, Reliability and Related Knowledge-Based Approaches* (Vol. 1, pp. 3-33). Dordrecht, Holland: D. Reidel Publishing Company.

Isermann, R., 1993, "Fault Diagnosis of Machines via Parameter Estimation and Knowledge Processing—Tutorial Paper", *Automatica*, Vol. 29, No. 4, pp. 815-835.

Isermann, R. and P. Ballé, 1997, "Trends in the Application of Model-Based Fault Detection and Diagnosis of Technical Processes", *Control Engineering Practice*, Vol. 5, No. 5, pp. 709-719.

Jiang, Y., J. Li, and X. Yang, 1995, "Fault Direction Space Method for On-line Fault Detection," *ASHRAE Transactions*, Vol. 101, Pt. 2, pp. 219-228.

Jones, A.H. and S.E. Burge, 1987, "An Expert System Design Using Cause-Effect Representations and Simulation for Fault Detection." In S. Tzafestas, M. Singh, and G. Schmidt (Ed.), *System Fault Diagnostics, Reliability and Related Knowledge-Based Approaches* (Vol. 2, pp. 71-80). Dordrecht, Holland: D. Reidel Publishing Company.

Kaler Jr., G.M., 1990, "Embedded Expert System Development for Monitoring Packaged HVAC Equipment," *ASHRAE Transactions*, Vol. 96, Pt. 2, pp. 733-742.

Krafthefer, B.C. Rask, and D.R. Bonne, 1987, "Air-conditioning and heat pump operating cost savings by maintaining coil cleanliness," *ASHRAE Transactions*, Vol. 93, Pt. 1, pp. 1458-1473.

Kumamaru, T., T. Utsunomiya, Y. Yamada, Y. Iwasaki, I. Shoda, and M. Obayashi, 1991, "A Fault Diagnosis System for District Heating and Cooling Facilities," *Proceedings of the International Conference on Industrial Electronics, Control, and Instrumentation,* Kobe, Japan (IECON '91), Vol. 1, pp. 131-136.

Lee, W.Y., C. Park, and G.E. Kelly, 1996, "Fault Detection in an Air-Handling Unit Using Residual and Recursive Parameter Identification Methods," *ASHRAE Transactions*, Vol. 102, Pt. 1, pp. 528-539.

Lee, W.Y., J.M. House, C. Park, and G.E. Kelly, 1996, "Fault Diagnosis of an Air-Handling Unit Using Artificial Neural Networks," *ASHRAE Transactions*, Vol. 102, Pt. 1, pp. 540-549.

Lee, W.Y., J.M. House, and D.R. Shin, 1997, "Fault Diagnosis and Temperature Sensor Recovery for an Air-Handling Unit," *ASHRAE Transactions*, Vol. 103, Pt. 1, pp. 621-633.

Li, X., V. Hossein, and J. Visier, 1996, "Development of a Fault Diagnosis Method for Heating Systems Using Neural Networks," *ASHRAE Transactions*, Vol. 102, Pt. 1, 607-614.

Li, X., J. Visier, and H. Vaezi-Nejad, 1997, "A Neural Network Prototype for Fault Detection and Diagnosis of Heating Systems," *ASHRAE Transactions*, Vol. 103, Pt. 1, pp. 634-644.

Mangoubi, R.S., 1998, *Robust Estimation and Failure Detection*, Springer, New York.

March, P.A. and C.W. Almquist, 1989, "New techniques for monitoring condenser flow rate, fouling," *Power*, Vol. 133, March, pp. 73-76.

McKellar, M.G., 1987, *Failure Diagnosis for a Household Refrigerator*, Master Thesis, School of Mechanical Engineering, Purdue University.

Norford, L.K. and R.D. Little, 1993, "Fault Detection and Load Monitoring in Ventilation Systems," *ASHRAE Transactions*, Vol. 99, Pt. 1, pp. 590-602.

Pape, F.L.F. and J.W. Mitchell, 1990, "Optimal Control and Fault Detection in Heating, Ventilating, and Air-Conditioning Systems," *ASHRAE Transactions*, Vol. 97, Pt. 1, pp. 729-736.

Patton, R., P. Frank, and R. Clark, 1989, *Fault Diagnosis in Dynamic Systems*, Prentice Hall, New York.

Patton, R.J. and J. Chen, 1994, "Robust Fault Diagnosis of Stochastic Systems with Unknown Disturbances," *Control '94*, Conference Publication No. 389, pp. 1340-1345.

Patton, R.J., J. Chen, and T.M. Siew, 1994, "Fault Diagnosis in Nonlinear Dynamic Systems via Neural Networks," *Control '94*, Conference Publication No. 389, pp. 1346-1351.

Phelan, J., M. Brandemuehl, and M. Krarti, 1997, "Review of Laboratory and Field Methods to Measure Fan, Pump, and Chiller Performance," *ASHRAE Transactions*, Vol. 103, Pt. 2, pp. 914-925.

Redden, G.H., 1996, "Effect of Variable Flow on Centrifugal Chiller Performance," *ASHRAE Transactions*, Vol. 102, Pt. 2. pp. 684-687.

Tsutsui, H. and K. Kamimura, 1996, "Chiller Condition Monitoring Using Topological Case-Based Modeling," *ASHRAE Transactions*, Vol. 102, Pt. 1, pp. 641-648.

Tzafestas, S.G., 1987, "A Look at the Knowledge-Based Approach to System Fault Diagnosis and Supervisory Control." In S. Tzafestas, M. Singh, and G. Schmidt (Ed.), *System Fault Diagnostics, Reliability and Related Knowledge-Based Approaches* (Vol. 2, pp. 3-15). Dordrecht, Holland: D. Reidel Publishing Company.

Wagner, J. and R. Shoureshi, 1992, "Failure Detection Diagnostics for Thermofluid Systems," *Journal of Dynamic Systems, Measurement, and Control*, Vol. 114, No. 4, pp. 699-706.

Willsky, A.S., 1976, "A Survey of Design Methods for Failure Detection in Dynamic Systems," *Automatica*, Vol. 12, pp. 601-611.

Yoshida, H., T. Iwami, H. Yuzawa, and M. Suzuki, 1996, "Typical Faults of Air-Conditioning Systems and Fault Detection by ARX Model and Extended Kalman Filter," *ASHRAE Transactions*, Vol. 102, Pt. 1, pp. 557-564.

Yoshimura, M. and N. Ito, 1989, "Effective Diagnosis Methods for Air-Conditioning Equipment in Telecommunications Buildings," In *Proceedings of IEEE INTELEC 89: The Eleventh International Telecommunications Energy Conference*, October 15-18, 1989, Centro dei Congressi, Firenze, Vol. 21.1: 1-7.

APPENDICES

Appendix A: Detailed Test Stand Documentation

A.1 Equipment

The complete test stand consists of a chiller integrated into a simulated building load as well as all the instrumentation required to collect the pertinent data. The construction of the test facility proceeded through the first part of 1999, with the official commissioning of the chiller occurring on June 24, 1999.

A.1.1 Chiller

The nameplate on the centrifugal compressor reads; Model: CE048JAH10RAX, Style: 700508GG60, Serial: 5UH0075901, Motor Style: 5970934G11, Speed Code: AH. This information seems to indicate that the impeller is 4.8 inches in diameter; however, the speed code does not correspond with this kind of impeller. The actual speed code is AE, the gear ratio was modified without the compressor nameplate being updated—impeller tip velocity should be 657 ft/second.

The nameplate on the front of the chiller reads; Model: PEH048J, Serial: ENG-LAB-1, Compressor: Volts 460, Hz 60, Phase 3, RLA: 105, LRA WYE 163, LRA DELTA 488, Refrigerant: 134a, Charge: 300 lbs. The following supplementary information corresponds with what was given on the nameplate: rated load amps is 105 during normal operation, locked rotor amps is 163, and start-up locked rotor amps is 488. The chiller was originally used in one of McQuay's engineering test facilities for approximately 10 years before being donated to Herrick Laboratories for this project.

The controller is a Series 200 MicroTech controller. Energy Line manufactures the MicroTech controller; MicroTech is simply a brand name reserved exclusively for McQuay. The MicroTech controller contains a microprocessor that keeps track of a large number of sensor readings and can also communicate on a network via an N2 bus or

modem. A large amount of documentation is available from McQuay on the MicroTech controller, relating to the user interface screens as well as the internal wiring.

Some of the sensors mounted on the chiller provide the following measurements:

- Evaporator leaving water temperature
- Evaporator entering water temperature
- Compressor suction temperature
- Condenser liquid line temperature
- Condenser entering water temperature
- Condenser leaving water temperature
- Percent unit amps
- Compressor discharge temperature
- Oil feed temperature
- Oil sump temperature
- Oil vent pressure
- Evaporator refrigerant pressure
- Condenser refrigerant pressure
- Oil feed gauge pressure

From these measurements the following temperatures and pressures are calculated:

- Evaporator temperature derived from saturation tables
- Condenser temperature derived from saturation tables
- Net oil pressure calculated from oil gauge pressure minus oil vent pressure
- Lift pressure calculated from condenser pressure minus evaporator pressure
- Suction superheat calculated from suction line temperature minus evaporator temperature
- Discharge superheat calculated from discharge temperature minus condenser temperature
- Liquid subcooling calculated from condenser temperature minus liquid line temperature

- Condenser approach temperature calculated from condenser temperature minus leaving condenser water temperature
- Evaporator approach temperature calculated from leaving evaporator water temperature minus evaporator temperature

These sensor readings are utilized in the following fault/alarm monitoring by the MicroTech controller:

- Low discharge superheat (<0°F @ 100% RLA or <0°F @ 40%RLA)
- High discharge superheat (>32°F @ 100% RLA or >35°F @ 40% RLA)
- Low evaporator pressure (<30 psig): inhibits loading
- Low evaporator pressure (<28 psig): unloads compressor
- High discharge temperature (>170°F): loads compressor
- Condenser freeze protect (<34°F): condenser water pump started
- Evaporator freeze protect (<34°F): evaporator water pump started
- Low evaporator pressure (<26 psig): compressor shut down
- Low net oil pressure (<50 psig): compressor shut down
- Low oil delta temperature (<20°F): compressor shut down
- High oil feed temperature (>140°F): compressor shut down
- Low motor current (<10%): compressor shut down
- High motor current (>10%): when compressor is shut down
- High discharge temperature (>190°F): compressor shut down
- High condenser pressure (>140 psig): compressor shut down
- High motor temperature: compressor shut down
- High suction superheat (running >25°F; startup >90°F): compressor shut down
- No starter transition: compressor shut down
- No evaporator water flow: compressor shut down
- No condenser water flow: compressor shut down
- Starter fault: compressor shut down
- Various sensor failures: compressor shut down

As can be observed by this list, the chiller controller is already monitoring many simple faults.

A.1.2 Test Stand

The chiller test stand is comprised of multiple water loops, a city water supply, and a steam supply. The condenser water loop consists of the following components:

- Water pump: B&G Model 1531, size 3AC with 10 HP/3500 RPM motor
- Suction diffuser: B&G Model EE-3X
- Triple duty valve: B&G Model 3DS-4S
- Shell and tube heat exchanger: B&G Model WU104-2
- Rolairtrol air separator: B&G Model RL-4
- B&G 15 gallon compression tank
- Fill valve: B&G Model B-38
- Pressure relief valve: B&G Model 790-30
- Automatic vent valve: B&G Model 87
- Vortex flow meter: Fluidyne Hydro-Flow Model 2200
- Electronically actuated 3-way valve: JCI VB-4322-13
- Electronically actuated 2-way valve: JCI VB-3970-17

The evaporator water loop consists of the following components:

- Water pump: B&G Model 1531, size 3AC with 3 HP/1750 RPM motor
- Suction diffuser: B&G Model EE-3X
- Triple duty valve: B&G Model 3DS-4S
- Shell and tube heat exchanger: B&G Model WU105-2
- Rolairtrol air separator: B&G Model RL-4
- B&G 15 gallon compression tank
- Fill valve: B&G Model B-38
- Pressure relief valve: B&G Model 790-30
- Automatic vent valve: B&G Model 87

- Vortex flow meter: Fluidyne Hydro-Flow Model 2200
- Electronically actuated 2-way valve: JCI VB-3970-17

The hot water loop consists of the following components:

- Water pump: B&G Model 1531, size 1-1/2AC with 1 HP/1750 RPM motor
- Suction diffuser: B&G Model BA-3X
- Triple duty valve: B&G Model 3DS-2S
- Shell and tube heat exchanger: B&G Model WU104-2
- Shell and tube steam heat exchanger: B&G Model SU62-2
- Air separator: B&G Model EAS-2
- B&G 15 gallon compression tank
- Fill valve: B&G Model B-38
- Pressure relief valve: B&G Model 790-30
- Automatic vent valve: B&G Model 87
- Electronically actuated valve: JCI VG7241PT

The city water and steam supply have the following valves:

- Electronically actuated valve: JCI VG7241ST
- Electronically actuated valve: JCI VG7241GT
- Electronically actuated valve: JCI VG7241LT

In addition to these components, there were 12 1000Ω Platinum RTDs (Resistance Temperature Detectors) and various relays to turn pumps and valves on and off. Finally, a Scientific Columbus power transducer, Model XL31K5PAN7-2, was mounted in the starter to measure the instantaneous power consumption of the compressor.

Pressure gages are mounted across each water pump for troubleshooting. These gages are most frequently used to ensure that the proper amount of water was charged into the system. While the condenser water pump is off, the pressure reading will be in the neighborhood of 18 psig. When the condenser water pump is running the suction pressure will be about 18 psig and the discharge pressure fluctuating around 51 psig. The evaporator water pump standing pressure is about 21 psig; when running the suction pressure is 21 psig, and the discharge pressure is 32.5 psig. The hot water pump standing

pressure is 20 psig; when running the suction pressure is 19 psig, and the discharge pressure is 32.5 psig. Deviations of ± 3 psig from the above reference values are meaningless.

The condenser water pump originally had a 3HP motor that was later replaced by a 10HP motor running at double the RPM (the impeller was also trimmed down to 5.125 inches). These modifications were made in order to obtain higher flow rates.

A.1.3 AHU Controllers and Magic Box

A total of three Johnson Controls Inc. Air-Handling Unit (AHU) controllers were used to operate the test stand. Typically a computer communicates to the AHU controllers on an N2 bus by utilizing the JCI MM-CVT101-0 (which converts the computer's RS-232 communication standard to the N2 bus' RS-485 communication standard). However, in order to also incorporate communications from the MicroTech controller it was necessary to replace the MM-CVT101-0 (referred to as the 'black box') with a conversion box manufactured by Field Diagnostic Services Inc. (referred to as the 'magic box'). More information on the communications' interface is described in Appendix A.2.2.

Table A.1 shows the various connections used on the three AHU controllers. Each AHU controller has 8 analog inputs (0-10 VDC, 4-20mA, various RTDs, etc.), 8 binary inputs (15 VDC), 6 analog outputs (0-10 VDC or 4-20mA), and 10 binary outputs (24 VAC). The AHUs were labeled 'AHU 1', 'AHU 2', and 'AHU 3' based on physical location. The analog inputs are abbreviated AI, the binary inputs are abbreviated BI, the analog outputs are abbreviated AO, and the binary outputs are abbreviated BO. Table A.2 shows additional physical information pertaining to the installation and wiring of the test stand.

Table A.1: Equipment list and location.

Designation	Description	Location	AHU connection
TCI	RTD	Chiller condenser water in	AHU 1 AI 1
TCO	RTD	Chiller condenser water out	AHU 1 AI 2
TWI	RTD	City water into WU104-25	AHU 1 AI 3
TWO	RTD	City water out of WU104-25	AHU 1 AI 4
TEI	RTD	Chiller evaporator water in	AHU 1 AI 5
TEO	RTD	Chiller evaporator water out	AHU 1 AI 6
TSI	RTD	Condenser water out of WU104-25	AHU 2 AI 1
TSO	RTD	Condenser water out of WU105-28	AHU 2 AI 2
THI	RTD	Hot water into WU104-25	AHU 2 AI 3
THO	RTD	Hot water out of WU104-25	AHU 2 AI 4
TBI	RTD	Evaporator water into WU104-25	AHU 2 AI 5
TBO	RTD	Evaporator water out of WU104-25	AHU 2 AI 6
FWC	Flow Meter	Condenser water between WU104-25 and WU105-28	AHU 3 AI 1
FWE	Flow Meter	Evaporator water between WU105-28 and WU104-25	AHU 3 AI 2
WATT	Power Transducer	Inside Starter Cabinet, also utilizes two current transformers	AHU 3 AI 3
VSSR	Relay	Controls power to transformer which supplies actuator on valve VSS	AHU 1 BO 1
VSLR	Relay	Controls power to transformer which supplies actuator on valve VSL	AHU 1 BO 2
VHR	Relay	Controls power to transformer which supplies actuator on valve VH	AHU 1 BO 3
VMR	Relay	Controls power to transformer which supplies actuator on valve VM	AHU 1 BO 4
VSS	1/2 inch Steam valve	Steam valves mounted in parallel	AHU 1 AO 1
VSL	3/4 inch Steam valve	Steam valves mounted in parallel	AHU 1 AO 2
VH	1 1/4 inch 2-way valve	Actuator used to control valve (Hot water loop)	AHU 1 AO 3
VM	4 inch 3-way valve	Actuator used to control valve (Condenser water loop)	AHU 1 AO 4
VCR	Relay	Controls power to transformer which supplies actuator on valve VC	AHU 2 BO 1
VER	Relay	Controls power to transformer which supplies actuator on valve VE	AHU 2 BO 2
VWR	Relay	Controls power to transformer which supplies actuator on valve VW	AHU 2 BO 3
VC	4 inch 2-way valve	Actuator used to control valve (Condenser water loop)	AHU 2 AO 1
VE	4 inch 2-way valve	Actuator used to control valve (Evaporator water loop)	AHU 2 AO 2
VW	2 inch 2-way valve	Actuator used to control valve (City water loop)	AHU 2 AO 3
PWC	Pump Motor	Condenser water loop, contactor in electrical cabinet labeled west pump	--
PWE	Pump Motor	Evaporator water loop, contactor in electrical cabinet labeled middle pump	--
PWH	Pump Motor	Hot water loop, contactor in electrical cabinet labeled east pump	--
PWCR	Relay	Relay kit used to control contactor (Condenser water pump)	AHU 3 BO 1
PWER	Relay	Relay kit used to control contactor (Evaporator water pump)	AHU 3 BO 2
PWHR	Relay	Relay kit used to control contactor (Hot water pump)	AHU 3 BO 3

Table A.2: Equipment wiring and miscellaneous notes.

Designation	Box	Wire	Color Hot (+)	Color Com (-)	Notes
TCI	McQ1	01	White / Orange	Orange	Calibrated for -0.67
TCO	McQ1	01	White / Brown	Brown	Calibrated for -0.59
TWI	McQ1	01	White / Green	Green	Calibrated for -0.78
TWO	McQ1	02	White / Orange	Orange	Calibrated for -1.35
TEI	McQ1	02	White / Brown	Brown	Calibrated for -0.71
TEO	McQ1	01	White / Blue	Blue	Calibrated for -0.54
TSI	McQ2	04	White / Brown	Brown	Calibrated for -1.60
TSO	McQ2	04	White / Orange	Orange	Calibrated for -1.76
THI	HX1	06	White / Brown	Brown	Calibrated for -1.22
THO	HX1	06	White / Orange	Orange	Calibrated for -1.77
TBI	HX1	06	White / Blue	Blue	Calibrated for -0.98
TBO	HX1	06	White / Green	Green	Calibrated for -0.99
FWC		41	Yellow / Green	Blue / Violet	Serial Number: H981021.004 Max flow for 276 GPM
FWE		41	Black / Brown	Red / Orange	Serial Number: H981021.005 Max flow for 221 GPM
WATT		42	Red	Black	
VSSR		11	Red	Black	See diode full wave rectification circuit because relay needs DC
VSLR		11	Orange	Black	See diode full wave rectification circuit because relay needs DC
VHR		11	Blue	Black	See diode full wave rectification circuit because relay needs DC
VMR		11	White	Black	See diode full wave rectification circuit because relay needs DC
VSS	Power 21	13	Red	Black	All the way in at 0%, spring will close if power cut off
VSL	Power 22	13	Orange	Black	All the way in at 0%, spring will close if power cut off
VH	Power 23	13	Blue	Black	All the way in at 0% (closed)
VM	Power 24	13	White	Black	All the way out at 0% (full bypass)
VCR		12	Red	Black	See diode full wave rectification circuit because relay needs DC
VER		12	Orange	Black	See diode full wave rectification circuit because relay needs DC
VWR		12	Blue	Black	See diode full wave rectification circuit because relay needs DC
VC	Power 25	14	Red	Black	All the way out at 0% (closed)
VE	Power 26	14	Orange	Black	All the way out at 0% (closed)
VW	Power 27	14	Blue	Black	All the way in at 0% (closed)
PWC					Can also be turned on manually by cabinet switch
PWE					Can also be turned on manually by cabinet switch
PWH					Can also be turned on manually by cabinet switch
PWCR		31	Green	Black (24VAC)	
PWER		31	White	Red (24VAC)	
PWHR		32	Green	Black (24VAC)	

Setting the offsets for the RTDs is described in Appendix A.2.1. Additional electronics are used to convert the 24 VAC binary output of the AHU into 24 VDC that the electronic valve relays can utilize. The extra circuits built for each relay are mostly contained within the AHU box and consist of four diodes, a 1.2 kΩ resistor, a 10 μF capacitor, and a 1000 μF capacitor (in transformer box).

A.1.4 Computer

A dedicated PC was used to collect the information from the test stand and chiller. The PC had two active COM ports, one was connected to the 'magic box' to interface with the JCI N2 bus and the other was connected to the MicroTech controller (refer to Figure 3.4). In case the computer malfunctions in such a way that communications cannot be reestablished (sometimes Windows will conflict with the BIOS), it is worth

checking the IRQ settings for the COM ports: COM1 03F8-03FF IRQ4 and COM2 02F8-02FF IRQ3 are two settings that work—and there will be others). It is important to note that the VisSim program is initialized in such a way that the 'magic box' must be connected to COM1 and the MicroTech connected to COM2.

The computer also contains the HVAC PRO, MicroTech Monitor, and VisSim programs that were used to communicate with the test stand and chiller. HVAC PRO is a program developed specifically by Johnson Controls to talk to the AHU controllers. MicroTech Monitor is a program specifically designed for McQuay chillers. And VisSim is a generalized simulation software package that had custom DLLs written for it that allows it to take the place of both HVAC PRO and MicroTech Monitor, but only when collecting data. It is necessary to use the specially designed software packages to perform complex tasks, such as commissioning.

A.2 Data Acquisition and Control

A.2.1 Programming the AHU Controllers

There were three configuration files constructed using HVAC PRO: 'fddahu1.cfg', 'fddahu2.cfg', and 'fddahu3.cfg' to be used with 'AHU 1', 'AHU 2', and 'AHU 3' respectively. Once HVAC PRO is running, simply load up the desired configuration and then click on the input and output buttons to see how that particular AHU is configured. To directly communicate with the chosen AHU using HVAC PRO, go to the menu labeled 'Commission' and select 'Current Configuration'. Select 'Comm. Port: 1', 'Bus Type: N2 Bus', and the corresponding 'N2 Device Address' (1, 2, or 3). To upload a configuration from the controller, select menu 'Commission' and 'Configuration in Controller'. To download a configuration to the controller, select menu option 'Download' and 'Current Configuration'. Communication is only possible with one AHU at a time using HVAC PRO; moreover, any configurations uploaded from a controller will lack the customized titles normally attached to each input and output.

The HVAC PRO device type should be set to AHU-AHU102-0 (Rev. C06). The AHU addresses on the N2 bus are defined by jumper settings located on the boards (which were set to 1, 2, and 3). In addition to setting the configuration properly for the analog inputs, it is also necessary to adjust the jumper settings for Current, Voltage, or Resistance (Temperature). Consult the JCI AHU controller manual for more details.

To change internal offsets in the AHU controllers it is necessary to use the AS-CBLPRO2 (referred to as the 'white box'). One end of the 'white box' connector goes into COM port 1 and the other end goes into the J12 slot on the AHU board (an 8-pin connector, similar to a 10 base T connector). When commissioning in this setup it is necessary to chose Zone Bus instead of N2 Bus. It is not possible to change offsets using the N2 Bus; therefore, the 'white box' must be physically connected to each AHU in turn in order to change all the offsets. Also be aware of the possibility that the offsets may be erased when downloading new configuration files (a box must be checked to clear the offsets).

When first putting the data acquisition system together, one of the possible options not chosen was the following: AS-MIG201-0 Circuit board (Integrator), TL-SWOMIG-0 Software, EN-EWC13-0 Enclosure/transformer, and MM-CPN101-0 PC Companion. The Integrator would have allowed the MicroTech controller to function on the same N2 bus (RS-485) as the AHU controllers. PC Companion would have replaced VisSim as the control software on the computer and HVAC PRO as the commissioning software. This option was not chosen because its quickest sampling rate was once per minute.

A.2.2 VisSim Program

Open the VisSim program 'C:\Chiller FDD Data\chiller automatic control.vsm'. The main screen contains a few general plots, a picture of the chiller, and a number of compound blocks. Whenever a compound block is selected (right mouse click), the compound block is opened, thus revealing a new screen. The main compound blocks found in this program are:

- ‘To the Manual Control Screen’ – an interactive screen that allows every facet of the chiller and test stand to be controlled in one place. Color-coded blocks are used to help separate inputs and outputs for the AHU controllers and MicroTech controller. It also contains two additional compound blocks (‘Interpreting Unit Status’ and ‘Interpreting Fault Status’) that help interpret the chiller’s status without having to consult McQuay’s ‘Open Protocol Manual’.
- ‘MicroTech Sensor Data Plots’ – a collection of plots of various measurements made by the MicroTech controller
- ‘JCI Sensor Data Plots’ – a collection of plots of various measurements made by the JCI AHU controllers
- ‘Initialize JCI AHU controller communication’ – contains the custom DLL blocks that enable VisSim to communicate with the JCI AHU controllers
- ‘Initialize MicroTech controller communication’ – contains the custom DLL blocks that enable VisSim to communicate with the MicroTech controller
- ‘Mathematic Calculations’ – contains calculations for COP, kW/ton, and Heat Balance. Also contains the following compound blocks: ‘Temperature Deltas’ which defines variables based on temperature differences, ‘Heat transfer loads’ which calculates the heat transfer rates across the various heat exchangers, and ‘Flow rates’ that estimates flow rates in the test stand that are not measured directly by flow meters (primarily for troubleshooting purposes).
- ‘Export Data’ – exports the measured data into two files called ‘C:\Chiller FDD Data\FDD Data Part A.dat’ and ‘C:\Chiller FDD Data\FDD Data Part B.dat’. These files are tab delimited. The reason for two files is simply that VisSim has a limit to how many variables can be exported through one export block.
- ‘Import Data’ – imports data from the file called ‘C:\Chiller FDD Data\control setpoints.dat’ which contains the information needed for the VisSim program to run in automatic mode. The variables imported are given variations of

names of other variables already in the VisSim program. When the 'Emergency Override Button' is pushed in the 'Manual Control Screen' a series of Boolean blocks switch the control variables from the 'auto' labeled variables to those that are directly controlled within the 'Manual Control Screen'. Consult Appendix B.4 for further information.

Whenever new sensors are added to the test stand it will be necessary to reconfigure the AHU controllers as described in Appendix A.2.1. It will also be necessary to change the initialization files in the VisSim program. There are four blocks relevant to communication between VisSim and the JCI AHU controllers (found in menu option 'Blocks', 'JCIAHU'). As mentioned in Appendix A.1.3, the AHU controllers have analog inputs (AI), analog outputs (AO), binary inputs (BI) and binary outputs (BO). Each of the four VisSim blocks pertains specifically to one of these AHU connections: there is a 'JCI AHU AI' block, a 'JCI AHU AO' block, a 'JCI AHU BI' block, and a 'JCI AHU BO' block. The format of each block is identical: the top connector tab is for the AHU address (1,2, or 3), the second connector tab is for the specific number of the connection in the AHU (1-8 for AI, 1-6 for AO, 1-8 for BI, and 1-10 for BO), the third is to activate the override (0 for outputs and 1 for inputs), and the fourth is to provide an override value (leave 0 for an input variable and connect to one of the global control variables for an output variable).

There are a total of 6 outputs and 65 inputs to the MicroTech controller, not all of these are currently utilized in VisSim. Two basic blocks are available to initiate communication between VisSim and the MicroTech controller (found in menu option 'Blocks', 'MicroTech'). A right mouse click on these blocks will provide a dialog box that gives a choice as to which item number to choose (a help menu shows which item number corresponds to each output/input). The possible write blocks (i.e. outputs) are listed in Table A.3 and the possible read blocks (i.e. inputs) are listed in Table A.4.

Table A.3: List of write blocks available in VisSim for communication with MicroTech controller.

Description	Item number
Capacity Limit Percent	1
Clear Current Fault	2
Chiller Operation Mode	3
Chilled Water Temperature Setpoint	4
Communications Signal	5
Outdoor Air Temperature BAS	6

Table A.4: List of read blocks available in VisSim for communication with MicroTech controller.

Description	Item Number
Chilled Water Temperature Active Setpoint	1
Chiller Unit Temperature Type	2
Communication Status	3
Compressor Lift Pressure	4
Compressor Motor Current	5
Compressor Motor Current Percent	6
Compressor Number of Starts	7
Compressor Operating Hours	8
Compressor Suction Temperature	9
Compressor Superheat Discharge	10
Compressor Superheat Suction	11
Condenser Approach Temperature	12
Condenser Heat Recovery Unit Present	13
Condenser Heat Recovery Temperature – Delta	14
Condenser Heat Recovery Temperature – Entering	15
Condenser Heat Recovery Temperature – Leaving	16
Condenser Pump Status	17
Condenser Pump #1 Operating Hours	18
Condenser Pump #2 Operating Hours	19
Condenser Refrigerant Pressure	20
Condenser Refrigerant Temperature	21
Condenser Subcooling Temperature	22
Condenser Water Flow Rate	23
Condenser Water Flow Status	24
Condenser Water Rate Sensor, 0 = Not Present, 1= Present	25
Condenser Water Temperature – Delta	26

Table A.4: Continued.

Description	Item Number
Condenser Water Temperature - Entering	27
Condenser Water Temperature - Leaving	28
Cooling Tower Control, 0 = External, 1 = Chiller	29
Cooling Tower Stage	30
Cooling Tower Valve Position	31
Discharge Refrigerant Temperature	32
Evaporator Approach Temperature	33
Evaporator Pump Status	34
Evaporator Pump #1 Operating Hours	35
Evaporator Pump #2 Operating Hours	36
Evaporator Refrigerant Pressure	37
Evaporator Refrigerant Temperature	38
Evaporator Water Flow Rate	39
Evaporator Water Flow Status, 0 = No flow, 1 = Flow	40
Evaporator Water Flow Sensor, 0 = Not Present, 1 = Present	41
Evaporator Water Temperature - Delta	42
Evaporator Water Temperature - Entering	43
Evaporator Water Temperature - Leaving	44
Fault Current Active	45
Last Start Hour	46
Last Start Minute	47
Last Start Month	48
Last Start Date	49
Last Start Year	50
Last Stop Hour	51
Last Stop Minute	52
Last Stop Month	53
Last Stop Date	54
Last Stop Year	55
Liquid Line Refrigerant Temperature	56
Oil Pressure - Feed	57
Oil Pressure - Net	58
Oil Pressure - Vent	59
Oil Temperature - Feed	60
Oil Temperature - Sump	61
Outdoor Air Temperature - Network	62
Refrigerant Detection Sensor, 0 = Not Present, 1 = Present	63
Refrigerant Leak Detection Limit	64
Unit Status	65

As mentioned in Appendix A.1.4, a couple custom DLLs were written for VisSim that allows it to communicate with both the JCI AHU controllers and with the MicroTech controller. There are other documents written to explain the process of building the DLLs, this will be a brief explanation of the vital components. The DLL written for the JCI AHU controllers is called 'jciahu.dll' and the DLL written for the MicroTech controller is called 'mtech.dll'. These files must be copied into the VisSim folder in addition to adding the following lines in the file 'C:\Windows\vissim.ini':

addons32 = mtech.dll

addons32 = jciahu.dll

In case the DLLs need to be modified it will be necessary to have the following files for the JCI AHU DLL: jciahu.c, jciahu.h, jciahu.rc, c2cpp.cpp, c2cpp.h, talkn2.h, talkn2.cpp, netcomm.h, netcomm.cpp, vsuser.h, and vissim32.lib; and the following files for the MicroTech DLL: mtread.c, mtread.h, mtread.rc, c2cpp.cpp, c2cpp.h, talkn2.h, talkn2.cpp, netcomm.h, netcomm.cpp, vsuser.h, and vissim32.lib. An intern from Field Diagnostic Services Inc. wrote the DLLs and the 'magic box' was also supplied by them. One of the features of the 'magic box' is that its LEDs flash when sending and receiving data. This is useful for troubleshooting whether a communication problem is occuring from the computer or from the JCI AHU controllers.

A.2.3 Achieving the Desired Operating Conditions

The operating conditions imposed on the test stand can be determined by the following controls:

- Chilled water setpoint via the MicroTech controller
- Maximum compressor power draw via the MicroTech controller
- 3-way mixing valve in condenser water loop via JCI AHU controller – can load the evaporator loop from 0-90 tons depending on temperature difference between condenser and evaporator water loops
- Valve on city water supply via JCI AHU controller – affects condenser water temperature

- Valves on steam supply via JCI AHU controller – can load the evaporator loop by approximately an additional 0-15 tons

There is no direct control for the condenser water temperature or the chiller loading—both are controlled indirectly. Adjusting the mixing valve affects both the chiller loading and the condenser water temperature to a high degree. Adjusting the other valves may or may not have as much of a cross effect, depending on the setting of the mixing valve.

To determine what was possible for the test stand, each valve was changed through a spectrum of settings at different chilled water temperatures. The following information was learned from these tests: possible steady state temperatures, ability to reach a chilled water setpoint (not possible when too much load was imposed), and corresponding chiller load for certain valve settings. A few additional tests found that the condenser water entering temperature should be kept below 85°F to avoid activating the high condenser pressure alarm (and surge limit); moreover, the chiller load must be generally kept above 20-25 tons to prevent the low evaporator pressure alarm from triggering.

Each test run was designed to incorporate 27 tests in order to get a wide range of operating conditions within a reasonable length of time. The 27 tests are based on a 3x3x3 matrix consisting of chiller load, condenser water entering temperature, and chilled water setpoint. The earlier test runs were studied to determine which valve settings would permit each desired operating condition. The first trial run achieved good results for approximately two-thirds of the tests. It was soon discovered that transients from different operating conditions could not be anticipated beforehand; moreover, there was some valve hysteresis that also complicated the process. It took another 10 test runs with fine-tuning to get a good approximation of the desired operating conditions at all 27 tests. At this time it was obvious that some feedback control was necessary (for example, the city water supply temperature regularly changes by as much as 5 degrees, which has a significant impact on the condenser water temperature). The decision to add some feedback control was difficult because the control had to be implemented within VisSim, and there was uncertainty about how it would interact with the MicroTech controller's chilled water setpoint control.

To keep VisSim's cycle time short (it collects data every 10 seconds), a simple feedback control system was developed. The approximate valve settings to achieve the desired operating conditions were already known; therefore, only a few of the valve settings (the valves controlling the city water supply and the steam supply) needed to be occasionally tweaked if a temperature drifted too far away from the desired condition. The two conditions requiring additional feedback control are: maintaining the condenser water entering temperature and reducing the chiller load when it is unable to maintain the chilled water setpoint.

It is possible to use the difference between the evaporator leaving water temperature and the chilled water setpoint as the basis in deciding when to reduce the chiller load. Reducing the chiller load is accomplished by closing one of the valves controlling the steam supply. The changes in the valve setting are not cumulative from one rule to the next (i.e. only one is applied at a time). The valve position is modified according to the following rules:

- If the actual evaporator leaving water temperature is more than 0.5°F above the chilled water setpoint, the valve is closed an additional 5%
- If the actual evaporator leaving water temperature is more than 1°F above the chilled water setpoint, the valve is closed an additional 10%
- If the actual evaporator leaving water temperature is more than 2°F above the chilled water setpoint, the valve is closed an additional 15%
- If the actual evaporator leaving water temperature is more than 3°F above the chilled water setpoint, the valve is closed an additional 30%

To implement the other feedback control, an additional control variable was added to the import file 'control setpoints.dat' that specified a desired condenser water entering temperature for each test (as a side note: the entire series of valve setting changes is contained within the file 'control setpoints.xls'—thus it is possible to see when this column was added; this Excel file was the working file, with only the numbers then copied into the 'control setpoints.dat' file). The predetermined valve settings for the city water supply were reduced by about 5% so that the condenser water temperature would always be too high—without some correction. The VisSim program then

compares the actual condenser water entering temperature with the desired temperature and makes the following modifications to the assigned valve position:

- If the actual temperature is more than -0.5°F above the desired temperature, the valve is opened an additional 2% (recall that the valve setting is artificially lower than it should be)
- If the actual temperature is more than -0.2°F above the desired temperature, the valve is opened an additional 5%
- If the actual temperature is more than 0.3°F above the desired temperature, the valve is opened an additional 8%
- If the actual temperature is more than 0.8°F above the desired temperature, the valve is opened an additional 12%
- If the actual temperature is more than 1.2°F above the desired temperature, the valve is opened an additional 18%
- If the actual temperature is more than 1.5°F above the desired temperature, the valve is opened an additional 25%

It may seem strange to implement the control this way, nevertheless, the logic is extremely simple, consumes little processing time, and is extremely robust. Moreover, keeping the condenser water temperature within ± 1°F is more than adequate to ensure proper spacing between the different tests.

Although rare, there have been some isolated tests where the MicroTech controller displayed excessive oscillation around the setpoint. In most cases this was not repeatable in subsequent tests; however, during the low refrigerant charge tests it was necessary to limit the compressor power to prevent the oscillation.

Another control variable was added just before commencing most of the fault tests. This variable controlled the 2-way condenser valve position. It was necessary to include this variable into the automatic controls because the 3-way mixing valve also mounted in the condenser water loop causes a 10% variation in the water flow rate without any correction. Hence, for each mixing valve position, the 2-way condenser

valve is adjusted to maintain a constant flow rate. Under most circumstances the corrected flow variation is less than ± 1%, which is within the sensor tolerance.

A.2.4 Exporting to Excel

Due to the repetitive nature of the data analysis, several macros and Excel templates were created to speed up the process. There are two essential files found in the 'C:\Chiller FDD Data' folder that process the data: 'headings.xls' and 'macros.xls'. It is only necessary to open the 'macros.xls' file. Once opened, a macro can be chosen by either choosing menu 'Tools-> Macro-> Macros…' or simply pressing Alt-F8. There are twelve macros, two of which are actually just a combination of the others. The macros do the following tasks:

- Step1_dat_to_xls_conversion – import data from test run into Excel and saves as 'temporary working file.xls'.
- Step2_check_spikes – creates a graph that allows the user to easily spot sensor dropouts; simply go into the main data file and replace any sensor dropouts with the data in the previous time step. It is necessary to delete this graph before saving and exiting the 'temporary working file.xls' spreadsheet.
- Step3_sift_data – creates a new database that removes 11 out of every 12 time steps, thus leaving only one time step every two minutes.
- Step4_sift_data_2 – finishes the job started by Step3 (the code is too long to fit into one macro).
- Step5_second_to_minutes – converts the 'seconds' column to 'minutes' in the reduced database created by Step3 and Step4.
- Step6_build_reduced_graph – creates a graph of relevant operating parameters based on the reduced database.
- Step7_grab_steady_state – takes the last five time steps of each test run from the reduced database and creates a new database.

- Step8_grab_steady_state – averages the five time steps collected by Step7 and deletes the previous database while creating a new one consisting only of averaged steady state values.
- Step9_regression_setup – creates a new database that organizes the necessary information needed for a regression analysis.
- Step10_power_curve_tables – creates the final database that is ultimately used to record the regression analysis.
- Steps1and2 – runs Step1 and Step2.
- Steps3456789and10 – runs Step3, Step4, Step5, Step6, Step7, Step8, Step9, and Step10.

It will be necessary to hit the 'Ok' button during Step8 when one of the worksheets is deleted. The 'headings.xls' file is used during the process of importing the data from 'FDD Data Part A.dat' and 'FDD Data Part B.dat' mentioned in Appendix A.2.2. One of the worksheets in the 'macros.xls' file is used as a template that is copied into the 'temporary working file.xls' during Step10. Unfortunately, the regression analysis itself could not be included in a macro (a limitation of Excel).

A.3 Servicing Equipment

For major servicing it is recommended to call McQuay first. A good general-purpose manual to consult is McQuay's Operating and Maintenance Manual "Single/Dual Compressor Centrifugal Chillers", OM 307-5.

A.3.1 Checking Oil

The compressor case has three sight glasses located on the suction side. The top sight glass is simply for troubleshooting purposes; if it is full, the jet-pump is not working properly. The middle sight glass indicates where the oil level should be (ideally at the bottom) and may show some foam when the compressor is running. The bottom sight glass indicates the machine is out of oil (whenever the oil level is visible through it). Top

off the amount of oil when the compressor is running under full load conditions. A 3/8-inch flare valve is used to drain the oil; the same port is used with a hand pump to charge the unit. McQuay's OM 307-5 manual provides recommendations of the kind of oil to use. An obscure specification sheet mentions that the PEH048J chiller holds a nominal 2.75 gallons of oil. When changing the oil out of the compressor, approximately 1.6 gallons was drained (the rest would have been difficult to get to). The oil was replaced with 1.75 gallons of Mobil-Copeland 998-D022-01 EAL22.

Immediately projecting out of the compressor plate where the sight glasses are located is a stem with a flat head screw adjustment. This screw is turned clockwise to raise the oil pressure within the compressor. Lower oil pressures often cause slower response times in loading the chiller (vanes are adjusted hydraulically with oil).

A.3.2 Percent Rated Load Amps

The Percent Rated Load Amps (%RLA) reading of the MicroTech controller is adjusted using a small screwdriver. Open up the door with the display panel and look near the bottom left corner for a small yellow box (1/4 x 1/4 x 3/4 inches). Adjusting the screw on the top of this rheostat will change the %RLA reading on the display panel. The reading is not reliable enough for power measurements (it is possible to calibrate this measurement by equating the amp reading with an independent ammeter; however, only the third power phase is being measured and its amperage was sometimes 8-10% lower than the other phases. Furthermore, McQuay's suggested power factor of 0.88 is based on an average for many different motor sizes). The %RLA for the data collected in this thesis was calibrated by placing the chiller in a loading condition where the vanes were wide open. Since the only useful purpose of the %RLA is to limit the maximum compressor loading, the %RLA was set to around 98-99% under this condition. The MicroTech controller has a maximum loading setpoint that allows the user to specify the maximum allowable %RLA (available in menu 4). When the chiller reaches the setpoint, it no longer allows the vanes to open up. If the chiller load continues to drift higher, the vanes will begin to close when the %RLA is approximately 5% higher than the setpoint.

A.3.3 Setting the Pilot Valve

The pilot valve is a thermal expansion valve that regulates the main valve, which in turn controls the liquid line flow between the condenser and evaporator. A hex nut on the side of the pilot valve must be removed in order to get to the adjustable setscrew. Do not remove the hex nut unless the chiller is operating (refrigerant will leak through the setscrew when the chiller is off). Turning the setscrew counterclockwise (out) will lower the superheat. To minimize overshoot, it is best to turn the setscrew less than 360 degrees at any given time. The superheat should be adjusted to about 1.5°F superheat under full load conditions and at an evaporator water outlet temperature of 40°F. At higher evaporator water out temperatures the superheat will increase to as much as 5°F. If the pilot valve doesn't seem to be working, it is possible to jack open the main valve as much as 75% in order to diagnose the problem as being from the main valve or pilot valve.

A.3.4 General Valve Information

There is another valve upstream of the main valve that is called the King valve (located just below the main valve physically). This valve can be closed to disconnect the evaporator from the condenser (e.g. in order to pump refrigerant from the evaporator to the condenser for storage). However, it should also be noted that refrigerant is taken from the liquid line before the King valve and sent to the compressor shell to cool the motor. This motor cooling line then returns as superheated gas to the liquid line shortly after the main valve and just before the evaporator. Therefore, it is also important to close off the valves on this motor cooling line—depending on the kind of service done to the chiller.

A.3.5 Using the MicroTech Controller

There are two ways to change setpoints and alarm conditions in the MicroTech controller. The first method is using the display panel—consult McQuay's manual, Operations and Maintenance Data "200-Series MicroTech Control Panel: For Centrifugal Chillers", Bulletin No. OM 125, pages 10 through 39. To change a value it is first necessary to press the 'enter' key; upon being prompted for a password, press the 'enter' key four more times. To change offsets for the pressure transducers (menu 24) requires a special password (which McQuay does not want made public knowledge). The pressure transducers were calibrated according to a laboratory grade pressure gauge so that the condenser pressure was offset by +1.0 psi and the evaporator pressure was offset by –1.3 psi.

The other method is to use MicroTech Monitor, McQuay's proprietary software. For the controller used on centrifugal chiller, the password to connect is 86672775. Connecting with the correct password automatically enables all the normal setpoints to be changed (but not the offsets) whenever the mouse is positioned over them. Note that it is not possible to use VisSim and MicroTech Monitor to communicate with the controller at the same time (one of the programs must be completely exited before changing to the other).

Appendix B: Test Stand Operation

B.1 Mechanical Inspection Checklist

1. Refer to 'Operating and Maintenance Manual' OM 307-5, "PEH 050 Single Compressor Centrifugal Chillers" for more information on seasonal and annual servicing.
2. Check for water leakage along city water loop.
    a. Main water valve
    b. Heat exchanger
    c. Electronically actuated valve
    d. Thermally actuated valve
    e. Two plastic manual drainage distribution valves
3. Check for water leakage along condenser water loop.
    a. Condenser water out (5-inch to 4-inch adapter)
    b. Air separator
    c. Water pump
    d. Manual valve
    e. City water heat exchanger
    f. Flow meter
    g. Bypass T-junction
    h. Shared heat exchanger
    i. Electronically actuated valves (2-way and 3-way)
    j. Manual plastic valve
    k. Condenser water in (4-inch to 5-inch adapter)
4. Check for water leakage along evaporator water loop (don't confuse condensation with leakage).
    a. Evaporator water out (5-inch to 4-inch adapter)

   b. Air separator
   c. Water pump
   d. Manual valve
   e. Electronically actuated valve
   f. Shared heat exchanger
   g. Flow meter
   h. Hot water heat exchanger
   i. Manual plastic valve
   j. Evaporator water in (4-inch to 5-inch adapter)
5. Check for water leakage along hot water loop.
   a. Water pump
   b. Hot water heat exchanger
   c. Electronically actuated valve
   d. Air separator
   e. Steam heat exchanger
6. Check for oil leakage around chiller.
7. Check for loose power wires and sensor wires.
8. Check refrigerant pressure relief system (rubber stopper should be present just outside window).
9. General housekeeping.

B.2 Start-up Procedures

1. Go through mechanical inspection checklist.
2. Turn on all circuit breakers (the order is not important—except that the oil heater should be on 24 hours prior to start up).
   a. Main breaker for chiller compressor is located near exit of room 90 (labeled #2).
   b. Oil heater and MicroTech controller breaker is located above chiller controller cabinet (labeled #3).

c. Turn on power switch for electronic valves and relays next to oil heater breaker mounted on side of gray box above chiller control cabinet (labeled #7).
d. Water pump breakers are mounted vertically on top of one another in the main electrical distribution cabinet facing the south wall in room 90 and are the furthest from the exit door. They are labeled west pump (condenser, labeled #4), middle pump (evaporator, labeled #5), and east pump (hot water, labeled #6). Manual override switches are also located on the same panel as the breaker (and should be left off, since the PC can turn these pumps on remotely).

3. Check that the internal power switches to the Johnson Controls AHU controllers are on; proper operation is indicated by the flashing green zone bus light on the middle of the front panel. These controllers are normally left on. The programs used in these AHU controllers are downloaded from the PC using the software packaged called 'HVAC PRO'. Only physical changes in the test stand will require a modification of these programs (offsets of the RTDs are also applied within the controllers before being sent to the PC). The power supply to the 'magic box' (labeled #8) connected between the computer and the JCI AHU controllers must be plugged into a standard 115V outlet.
4. Verify that manual valves on the city water supply are open (there are three of them, one upstream of the heat exchanger (labeled #9) which should be positioned 100% open and two plastic valves downstream of the heat exchanger which should be about 90% open).
5. Turn on the PC (labeled #1) and start VisSim. Load up the chiller control program: either the 'chiller manual control' program or the 'chiller automatic control' program. Both can be easily found under the 'file' menu.
6. Start running the simulation within VisSim. The manual control program should be started with the chiller set in the off position. The automatic program requires no adjustments (setpoint changes and timing are controlled from the input file). If running the manual program, ensure that no condenser water flow is bypassed when starting the chiller. Next, open the city water valve to the 30% open position and turn the three water pumps on.

7. Switch the McQuay MicroTech controller switch to the Auto position and press the 'Control' category key to get to menu 11 in order to verify that the control mode is 'Auto:Network'. While in 'Auto:Network' mode the controller expects a communications' signal once a minute. If it does not receive any communication for 5 minutes it will resort back to local setpoint control and a 'Comm error' alarm will appear (red alarm light will turn on). It is possible to clear the alarm by pressing the 'Alarm' category key (menu 27) and then the 'clear' key (or by using the 'clear fault' button in VisSim). Note that if the evaporator or condenser water pumps are off, then alarms will also appear indicating no evaporator water flow or condenser water flow. Once the alarms are cleared, the chiller may be started manually using the manual VisSim program. The automatic program will run a few minutes before it attempts to start the chiller, thus giving the user some time to clear any alarms.

B.3 Shut Down Procedures

B.3.1 McQuay Chiller and Load Stand Shutdown Procedure (manual)

1. Ensure that evaporator water temperature leaving chiller is above 40°F. It is not necessary to unload chiller first, since the chiller automatically takes the time to unload before shutting the compressor down.
2. Turn chiller off through VisSim program while simulation is running.
3. Close the steam heating valves through VisSim program while simulation is running.
4. Allow temperatures to equalize for next 5 minutes (approximately within 5°F of the city water supply temperature) and then shut off city water valve and pumps via VisSim.
5. Stop the VisSim simulation and then check and rename (or move) the data export files, otherwise data will be appended to those files during the next simulation.
6. Switch the MicroTech controller to the off position.

B.3.2 McQuay Chiller and Load Stand Shutdown Procedure (automatic)

1. Allow VisSim to finish its test cycle, turn the chiller off, equalize system temperatures, and turn the test stand off.
2. The VisSim simulation should be timed to shut itself off soon thereafter.
3. Check and rename (or remove) the data export file, otherwise data will be appended to those files during the next simulation.
4. Switch the MicroTech controller to the off position.

B.3.3 Optional Shutdown Step for Manual or Automatic Operation

1. If the equipment will not be run for several days or if servicing is needed, then several additional steps may be taken.
2. Turn off the circuit breakers (the order is not important).
    a. Main breaker for chiller compressor (labeled #2) is located near exit of room 90 (normally left on because other research projects require power routed through this circuit).
    b. Oil heater and MicroTech controller breaker (labeled #3) is located above chiller controller cabinet (only turn this off if servicing is required or chiller will be off for many weeks).
    c. Power switch for electronic valves and relays (labeled #7) next to oil heater breaker mounted on side of gray box above chiller control cabinet.
    d. Water pump breakers are mounted vertically on top of one another in the main electrical distribution cabinet facing the south wall in room 90 and are the furthest from the exit door. They are labeled west pump (condenser, labeled #4), middle pump (evaporator, labeled #5), and east pump (hot water, labeled #6).

B.3.4 McQuay Chiller and Load Stand Emergency Shutdown Procedure

1. In the event of a fire or mechanical damage to the chiller, turn off the main circuit breaker (labeled #2) located next to the exit of room 90 (a fire extinguisher is also located next to the door).
2. If water is not draining properly and spilling onto the floor, begin to close the main city water valve (labeled #9) located upstream from the heat exchanger (18 inches from the elbow where the city water pipe drops from the ceiling). If it is necessary to shut the valve significantly then proceed to turn the chiller switch to the 'off' position and the chiller will begin its shutdown routine (there is adequate time for the chiller to shut off before it overheats).
3. If the steam valves are not closing properly, simply turn their power supply off on the gray box mounted above the chiller control cabinet (labeled #7). These valves are spring-loaded and will close when no power is present. None of the other electronically actuated valves are spring-loaded, and they will therefore remain in the same position. The manual shutoff valve for the steam lines is mounted about 10 feet above the PC.

If manual control is desired while running the automatic control program, it is possible to obtain control by activating the Emergency Manual Override button in the Manual Control Screen in VisSim. When this button is activated, the program will simply ignore the imported setpoint information (if Emergency Manual Override is deactivated the program will revert back to Automatic operation). Make sure all the manual settings are properly set before activating the Override button; otherwise the chiller may be inadvertently turned off.

B.4 VisSim Automatic Chiller Control Program

This is a supplementary section to further elaborate on information described in other parts of the Appendices. There are 28 total screens (pages) within the Automatic Chiller Control Program 'C:\Chiller FDD Data\chiller automatic control.vsm'. The

automatic program evolved from the manual program 'C:\Chiller FDD Data\chiller manual control.vsm'. It is possible to use the automatic program for manual control when the 'Emergency Override Button' is pressed; hence no further mention will be made of the manual control program.

Within the main screen of the automatic control program there is access to eight additional screens (VisSim refers to these as compound blocks). Only one of these compound blocks needs to be regularly accessed, and it was given a special oversized bitmap that reads 'To the Manual Control Screen'. A right mouse click on this bitmap will send the user to a screen that provides online control of all controllable functions as well as displaying all measured data and important calculations. Note that both this screen and the main screen are usually left in the display mode. To edit these screens requires that the display mode be turned off.

Each set of controls and displays is contained within a color-coded group. The large red button labeled 'Emergency Manual Override' will change to a green button when activated. The override button is connected to a number of Boolean logic blocks (buried in the initialization screens) that control whether the imported control variables are used or the controls located on the manual control screen. It is important to note that some of the manual controls are always active (consult Table B.1).

Table B.1: List of controllable variables.

Name	Additional notes	Type
Chiller On/Off	Remote Chiller Start	Manual and Automatic Toggle Button
Clear Fault	Clear Chiller Alarm	Manual Toggle Button
Chilled Water Setpoint	Adjustable to 0.5°F	Manual and Automatic Slider
Max. Chiller Capacity	Limits RLA%	Manual and Automatic Slider
PWCR	Condenser Water Pump	Manual and Automatic Toggle Button
PWER	Evaporator Water Pump	Manual and Automatic Toggle Button
PWHR	Hot Water Pump	Manual and Automatic Toggle Button
VSSR	Small Steam Valve Relay	Manual Toggle Button
VSLR	Large Steam Valve Relay	Manual Toggle Button
VHR	Hot Water Valve Relay	Manual Toggle Button
VMR	Mixing Valve Relay	Manual Toggle Button
VCR	Condenser Valve Relay	Manual Toggle Button

Table B.1: Continued.

Name	Additional notes	Type
VER	Evaporator Valve Relay	Manual Toggle Button
VWR	City Water Valve Relay	Manual Toggle Button
VSS	Small Steam Valve Setpoint	Manual and Automatic Slider
VSL	Large Steam Valve Setpoint	Manual and Automatic Slider
VH	Hot Water Valve Setpoint	Manual Slider
VM	Mixing Valve Setpoint	Manual and Automatic Slider
VC	Condenser Valve Setpoint	Manual and Automatic Slider
VE	Evaporator Valve Setpoint	Manual Slider
VW	City Water Valve Setpoint	Manual and Automatic Slider

The relay buttons control power to the corresponding valves by the same name. These valves will not move when the relay has cut power to them, and the spring valves will close because they are spring-loaded. Therefore, it is customary practice to leave the relay buttons toggled to the ‘on’ position. Table B.2 contains a sample file used for importing control variables into VisSim.

Table B.2: Import file for automatic chiller test run.

Time	Chiller on/off	PWCR	PWER	PWHR	TWE_set	Max Chiller%	VSS%	VSL%	VM%	VW%	VC%	TCI_set
0	0	0	0	0	50	60	0	0	100	0	57	85
10	0	1	1	1	50	60	0	0	100	30	57	85
290	0	1	1	1	50	60	0	0	100	30	57	85
300	1	1	1	1	50	100	0	0	100	30	57	85
450	1	1	1	1	50	100	0	0	100	30	57	85
460	1	1	1	1	49	100	90	90	60	20	51	85
1050	1	1	1	1	49	100	90	90	45	20	49	85
1060	1	1	1	1	49.5	100	90	0	46	22	49	85
2850	1	1	1	1	49.5	100	90	0	46	22	49	85
2860	1	1	1	1	50	70	40	0	25	17	49	85
4650	1	1	1	1	50	70	70	0	25	17	49	85
4660	1	1	1	1	50	60	0	0	15	17	49	85
4950	1	1	1	1	50	60	0	0	15	12	49	85
4960	1	1	1	1	50	60	40	0	5	12	49	85
6450	1	1	1	1	50	60	40	0	5	12	49	85
6460	1	1	1	1	49	100	40	0	25	18	49	85
6750	1	1	1	1	49	100	40	0	40	18	49	85
6760	1	1	1	1	49	100	90	100	100	38	57	75
8250	1	1	1	1	49	100	90	100	100	40	57	75
8260	1	1	1	1	49.5	80	90	0	80	42	50	75
8550	1	1	1	1	49.5	80	90	0	40	42	47	75
8560	1	1	1	1	50	65	80	0	32	30	47	75
10050	1	1	1	1	50	65	80	0	32	30	47	75
10060	1	1	1	1	50	55	45	0	10	17	47	75
11850	1	1	1	1	50	55	45	0	10	14	47	75
11860	1	1	1	1	49	100	90	50	50	38	48	75
12150	1	1	1	1	49	100	90	50	50	38	48	75
12160	1	1	1	1	49.5	100	90	100	100	52	56	70
13650	1	1	1	1	49.5	100	90	100	100	52	56	70
13660	1	1	1	1	50	60	50	0	80	42	56	65
15450	1	1	1	1	50	60	50	0	80	42	56	65
15460	1	1	1	1	50	50	30	0	40	42	47	62
17250	1	1	1	1	50	50	30	0	40	42	47	62
17260	1	1	1	1	44	100	70	100	85	17	56	85
17850	1	1	1	1	44	100	70	30	35	17	53	85
17860	1	1	1	1	44.5	100	85	0	35	22	49	85
19650	1	1	1	1	44.5	100	85	0	35	25	49	85
19660	1	1	1	1	45	75	70	0	20	20	49	85
21450	1	1	1	1	45	75	70	0	20	20	49	85
21460	1	1	1	1	45	60	30	0	5	13	49	85
23250	1	1	1	1	45	50	30	0	5	13	49	85
23260	1	1	1	1	44	100	0	0	20	17	49	85
23550	1	1	1	1	44	100	0	0	40	17	49	85
23560	1	1	1	1	44	100	90	30	70	35	53	75
25050	1	1	1	1	44	100	90	30	70	35	53	75
25060	1	1	1	1	44.5	70	90	0	25	34	48	75
26850	1	1	1	1	44.5	70	90	0	25	34	48	75
26860	1	1	1	1	45	50	20	0	10	17	48	75
28650	1	1	1	1	45	50	20	0	10	17	48	75
28660	1	1	1	1	44	100	90	0	20	17	48	75
28950	1	1	1	1	44	100	30	0	50	17	48	75
28960	1	1	1	1	44	100	90	100	100	52	57	70
30450	1	1	1	1	44	100	90	100	80	52	57	70
30460	1	1	1	1	44.5	60	20	0	65	42	51	65
32250	1	1	1	1	44.5	60	45	0	65	42	51	65
32260	1	1	1	1	45	60	0	0	50	42	48	65
32550	1	1	1	1	45	45	0	0	30	42	47	65
32560	1	1	1	1	45	45	35	0	23	42	47	65
34050	1	1	1	1	45	45	35	0	23	42	47	65
34060	1	1	1	1	39	100	80	0	60	17	49	80
34650	1	1	1	1	39	100	80	0	40	22	49	80
34660	1	1	1	1	39.5	100	80	30	36	25	49	80
36450	1	1	1	1	39.5	100	80	30	36	28	49	80
36460	1	1	1	1	40	70	50	0	23	18	49	80
38250	1	1	1	1	40	65	50	0	23	18	49	80
38260	1	1	1	1	40	55	20	0	8	15	49	80
40050	1	1	1	1	40	55	20	0	8	15	49	80
40060	1	1	1	1	39	100	0	0	20	17	49	80
40350	1	1	1	1	39	100	30	30	50	17	49	80
40360	1	1	1	1	39	100	80	30	85	45	57	70
41850	1	1	1	1	39	100	80	30	85	46	57	70
41860	1	1	1	1	39.5	65	50	0	33	38	48	70
43650	1	1	1	1	39.5	65	50	0	33	34	48	70
43660	1	1	1	1	40	50	30	0	15	28	48	70
45450	1	1	1	1	40	50	30	0	15	26	48	70
45460	1	1	1	1	39	100	50	0	20	22	48	70
45750	1	1	1	1	39	100	50	0	60	22	50	70
45760	1	1	1	1	39.5	100	80	0	100	55	57	65
47250	1	1	1	1	39.5	100	80	0	100	55	57	65
47260	1	1	1	1	40	60	40	0	50	45	48	65
49050	1	1	1	1	40	60	60	0	50	45	48	65
49060	1	1	1	1	40	50	25	0	22	45	47	65
50850	1	1	1	1	40	50	25	0	22	45	47	65
50860	1	1	1	1	40	60	0	0	50	30	48	85
51150	1	1	1	1	40	60	0	0	100	30	56	85
51160	1	1	1	1	40	60	0	0	100	30	56	85
51450	1	1	1	1	40	60	0	0	100	30	56	85
51460	0	1	1	1	40	60	0	0	100	30	56	85
51750	0	1	1	1	40	60	0	0	100	30	56	85
51760	0	0	0	0	40	60	0	0	100	0	56	85

The time column (in seconds) indicates when a particular command is to be executed. The sampling rate in VisSim is every 10 seconds; therefore, when commands are issued to change variables in subsequent time steps, the variables will immediately change to the next setpoint (keeping in mind that the valves take approximately one minute to travel from one end of their stroke to the other). However, if there is more than one time step between changes in variable settings, then VisSim will interpolate a value based on the current time and the time between the changes. Thus it would be a mistake to send a toggle command (e.g. a '0' to '1' transition for starting the chiller) unless the subsequent commands were only 10 seconds apart. However, if it were desired to gradually change a valve position, then it would be appropriate to specify an ending valve position some time later than the starting valve position.

The three other color-coded blocks contain sensor information and calculated values. All this information is exported into the files 'C:\Chiller FDD Data\FDD Data Part A.dat' and 'C:\Chiller FDD Data\FDD Data Part B.dat' as described in Appendix A.2.2. A description of the exported data is contained in Chapter 3.

The MicroTech controller must be in remote communications mode (menu 11) before it will accept commands from VisSim. Moreover, the MicroTech controller will ignore startup commands until all alarms (i.e. faults) have been cleared. Some of the common alarms are 'No Evaporator Water Flow', 'No Condenser Water Flow', and 'Communications Error' (occurs when MicroTech controller receives no communication for approximately five minutes—the VisSim simulation must be active for communication to occur). Table B.3 has a complete list of all alarms and can also be obtained by a right mouse click on the button 'Interpreting Fault Status', which will also show a red light next to the fault for easy identification while working in VisSim. Some alarms may show up during operation, such as 'Low Evaporator Pressure'. As long as it is just a warning, the alarm may reset itself when the alarm condition no longer exists. However, if conditions continue to get worse the alarm will automatically cause the compressor to shut down and the alarm must be reset manually (consult Appendix A.1.1 for a list of alarm conditions).

Table B.3: Interpreting the fault status condition.

Fault Condition	Value
No Fault	0
Liquid Line Sensor Failure	1
Entering Evaporator Water Sensor Failure: Warning	2
Leaving Condenser Water Sensor Failure	3
Low Discharge Superheat	4
High Discharge Superheat	5
Entering Evaporator Water Sensor Failure: Problem	6
Outside Air Temperature Sensor	7
Low Evaporator Pressure – No Load	8
Low Evaporator Pressure – Unload	9
High Discharge Temperature – Load	10
Condenser Freeze Protection	11
Evaporator Freeze Protection	12
Evaporator Pump #1 Failure	13
Evaporator Pump #2 Failure	14
Condenser Pump #1 Failure	15
Condenser Pump #2 Failure	16
Compressor Vanes Open at Startup	17
Low Evaporator Pressure	18
Low Oil Pressure Delta	19
Low Oil Feed Temperature	20
High Oil Feed Temperature	21
Low Compressor Motor Current	22
High Discharge Temperature	23
High Condenser Pressure	24
Mechanical High Condenser Pressure	25
High Compressor Motor Temperature	26
Surge-High Suction Superheat	27
Compressor Motor	28
No Evaporator Water Flow	29
No Condenser Water Flow	30
High Compressor Motor Current	31
Compressor Motor Starter Fault	32
Leaving Evaporator Water Sensor Failure	33
Evaporator Pressure Sensor Failure	34
Entering Condenser Water Sensor Failure	35
Suction Temperature Sensor Failure	36
Discharge Temperature Sensor Failure	37
Condenser Pressure Sensor Failure	38
Oil Feed Pressure Sensor Failure	39
Oil Feed Temperature Sensor Failure	40
Oil Sump Temperature Sensor Failure	41
Oil Sump Pressure Sensor Failure	42
Voltage Ratio Sensor Failure	43
Communications Error	44

Table B.4 contains information that is available by right clicking on the compound block called 'Interpreting Unit Status'. When first starting VisSim, the chiller will usually be in an alarm condition and the Unit Status will be '1'. Once the alarm is cleared the Unit Status will be '6' until the chiller receives the startup command.

Table B.4: Interpreting the unit status condition.

State Name	Value
Off: All Systems	0
Off: Alarm	1
Off: Ambient Temperature Lockout	2
Off: Panel Rocker Switch	3
Off: Manual	4
Off: Remote Switch	5
Off: Remote Communications	6
Off: Time Schedule	7
Start Requested	8
Waiting for Low Oil Sump Temperature	9
Evaporator Pump Off	10
Evaporator Pump On – Recirculation	11
Evaporator Pump On – Cycle Timer	12
Evaporator Pump On – Waiting for Load	13
Oil Pump Off	14
Oil Pump On – Waiting for Load	15
Condenser Pump Off	16
Condenser Pump On – Waiting for Flow	17
Compressor Motor – Startup Unloading	18
Compressor Motor – Started	19
Compressor Motor – Running OK	20
Compressor Motor – Rapid Shutdown	21
Compressor Motor – Shut Down Unloading	22
Compressor Motor – Off Normal Shutdown	23
Condenser Pump – Off/Shut Down	24
Evaporator Pump – Off/Shut Down	25
Compressor Post Lubrication	26
Oil Pump – Off/Shut Down	27

In controlling the city water supply, a few things should be kept in mind. The city water supply normally stays within 55°F to 60°F (initially it will be higher until standing water in the pipe has been flushed out). Five valves were originally mounted to control the city water flow rate. The main valve is upstream of the heat exchanger and should always be at least 75-100% open (the import file was designed for 100% open). Two valves are mounted in parallel immediately downstream from the heat exchanger; one valve is electronically actuated from the PC via VisSim and the JCI AHU controllers, the other valve acts as a safety net and is thermally actuated from the temperature of the condenser shell (manufacturer specifications indicate that at 80°F it is fully closed and at 120°F it is fully open; nevertheless, the MicroTech controller makes the valve obsolete as a safety net and it always remains closed during the testing sequence). Downstream from these control valves are two manual valves that are used to regulate the distribution of the wastewater to two drainage pipes (both of these valves should be 80-100% open). The distribution valves must be adjusted so that the drainage pipes do not overflow when all the other valves (excluding the thermally actuated valve) are fully open.

The condenser vessel should be kept below 138°F when running (max rated pressure of 225 psig). The MicroTech controller is set to turn the chiller off when the condenser pressure exceeds 140 psig (about 108°F). If this fails, there is a digital switch that opens at 195 psi (about 128°F). The evaporator vessel should be kept below 122°F when running (max rated pressure of 180 psig). There is no direct shut-off for high evaporator pressure, except that the condenser high-pressure warning should activate well before the evaporator reaches this pressure. When the evaporator leaving water temperature is near the freezing point the potential exists for severe damage to the chiller; consequently, the lowest possible chilled water setpoint is 34°F. The MicroTech controller will normally attempt to decrease the load at low temperatures, since the corresponding pressure will likely be in an alarm state (with automatic shutdown occurring at 26 psig or 30°F). The evaporator water temperature should be brought up above 45°F before the evaporator water pump is turned off, so that freezing water in the evaporator tubes is avoided. A differential pressure switch is mounted across the

evaporator and condenser pumps, so that in the event that the pump fails, the chiller will immediately shut down (this is hardwired into the chiller controller).

When the chiller is running it is necessary for the PC to also be on and running VisSim. The PC communicates to the MicroTech chiller through VisSim. If VisSim is turned off, then control will be lost. The chiller will recognize that communications have been lost and either maintain its local setpoint, or turn itself off.

There are many different manual switches that regulate power to the test stand and chiller. There are individual switches for each of the three water pumps (a main power switch and a manual control switch—the manual switch duplicates the function of the remote relay control for the pump), there is a switch that provides power to all valves, a switch for the chiller compressor, and finally another switch for the chiller oil heater and control panel. All these switches except the last may be turned on immediately before testing. Since the last switch controls the oil heater, it is necessary for it to be on at least two hours prior to testing and ideally 24 hours before testing. The oil temperature setpoint is 112°F (with a float of about ± 10°F) and it will be necessary to wait for the oil sump temperature to reach 110°F before starting (otherwise the bearings in the motor will be destroyed).

According to ARI Standard 550, the evaporator water loop should have a flow rate of 2.4 gpm/ton and the condenser water loop a flow rate of 3.0 gpm/ton. For a 90-ton chiller this translates to 216 gpm of water in the evaporator and 270 gpm of water in the condenser. Initially the condenser water flow rate was unable to meet ARI specifications; therefore, all data recorded through August 1999 shows a maximum flow rate of approximately 230 gpm. Furthermore, depending on the position of the mixing valve, the condenser water flow rate would drop as low as 205 gpm (refer to Appendix A.2.3). Tests run after September 8, 1999 were done using a more powerful motor on the condenser water pump that is capable of achieving flow rates of 310+ gpm. The flow meters on the condenser and evaporator water loops are specifically calibrated for this installation. Although the flow meter display will read flow rates exceeding the calibration, the JCI AHU controller will display a maximum flow rate of 276 gpm for the condenser water loop and 221 gpm for the evaporator water loop. The triple duty valve

on the condenser water loop is only opened to 10%, thus creating a large enough pressure drop to offset the more powerful motor and bring the flow rate down near to design conditions (which the electronic condenser valve is able to control).

B.5 Introducing Faults

The first fault introduced was an unintentional fault, the defective pilot valve. It is not clear when the pilot valve became defective; however, the inability to adjust it to reduce superheat was one reason leading to its replacement. The pilot valve assembly was replaced on August 19, 1999. The pilot valve is essentially a thermal expansion valve that is connected to a larger valve called the main valve; the main valve directly controls the amount of refrigerant flow in the system.

The first intentional fault introduced was reduced water flow rate in the condenser. The approximate condenser valve settings for each fault are shown in Table B.5. It is important to note that a weaker pump motor was used for the 30% and 40% reduced flow rate fault conditions; moreover, the triple duty valve was set to about 10% open for the 10% and 20% reduced flow rate conditions. The settings in Table B.5 were incorporated into the automatic control import file. Some additional fine-tuning in the control program may have been required to achieve the correct flow rates due to valve hysteresis. These settings normally maintained the desired flow rate within ±2%.

Table B.5: Condenser valve settings for reduced water flow rate faults.

Mixing Valve Position	Normal Condenser Water Flow	10% Condenser Water Flow Reduction	20% Condenser Water Flow Reduction	30% Condenser Water Flow Reduction	40% Condenser Water Flow Reduction
100%	57%	46%	40%	56%	45%
90%	57%	46%	40%	56%	45%
80%	57%	45%	40%	55%	45%
75%	53%	44%	40%	53%	44%
70%	52%	43%	39%	51%	44%
60%	50%	43%	37%	50%	43%
50%	48%	43%	35%	48%	42%
40%	48%	42%	35%	47%	42%
30%	48%	42%	35%	47%	42%

The evaporator valve setting was never incorporated into the import file, thus only one setting is required for each test. At the beginning of each test the evaporator valve setting was manually set approximately to the values indicated in Table B.6.

Table B.6: Evaporator valve settings for reduced water flow rate faults.

Normal Evaporator Water Flow	10% Evaporator Water Flow Reduction	20% Evaporator Water Flow Reduction	30% Evaporator Water Flow Reduction	40% Evaporator Water Flow Reduction
56%	42%	37%	33%	30%

The refrigerant leak testing was simulated by removing refrigerant from the chiller. Initially, all the refrigerant from the chiller was removed, a total of approximately 292 pounds (nominal charge is 300 pounds). About 180 pounds of refrigerant were charged back into the system to simulate the worst fault level of a 40% loss of refrigerant. Each subsequent fault level was introduced by adding 30 pounds of refrigerant between each test run. The scale used to measure the refrigerant transfer was accurate to ±0.5 pounds.

The refrigerant overcharging faults progressed naturally from the refrigerant leak testing. After finishing the refrigerant leak tests, 30-pound increments of refrigerant were

added between test runs to introduce the refrigerant overcharge conditions (by coincidence, the refrigerant supply canisters also contained 30 pounds of refrigerant each—thus simplifying the charging process).

Excess oil was introduced to the compressor via the normal charging port using a hand pump. The amount of oil added was determined by weight, not volume. For the first fault, only three pounds of oil was added because it conveniently emptied a previously used oil can. The next fault used half the oil in a new can, with the third fault then using the remaining half. To make the fourth fault more severe, an entire can of oil was used (one gallon, eight pounds). However, this proved to be too much oil for an effective test run and several pounds of oil were removed. Nevertheless, the first operating condition never reached steady state; so another pound of oil was removed, thus causing the fourth fault level increment to equal the previous fault level increments. The first test in this test run also had problems reaching steady state, and the data used in the analysis excludes the first test run.

The condenser fouling tests were simulated by plugging tubes in the condenser. The condenser is a two pass design, so the plugged tubes were evenly distributed among the two passes. The tubes were plugged with expansion plugs (a rubber stopper bounded by two washers and an internal screw that can lock the plug into place by compressing the stopper so that its outside diameter increases). As can be seen back in Figure 4.22, the condenser has already seen considerable use and was technically already fouled before the simulated fouling tests were conducted. Nevertheless, this is not a problem, since both the benchmark test and fault tests are equally affected (and the fault tests are only compared to the benchmark test).

The non-condensables in the refrigerant tests were simulated by adding laboratory grade nitrogen to the system. The initial amount of nitrogen charged into the system proved to be more severe than anticipated (about 1.5 pounds was originally added). The chiller suffered from high-pressure surge at most operating conditions; therefore, it was decided to start over and remove all the nitrogen. Unfortunately, it is more difficult to remove nitrogen than it is to introduce it into the system.

First, the entire refrigerant charge was recovered from the chiller and a vacuum was pulled on it. Nitrogen was then purged from the recovery tanks; however, not enough time was allowed to bring the tanks to equilibrium during the process. Hence, nitrogen was still present in the recovery tanks when the refrigerant was recharged into the chiller. Based on calculations made using Dalton's law of additive (partial) pressures, about 0.6 pounds of nitrogen remained in the refrigerant.

The chiller worked better than before, but some difficulties in operation prompted the removal of another 0.06 pounds of nitrogen. This time the nitrogen was removed from the highest point in the chiller—the suction port to the compressor—while the unit was turned off (the molecular weight of nitrogen is 28 kg/kgmol, whereas the molecular weight of R134a is 102 kg/kgmol, thus nitrogen will naturally migrate upwards). After modifying the test run to eliminate operating conditions that caused high-pressure surge, the worst fault case became the first one tested.

Removing refrigerant from the highest point in the chiller while it was turned off was not as efficient a method as was hoped for (anywhere from 5 to 60 pounds of refrigerant must be removed to purge 0.1 pounds of nitrogen—the larger quantities are required when the nitrogen concentration is very small). Therefore, since nitrogen is trapped in the condenser during operation, it was believed that it could be recovered from the top of the condenser shell while the chiller was turned on. Unfortunately, the amount of nitrogen purged was undetectable. The only explanation is that the influx of refrigerant in the condenser caused the nitrogen to mix with the refrigerant vapor throughout the condenser instead of settling at the top of the shell as was originally thought.

Nitrogen was removed from the system a small amount at a time in order to test the less severe faults. The contaminated refrigerant was always recovered to the same tank and the chiller's refrigerant charge was brought back to nominal by using refrigerant from the container's liquid recovery port. The nitrogen was very slowly purged from the container's vapor port after it had been left to reach equilibrium (5 to 10 hours) by using a laboratory grade pressure gauge and NIST traceable digital thermometer accurate to ± 0.01°F (to determine the saturation pressure).

Due to the initial problem of introducing too much nitrogen, it was subsequently not possible to precisely determine how much nitrogen was in the system. Instead, it was possible to calculate the theoretical nitrogen content based on Dalton's law of additive pressures (the partial pressure due to nitrogen added to the partial pressure of the refrigerant vapor equaled the total measured pressure—the only unknown to solve for was the partial pressure due to nitrogen since the refrigerant partial pressure could be determined from pressure-temperature tables). The mass of nitrogen in the refrigerant is calculated from the partial pressure by using the ideal gas law. The volume of the system was estimated while recharging refrigerant into the system—determined from the mass introduced and the measured pressure and temperature just before saturation was reached (this was done so that the scale error was minimized when doing the calculation). The calculations were iteratively performed in EES using the following code with equations taken from Wark (1988).

```
{Estimate nitrogen content in refrigerant}
Volume=21.5 {volume of refrigerant system in ft^3}
T_r=70 {temperature of refrigerant in F}
P_meas=75.8 {pressure of refrigerant/nitrogen mixture in psig}
T1=T_r
P1=P_meas+14.7 {convert pressure to psia}
P_r=PRESSURE(R134A,T=T1,x=0.5) {find saturation pressure of refrigerant in psia}
rho_n=DENSITY(N2,T=T1,P=P1) {find density of nitrogen in lb/ft^3}
rho_r=DENSITY(R134A,T=T1,x=1) {find density of refrigerant vapor in lb/ft^3}
rho_rl=DENSITY(R134A,T=T1,x=0) {find density of refrigerant liquid in lb/ft^3}
MW_n=MOLARMASS(N2) {find molecular weight of nitrogen}
MW_r=MOLARMASS(R134A) {find molecular weight of refrigerant}
mass_r=(Volume-(300-mass_r)/rho_rl)*rho_r {find mass of refrigerant in pounds}
mass_n_m=mass_n*CONVERT(lbm,g) {find mass of nitrogen in pounds}
N_n=mass_n/MW_n {find number of moles of nitrogen}
N_r=mass_r/MW_r {find number of moles of refrigerant}
N_m=N_n+N_r {find total number of moles}
y_n=N_n/N_m*100 {find fraction of nitrogen in vapor in %}
y_r=N_r/N_m*100 {find fraction of refrigerant in vapor in %}
```

```
pp_n=N_n/N_m*P1 {find partial pressure of nitrogen in psia}
P_r=N_r/N_m*P1 {constraint imposed on mole calculation}
P_rg=P_r-14.7 {find saturation pressure of refrigerant in psig}
```

Appendix C: Chiller Component Modeling

To model the refrigerant flow path between the condenser and evaporator requires some knowledge about the two additional liquid lines that branch off from the main liquid line leaving the condenser. The first branch sends refrigerant to the motor cavity where it in turn cools the motor and the oil. The second branch is used to regulate the main expansion valve (via the pilot valve discussed in Chapter 4). This second branch returns to the main liquid line at the main valve. The motor cooling line returns to the main liquid line just after the main valve and before the evaporator (both the evaporator and condenser see the full refrigerant flow).

The key component of the chiller system is the compressor. Some modeling was done on the compressor, but it involved using confidential information. Future researchers may find some of the information listed in Table C.1 useful for their own modeling.

Table C.1: Compressor physical characteristics.

Parameter	Dimension	Units
Impeller diameter	4.8	inches
Motor speed	3521	rpm
Gear ratio	8.909	--

Guide vanes are positioned at the inlet of the compressor to control the compressor loading. The onboard chiller controller has no means of tracking the vane position. However, it can be assumed that at the highest loads during normal tests the vanes are at least 90% open (particularly when the chilled water setpoint is not achieved). When the vanes are fully closed the suction aperture is approximately 10-15% of the fully open aperture size.

The following program written in EES was used to obtain the results given in Chapter 6.

```
PROCEDURE WATER_PROPERTIES (wfc,wfe,TEI,TEO,TCI,TCO,T_e,T_c : cp_wc,cp_we,
        m_dot_wc,m_dot_we,h_wc,h_we,cond_area_i,cond_area_o,evap_area_i,evap_area_o,
        evap_tube_od, cond_tube_od)
cxa_wc:=(PI/4*(3.826/12)^2) {cross sectional area of condenser water pipe}
cxa_we:=(PI/4*(3.826/12)^2) {cross sectional area of evaporator water pipe}
q_dot_wc:=wfc*CONVERT(gpm,cfm)/60 {convert to ft^3 per second}
q_dot_we:=wfe*CONVERT(gpm,cfm)/60 {convert to ft^3 per second}
v_dot_wc:=q_dot_wc/cxa_wc {velocity of condenser water in pipe in ft/s}
v_dot_we:=q_dot_we/cxa_we {velocity of evaporator water in pipe in ft/s}
rho_wc:=DENSITY(WATER,T=(TCI+TCO)/2,P=14.7) {water density in condenser}
rho_we:=DENSITY(WATER,T=(TEI+TEO)/2,P=14.7) {water density in evaporator}
m_dot_wc:=q_dot_wc*rho_wc {mass flow rate of condenser water}
m_dot_we:=q_dot_we*rho_we {mass flow rate of evaporator water}
cp_wc:=SPECHEAT(WATER,T=(TCI+TCO)/2,P=14.7) {specific heat of water in condenser}
cp_we:=SPECHEAT(WATER,T=(TEI+TEO)/2,P=14.7) {specific heat of water in evaporator}

cond_tube:=164 {total number of condenser tubes for both passes}
cond_tube_od:=0.75/12 {condenser tube outside diameter in feet}
cond_tube_id:=0.051 {condenser tube inside diameter in feet}
cond_tube_length:=8 {condenser tube length in feet}
cond_tube_cxai:=PI/4*cond_tube_id^2 {condenser tube inside cross sectional area in ft^2}
cond_tube_sfa:=PI*cond_tube_od {condenser tube surface area per foot of tube}
cond_cxa:=cond_tube_cxai*cond_tube/2 {total cross sectional area per pass}
cond_area_i:=cond_tube_id*PI*cond_tube_length*cond_tube {total heat transfer area inside
        tubes}
cond_area_o:=cond_tube_od*PI*cond_tube_length*cond_tube {total heat transfer area inside
        tubes}

k_wc:=CONDUCTIVITY(WATER,T=(TCI+TCO)/2,P=14.7) {Btu/hr-ft-R}
mu_wc:=VISCOSITY(WATER,T=(TCI+TCO)/2,P=14.7) {lbm/ft-hr}
cond_v_dot:=q_dot_wc/cond_cxa {velocity of condenser water in shell in ft/s}
```

```
Re_c:=rho_wc*cond_v_dot*cond_tube_id/(mu_wc/3600) {Reynolds number for condenser water
      flow}
Pr_c:=cp_wc*mu_wc/k_wc {Prandtl number for condenser water flow}
LMTD_c:=(TCO-TCI)/LN((T_c-TCI)/(T_c-TCO))
f_c:=(0.79*LN(Re_c)-1.64)^(-2) {friction factor eq. 8.21}
Nus_c:=((f_c/8)*Re_c*Pr_c)/(1.07+12.7*(f_c/8)^0.5*(Pr_c^0.67-1)) {nusselt number for
      condenser water flow eq.8.62}
h_wc:=[omitted]*(k_wc/cond_tube_id)*Nus_c {condenser water heat transfer coefficient}

evap_tube:=149 {total number of evaporator tubes for both passes}
evap_tube_od:=0.0643 {evaporator tube outside diameter in feet}
evap_tube_id:=0.0527 {evaporator tube inside diameter in feet}
evap_tube_length:=8 {evaporator tube length in feet}
evap_tube_cxai:=PI/4*evap_tube_id^2 {evaporator tube inside cross sectional area in ft^2}
evap_tube_sfa:=PI*evap_tube_od {evaporator tube surface area per foot of tube}
evap_cxa:=evap_tube_cxai*evap_tube/2 {total cross sectional area per pass}
evap_area_i:=evap_tube_id*PI*evap_tube_length*evap_tube {total heat transfer area inside
      tubes}
evap_area_o:=evap_tube_od*PI*evap_tube_length*evap_tube {total heat transfer area inside
      tubes}

k_we:=CONDUCTIVITY(WATER,T=(TEI+TEO)/2,P=14.7){Btu/hr-ft-R}
mu_we:=VISCOSITY(WATER,T=(TEI+TEO)/2,P=14.7){lbm/ft-hr}
evap_v_dot:=q_dot_we/evap_cxa {velocity of evaporator water in shell in ft/s}
Re_e:=rho_we*evap_v_dot*evap_tube_id/(mu_we/3600) {Reynolds number for evaporator water
      flow}
Pr_e:=cp_we*mu_we/k_we {Prandtl number for evaporator water flow}
LMTD_e:=(TEI-TEO)/LN((TEI-T_e)/(TEO-T_e))
{f_e:=(0.79*LN(Re_e)-1.64)^(-2) {friction factor eq. 8.21}}
f_e:=-0.5087+0.2768*LOG10(Re_e)-0.0339*(LOG10(Re_e))^2 {for Re_e < 20000}
Nus_e:=((f_e/8)*(Re_e-1000)*Pr_e)/(1+12.7*(f_e/8)^0.5*(Pr_e^0.67-1)) {nusselt number for
      evaporator water flow eq.8.63}
h_we:= [omitted]*(k_we/evap_tube_id)*Nus_e {evaporator water heat transfer coefficient}
END
```

```
PROCEDURE HEAT_TRANSFER_COEFFICIENTS (q_e_flux,evap_tube_od,cond_tube_od,
        m_dot_r,T1,P1,T3,P3,delta_Tc : h_re,h_rc,h_re_sh,h_rc_sc)
{Calculating boiling heat transfer coefficient}
h_re:= [omitted]+q_e_flux*[omitted]

{Calculating refrigerant side heat transfer coefficient in superheat region}
k_e_sh:=CONDUCTIVITY(R134A,T=T1,P=P1){Btu/hr-ft-R}
rho_e_sh:=1/DENSITY(R134A,T=T1,P=P1) {lb/ft^3}
mu_e_sh:=VISCOSITY(R134A,T=T1,P=P1){lbm/ft-hr}
Pr_e_sh:=PRANDTL(R134A,T=T1,P=P1)
v_dot_e_sh:=m_dot_r*60/(rho_e_sh*8) {ft/hr}
Re_e_sh:=rho_e_sh*v_dot_e_sh*evap_tube_od/mu_e_sh
Nus_e_sh:=1.13*0.5*Re_e_sh^0.5*Pr_e_sh
h_re_sh:= [omitted]*(k_e_sh/evap_tube_od)*Nus_e_sh {refrigerant heat transfer coefficient in
        superheat region of evaporator} {multiplier is for enhanced tubes}

{Calculating condensing heat transfer coefficient}
rho_rl:=DENSITY(R134A,T=T3,P=P3){lb/ft^3}
rho_rg:=DENSITY(R134A,P=P3,x=0.5){lb/ft^3}
k_rl:=CONDUCTIVITY(R134A,T=T3,P=P3){Btu/hr-ft-R}
mu_rl:=VISCOSITY(R134A,T=T3,P=P3){lbm/ft-hr}
h_fg:=ENTHALPY(R134A,P=P3,x=1)-ENTHALPY(R134A,P=P3,x=0){Btu/lb}
h_fg_prime:=h_fg+0.68*SPECHEAT(R134A,T=T3,P=P3)*delta_Tc {eq. 10.26}
h_rc:=[omitted]*0.729*((32.2*3600^2*rho_rl*(rho_rl-rho_rg)*k_rl^3*h_fg_prime)
        /(mu_rl*delta_Tc*cond_tube_od))^0.25 {eq. 10.41} {refrigerant heat transfer coefficient
        in condensing region of condenser} {multiplier is for enhanced tubes}

{Calculating refrigerant side heat transfer coefficient in subcooled region}
k_c_sc:=CONDUCTIVITY(R134A,T=T3,P=P3){Btu/hr-ft-R}
rho_c_sc:=1/DENSITY(R134A,T=T3,P=P3) {lb/ft^3}
mu_c_sc:=VISCOSITY(R134A,T=T3,P=P3){lbm/ft-hr}
Pr_c_sc:=PRANDTL(R134A,T=T3,P=P3)
v_dot_c_sc:=m_dot_r*60/(rho_c_sc*8) {ft/hr}
Re_c_sc:=rho_c_sc*v_dot_c_sc*cond_tube_od/mu_c_sc
Nus_c_sc:=1.13*0.5*Re_c_sc^0.5*Pr_c_sc
```

```
h_rc_sc:= [omitted]*(k_c_sc/cond_tube_od)*Nus_c_sc {refrigerant heat transfer coefficient in
        subcooled region of condenser}{multiplier is for enhanced tubes}
END

{x=1}{uncomment to solve for just one lookup value}
{Imported Values}
TEI=LOOKUP(x, 1) {temperature of evaporator water in}
TEO=LOOKUP(x, 2) {temperature of evaporator water out}
TCI=LOOKUP(x, 3) {temperature of condenser water in}
TCO=LOOKUP(x, 4) {temperature of condenser water out}
Cond_ton=LOOKUP(x, 5) {heat rejection of condenser in tons}
Evap_ton=LOOKUP(x, 6) {cooling capacity in tons}
Motor_kw=LOOKUP(x, 7) {power consumption of motor in kW}
wfc=LOOKUP(x, 8) {gpm of water flow through condenser}
wfe=LOOKUP(x, 9) {gpm of water flow through evaporator}
P_e=LOOKUP(x, 10)+14.7 {refrigerant pressure in evaporator}
P_c=LOOKUP(x, 11)+14.7 {refrigerant pressure in condenser}
T_sub=LOOKUP(x, 12) {liquid subcooling}
Tsh_suc=LOOKUP(x, 13) {superheat of refrigerant out of evaporator}
Tsh_dis=LOOKUP(x, 14) {superheat of refrigerant out of compressor}

Motor_btu=Motor_kw*1000/60*3.413 {power consumption of motor in Btu/min}
T_c=TEMPERATURE(R134A,P=P_c,x=0.5) {condenser temperature}
T_e=TEMPERATURE(R134A,P=P_e,x=0.5) {evaporator temperature}

{Compressor}
idia=4.8/12 {impeller diameter in feet}
rpm=3521*8.909 {impeller rpm, motor rpm times gear ratio}
U_t=rpm/60*idia*PI {impeller tip speed in ft/s}
a_s=483 {suction acoustic velocity in ft/s}
mach=U_t/a_s {machine mach number}

CALL
        WATER_PROPERTIES(wfc,wfe,TEI,TEO,TCI,TCO,T_e,T_c:cp_wc,cp_we,m_dot_wc,
        m_dot_we,h_wc,h_we,cond_area_i,cond_area_o,evap_area_i,evap_area_o,evap_tube_od
        , cond_tube_od)
```

{Thermodynamic Cycle}

{State 1 - Suction}

T1=T_e+Tsh_suc

P1=P_e-1

H1=ENTHALPY(R134A,T=T1,P=P1)

S1=ENTROPY(R134A,T=T1,P=P1)

v1=1/DENSITY(R134A,T=T1,P=P1)

{State 2 - Discharge}

T2=T_c+Tsh_dis

P2=P_c+1

v2=1/DENSITY(R134A,T=T2,P=P2)

H2s=ENTHALPY(R134A,P=P2,S=S1)

H2=ENTHALPY(R134A,T=T2,P=P2)

eta_s=(H2s-H1)/(H2-H1) {isentropic efficiency}

Work_gas=(H2-H1)*m_dot_r

H_i=H2s-H1 {isentropic lift}

mu_i=(778.16*32.174)*H_i/U_t^2 {isentropic head coefficient, dimensionless}

QNDC=(PI/60*m_dot_r*v1)/(U_t*idia^2) {flow coefficient, dimensionless}

m_dot_r=(Cond_ton*12000/60)/(H2-H3) {mass flow rate of refrigerant, lb/min}

{State 3&4 - Subcooled Liquid}

P3=P_c

T3=T_c-T_sub

H3=ENTHALPY(R134A,T=T3,P=P3)

H4=H1-Evap_ton*12000/60/m_dot_r

P4=P_e

m_dot_re=(Evap_ton*12000/60)/(H1-H4) {a check of refrigerant mass flow rate, lb/min}

H_c=ENTHALPY(R134A,P=(P3+P2)/2,T=130)

m_dot_cooling=(Motor_btu-Work_gas)/(H_c-H3) {lb/min}

{First Law Energy Balance}

Heat_Balance=-(Cond_ton*12000/60)+(Evap_ton*12000/60)+Motor_btu{Btu/min}

Heat_Balance%=Heat_Balance/(Cond_ton*12000/60)*100

```
{Compressor Power}
rho_s=DENSITY(R134A,T=T1,P=P1)
cfm=1/rho_s*m_dot_r
Work_gas_hp=cfm*rho_s*H_i/42.4/eta_s {hp to compress gas}
Work_gas_check=Work_gas_hp*2545/60 {convert hp to Btu/min to check earlier result}

{Polytropic Work and Efficiency}
W_p=((P2*v2-P1*v1)/LN((P2*v2)/(P1*v1)))*LN(P2/P1)*(144/778.16)
eta_p=W_p/(H2-H1)

{Fouling factors}
ff_c=0.0005 {condenser fouling factor}
ff_e=0.0001 {evaporator fouling factor}

CALL   HEAT_TRANSFER_COEFFICIENTS   (q_e_flux,evap_tube_od,cond_tube_od,m_dot_r,
          T1,P1,T3,P3,delta_Tc : h_re,h_rc,h_re_sh,h_rc_sc)

{Evaporator heat transfer calculations}
cp_re=SPECHEAT(R134A,P=P1,T=T1)
c_re=cp_re/cp_we
H4a=ENTHALPY(R134A,P=P4,x=1) {enthalpy at vapor/liquid boundary}
Q_dot_e=m_dot_r*60*(H4a-H4){(m_dot_r-m_dot_cooling)*60*(H4a-H3)}
Q_dot_e=epsilon_e*m_dot_we*3600*cp_we*(TEI-T_e)
epsilon_e=1-EXP(-UA_e/(m_dot_we*3600*cp_we))
{A_e=m_dot_we*3600*cp_we/UA_e*LN(1/(1-epsilon_e))}
A_sh=1-A_e {fractional evaporator shell heat transfer area for superheating}
NTU_sh=UA_sh/(m_dot_we*3600*cp_we)
epsilon_sh=2/(1+c_re+(1+c_re^2)^0.5*((1+EXP(-NTU_sh*(1+c_re^2)^0.5)/(1-EXP(-
          NTU_sh*(1+c_re^2)^0.5)))))
Q_dot_sh=epsilon_sh*m_dot_we*3600*cp_we*(TEI_i-T_e)
Q_dot_sh=m_dot_we*3600*cp_we*(TEI_i-TEO_est)
Q_dot_sh=m_dot_r*60*cp_re*T_sh

1/UA_e=1/(h_re*evap_area_o*A_e)+1/(h_we*evap_area_i)+ff_e/evap_area_i
1/UA_sh=1/(h_re_sh*evap_area_o*A_sh)+1/(h_we*evap_area_i)
Q_dot_e_tons=Q_dot_e/12000
```

```
Q_dot_sh_tons=Q_dot_sh/12000
Q_dot_et_tons=Q_dot_e_tons+Q_dot_sh_tons
Q_dot_et_tons*12000=m_dot_we*3600*cp_we*(TEI-TEO_est)

q_e_flux=Q_dot_e/(evap_area_o)
U_e=UA_e/evap_area_i
U_e_sh=UA_sh/evap_area_i

{Condenser heat transfer calculations}
cp_rc=SPECHEAT(R134A,P=P3,T=T3)
c_rc=cp_rc/cp_wc
H3a=ENTHALPY(R134A,P=P3,x=0) {enthalpy of vapor/liquid boundary}
Q_dot_c=m_dot_r*60*(H2-H3a)
Q_dot_c=epsilon_c*m_dot_wc*3600*cp_wc*(T_c-TCI_i)
epsilon_c=1-EXP(-UA_c/(m_dot_wc*3600*cp_wc))
{A_c=m_dot_wc*3600*cp_wc/UA_c*LN(1/(1-epsilon_c))}
A_sc=1-A_c {fractional condenser shell heat transfer area for subcooling}
NTU_sc=UA_sc/(m_dot_wc*3600*cp_wc)
epsilon_sc=2/(1+c_rc+(1+c_rc^2)^0.5*((1+EXP(-NTU_sc*(1+c_rc^2)^0.5)/(1-EXP(-
        NTU_sc*(1+c_rc^2)^0.5)))))
Q_dot_sc=epsilon_sc*m_dot_wc*3600*cp_wc*(T_c-TCI)
Q_dot_sc=m_dot_wc*3600*cp_wc*(TCI_i-TCI)
Q_dot_sc=m_dot_r*60*cp_rc*T_sc

1/UA_c=1/(h_rc*cond_area_o*A_c)+1/(h_wc*cond_area_i)+ff_c/cond_area_i
1/UA_sc=1/(h_rc_sc*cond_area_o*A_sc)+1/(h_wc*cond_area_i)
Q_dot_c_tons=Q_dot_c/12000
Q_dot_sc_tons=Q_dot_sc/12000
Q_dot_ct_tons=Q_dot_c_tons+Q_dot_sc_tons
Q_dot_ct_tons*12000=m_dot_wc*3600*cp_wc*(TCO_est-TCI)

LMTD_c=(TCO-TCI_i)/LN((T_c-TCI_i)/(T_c-TCO))
UA_c_avg=Q_dot_c/LMTD_c

delta_Tc=Q_dot_c_tons*12000/(h_rc*cond_area_o)
q_c_flux=Q_dot_c/cond_area_o
```

U_c=UA_c/cond_area_i
U_sc=UA_sc/cond_area_i

Q_dot_sub=m_dot_r*60*(H3a-H3)/12000

mass_evap=([omitted]*A_sh)/v1+([omitted]*A_e)*DENSITY(R134A,T=T1,x=0)
mass_cond=([omitted]*A_c)/v2+([omitted]*A_sc)*DENSITY(R134A,T=T3,P=P3)
mass_total=mass_evap+mass_cond
{mass_total=290}
A_liquid=A_e+A_sc
A_gas=A_sh+A_c